SAND2004-3632 C.1
RECORD COPY

SANDIA REPORT

SAND2004-3632
Unlimited Release
Printed October 2004

Case Study for Model Validation: Assessing a Model for Thermal Decomposition of Polyurethane Foam

Kevin J. Dowding, Richard G. Hills, Ian Leslie, Martin Pilch, Brian M. Rutherford, and Michael L. Hobbs

Prepared by Sandia National Laboratories
Albuquerque, New Mexico 87185 and Livermore, California 94550

Sandia is a multiprogram laboratory operated by Sandia Corporation, a Lockheed Martin Company, for the United States Department of Energy's National Nuclear Security Administration under Contract DE-AC04-94AL85000.

Sandia National Laboratories

TOTAL PAGES: 196
COPY

Issued by Sandia National Laboratories, operated for the United States Department of Energy by Sandia Corporation.

Available to DOE and DOE contractors from
U.S. Department of Energy
Office of Scientific and Technical Information
P.O. Box 62
Oak Ridge, TN 37831

Telephone: (865)576-8401
Facsimile: (865)576-5728
E-Mail: reports@adonis.osti.gov
Online ordering: http://www.osti.gov/bridge

Available to the public from
U.S. Department of Commerce
National Technical Information Service
5285 Port Royal Rd
Springfield, VA 22161

Telephone: (800)553-6847
Facsimile: (703)605-6900
E-Mail: orders@ntis.fedworld.gov
Online order: http://www.ntis.gov/help/ordermethods.asp?loc=7-4-0#online

SAND2004-3632
Unlimited Release
Printed October 2004

Case Study for Model Validation: Assessing a Model for Thermal Decomposition of Polyurethane Foam

Kevin J. Dowding
Validation and Uncertainty Quantification Processes
Sandia National Laboratories
P. O. Box 5800
Albuquerque, New Mexico 87185-0828

Richard G. Hills and Ian Leslie
Department of Mechanical Engineering
New Mexico State University
Las Cruces, New Mexico 88003

Martin Pilch
Validation and Uncertainty Quantification Processes
Sandia National Laboratories
P. O. Box 5800
Albuquerque, New Mexico 87185-0828

Brian M. Rutherford
Independent Surveillance Assessment & Statistics
Sandia National Laboratories
P. O. Box 5800
Albuquerque, New Mexico 87185-0829

Michael L. Hobbs
Thermal and Reactive Processes
Sandia National Laboratories
P. O. Box 5800
Albuquerque, New Mexico 87185-0836

Abstract

A case study is reported to document the details of a validation process to assess the accuracy of a mathematical model to represent experiments involving thermal decomposition of polyurethane foam. The focus of the report is to work through a validation process. The process addresses the following activities. The intended application of mathematical model is discussed to better understand the pertinent parameter space. The parameter space of the validation experiments is mapped to the application parameter space. The mathematical models, computer code to solve the models and its (code) verification are presented. Experimental data from two activities are used to validate mathematical models. The first experiment assesses the chemistry model alone and the second experiment assesses the model of coupled chemistry, conduction, and enclosure radiation. The model results of both experimental activities are summarized and uncertainty of the model to represent each experimental activity is estimated. The comparison between the experiment data and model results is quantified with various metrics. After addressing these activities, an assessment of the process for the case study is given. Weaknesses in the process are discussed and lessons learned are summarized.

Executive Summary

A case study is reported to document the details of a validation process to assess the accuracy of a mathematical model to represent experiments involving thermal decomposition of polyurethane foam. The focus of the report is the validation process and not the specific outcome for the model studied. The goal of report is to work through the validation process and present the details for a thermal application.

In the report, all steps in the process are covered with sufficient detail and references so that others interested in validation may gain enough insight to apply the process to a different problem. The report and process begins with a discussion of model application requirements and planning (Chapter 2). A brief description of the mathematical model, computer code that solves the mathematical model, and code verification follow (Chapter 3). Experimental activities to collect data for assessing the accuracy of the model are then described, including presentation of the test matrix and experimental data (Chaper 4). Two separate experiments are used in this study. Modeling results for the experimental measurements, including model uncertainty due to input parameters, are discussed next (Chapter 5). Various metrics are applied to quantify differences between experimental measurements and model results (Chapter 6). Then, the outcome of the comparison/process is assessed (Chapter 7). The report concludes with a summary and recommendations (Chapter 8).

The model assessed in this study is chemical-structure-based polyurethane foam (CPUF). Two models are assessed in the report. A chemical kinetics model to represent the thermal decomposition of foam is assessed first. The chemical kinetics model is assessed with data collected on a thermal gravimetric analyzer (TGA). TGA experiments study small, 1-10 mg, foam samples. A TGA apparatus measures the sample mass for a control temperature history. Measured mass is usually normalized by the initial mass to calculate the solid fraction, which ranges from 0 to 1. TGA experiments investigate the effects of temperature history (isothermal or continuous ramping) and pressures (1 to 30 atm) on the decomposition. The chemical kinetics model is assessed through quantifying the error in various physical quantities. Physical quantities studied include: the temperature to reach a prescribed solid fraction, solid fraction at burnout temperature (completion of decomposition), and solid fraction over the range of temperatures from the onset of decomposition to completion.

The decomposition of larger foam samples, 100-300 g, is studied in the benchmark experiments. For the larger samples, in addition to chemical kinetics in the mathematical model, models for transient conduction, material removal when the foam decomposes (element death), and enclosure radiation across the voids resulting from element death are included. In these experiments, the polyurethane foam samples are encased in a stainless steel cylinder with steel end caps. The temperature of one end of the cylinder is controlled, ramping from ambient temperature to a steady hold temperature, (600, 750, 900, or 1000 °C) over approximately 90 seconds. The test matrix

for the benchmark experiments studied the effects of hold temperature, foam density, and orientation of the heated surface relative to gravity. The benchmark experiments employ X-ray imagery of the foam to track the location of a decomposing front. The model was assessed based on front location as a function of time and slope of the front location as a function of time curve.

Two metrics, or more appropriately analyses, were undertaken to assess the accuracy of the models. Applying various metrics was done for demonstration purposes and to gain greater insight into model accuracy. For the first approach, the difference between the experimental measurement and the model result, call it the prediction error, was quantified and statistics of prediction error, mainly mean, standard deviation, and correlation coefficient, were estimated. The prediction error has contributions from variability/uncertainty in the model inputs, like material properties and boundary conditions, and experimental measurement uncertainty. For the second approach, the effects of model uncertainty and measurement uncertainty are estimated independently. Then, a (hypothesis) test of whether the prediction error is consistent with the model and measurement uncertainty is made. The second approach provides some insight into whether the observed prediction error could be described by model input and measurement uncertainty.

Comparison of the chemical kinetics model with the TGA experiments indicated the error in the model to represent the physical process was relatively small. The following variables were quantitatively studied.

- ***Temperature to achieve prescribed solid fractions.*** For solid fractions of 0.8, 0.6, 0.4, and, 0.1 relative errors ranged in magnitude from –10% to 5%. The largest errors were observed at the 0.1 solid fraction and higher pressures. In most cases, the mean error was less than 1% with standard deviation of 1 to 2%. A dependence of the error on pressure, as indicated by the correlation coefficient, was observed.
- ***Solid fraction at the burnout temperature.*** The absolute error in solid fraction at the burnout temperature (temperature signifying the completion of decomposition) was a function of pressure, with mean ranging 0.01 to 0.05 for pressures from ambient to 10 atm and standard deviation about a consistent 0.02 over the range of pressures.
- ***Solid fraction as a function of temperature.*** Error in solid fraction over the temperature range from onset to completion of decomposition was assessed relative to the uncertainty due to model inputs and experimental measurement uncertainty. Error in solid fraction was consistent with model uncertainty and measurement uncertainty for ambient pressure experiments, but the outcome was sensitive to the magnitude of the measurement uncertainty. Error in solid fraction was not consistent with model and measurement uncertainty at higher pressures. Errors at lower solid fractions deviated significantly from measurement and model uncertainty.

Assessing the mathematical model, included chemical kinetics, conduction, element death, and enclosure radiation, with the benchmark experiments demonstrated a large prediction error for the mathematical model to represent the experiment. The error was strongly dependent on the boundary temperature and independent of orientation. Because the tests were concentrated at a boundary temperature of 750 °C, it is unclear what the source of the error may be. The physical quantities investigated and a summary of the quantification is discussed below.

- ***Slope of the front recession curve.*** Logarithmic error in slope between 1 cm and 2 cm of decomposition was quantified. The slope of the front recession curve is proportional to the velocity of the front. For a 750 °C hold temperature, the logarithmic error, which is comparable to the relative error for small errors, had a mean of 0.11 and standard deviation of 0.26 and showed no dependence on orientation. The error at 600 °C hold temperature was significantly larger and negative, -0.36. The error at 900 °C and 1000 °C was large and positive, 0.26 and 0.32, respectively.
- ***Front location as a function of time.*** The error in front location as a function of time was assessed relative to the model and measurement uncertainty. Except for a single experiment, which is significantly different from the other experiments with a 750 C hold temperature, the error is consistent with model and measurement uncertainty. Engineering judgment estimates measurement uncertainty to have a standard deviation of 0.075 cm, this uncertainty is significantly less than model uncertainty. Errors are not consistent with uncertainty at the 900 °C hold temperature. Errors are consistent for the 600 °C hold temperature, but model uncertainty swamps the error.

Four main lessons are taken from our study of validation process for the foam decomposition model.

1. Validation experiments need a clearly defined target application. Without requirements to specify what prediction is needed from the model and the accuracy of the prediction, we can only speculate on model's performance relative to the accuracy needed for the intended application. Furthermore, the validation exercise may not investigate the model's performance for quantities of interest for the application.

2. Validation experiments should be performed in the parameter range anticipated for the intended application. The size of materials and test conditions should be selected to map directly to the intended application.

3. Validation experiments should be designed to provide/investigate responses that are meaningful to the application. Carefully managing the data collected and experimental procedures can greatly improve the insight provided during the validation. Specifically,

a. Use statistical design to define the experimental test matrix. The main goals are to efficiently coverage the parameter space and data to assess the experimental variability.

b. The effect of uncertainty on the measured response needs to be estimated. Quantifying measurement errors is challenging, and may require additional experiments. Considering this issue during the experimental design phase may suggest ways to reduce the effect.

c. Uncertainty in measured boundary and initial conditions need to be estimated.

The computational model should be used to study the effect of uncertainty prior to conducing the experiments to understand the important parameters/boundary conditions needed to model the experiment.

Acknowledgements

The authors would like to thank Dean Dobranich, Rob Easterling, Roy Hogan, Jaime Moya, Bill Oberkampf, and Tim Trucano for reviewing this report. Ken Erickson and T.Y. Chu coordinated the experimental activities and provided the experimental data used in the report. Ben Blackwell helped generate verification results.

Sandia is a multiprogram laboratory operated by Sandia Corporation, a Lockheed Martin Company, for the United States Department of Energy under Contract DE-AC04-94AL85000.

Nomenclature

A_j	area (m^2)
c	specific heat (J/kg °C)
D	experimental data
e	prediction error, difference between experimental measurement and model result
e_T	temperature error (°C)
e_{sf}	solid fraction error
$E()$	experimental physical process
E_j	activation energy j (cal/mol)
F_{k-j}	view factor
h	characteristic mesh dimension
H_0	norm of temperature (°C)
H_1	norm of temperature gradient (°C/m)
k	thermal conductivity (W/m°C)
k_j	kinetic coefficient
L_∞	norm of maximum temperature(°C)
L, L_0	bridge (adipate) population
M()	mathematical model process
M_i	chemical symbol for species i
N_i	concentration of species I
P	pressure (atm)
q	heat flux (Wm^2)
Q_c	volumetric energy (W/m^3)
Q_i	net surface energy loss (W)
R	universal gas constant (kJ/kmol K)
r^2	r^2 statistic
r_ρ	correlation coefficient
s_f	solid fraction
S	mathematical model result
Sp	mathematical model error due to input error
T	temperature
t	time
v',v''	stoichiometric coefficients
x	front location
X	factor
z	boundary condition

Greek

ϕ	mathematical model parameters
α	parameter vector
μ	concentration exponent
μ_p	mean error for variable p
γ	importance factor

ρ density (kg/m^3)
$\rho_{E_iE_j}$ correlation coefficient for variable E_i and E_j
δ front thickness (m)
δ_D experimental measure error (°C)
δ_n numerical mathematical model error
δ_{kj} delta function
σ Stefan-Boltmann constant (W/m^{2}K^4)
σ_p standard deviation of variable p
σ_E distributed activation energy parameter (cal/mol)
ξ extent of reaction parameter
Ω domain

$\|\bullet\|$ norm
^ corrupted with error

1.0 Introduction

The goal of the verification and validation (V&V) program as part of the Advanced Simulation and Computing Program (ASCP), the follow-on program to the Accelerated Strategic Computing Initiative (ASCI), is to establish confidence in computational simulations supporting the Stockpile Stewardship Program (SSP) through systematic demonstration and documentation of the accuracy of the computational simulations and their underlying models. In support of this goal, we document the results of a case study to assess the accuracy of a model for the thermal decomposition of polyurethane foam.

Validation of a computer model for a given application in defined in the DOE Defense Programs (DOE/DP) ASCI Program Plan (DOE, 2000) as:

> **Validation** – The process of determining the degree to which a computer model is an accurate representation of the real world from the perspective of the intended model applications.

This definition suggests three important aspects of model validation. First, model validation is a process with a number of interacting related technical tasks involved in computational modeling. Second, the process is application-driven and, consequently, closely tied to requirements of a specific computer-modeling application. We discuss validation methodology in terms of the application requirements. Third, the process is quantitative; we determine the degree of accuracy of a model to represent the real world. Metrics to quantitatively compare model results and experiments are discussed in this report.

Model validation (In the document, we use the term model to refer to a set of mathematical equations, usually in the form of differential equations, to represent a physical process.) is a process that can be viewed as one of several activities involved in performing a computational analysis using a code for a specific application. The application requirements dictate what predictive capabilities are needed to address application objectives and how well the code must perform to be useful in the analysis. The role of the validation process and specifically of the validation experiments within this framework is discussed in detail in Trucano, et al., (2002). The basic relationships are established in Figure 1.1, Trucano et al. (2002).

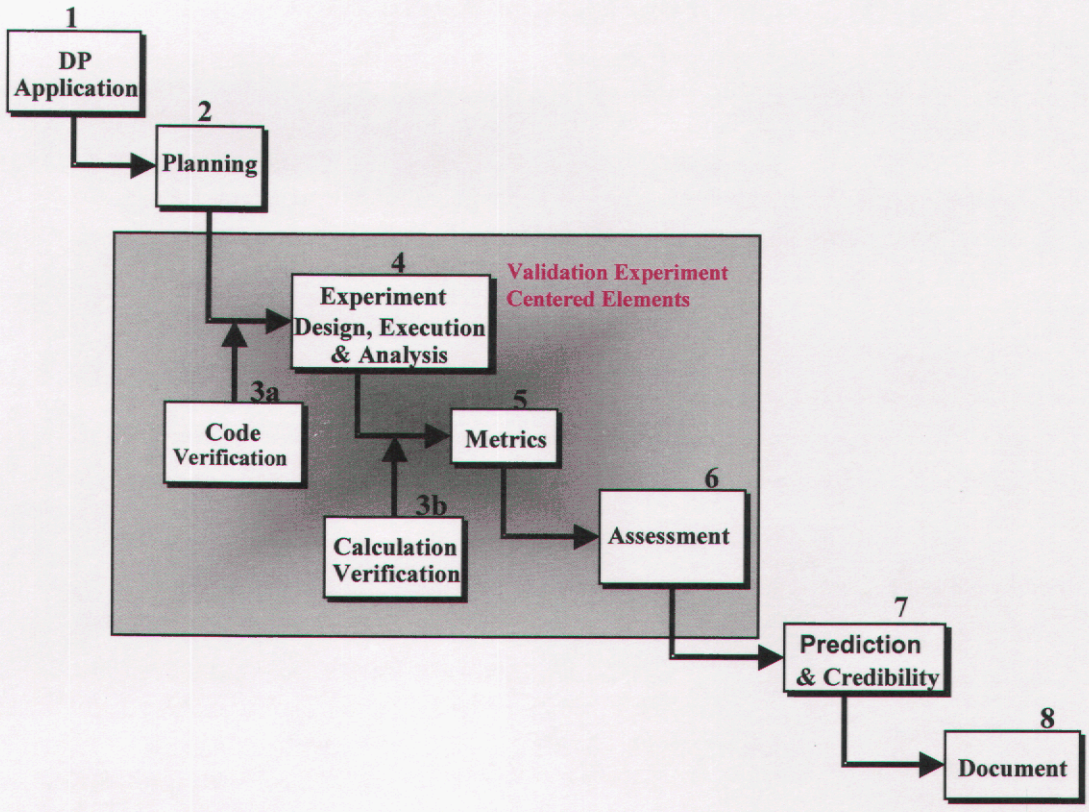

Figure 1.1 Validation process Trucano, et al. (2002)

The process schematically outlined in Figure 1.1 provides a framework for the methodology studied in this report. We apply the process to the code application of modeling the thermal decomposition of polyurethane foam. Our goal is to use the modeling and experimental activities supporting the thermal decomposition of foam and work through all of the steps in the process identified in Figure 1.1. However, because portions of the activities were performed for reasons other than for this study, limitations in specific activities may exist. In this report, we acknowledge and discuss limitations that were identified. We were more concerned with illustrating all steps in the validation process rather than refining each specific step of the process to the point of complete satisfaction. One can view the results presented here as eh first iteration of the validation process. In general, the process is iterative and applies lessons learned to improve subsequent iterations.

The design and implementation of a flexible and effective validation process is a topic of current research and development in areas of engineering, statistics, and mathematics. The recent literature includes a number of papers proposing a common framework for model validation, introducing techniques for comparing model to experimental results, and using the models for prediction. We discuss various frameworks later in this section.

The model studied in this document pertains to thermal decomposition of foam. We note that the purpose of our study is to demonstrate the validation methodology, as opposed to a arriving at a definitive assessment of the model. Because the experiments were conducted over two years prior to our work, direct input to address validation issues was not possible. Limitations in the data, and suggested improvements, are noted when applicable, which should benefit future activities on different foam. As discussed previously, validation is a process and it is anticipated that ultimately we will need to iterate over the steps in this process if complete credibility is to be achieved. The first iteration presented in this study will help improve future work supporting validation activities for similar models, as well as demonstrate the methodology.

In the remainder of Section 1.0 we briefly discuss the code application studied in the report, thermal decomposition of polyurethane foam. Then, a mathematical framework for comparing a computational model with physical experiments is presented. We conclude this section with an outline of the remaining sections of the report.

1.1 Thermal Decomposition of Foam

1.1.1 Introduction

In a weapon system, rigid foam is used to encapsulate critical components. The foam provides needed mechanical support. In an abnormal environment, such as a hydrocarbon fuel fire, the rigid foam will decompose when the temperature exceeds 250°C, exposing critical components to the harsh thermal environment. Historically, based on limited test data, radiation parameters in weapon models have been "tuned" to reflect the protective effect of foam. More recently, experiments have been conducted and compared with existing weapon models, Dobranich and Gill, (1999). The comparisons have shown that the historical approach of tuning is not adequate for predictive models, thus suggesting that physics-based models are needed for foam decomposition in an abnormal thermal environment. Subsequently, a model has been under development and a program has been initiated to validate this foam decomposition model (Hobbs *et al.*, 2003). The modeling and experimental efforts, which were jointly conducted, are discussed next.

1.1.2 Model Efforts

Chemical-structure-based polyurethane foam (CPUF) is a computational model to describe the thermal response of closed-cell polyurethane foam, as used in the B61 and W80 weapon systems, for thermal environments representative of fires (abnormal thermal environments). CPUF has three components to model the decomposition of polymeric materials: 1) a bond breaking mechanism, 2) a lattice statistics model, and 3) a vapor-liquid equilibrium model. The model predicts the mass and specie evolution of decomposing polyurethane depending on the temperature history.

To model the thermal response of foam under conditions of combined thermal diffusion, thermal radiation exchange, and chemical kinetics, the CPUF chemistry model

is implemented in a thermal diffusion/radiation code. A foam response model, which Hobbs et al. (2003) refer to as the CPUF foam response model, will include the CPUF chemistry model and thermophysical properties to model diffusion characteristics of foam. Experimental investigations supported physics discovery and model development, with some experiments used to calibrate the parameters in proposed models.

The foam response model is implement in thermal analysis codes Calore (Bova, et al., 2002A) and Coyote (Gartling, et al., 1994). The intent was to study the validation of the model as implemented in ASCI code Calore. However, because the model was not implemented in Calore in time to provide the necessary model results, Coyote model results were used in this report to compare with experimental data. We note that the computational models/algorithms in Calore are nearly identical to those in Coyote. Hence, we believe that studying model results from Coyote is insightful to validation issues of foam response models in Calore. Of course, we need to verify the implementation of the foam response model for the two computational codes, then make a case that the codes give "comparable" model results. Trucano (2002) discusses the issue of code-to-code comparisons. Alternatively, we can repeat the comparisons using code results from Calore. Issues surrounding code verification are addressed for Calore.

1.1.3 Experimental Efforts

Two types of experiment were conducted to support model development and validation. Thermal gravimetric analysis (TGA) experiments monitor the mass of a small specimen (4-6 mg) while controlling the thermal environment. TGA experiments support physical discovery and model development/calibration. The TGA experiments isolate the chemical processes to support developing a chemical kinetics model of the thermally driven decomposition. In the model development process, TGA experiments are used to estimate model parameters.

The second type of experiment is refereed to as the benchmark experiment in this document. The experiment tests a large foam sample (400 g) by imposing an incident heat flux representative of a fire and tracking the decomposition of the sample using X-ray imagery.

1.2 Mathematical Framework

To motivate a quantitative process, an overview of comparing model results with experimental measurements (the fundamental activity of validation) is provided. The model results are from the solution of a mathematical model (simulation), S, of the physical process in the experiment. Experimental data, D, are measured quantities from the physical experiment. The modeling and experimental process are discussed and summarized individually followed by a subsection discussing their comparison.

1.2.1 Model Simulations

The model values that are compared to the experimental measurements are typically based on the solution of a (or set of) differential equation(s). We can conceptualize the solution of the differential equation as a transfer operator. Given physical parameters, ϕ, and boundary and initial conditions, z, we can solve the equation, i.e., evaluate operator $\mathbf{M}(\phi)$, and get model results

$$z \rightarrow \mathbf{M}(\phi) \rightarrow S(\phi, z). \qquad (1.1)$$

The mathematical model "transforms" physical (and possibly empirical) parameters and boundary/initial conditions to model outputs. Parameters, ϕ, are coefficients or empirical constants required for the mathematical model. Numerical values of ϕ are selected based on the experimental dependence, X (discussed next). Boundary/initial conditions, z, are inputs to the model that are controlled or measured in the experiment. These inputs are the "driving" terms in the model. That is to say, the boundary/initial conditions are the "cause," of the model's output ("effect").

For the present application, ϕ are the activation energies and thermophysical properties and other associated parameters of foam and stainless steel. The initial/boundary conditions, z, are the measured temperatures of the heated plate and can, and the model output, $S(\phi,z)$, is the foam decomposition front location as a function of time or velocity.

1.2.2 Experimental Data

An experiment, or "physical simulation," provides data representative of the physical process. Similar to the math model, the data depends upon the boundary/initial conditions and physical attributes of the experimental hardware. We represent the physical attributes of the experiment by X. By imposing boundary/initial conditions, z, on selected hardware described by factors, X, we can measure an experimental outcome

$$(z) \rightarrow \mathbf{E}(X) \rightarrow D(X, z) \qquad (1.2)$$

The operator **E(X)** is the physical process that transforms boundary/initial conditions and physical characteristics of the experiments, X, to an observed or measured response, $D(X,z)$. The boundary/initial conditions, z, are separated from all other experimental factors, X, because the boundary/initial conditions are the active or driving factors in the process and directly link the experiment to the model.

In the benchmark experiment, a plate is radiantly heated to impose the boundary condition on the end surface of the can. The magnitude of this heating is controlled and measured to produce a given temperature history. Additionally, the transient temperature of the outer surface of the can is measured to identify this boundary condition. The physical characteristics of the experiment, or factors, X, are the geometry, materials (foam and stainless steel), presence and type of component, orientation, etc. Values of physical parameters for the mathematical model, ϕ, are related to the experimental characteristics, X. For example, we specify thermophysical properties for the model

based on knowing the experiment has polyurethane foam of a certain density. It is important to select an appropriate X-space to study the model's accuracy. Because the number of variables in X can be large, it is also necessary to identify a subset of X that is important and relevant to the application.

1.2.3 Comparison of Experimental Measurements and Model Results

The goal of comparing a model to experiments is to assess the accuracy of the mathematical model, $\mathbf{M}(\phi)$, to represent the physical process, $\mathbf{E}(X)$, for the intended application. If we demonstrate that the mathematical model is adequately accurate for the application, we can use it, within some bounds, in place of physical experiments. The raw data we have for assessing the accuracy of the math model are model simulations, $S(\phi,z)$, and experimental measurements, $D(X,z)$.

To quantitatively study the accuracy of the model, differences between experimental data and model results must be studied. Differences are a sensitive indicator of the relationship between an experiment and a model. Define the difference between the "exact" experimental measurements and model results (no error in either value) as

$$\varepsilon \equiv D(X,z) - S(\phi,z). \qquad (1.3)$$

This difference directly indicates the accuracy of the model to represent the physical process. We want to think of ε as model inadequacy or model form error. It (ε) has no dependence on lack of information about the experiment (or model) or measurement error and is purely the result of the model approximating nature. The difference should be due to the model approximating the physical process, or "missing physics."

A fundamental difficulty with validation is that the data we have for the experimental measurements and model results are corrupted with error; hence, we cannot directly quantify ε. The experimental data are corrupted with measurement error, bias and variablility, and we measure

$$\hat{D}(X,z) \equiv D(X,z) + \delta_D, \qquad (1.4)$$

where δ_D is the measurement error. We also have measurement error in the boundary/initial conditions, but discuss the effect of this measurement error later.

The model is corrupted with error through "misalignment" of the model with the experiment. We align the experiment and model through $(X,\phi,z,)$. The boundary/initial conditions are measured, or inferred, from the experiment and corrupted with error. Physical parameters are typically estimated from previous experiments (hopefully for similar X), which will result in estimation error. Furthermore, many of these parameters vary (perhaps randomly) from experiment to experiment. A critical aspect of modeling is to select the values of parameters, ϕ, based on X and quantify the effect of uncertainty due to using selected values of ϕ to model the experiment. Consequently, model results (of the validation experiment) use measurements/estimates for (ϕ,z), call them $(\hat{\phi},\hat{z})$. In addition, by solving the mathematical model on the computer we incur numerical errors,

δ_n. The numerical error is due to discretization and other numerical issues associated with solving the mathematical equations on the computer. Calculation verification is intended to address the numerical error. The relationship between the "exact" model and model using measurements/estimates for parameters and boundary/initial conditions and solved on the computer is

$$S(\phi, z) = S(\hat{\phi}, \hat{z}) + S_p(\phi - \hat{\phi}, z - \hat{z}) + \delta_n . \qquad (1.5)$$

This relationship is conceptual; we only know the first term on the right side of the equation other terms can be estimated, but recognize that the model result for the validation experiment (left side of equation) differs from the known value. We (potentially) have error due to the estimation/measurement error in inputs $(\phi - \hat{\phi}, z - \hat{z})$ and error due to numerically solving for the model results, δ_n. The error due to input error can be approximated as

$$S_p(\phi - \hat{\phi}, z - \hat{z}) \approx \frac{\partial S}{\partial \hat{\phi}}(\phi - \hat{\phi}) + \frac{\partial S}{\partial \hat{z}}(z - \hat{z}) + O\left[(\phi - \hat{\phi})^2, (z - \hat{z})^2\right]. \qquad (1.6)$$

As the approximation shows, the error is a function of how sensitive the model is to the parameters, i.e., the gradient, and the magnitude of the error in the inputs.

The data (experimental and model results) are corrupted by various sources of error. Define the difference between the corrupted values as the *prediction error*

$$e \equiv \hat{D}(X, z) - S(\hat{\phi}, \hat{z}) . \qquad (1.7)$$

We have data to quantify the prediction error, e, in Eq. (1.7). The prediction error can be related to ε in Eq. (1.3),

$$e = \delta_D + S_p(\phi - \hat{\phi}, z - \hat{z}) + \delta_n + \varepsilon . \qquad (1.8)$$

Although data exists to quantify e, its relationship to ε, the error in the model's ability to represent the physical process, is confounded with additional measurement and modeling input error. As this equation demonstrates, four sources could potentially contribute to the difference (e).

- Experimental response measurement error, δ_D. Random and bias errors in the instrumentation affect the experimental measurements. Such errors impact the measured experimental response, D, and measured boundary/initial conditions, z. Characterizing the resolution of diagnostics will help quantify this error. In many cases, however, diagnostic installation issues have a larger effect than diagnostic resolution and are more difficult to quantify.
- Error in the physical parameters and boundary/initial conditions input to the model, $S_p(\phi - \hat{\phi}, z - \hat{z})$. Note that this error depends on the magnitude of error or misalignment, $(\phi - \hat{\phi}, z - \hat{z})$, and on the model's dependence on this misalignment. Techniques exist for quantifying the effect of misalignment on the

model, but rely on, often unavailable, characterization of the misalignment (input errors).

- Error associated with numerically solving the mathematical equations on the computer, δ_n. Assessing convergence and studying numerical dependencies is required to gain insight to this error.
- Error due to the model not representing the physics, ε. Conceptually, this is the error we would like to quantify through the validation process.

In practice, we expect that all four sources will contribute to the observed differences. Separating and quantifying the effects is extremely challenging and not always possible. In some cases, with additional data we may be able to separate the contributions and isolate a component. In other cases, we may wish to quantify the combined effect of the errors. It is important, however, to understand what errors could impact the comparison. The better understanding we have about what components contribute to e, the more confidence we will have in understanding what e in the validation exercise indicates about the application, the more insight we will have to the accuracy of the model, and finally, the better our chance of identifying how to improve on the process.

1.3 Validation Framework

We note that, as this is a research area, there are aspects of the validation process that are still being debated. This is particularly true of frameworks to describe the process and metrics. We have not tried to debate issues further in this document. Rather, we apply various metrics that are under consideration and discuss the resulting inferences. Frameworks for validation are discussed in Easterling and Berger (2002), Bayarri et al. (2002), Kennedy and OHagan (2002), Rutherford and Dowding (2003), and Hills et al. (2002).

1.4 Outline

The material in the remaining sections of the report can be related to the Eq. (1.6) and (1.7) and Figure 1.1. We relate the topic(s) of each section to them.

Section 2 discusses the DP Application (1) and Planning (2). We relate requirements on the application to requirements on the validation activity and other planned validation work supporting the application. Specifically, we identify the parameter space, X, ϕ, and z, of interest for the application.

Code Verification (3a) is addressed in Section 3 (we save Calculation Verification (3b) until Section 5). The code verification status, math models required for the code application validation, and math model/ algorithm verification are summarized. This material is aimed at the numerical error, δ_n.

The experimental activities, including Experiment Design and Execution (4), are summarized in Section 4. Experimental activities that provide the data to support validation are discussed. We discuss the experimental design and mapping to the application parameter space, as well as experimental measurement error, δ_D.

Application of the code to analyze the experiments (4) is discussed in Section 5. This section presents the computational model results of the experiments, include model uncertainty, to estimate the effect of $S_p(\phi - \hat{\phi}, z - \hat{z})$, and Calculation Verification (3b), δ_n.

Section 6 applies metrics/analyses (5) to quantitatively compare code application results with experimental measurements. We quantify the error, e, assess its dependence, and possible contributors.

Section 7 provides an Assessment (6) of the process and discusses Prediction and Credibility (7).

Section 8 summarizes the main points learned in this process and gives guidance for future validation activities.

2.0 Application Requirements and Planning

Validation activities should be aligned, as close as possible, with the intended application and the requirements of the intended application. The W80 weapon system in an abnormal thermal environment is the intended application for the foam thermal decomposition model. At the time of writing this document, an integrated plan for the W80 system was in preparation, but not available. A plan for the W76 system in an abnormal environment was available, however, Tieszen et al. (2002). Although the W76 uses different foam, the application requirements are similar. We draw on the information in the W76 plan to identify the application requirements pertinent to modeling the thermal decomposition of foam in an abnormal environment.

In an abnormal environment, system metrics involving safety issues are the main concern for the application. In particular, assessing the "thermal race" and failure of the AF&F exclusion region barrier (ERB) are pertinent system metrics, Tieszen et al. (2002). The thermal race is the time differential between safety critical components reaching their failure temperatures. The ERB provides electrical protection of critical components and fails when the container is breached. The safety issues are to be studied for abnormal thermal environments where high and medium flux levels are anticipated. Medium heat fluxes are typical of a hydrocarbon fuel fire and high heat fluxes are typical of a propellant fire. (For the W80 system propellant fires are not relevant.)

Thermally induced foam decomposition and recession are rated as a phenomenon of high importance to the system metrics. This means the phenomenon is expected to have a first order effect on application issues of interest. First order importance is implied because foam encapsulates critical components, thus affecting their thermal response and the thermal race. Furthermore, decomposition of foam produces gas, which can pressurize the ERB and result in a thermal-mechanical failure. Since the application ranks thermal issues associated with foam as having high importance, a closely integrated plan of model development, code development, and verification and validation activities exists, Tieszen et al. (2002).

The application requirements are not detailed to the point of providing specific numerical modeling requirements on geometry, environment, etc. In the next sub section we discuss identifying specific application requirements, in particular the expected thermal, pressure, and physical environments. The application requirements on the model are not specific enough to establish required accuracy of the foam model either. As Romero et al. (2000) indicate, the ultimate accuracy needed for an application can be achieved through a non-unique assembly of component models that support the application. Only through application-level studies can we identify feasible sets of requirements (on component models) that can satisfy an application requirement.

2.1 Application Parameter Space

The parameter space of the application can be separated into three categories:

- Thermal environment – abnormal environments are characterized by high temperatures and large heat fluxes.
- Pressure/Confinement – the decomposition of organic foam is known to produce gases, which will pressurize a sealed region and affect the decomposition chemistry.
- Physical attributes – the regions of the weapon that are occupied by foam have a typical thickness and density of foam.

Quantifying the expected range of each category for the application is ideally performed using weapon or component models, experiments, and/or expert elicitation. To define the application parameter space we rely on model studies performed for the W76 in an abnormal environment, Dobranich and Dempsey, (1998), testing/modeling on the W80 fireset, Boucheron (1995), and basic engineering analyses and judgment. In the remainder of this section, we describe these categories in more detail.

2.1.1 Thermal Environment

In an abnormal environment, the incident heat flux is large. The large heat flux causes the temperature of a weapon's outer surface to increase rapidly. A reasonable (nominal) estimate for the surface temperature of a weapon exposed to an engulfing hydrocarbon fuel fire is 1000°C, Boucheron (1995). The temperatures of the internal structures that encase the foam also increase rapidly, Dobranich and Dempsey (1998) and Boucheron (1995), but more slowly than the outer surface of the weapon. In addition, the internal temperatures may have a period of rapid increase, followed by a period of more moderate increase Dobranich and Dempsey (1998).

The foam in a weapon is anticipated to be exposed to a thermal environment that is highly transient and bounded by the maximum temperature of a hydrocarbon fuel fire, 1000°C. The structure of the hardware surrounding the foam and its thermal connection to the weapon's surface will dictate the thermal response the foam "sees." Foam that is near the weapon's outer surface may see approximately a step change in temperature from ambient to 1000°C. Foam that is farther from the weapon's surface will see a more moderate increase in temperature. We estimate that the weapon should have rates of temperature increase in the range of 10s-100s C/min. The temperature will be transient until it reaches the fire temperature.

The foam's temperature cannot exceed that of the surroundings, but its rate of increase in temperature may exceed that of its surroundings. The high temperature surroundings and low thermal diffusivity cause the surface of the foam to heat rapidly and start decomposing. We can estimate the foam's heating rate by knowing the rate of decomposition, thickness of the decomposition front, and temperature differential over the decomposition front. We can get approximate values from the benchmark experiments/model. The thickness of the decomposition front (δ) is 2.0 cm to 0.4 cm and the front recedes at a rate (v) of 0.13 cm/min to 0.56 cm/min, respectively, when exposed to a boundary temperature in the range from 600°C to 1000°C, respectively. The temperature differential across the front (ΔT) is about 500°C, independent of boundary

temperature. We can approximate the rate of temperature increase for the foam specimen as the temperature increase divided by the time required for this increase, Δt. The time required is related to the thickness of the front divided by the front velocity, giving

$$\dot{T} = \frac{\Delta T}{\Delta t} = \frac{\Delta T}{\delta / v}. \qquad (2.1)$$

Applying the numerical values from above discussion gives a rate of temperature increase from 32.5°C/min to 700°C/min, depending on the temperature the foam is exposed to. Note, that this rate of increase is applicable to the foam near the decomposing front and is likely different from the rate of increase for the weapon.

2.1.2 Pressure/Confinement

The application may confine the decomposition products and pressurize the structure encasing the decomposing foam. Whether the structure pressurizes, and to what magnitude, depends on the integrity of the seal and volume of gas produced. If the structure is hermetically sealed, it is anticipated that, even for a moderate amount of decomposition, gasses will pressurize the structure because of the limited amount of free volume. The pressure is expected to continuously increase. The pressure at which the structure will yield is unclear because it could be compromised in several failure modes (material yielding or welded joint yielding). If the structure were not hermetically sealed, or relieves pressure quickly, even though the structure will not pressurize, the decomposition products are expected to be confined in the proximity of the decomposing foam. We anticipate that the decomposition will proceed with the effect of confinement and, at least for a short time, pressurization will occur in the application.

2.1.3 Physical Attributes

Foam fills the gaps between components in the electronics package of the weapon system. The foam provides structural support to critical parts in the electronics package. The package is a reasonably compact assembly densely filled with components. The package is encased in a metallic structure that has little free volume. The voids between the components are estimated to be nominally, 1 to 2 cm. Foam densities in the range 5 lb/ft^3 to 20 lb/ft^3 are anticipated. Higher densities are desired for more structural support, but lower densities may be required to satisfy weight constraints or to reduce stress on fragile components, such as circuit boards.

3.0 Mathematical Models and Code Verification

Before embarking on a validation exercise, the analyst should have evidence to support the accuracy and readiness of the computer code to be used for validation activities. It is not fruitful to compare model results that are not an accurate solution of the mathematical models or affected by bugs in the computer code. Code verification is a process to determine whether a computer code is performing well enough for use in validation activities. As Trucano et al. (2002) point out, this involves verifying the code as a product and assessing the numerical accuracy of mathematical models/algorithms in the code. We rely on the code development team, Calore (2002), to provide the evidence supporting readiness of code through the verification plan, performance testing, version control, programming practices, and math model verification.

In this section we describe the mathematical models solved in the computational code Calore. We summarize and reference data supporting code activities that document the code's readiness for validation. In support of the validation readiness we identified and conducted a suite of verification problems to assess math model/algorithms needed for the code application validation. Results from verification problems we studied are summarized at the end of this section.

3.1 Description of Code (Calore)

We are validating the application of a computational model to the physical process of thermal decomposition of foam. The computer code Calore (Bova et al.) formulates and solves the computational model. Calore is a computer program (code) that numerically solves the energy equation based on a finite element discretization. Calore can couple the energy equation with chemical kinetics and radiation transport. A (modified) version of CHEMEQ (Young) is a subroutine in Calore for solving the equations associated with chemical kinetics. The independent program Chaparral, Glass (1995), is linked with Calore and provides viewfactors and the radiosity solution.

Calore has been developed in the SIERRA framework, Edwards et al. (2002), and software development is managed using the SIERRA code management system (SCMS). The framework provides an object-oriented software architecture and set of services to support general applications. The SCMS provides tools to create, modify, test, and version control software. Calore relies on SIERRA support services to manage and test the software.

The SCMS has the capability to run a suite of tests on a regular basis. These tests are referred to as regression tests. The objective of regression testing is to ensure that the solution for a given problem does not change during the evolving implementation status of code development. Calore has a collection of 81 regression tests that are run on a nightly basis. The regression test suite collectively covers capability that has been implemented in Calore. Periodically, the amount of code functionality covered by regression tests can be quantified; recent numbers indicate ~85 percent coverage (of

Calore code) by the current regression test suite. The outcome of the nightly regression testing is compiled on the Calore web site.

The verification plan, Bova et al. (2002), describes activities to support mathematical model/algorithm verification in Calore. The plan details using unit testing of operators and analytical solution (exact and "manufactured") of model equations to address verification. Planned verification problems are identified to provide coverage of the mathematical models/algorithms in Calore. Since model verification of Calore is just beginning, we identified the math models needed for the validation activities and identified verification problems. We discuss this verification work next.

3.2 Summary of Mathematical Models

The mathematical equations required for modeling the validation experiments are summarized in this subsection. Mathematical equations for thermal diffusion, chemical kinetics, and radiation transport are included, Gartling et al. (1994). In addition, the removal of material due to thermal effects is modeled with a process called "element death." The mathematical equations and processes are discussed next.

3.2.1 Thermal Diffusion

Based on conservation of energy and Fourier's law a partial differential equation describing thermal diffusion within a solid can be derived

$$\nabla(k\nabla T) + Q_c = \rho c \frac{\partial T}{\partial t} \qquad (3.1)$$

where, temperature is T, thermal conductivity is given by k, density by ρ, specific heat by c, and t is time. The volumetric energy term, Q_c, accounts for the energy associated with chemical kinetics. The energy due to radiation transport is coupled to thermal diffusion through (flux) boundary conditions. Separate, coupled mathematical equations describe chemical kinetics and radiation transport.

3.2.2 Chemical Kinetics

A set of equations describe the allowable chemical reactions for J reactions and I species

$$\sum_{i=1}^{I} \nu'_{ij} M_i \rightarrow \sum_{i}^{I} \nu''_{ij} M_i \quad j = 1,...,J\,. \qquad (3.2)$$

In Eq. (3.2) ν''_{ij}, ν'_{ij} are stoichiometric coefficients and M_i is the chemical symbol for species i. Each reaction proceeds at rate given by

$$r_j = k_j(T) \prod_i [N_i]^{\mu_{ij}} \quad j = 1,...,J \qquad (3.3)$$

where N_i is the concentration of species i and μ_{ij} is the concentration exponent. The kinetic coefficient is expressed in Arrhenius form

$$k_j = A_j \exp\left(\frac{-E_j}{RT}\right) \tag{3.4}$$

where A_j is the pre-exponential factor, E_j is the activation energy, T is the temperature (from thermal diffusion) and universal gas constant is R. The rate of change in concentration for each species is written as

$$\frac{d}{dt}[N_i] = \sum_i (\nu''_{ij} - \nu'_{ij}) r_j \quad i = 1,...,I. \tag{3.5}$$

The chemical reaction process is coupled to thermal diffusion through a volumetric energy term

$$Q_c = \sum_j r_j q_j \tag{3.6}$$

where q_j is the energy change due to reaction j.

3.2.3 Radiation Transport

Exchange of energy by radiation between N surfaces defining an enclosure is described by

$$\sum_{j=1}^{N}\left[\frac{\delta_{kj}}{\varepsilon_j} - F_{k-j}\left(\frac{1-\varepsilon_j}{\varepsilon_j}\right)\right]\frac{Q_j}{A_j} = \sum_{j=1}^{N}\left(\delta_{kj} - F_{k-j}\right)\sigma T_j^4 \tag{3.7}$$

The net energy loss from a surface, Q_j, is related to the surface temperature, T_j, of each surface in an enclosure through Eq. (3.7). Surface area is A_j, emissivity is ε_j, and σ is the Stefan-Boltzmann constant. The view factor, F_{k-j}, is the fraction of energy leaving surface k that arrives at a second surface j. These equations are coupled to thermal diffusion through the net flux on a surface. Because these equations have a nonlinear dependence on temperature, a "lagged" algorithm is used to couple the radiation and thermal diffusion to simplify the numerical treatment, Gartling et al. (1994).

3.2.4 "Element Death"

When heated, the foam undergoes chemical kinetics that result in the (solid) structure transitioning to various gas, liquid, and solid decomposition products, Hobbs et al. (2003). If heated long enough, the foam will fully decompose to gas products. A simple approach to modeling this complex physical process is to adjust the material domain of the computational model based on the solid fraction of condensed material.

This can be implemented in a finite element code by removing elements that define the foam material in the thermal diffusion model once the mass from the chemical kinetics is below a specified value. This process is called "element death," and is an engineering model to account for material removal in a thermal diffusion code.

3.3 Verification of the Mathematical Models

The coupled mathematical equations of thermal diffusion, chemical kinetics, and radiation transport constitute the mathematical model (with appropriate boundary initial conditions and solution/coupling algorithms) that is addressed in this validation activity. We need to assess code verification status for the math model required. Because the mathematical model is too complex to generate a single solution that couples all three equations, we use problems that can address specific math equations independently, or as coupled subsets of equations, and are amenable to analytical solution. With this approach, we can define a verification test suite (VERTS) to address verification status of the math model.

3.3.1 VERTS Problems (Requirements)

A minimal set of problems is identified to address verification of the mathematical equations solved in Calore that are needed for simulating the validation experiments. The approach taken is to verify the solution of the mathematical equations separately, then coupled, when it is possible to get an analytical solution. The Problem suite is summarized in Table 3.1. Cases 1-3 address the math equations for thermal diffusion covering linear steady, linear transient, and nonlinear transient. Case 4 covers the chemical kinetics solution and Case 5 addresses coupled chemistry and diffusion. The 3rd party library, Chaparral, is verified with Case 6. Cases 7 and 8 were to verify coupling thermal diffusion and radiation transport and coupled diffusion, chemistry and element death. However, solutions for these complex problems were not obtained as part of this activity but are being pursued as part of follow on activities.

3.3.2 Summary of Code Verification Results

The results for the verification studies are documented on the Calore web page (http://www.engsci.sandia.gov/calore/verification/model_eqns/index.html). The approach taken was to compare an analytical solution for the given mathematical equations with the numerical solution from Calore to quantify the discretization error. The dependence of the error on discretization parameters was studied using local and/or global error measures, Copps and Stewart (2002). We note that verification problems for cases 1 through 6 have been studied with Calore. A catalog of documentation of the verification results is provided in the last column of Table 3.1. A problem has been identified for case 6 and analysis had been initiated. Problems for cases 7 and 8 are in progress. Results from a representative example verification problem are discussed in the following subsection.

Table 3.1 VERTS problems

Case	Mathematical Model	Description	Independent Solution	Reference
1	Thermal Diffusion (steady)	Radial heat flow in a cylinder and sphere with temperature BCs 2D heat flow with volumetric energy and mixture of Temperature, Flux, and Convective BCs	Exact Analytical	Blackwell (2002A,B) Blackwell (2002C) and Dowding (2002A)
2	Thermal Diffusion (transient)	1D heat flow with flux BC, other surface adiabatic	Exact Analytical	Blackwell (2002D)
3	Nonlinear Thermal Diffusion (transient)	1D heat flow, linear *k(T)* variation, constant c, non uniform IC and transient flux BCs	Exact Analytical	McMasters et al. (2002)
4	Chemistry	2-step reaction, isothermal	Exact Analytical	Dowding (2002B)
5	Thermal Diffusion and Chemistry	1-step reaction, non uniform (spatial) temperature	Manufactured Analytical	Zoeller and Voth (1999)
6	Enclosure Radiation (3rd Party Library)	Radiation exchange inside a hollow parallelepiped	Exact Analytical	
7	Thermal Diffusion and Radiation	N/A		
8	Thermal Diffusion and Chemistry with Element Death	N/A		

3.3.3 Verification Results for Steady-State Thermal Diffusion

The solution for steady diffusion in a two-dimensional region with a 2x1 aspect ratio is studied. The boundary conditions on the 2D region are as follows.

left face: specified heat flux of 3500 W/m^2

top face: convection with h = 60 $W/m^{2o}C$ and T_c = 25 °C

right face: isothermal, T = 1000 °C

bottom face: adiabatic

Material properties and geometry are as follows: k = 0.4 W/m-K, L_x = 0.1 m, L_y = 0.05 and L_z = 0.005 m. The volumetric source term is 1.353×10^5 W/m^3.

The coarsest three-dimensional finite element model of the region has 10 elements in the x-direction, 10 elements in the y-direction and a single element in the z-direction. (Note that the problem has 2D heat flow, but is solved in 3D, but there are no temperature gradient in the z-direction and only a single element in that direction.) We study the dependence on discretization by successively doubling the number of elements in x and y directions; we study solutions with 100, 400, 800, and 1600 total elements.

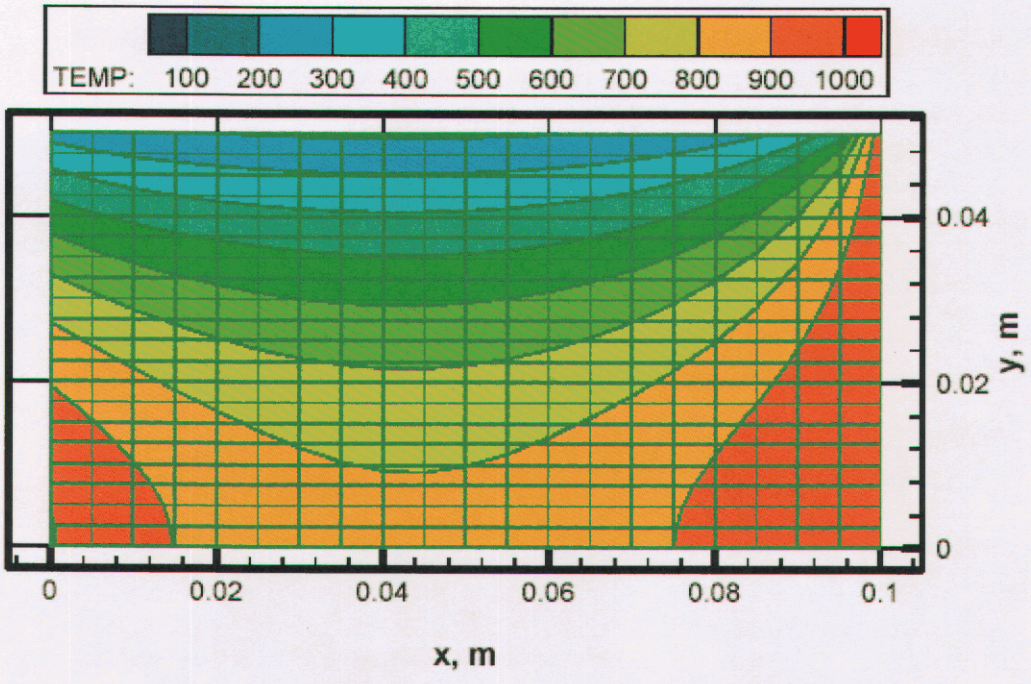

Figure 3.1 Temperature contours for steady diffusion verification problem, contour levels are in degrees C

The temperature contours for the Calore solution to this problem are given in Figure 3.1 for a solution using 400 (20x20x1) elements. The heat transfer is into the body through the left and right faces and out through the top. The largest regions of high temperature occur along the left and right faces.

The analytical solution for this problem was evaluated using the Cond3d code developed by Beck, et al. of Michigan State University. Using the numerical evaluation of the analytical solution as truth, errors in the Calore solution were computed. Error at specific locations in the body, local error, and error integrated over the spatial domain, global error, is studied.

The Calore (local) error results at the lower left (x=0, y=0) and upper left (x=0, y=.05) corners are shown in Fig 3.2. Results for all four grids are presented. For the lower left hand corner, the Calore results follow the 2nd order grid convergence line very closely. For the upper left hand corner where the temperature gradients are much steeper, the errors are larger in magnitude and the order of convergence is variable and less than 2. It is speculated that the lack of 2nd order convergence results are due to the steep temperature gradients in the upper left hand corner; this hypothesis is still under investigation. For comparison purposes, numerical results were also computed using a separate finite volume code called FCV. The Calore and FCV grid convergence results are nominally parallel with the Calore results having smaller errors.

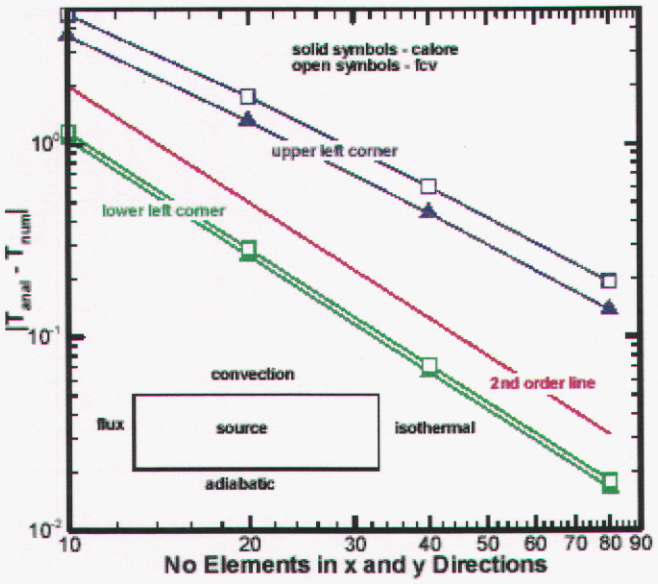

Figure 3.2 **Local grid convergence results**

Three error norms/seminorms are studied to quantify the difference between the analytical solution, T, and the approximate finite element solution, T^N. The first norm is based on the maximum error in the spatial domain of the solution

$$L_\infty = \max[T(x,y) - T^N(x,y)] \tag{3.8}$$

The second error norm integrates the squared differences in temperature over the domain

$$H_0 \equiv \left\{ \int_\Omega [T(x,y) - T^N(x,y)]^2 \, d\Omega \right\}^{1/2} \tag{3.9}$$

which is commonly called the "L-two" norm. The third error is a seminorm that involves the first derivative of the solution integrated over the domain

$$H_1 \equiv \left\{ \int_\Omega \left[\sum_{i=1}^{2} \left(\frac{\partial T(x,y)}{\partial x_i} - \frac{\partial T^N(x,y)}{\partial x_i} \right) \right]^2 d\Omega \right\}^{1/2} \tag{3.10}$$

Convergence of the finite element solution, as the mesh is refined spatially, is studied in these error measures.

The error norms for the four levels of mesh refinement are listed in Table 3.2 and plotted in Fig 3.3. A linear fit (on log-log scale) of the error as a function of mesh size is given at the bottom of Table 3.2. The convergence rate (slope) of the error is -1.74/-1.68 for H_0, -0.73/-0.71 for H_1, using a 2 pt/4 pt scheme (in each direction), respectively, to numerically integrate the norms, and 0.93 for L_∞.

Table 3.2 Error norms

num of elements		h		H_0 (°C)		H_1 (°C/m)		L_∞ (°C)
x	y	x	y	2 pt	4 pt	4 pt	2 pt	70.50
10	10	.01	.005	.0365	.0396	17.15	19.12	39.46
20	20	.005	.0025	.0115	.0127	10.84	12.01	20.50
40	40	.0025	.00125	.0034	.0038	6.519	7.130	10.27
80	80	.00125	.000625	.0010		3.767		2.79
			p	-1.74	-1.68	-0.73	-0.71	-0.93
			C	0.32	0.286	1.97	2.00	2.79

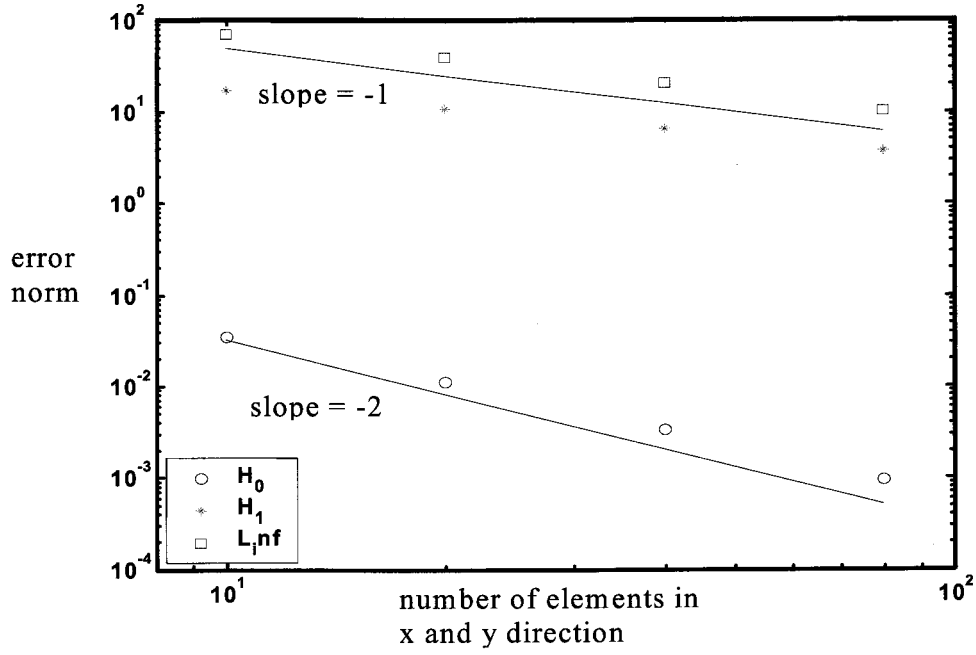

Figure 3.3 Convergence of error norms as the mesh is refined

The approximate error for a linear finite element solution can be derived [1] as

$$\|e\|_m = c' h^{s+1-m} \|T\|_{s+1} \qquad (3.11)$$

where c' is a constant (independent of h and T), h is the characteristic length of an element, s is the degree of polynomial in the finite element shape function, m is the order of the highest derivative appearing in the norm/seminorm expression. In Eq. (4) we have assumed the analytical solution T is sufficiently smooth, meaning the analytical solution has bound derivatives up to (at least) $s+1$. Linear elements are used for the analysis, i.e., $s = 1$, and the analytical solution, though having discontinuous derivatives at the corner, has bound second derivatives ($s+1$), meaning Eq. (3.11) can be rewritten as

$$\|e\|_m = Ch^{2-m} \qquad (3.12)$$

Hence, we expect second order ($1/n^2$) convergence for H_0, first order ($1/n$) convergence for H_1, and ($1/n^2 \log(1/n)$) dependence for L_∞ norm.

The discretization error (Table 3.2) does not converge at the theoretically expected rate, Eq. (3.12); H_0 decreases at a rate of 1.7 (2 is expected) and H_1 at a rate of 0.7 (1 is expected). The explanation for not obtaining the expected convergence rate may be the discontinuous gradient in temperature in the upper right corner of the domain. The contribution from the single element in this upper right corner to the H_0 norm is 82, 79, 90, and 65 percent, for the four mesh refinements studied. This issue is under further study, but does not appear to be a code issue.

4.0 Experiment Design and Execution

4.1 Description of Experimental Activities

Experimental data from two activities support assessing the model for thermal decomposition of polyurethane foam. The first activity collects data using a thermal gravimetric analyzer (TGA). This apparatus controls the thermal environment while monitoring mass and decomposition gas products. The second activity uses radiant heating to control the temperature of one end of a cylindrical can that is filled with foam. X-ray imagery monitors the location of the decomposing front within the can.

The experimental activities in this study follow a paradigm that is common in engineering. Math modelers and experimentalists cooperate to identify pertinent physical processes and an approach to modeling them using a well-controlled experiment (TGA). During the process, parameters in the math models may be calibrated with the experimental data. These experiments are typically well-characterized single physics experiments, Tier 1 in Trucano et al. (2002). In this application, after attaining an acceptable level of confidence in the math model through comparison with experimental data and possibly some calibration, a second set of experiments is conducted. These second experiments assess the math model in a predictive sense, with no further calibration. A simple coupling of physics, Tier 2, Trucano, et al. (2002) often exists in the second experiment. In this application, the second set of experiments is the radiant heating foam-in-a-can experiments, which we refer to as benchmark experiments.

In the remainder of this section, we summarize the experimental activities including the experimental design and execution. The analysis of the experiments (using the computational model) is presented in Section 5.0.

4.2 TGA (Tier 1, simple physics, some calibration)

A schematic of a TGA apparatus is shown in Fig 4.1. A small foam sample (1-20 mg) is loaded in the apparatus. The temperature of the reaction gas is measured and controlled. (It is assumed that the gas temperature is equal to the sample temperature.) In conjunction with measuring gas temperature, a microbalance measures sample weight/mass. These measurements provide the relationship between sample mass and temperature. Additionally, the gases that evolve during the decomposition are analyzed with Fourier Transform Infrared (FTIR) spectroscopy.

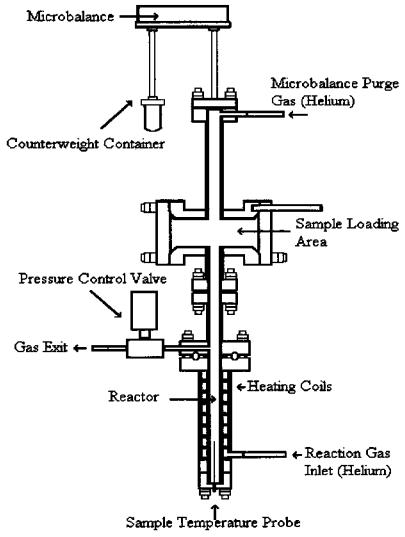

Figure 4.1 Schematic of TGA apparatus

Experiments were conducted on two different TGA apparatuses. Experiments at ambient pressure were conducted at SNL, Erickson, et al. (1999) Experiments at pressures greater than ambient were conducted at BYU, Clayton (2002). A series of ambient pressure experiments were also performed at BYU for lab-to-lab comparison.

4.2.1 Experimental Design (Test Plan)

The following factors were studied using the TGA apparatus, Erickson et al. (1999) and Clayton, (2002).

- Temperature environment
  - Ramp rate – temperature ramped continuously throughout the experiment at rates of 5, 20, and 50 °C/min
  - Isothermal – temperature ramped at 20 °C/min and then held at a constant value of 250, 270, and 300 °C
  - Dual-Isothermal – temperature ramped at 20 °C/min and held at constant temperature of 300 °C until mass stabilizes then ramped at 20 °C/min to a higher temperature and held at 400 °C
- Constant pressure (1 atm, 5 atm, 10 atm, 30 atm, and 70 atm)
- Miscellaneous
  - Sample configuration (mass, shape)
  - Purge gas (Ne or He and flow rate)
  - Density (high, low)

On the order of one hundred TGA experiments were performed. After eliminating the miscellaneous experiments, which were "shake-out" experiments, we are left with a

set of experiments that study the effect of temperature, pressure, and laboratory. For our purposes, further restrict these data to experiments conducted with a sample size in the range 4-6 mg to minimize the dependence on sample size. We utilized data for approximately 50 experiments, which are shown in Figure 4.2. The data plotted are solid fraction, $s_f = m/m_o$ as a function of time (isothermal experiments) or temperature (continuously ramped experiments).

The goal, at least initially, of these experiments was physics exploration and model development, rather than dedicated validation. With this goal, a detailed experimental design and mapping to the application parameter space (discussed in Section 2) were not of first importance. These data did provide a physical understanding and raw data to build a model. The test matrix for the TGA experiments is shown in Table 4.1.

Table 4.1 Test matrix for TGA Experiments

Thermal Environment	Temp (°C) / Temp rate (°C/min)	Pressure (atm)					
		1	5	10	30	50	70
Isothermal	250	3-SNL					
Isothermal	270	3-SNL					
Isothermal	300	3-SNL					
Dual Isothermal	300/400	2-SNL 4-BYU		1-BYU			
Ramp	5	1-SNL					
Ramp	20	14-SNL 4-BYU	8-BYU	6-BYU	5-BYU	1-BYU	1-BYU
Ramp	50	1-SNL					

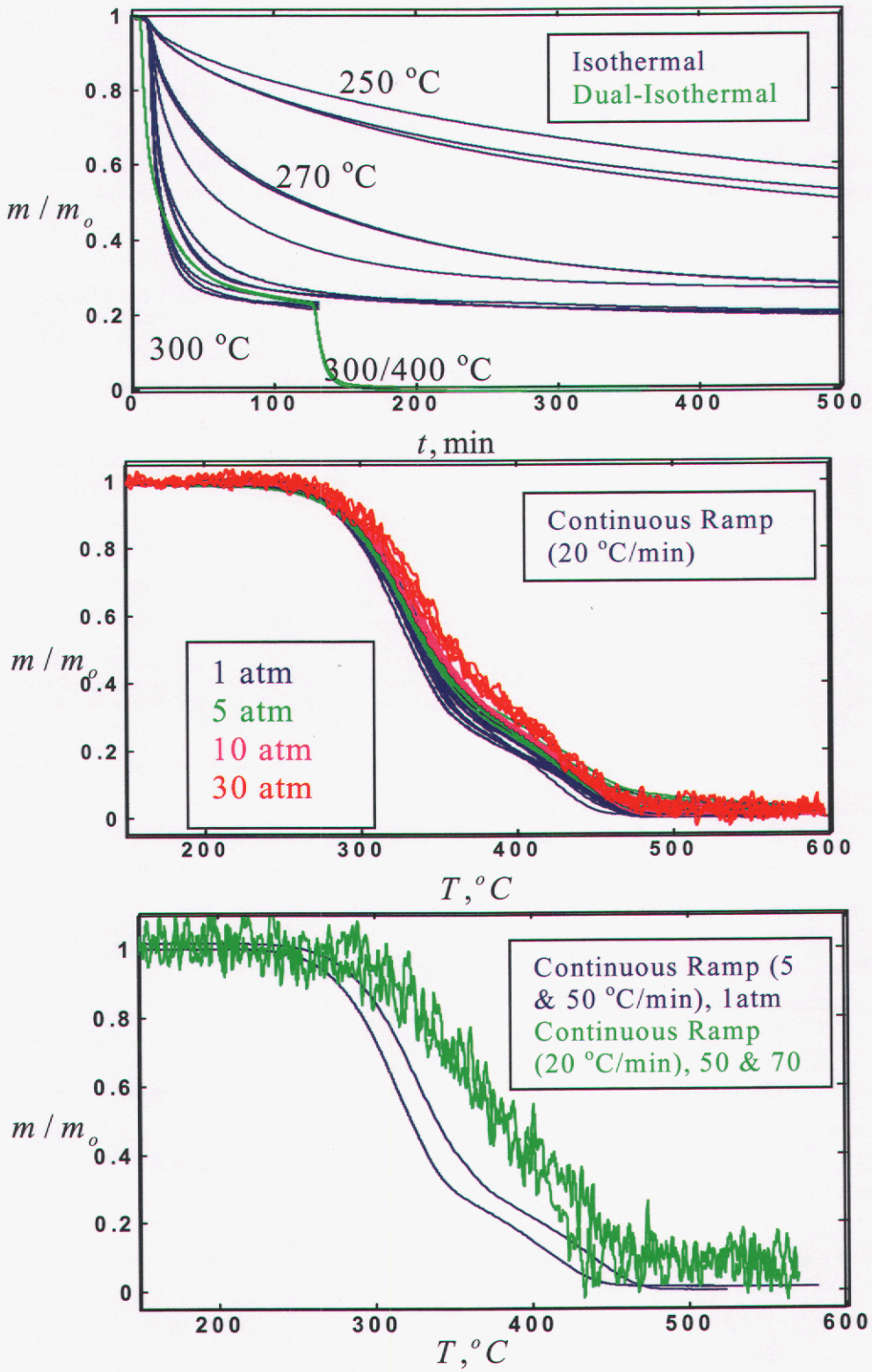

Figure 4.2 **Data from TGA experiments**

4.2.3 Mapping to the Application Parameter Space

The application parameter space was discussed in Section 2. In this subsection, we discuss how the parameter space investigated in the validation experiments relates to the application parameter space.

TGA experiments investigate the effects of temperature and pressure on thermal decomposition of foam. (The samples are made sufficiently small (4-6 mg) to neglect dependence on physical dimensions.) The thermal environment is ramped at 20°C/min for all but two of the experiments; these two experiments were ramped at 5 and 50°C/min. In some experiments, the temperature is ramped to a specified temperature value and then held constant. Experiments were conducted for pressures from ambient to 30 atm; two experiments at 50 and 70 atm were also run. See Table 4.1.

We estimate the rate of temperature increase for the foam (not the weapon) to be in the range 30-700°C/min for the application. Rates outside of this range, 20°C/min, were used in all but one of the TGA experiments. This means we are extrapolating the TGA experiments to the application parameter space. While we would prefer to interpolate from the validation experiments to the application parameter space, in this situation there are experimental concerns that require running the experiments outside the application parameter space. Though the apparatus can support higher heating rates, conducting experiments at high rates can result in the low diffusivity foam not being isothermal and interpreting the experimental data is considerably more difficult. Also, the heating rate must be high enough to produce decomposition products at sufficient rate to be detectable by the chemical analyses instrument (FTIR).

Although we anticipate pressurization in the application, the magnitude of pressure in the application is uncertain. Validation experiments (TGA) cover a pressure range from ambient to 70 atm, but only one experiment was conducted at 50 and 70 atm. Taking into account that the structure enclosing the foam is at high temperature, and the physical dimensions of the structure, we estimate pressures on the order of 10s of atmospheres could reasonably be expected. Because the TGA experiments covered the range from ambient to 30 atm, we expect to be within the application parameter space.

The effect of confining the gases produced by the decomposition, although anticipated to exist in the application, was not part of the validation data. TGA experiments have been run to study the effect of confinement and further analyses are on-going.

4.2.4 Measurement Uncertainty

TGA experiments provide measurements of temperature and mass as a function of time. Temperature is measured with a thermocouple probe that is inserted in close proximity to the sample in the gas flowing over the sample (Fig. 4.1). There are measurement errors due to the experimental sampling process. In addition, there may be a bias introduced by assuming the probe's temperature equals the sample temperature. Because the sample has a low thermal diffusivity, spatial thermal gradients could exist in

the sample, which this type of probe would not reflect. Independent quantitative estimates of the sampling and bias error are not available for the temperature measurement. We will use the experimental data to estimate the measurement error in mass. An estimate of measurement error is necessary for validation.

We can estimate measurement error for mass by analyzing the experiment before the decomposition begins. A plot of the experimentally measured solid fraction between 65°C and 75°C is shown in Figure 4.3 for the 18 experiments at ambient pressure. In this temperature range, thermal decomposition of the foam is almost negligible. Notice that the solid fraction for most experiments changes less than 0.001 between 65°C and 75°C. The four experiments conducted at BYU are the curves that demonstrate more variability over the temperature range. Variability from experiment-to-experiment is seen to be larger than the variability within an experiment. The mean value of solid fraction over the temperature range is plotted for each experiment in Figure 4.3. These data represents the error in our ability to measure a mass fraction equal to 1. The variability between experiments is $(0.00125)^2$. Assuming the errors are normally distributed, we would expect with 0.95 probability that future errors be within two standard deviations of the mean mass measurement, or 0.0025. Because the estimates are based on data when the experiment is essentially static, we expect larger errors during the dynamic response. Nevertheless, a quantitative lower bound is better than pure speculation.

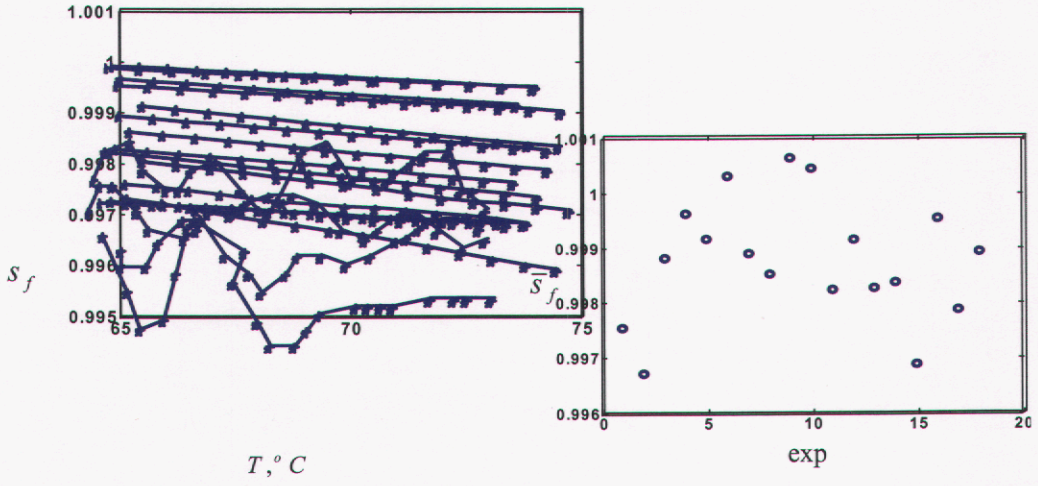

Figure 4.3 **Error in solid fraction measurement**

4.3 Benchmark (Tier 2, simplest coupling, validation)

A schematic diagram of the experimental setup is shown in Fig. 4.4. All the experimental setups included a polyurethane foam cylinder partially contained in a thin walled stainless steel sample cup. The foam cylinder was 8.8 cm in diameter and 14.6 cm long. The stainless steel cup consisted of a 0.5 mm thick walled cylinder 7.3 cm long. A 6 mm thick disk was press fit at one end. The inside diameter was closely matched to the foam cylinder. For some of the experiments, a solid stainless steel cylinder or hollow aluminum cylinder was embedded within the polyurethane foam to simulate a protected component. Heating of the foam was accomplished with an array of heat lamps. The relatively thick cup base results in uniform heating of the foam. Thermocouple measurements provide the temperature at boundaries, which are used for the model heat transfer calculations.

Shown in Fig 4.5 are the approximate locations of the vent holes and the thermocouples. Representative time history traces of temperature are also shown. The top three curves labeled '0' are from the 6 mm stainless steel plate (cup base). The remaining six traces are the side wall temperatures for the 600°C plate temperature experiment.

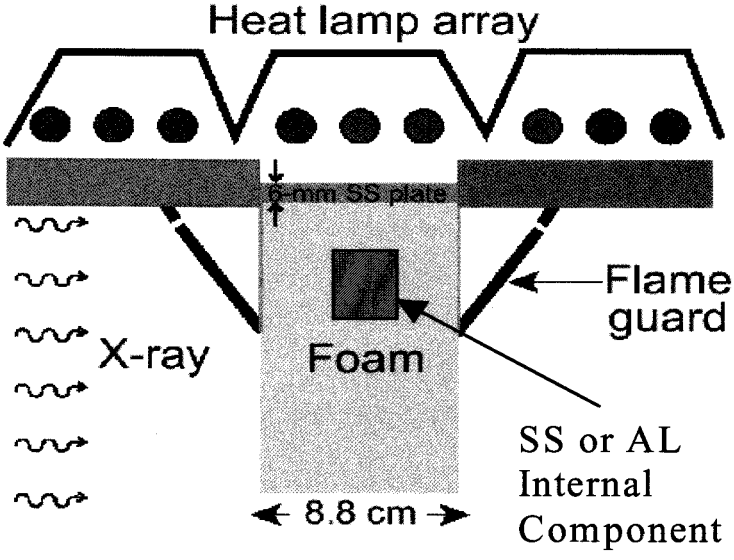

Figure 4.4 **Schematic diagram of foam heating apparatus in "top" configuration (Hobbs, 2003).**

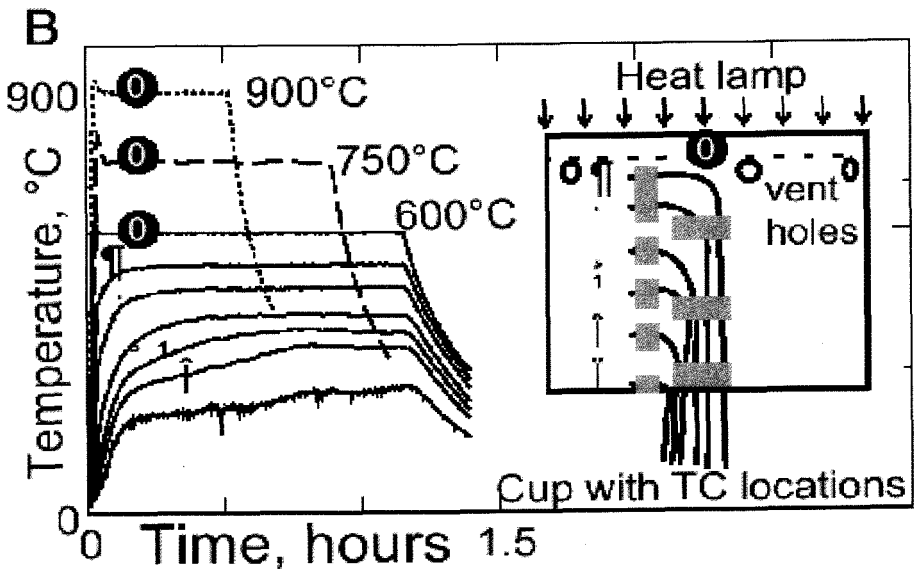

Figure 4.5 **Representative temperature history used as boundary conditions in the model calcuations.** Vent holes and thermocouple locations are also shown. (Hobbs et al., 2003)

4.3.1 Experimental Measurements

There were 16 scale-up experiments run at ambient pressure that included different configurations, orientations, and thermal boundary conditions, Bentz and Pantuso (1999). Of these 16 experiments, 14 were considered viable; a summary of these experiments is given in Table 4.2.

Table 4.2 Foam-in-can scale-up experiments

Experiment No.	Density (lb/ft^3)	Cup Plate Temperature (°C)	Orientation of Cup Plate	Component
1	22.7	600	Bottom	None
2	22.7	750	Bottom	None
5	22.7	750	Bottom	Stainless Steel
6	5.7	600	Bottom	None
7	5.7	900	Bottom	None
8	5.7	750	Bottom	Aluminum
9	5.7	750	Bottom	Stainless Steel
10	22.7	750	Top	None
11	22.7	750	Side	None
12	5.7	750	Side	None
13	22.7	750	Side	None
14	22.7	900	Bottom	None
15	22.7	750	Bottom	Aluminum
16	22.7	1000	Bottom	Stainless Steel

In addition to the temperature measurements shown in Fig. 4.5, X-rays were used to track the front location of the decomposing polyurethane. An example of the X-ray images from experiment number 2 (750 C bottom heated) is shown in Fig 4.6. The images show that the front has receded (approximately) 1.1, 2.2, and 4.0 cm.

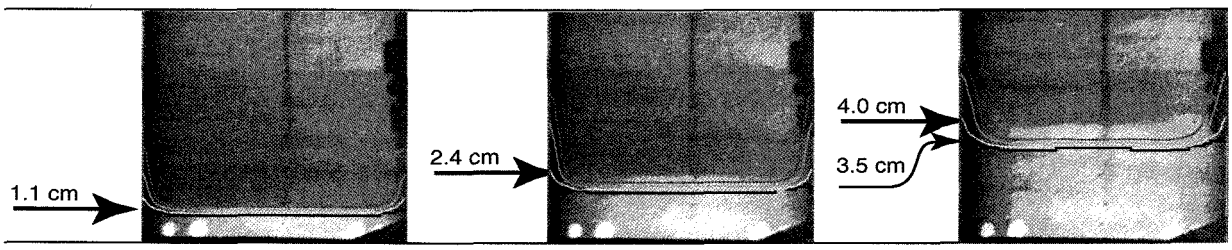

Figure 4.6 **X-ray images of front location of decomposing foam front.** Model results are overlaid on the X-ray (Hobbs et al., 2003)

For validation purposes, a quantitative comparison of the experimental results with the model is needed. To obtain quantitative information the X-ray images were digitized and the location of the decomposing front was tracked. Distance from the heated plate to the front provides a quantitative measure that can be extracted from the X-ray. With time-resolved images we can determine front location as a function of time. Typical data are shown in Figure 4.7 and numerical data are listed in Table B.1 through B.9 in Appendix B.

Of the 14 viable experiments, the X-ray diagnostic was not sensitive enough to clearly identify a front location for the five experiments that were run with a low-density foam sample. It is important to consider the fidelity of the diagnostic. Because we cannot quantify the experiments run at low density, the number of experiments available for validation is reduced to nine, all at the high density; this precludes assessing the effect of density.

In addition to thermocouples in the heated plate and attached to the outer surface of the plate, thermocouples were inserted into foam. These thermocouples were inserted from the outer radius towards the center of the cylindrical foam specimens and spaced along the length of the foam cylinder. Even though the X-ray images could be used to locate the thermocouples after installation, uncertainty in the location and movement of the thermocouple as the decomposition front approaches, made it impossible to use the measurements for quantitative comparison. There is also the potential for significant measurement bias when thermocouples are inserted into low diffusivity materials. Even if the thermocouples had not moved, uncertainty in the location may have outweighed the information content of the measurement.

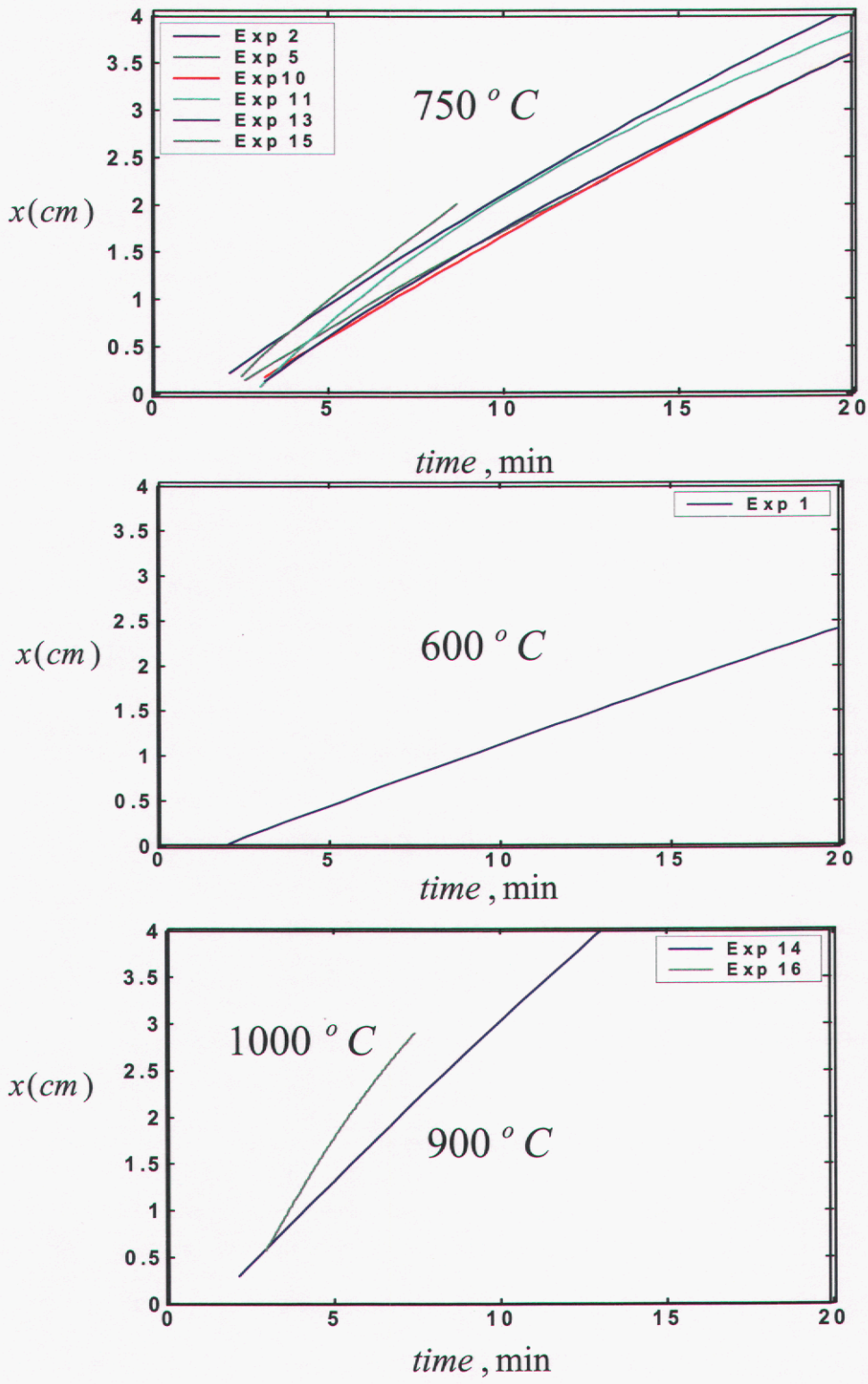

Figure 4.7 **Validation data from the benchmark experiments**

4.3.3 Experimental Design (Test Plan)

The test matrix for the benchmark validation experiments is discussed in this section. There are four factors (X), studied in the experiments:

1. Temperature of the cup's end surface (600, 750, 900, 1000°C)
2. Orientation of the heated surface relative to gravity (bottom, side, top)
3. Density of the foam (High-22.7 lb/ft^3, low-5.7 lb/ft^3)
4. Internal component (0-none, S-stainless steel slug, A-aluminum-shell)

The first factor is the constant temperature maintained on the end surface of the cup containing the foam. This factor prescribes the thermal environment that the foam "sees." Three temperature magnitudes were studied. (There is, approximately, a 1.5 min transient during which the temperature is ramped to the steady value.) The second factor is the orientation of the cup's heated surface relative to gravity. A flat end surface of the cup (cylinder) was always heated. This end surface was the bottom surface (vertical cylinder orientation), side surface (horizontal cylinder orientation), or top surface (vertical cylinder orientation). The third factor is the density of the foam. Two densities were studied. The fourth factor was whether the foam contained an embedded component. The test matrix to study these four factors is shown in the Table 4.3.

Table 4.3 Experimental test matrix for CPUF, O-No internal component, S-stainless steel internal component, A-aluminum internal component

high density foam (22.7lb/ft^3), low density foam (5.7lb/ft^3)

Boundary Temperature, °C	Top	Side	Bottom
1000	-	-	S
900	-	-	O O
750	O	OO O	O, S, A S, A
600	-	-	O O
	Top	Side	Bottom
	Orientation		

As Table 4.3 shows, most experiments are conducted with a cup temperature equal to 750°C and heating orientation from the bottom. All the experiments satisfy at least one of these two conditions. We have replicate experiments for 750°C side-heating orientation. In addition, the multiple experiments at 750°C bottom heated with and without internal components are replicates up to the time that the foam front reaches the internal component.

This is a "classic" one-factor-at-a-time (OFAT) experimental design in which all but one factor is held fixed while one factor is varied, sequentially, across a set of factors. In Table 4.3, the base condition is 750°C, bottom heating, from which we vertically consider other temperatures, then, horizontally other orientations. Unfortunately, this design is an inefficient way to evaluate the effects of multiple factors. The only true replicate is the 750°C-side heating orientation.

One way to build on the existing experimental results is to run experiments at the six untested combinations of temperature and orientation in Table 4.3. By less than a doubling of the existing number of experiments provides information about the effects of temperature and orientation on decomposition-front characteristics would increase substantially. For example, instead of having only two experiments by which to evaluate the difference between 600°C and 900°C there would be six, three at each temperature. Under the assumption that the effects of temperature and orientation (on the model and experiment) are linear, this set of 15 experiments would also provide a means of checking the linear assumption.

4.3.4 Mapping to the Application Parameter Space

In the application, we estimate that a weapon in an abnormal environment will respond transiently to a radiant environment at 1000°C, increasing at rates from 10-100°C/min depending on location within the weapon. The thermal environment for the benchmark experiments are ramped at rates of 300 to 500°C/min to temperatures of 600°C to 1000°C and then held at a constant temperature. The rate of increase studied in the validation experiments would appear to be at the upper level of that anticipated in the application. The application is not expected to attain a constant temperature until it reaches the fire temperature (1000°C). However, depending on the location in the weapon, after an initial ramp, the temperature will have a more moderate ramp to the fire temperature. Approximating the secondary ramp by holding the temperature fixed at levels bounding the range covered by the ramp seems reasonable.

Benchmark experiments were conducted such that up to 10 cm of foam was decomposed. In the application, we don't expect that the foam will exceed 5 cm and a nominal thickness would be 2 cm. Data of greater interest for the application would be the decomposition over the first couple of centimeters.

The effect of confining the gases produced by the decomposition, although anticipated to exist in the application, has not been studied. Experiments have been run to

study the effect of confinement (and pressure) but quantitative comparisons with the model have not been performed.

4.3.5 Experimental Uncertainty (Measurement)

Diagnostics for the benchmark experiment include time-resolved X-ray imagery and transient thermocouple measurements. Quantitative assessment of the random and bias errors associated with the measurements is not available. We discuss the potential impact of error in the measurement next.

The measured temperatures along the cylindrical sides and flat ends of the can are used as boundary conditions for the model. We expect that errors in the measured temperature along the side are not significant in the model. Errors in the measured end-plate temperature, particularly the heated plate, are likely to be significant because the measurement is the "driving" force in the model. During the analysis while comparing the experiment and model results it became clear that the measured temperature of the heated end-plate could have a significant impact on the comparison with experiments. The temperature was measured at two locations across the thickness of the 3.5 inch diameter, 0.25 inch thick plate. Although we had no quantitative estimate of the uncertainty in the measured temperature, plausible magnitudes of the uncertainty in the measurement were shown to have a significant effect on the model. This point is discussed further in Section 7.2.5.

We expect errors associated with the X-ray images due to resolution issues. The X-ray images have finite resolution and "smear" objects or features that are smaller than the minimum resolution. The manufacturer of the X-ray equipment could identify the minimum resolution. Possibly more important is the use of the digitized, time resolved X-ray images to extract front location as a function of time. The distance the front has moved is calculated by comparing the front location to a reference. The end plate of the can is selected as the reference. Relative misalignment between the can and X-ray field could bias the front location measurement.

5.0 Experiment Analysis (Model Results)

Details of the process to generate model results are presented in this section. We describe how the TGA data was used for calibrating activation energies in CPUF using a set of 18 experiments. Model results were calculated using a mean set of the activation energies and uncertainty quantified from statistics of the calibration. Then the computational model results for the benchmark experiments are discussed, including the process to estimate the effect of model input uncertainty. Finally, we discuss verification of the solution.

5.1 CPUF Model Calibration and Results

5.1.1 Model Calibration

CPUF includes 15 population species and 16 reactions, Hobbs et al. (2003). Each of these reactions has associated with it two Arrhenius factors, A_j and E_j. All the pre exponential factors, A_j, were set to a value of 3.0 x 10^{15} s^{-1}. There is a high degree of correlation between the A_j and E_j. Thus, with minor loss in fitting accuracy to the TGA results, the optimization procedure described below was more tractable. The extent of reaction is based on the population of adipate bridges found in the most probable structural unit of the polyurethane foam. The revised Arrhenius expression is:

$$k_j(T) = A_j \exp\left(E_j + \xi \sigma_E / RT\right) \tag{5.1}$$

where σ_E is the standard deviation of the activation energy and ξ is related to the adipate bridge population as given in Eq. (5.2)

$$\Phi(\xi) = 1 - \frac{L}{L_0} = \int_{-\infty}^{\xi} \frac{1}{\sqrt{2\pi}} \exp\left(\tfrac{1}{2} t^2\right) dt \tag{5.2}$$

where L and L_0 are the current and initial adipate bridge populations. Without loss of accuracy, the upper and lower limits of ξ were specified as:

$$\xi = \begin{cases} -2 & \Phi < 0.0228 \\ +3.5 & \Phi < 0.9997 \end{cases}. \tag{5.3}$$

Note that initial (before decomposition begins) activation energies are lower and increase with extent of reaction. For CPUF the standard deviation used with the distributed activation energy model (σ_E) is assumed the same for all of the bond-breaking reactions. Distributing the activation energies tends to smooth the bond-breaking reaction rates and eliminates abrupt changes in calculated solid fractions (weight loss), which is in agreement with experimental observations from the TGA experiments.

From each of the eighteen TGA experiments at ambient pressure ramped at 20 C/min, estimates of the 15 activation energies (E_j) and the standard deviation (σ_E) were

obtained. The method of estimation was to optimize the RMS agreement between the model and the experimental weight loss data (see Eq. (5.4) and Fig. 5.1).

$$RMS\ error = \sqrt{n\sum_{i=1}\left(s_{f_i}^{TGA} - s_{f_i}^{CPUF}\right)^2} \qquad (5.4)$$

where $s_f = m/m_o$, the mass of the sample divided by the initial mass of the sample. This optimization was performed with the Sandia code DAKOTA (Eldred et al., 2002). The complete calibration data set is given in Table A.1 in Appendix A. The mean and variance of these activation energies are listed in Table 5.1. The 18 sets of parameters were used to estimate the covariance matrix for the activation energies and the distribution parameter. The estimated covariance matrix for the activation energies is given in Table A.2 in Appendix A.

Table 5.1 Estimated Activation Energies

Parameters	Mean (cal/mol)	Variance $(cal/mol)^2$
E_1 (Activation Energy)	50209	$(238.8)^2$
E_2	50567	$(199.0)^2$
E_3	49374	$(107.3)^2$
E_4	50408	$(151.6)^2$
E_5	49985	$(131.0)^2$
E_6	49508	$(211.0)^2$
E_7	50397	$(78.36)^2$
E_8	49276	$(110.3)^2$
E_9	51513	$(127.6)^2$
E_{10}	49791	$(132.7)^2$
E_{11}	50195	$(141.4)^2$
E_{12}	50147	$(269.8)^2$
E_{13}	50201	$(137.8)^2$
E_{14}	51081	$(209.3)^2$
E_{15}	49608	$(168.6)^2$
E_{16}	49730	$(79.01)^2$
σ_E (distribution parameter)	3521.4	$(16.35)^2$

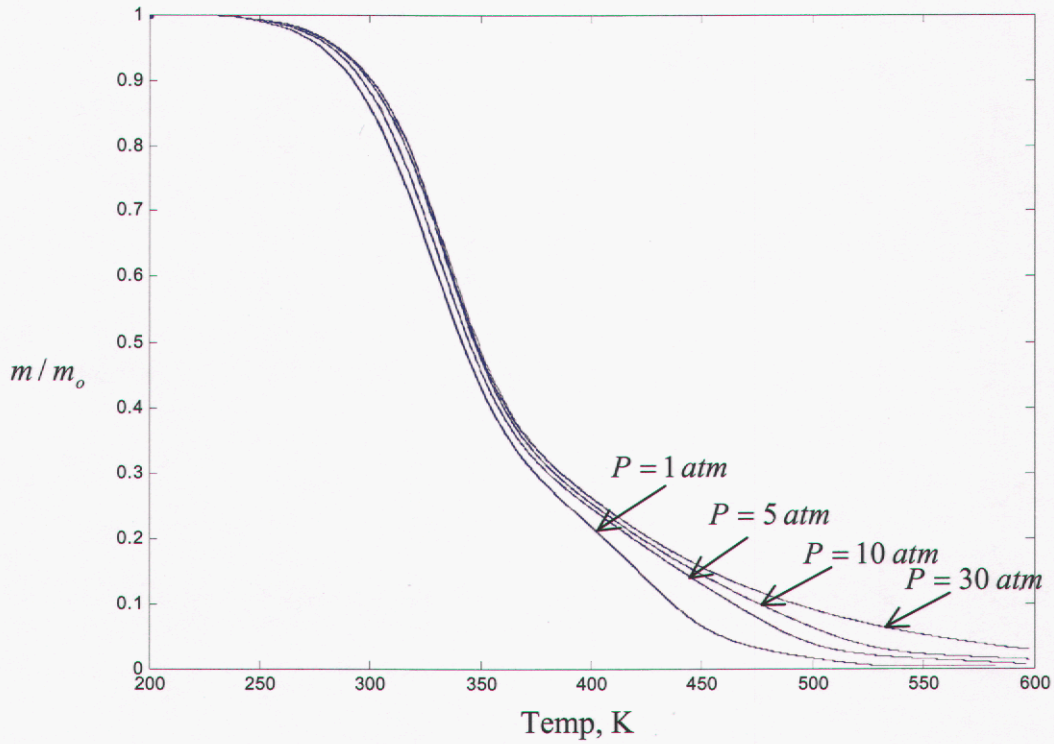

Figure 5.1 CPUF model results using mean activation energies

The variation in the estimated activation energies from the 18 experiments is an indication that a different set of activation energies would minimize the difference between the measured and modeled solid fraction. This can be interpreted in two ways. The first interpretation is that the material has physical variation between experiments and the variation in the activation energies represents variability in the material composition. A second interpretation is that the variation between experiments is due to error in the measured solid fraction and then variation in the activation energies represents the effect of measurement error on the estimates. Most likely both material variability and estimation error contribute to the variability in the estimated parameters. It is difficult to separate these effects without some independent estimate of covariance structure of the measurement error in solid fraction, in other words, further experimental study of the measurement error.

5.1.2 Model Results

Application of CPUF will use the mean values (of the 18 estimates) for the activation energies as listed in Table 5.1. Model results using mean activation energies are shown in Fig 5.1 for the 20 C/min ramped experiments. There are model results for each experiment (18 curves for P = 1 atm, 7 for P = 5 atm, 6 for P=10 atm, and 5 for P=30 atm). It is difficult to distinguish the individual curves for model results at a given pressure. The only difference between model results at a given pressure is the measured temperature provided to the model. Reproducibility of the model results for a given pressure suggests the measured thermal environment is accurately reproducible.

5.1.3 Model Uncertainty

As discussed earlier in this section, eighteen TGA experiments (20 °C/min, ambient pressure) were used to independently estimate the activation energies. The eighteen estimates (of 17 parameters) provide data to quantify the uncertainty (variance-covariance) in the activation energies. The covariance matrix is estimated as

$$\mathrm{cov}(E_i, E_j) = \sum_l \left(E_{i,l} - \overline{E}_i\right)\left(E_{j,l} - \overline{E}_j\right) \tag{5.5}$$

where $E_{i,l}$ is the lth estimate of activation energy i and $\overline{E}_i$ is the mean (of 18 estimates) for activation energy i. From the covariance matrix we can estimate correlation between the activation energies

$$\rho_{E_i E_j} = \frac{\mathrm{cov}(E_i, E_j)}{\sqrt{\mathrm{var}(E_i)}\sqrt{\mathrm{var}(E_j)}}. \tag{5.6}$$

A contour plot showing the magnitude of values in the correlation matrix is given in Fig. 5.2. The matrix is symmetric and identically equal to one along the diagonal (running from bottom left to top right). As a reference, values that are red have large positive correlation (correlation coefficient 0.7 to 1.0) and values that are dark blue have large negative correlation (correlation coefficient -.7 to -1.0); colors in the range orange to light blue have low correlation (correlation coefficient less than 0.5). The estimated activation energies demonstrate a high degree of correlation. This outcome is not surprising given the nature of the chemistry model and large number of parameters fit simultaneously. Given the correlation structure, it is not appropriate to assume the activation energies are independent; the full covariance matrix should be used for the uncertainty in the activation energies.

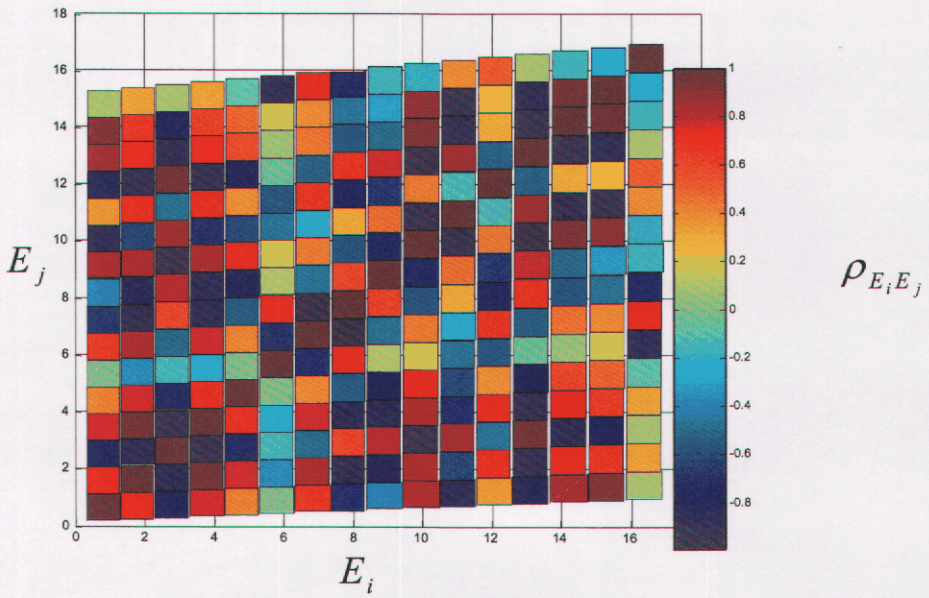

Figure 5.2 **Correlation coefficients for the estimated activation energies**

We can propagate the uncertainty in the activation energies (and its correlation structure) through the model to estimate the covariance of the model predictions for the solid fraction as follows

$$\mathrm{cov}(s_{f,\mathrm{mod}}) = \left[\nabla_{\mathbf{E}} s_{f,\mathrm{mod}}\right] \mathrm{cov}(E_i, E_j) \left[\nabla_{\mathbf{E}} s_{f,\mathrm{mod}}\right]^T . \qquad (5.7)$$

The sensitivity matrix, $\nabla_{\mathbf{E}} s_{f,\mathrm{mod}}$, is the partial derivative of solid fraction with respect to the activation energies and $\mathrm{cov}(E_i,E_i)$ is the covariance of the activation energies. Equation (5.7) assumes: 1) deviations in the input parameters from the mean value are random and described by $\mathrm{cov}(E_i,E_i)$, (matrix given in Table A.2) and 2) solid fraction, s_f, is locally linear, i.e., a linear function of parameter deviation from the mean. Errors in input parameters can be correlated and no assumptions concerning the distribution of the input errors are required. Only when we want to specify an interval that puts bounds on the *output,* are we required to make statements about the *output* distribution. Estimates using Eq. (5.7) are only as good as the quality of the covariance matrix describing input errors, $\mathrm{cov}(E_i,E_i)$, and the adequacy of the locally linear approximation.

A plot of the scaled sensitivity coefficients is shown in Fig. 5.3. All activation energies have a nonzero sensitivity, but some are clearly more important than others. The magnitude of the scaled sensitivity coefficients demonstrates the importance of the activation energy on the solid fraction.

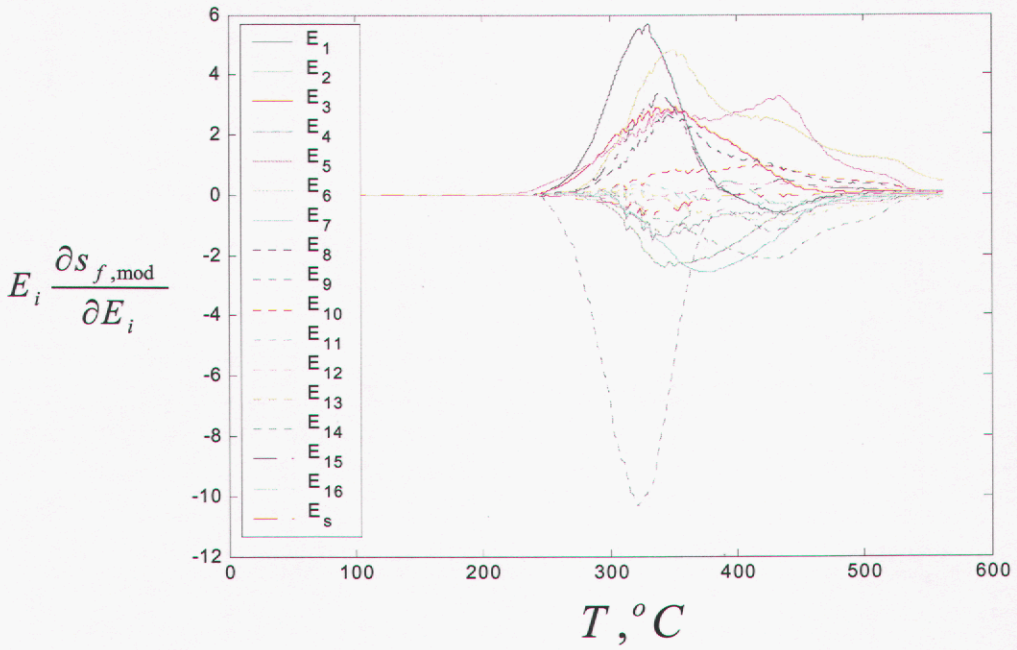

Figure 5.3 **Sensitivity of model prediction for experiment 1 (20°C/minute ramp ambient pressure)**

The mean of the activation energies estimated from the eighteen experiments is used in the model. The model predictions for solid fraction as a function of temperature are essentially equal for all eighteen experiments (See Fig. 5.1). We use the scatter of the eighteen estimates, i.e., covariance matrix of the activation energies, to quantify the uncertainty in the activation energies. The difference of the model with data is represented by a random model for the activation energies. The model predictions with the mean activation energies and an estimated uncertainty bar (for experiment 1) are shown in Fig. 5.4. The uncertainty represents a range, which the model prediction could lie, given that the activation energies have error in their values estimated by covariance matrix.

Assuming the activation energies are independent or uncorrelated, i.e., a diagonal covariance matrix, results in larger uncertainty bars in the temperature range from 260 °C to 350 °C than accounting for correlation the activation energies by using the full covariance matrix. At higher temperatures, (greater than 350°C) the uncertainty bars assuming uncorrelated parameters are comparable to those while accounting for the correlation.

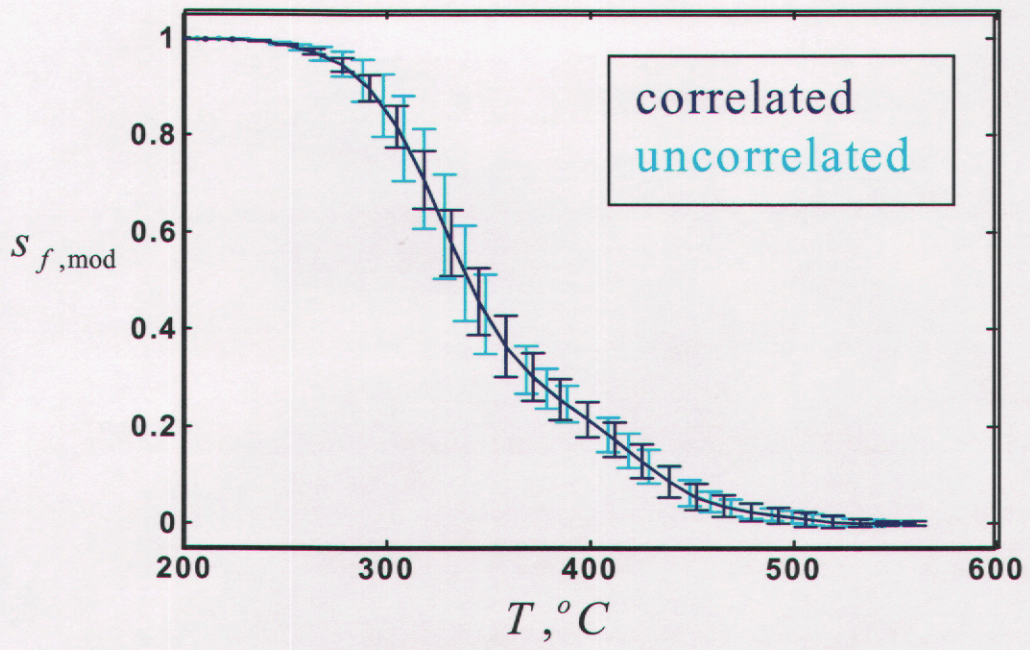

Figure 5.4 Model prediction for experiment 1 (20°C/minute ramp ambient pressure) with uncertainty bar approximated as $2\sigma_{s_f}$

The sensitivity of solid fraction to the activation energies and uncertainty of model results do not change significantly at higher pressures compare to results at ambient pressure. Figure 5.5 plots the scaled sensitivity coefficients and the model results with prediction intervals for a pressure of 5 atm. The uncertainty results at 5 atm are similar to those seen for ambient pressure.

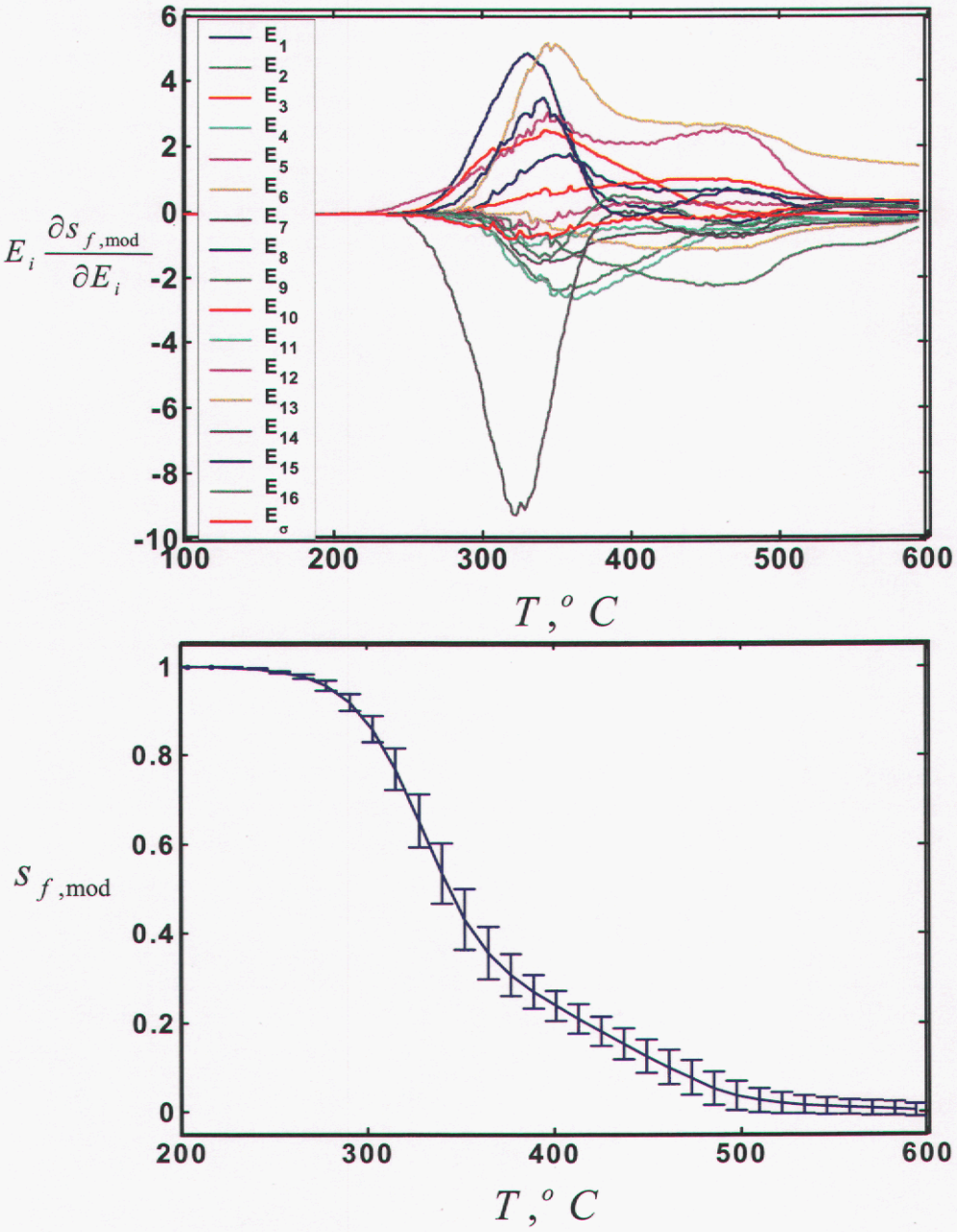

Figure 5.5 Model prediction for experiment 34 (20 °C/minute ramp 5 atm pressure) with uncertainty bar approximated as $2\sigma_{s_f}$

5.2 Benchmark Model Results

Model results for the benchmark experiments come from the thermal analysis code COYOTE, Gartling, et al., (1994) instead of the ASCI thermal analysis code Calore, Bova et al. (2002). Although the intent of this study was to validate the application of Calore, and all verification has addressed Calore, not all modeling capabilities had been implement in Calore with sufficient time to meet our schedule. Applying COYOTE in the validation study is relevant to understanding the accuracy of Calore. We say this because, we are validating the application of a computer code, in this case COYOTE. Stated another way, we are validating the mathematical models and algorithms that are executed when applying the code to the specified application. Because the mathematical model and algorithms in COYOTE are essentially identical to those in Calore, assessing the accuracy of COYOTE is indicative of the accuracy of Calore (for this application). Completing the validation process for an application of COYOTE does not guarantee Calore is valid for the same application, however. Some rational comparison between the two codes needs to be made to establish the accuracy of Calore. Trucano (2002) discusses the issues associated with comparing two codes and the comparison's role in verification and validation activities.

The mesh for the benchmark experiments is shown in Figure 5.6. Radial symmetry is assumed. The model has at least four material regions: reactive foam, non-reactive foam, 304 stainless steel heated plate, and 321 stainless can. In some cases a fifth material region, either 304 stainless steel or 6061 aluminum, is added when an internal component is included (a stainless steel slug is shown in Fig 5.2). The reactive foam will have chemical reactions (if temperature is sufficiently high), while the non-reactive foam will not have chemical reactions. Defining a block as non-reactive foam saves computations by not having to solve the chemical equations over the region that we know (from experimental data) will not reach temperatures to initiate a chemical reaction. The thermophysical properties are the same for reactive and non-reactive foam.

Boundary conditions for the model are taken from the experimental measurements (Figure 4.5). A thermocouple located within the heated plate provides the transient temperature imposed as a boundary condition along the heated surface, $T_p(t)$. Thermocouple measurements along the outer surface of the can are used to impose the transient temperature along the outer surface of the can, $T_c(x,t)$. Elements that are located between thermocouple locations interpolate to obtain the prescribed boundary temperature.

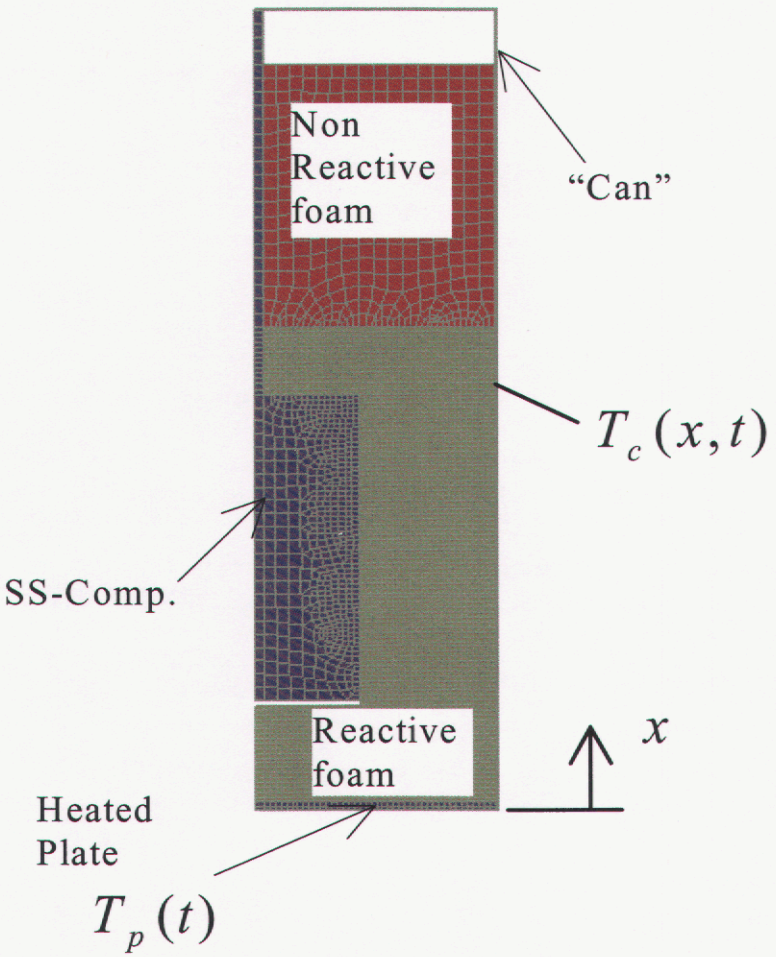

Figure 5.6 **Mesh for benchmark model results**

Table 5.2 Model Parameters*

Parameters	Mean	Variance
initial temp (T_i), °C	300	$(3)^2$
initial bond population (l_0)	0.78	$(0.05)^2$
Density (ρ), g/cm^3	0.364	$(0.0364)^2$
specific heat (c), cal/g °C	1	$(0.1)^2$
heat of reaction (h_r), cal/cm^3	20.6	$(2.06)^2$
Emissivity (ε)	0.8	$(0.05)^2$
σ+1	2.8	$(.28)^2$
death criteria (k_e)	0.036	$(.0069)^2$

* *Thermal conductivity is not included in this list because it was used as a discretization bias corrector (Hobbs et al., 2003). For an idea of the relative importance of thermal conductivity see Hobbs, et al. (1999).*

Table 5.3 Thermal Properties of Polyurethane foam

Temperature °C	Thermal Cond cal/s-cm-°C	Specific Heat cal/g-°C
-173	1.4 E-04	0.303
20	1.4 E-04	0.303
50	1.5 E-04	0.324
100	1.6 E-04	0.358
150	1.8 E-04	0.440
200	2.0 E-04	0.475
250	2.2 E-04	0.526
3227	1.3 E-03	0.526

Table 5.4 Thermal Properties of stainless steel

Temperature °C	Thermal Cond cal/s-cm-°C	Temperature °C	Specific Heat cal/g-°C
-223	0.0300	-223	0.096
-73	0.0300	-73	0.096
27	0.0325	27	0.114
127	0.0375	127	0.123
227	0.0450	227	0.133
477	0.0500	427	0.139
827	0.0625	727	0.146
1727	0.0900	1027	0.153
		3127	0.153

The mathematical model (Section 3) is coupled thermal diffusion, chemical kinetics, and enclosure radiation (after the reactive foam has decomposed and opens a void between the heated plate and surface of the foam). We need thermophysical properties, parameters for the chemical kinetics and (foam) decomposition, and radiation parameters. Values for these parameters are listed in Table 5.1 to 5.4; over 50 inputs are needed. Thermophysical properties of the foam, up to 250°C (onset of decomposition) are listed in Table 5.3; beyond this temperature, values are extrapolated. All grades of stainless steel use the thermophysical properties listed in Table 5.4. Activation energies for the foam were estimated from the TGA experiments (Table 5.1). Additional parameters are needed for the foam: initial bond population, density, heat of reaction, emissivity, degree of monomer (σ+1), and element death, these are given in Table 5.2.

Given the physical parameters and boundary conditions, the computer model calculates the foam mass fraction and temperature as a function of location and time. A quantitative measure of use for comparison with experiment is the location of the decomposing front. The front is signified by the region where the solid fraction transitions from 1 (no decomposition) to 0 (fully decomposed). The location of the 0.5 solid fraction is plotted in Fig. 5.7 for the model results of experiments with steady boundary temperatures, T_p, of 600°C, 750°C, and 900°C. We discuss quantifying the error in the model results in the next section.

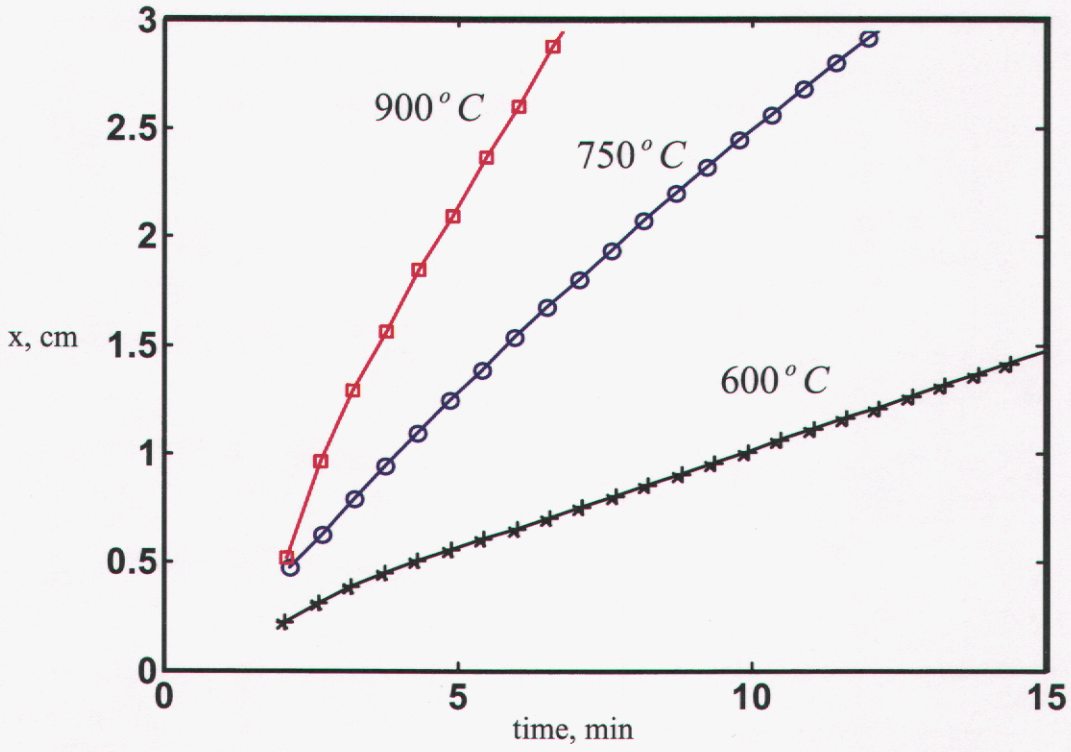

Figure 5.7 **Model results for location of 0.5 solid fractions using nominal input values**

5.2.1 Model UQ (Perturbation Method)

We consider twenty-five, of the 50+ input parameters, to have uncertainty in their values. The uncertain input parameters are the activation energies (Table 5.1) and parameters representing the thermophysical properties and assorted parameters for the foam model (Table 5.2). Uncertainty in the specific heat of the foam was assumed to shift the entire temperature-dependent curve, reducing uncertainty in this property to a single parameter. Uncertainty in thermophysical properties of stainless steel was assumed negligible, in comparison to the foam model uncertainties. The effect of model uncertainty due the use of measured temperatures for boundary conditions was not quantified as part of this study. It was not realized until after comparing the model to data that uncertainty due to the boundary conditions, particularly the measured temperature used as the boundary condition for the heated plate, was potentially significant. The issue of boundary condition uncertainty is discussed in Section 7.

We can estimate the covariance in the predicted front location due to the variance in these model parameters as follows (see Hills and Trucano, 2001):

$$\mathrm{cov}(\mathbf{x}_{\mathrm{model}}) = \nabla_{\alpha}\mathbf{x}\ \mathrm{cov}(\phi)\left[\nabla_{\alpha}\mathbf{x}\right]^{\mathrm{T}} \tag{5.8}$$

where $\mathrm{cov}(\phi)$ is the covariance matrix of the input parameters and $\nabla_{\alpha}\mathbf{x}$ is the sensitivity matrix

$$\nabla_{\alpha}\mathbf{x} = \begin{bmatrix} \frac{\partial x(t_1)}{\partial \phi_1} & \frac{\partial x(t_1)}{\partial \phi_2} & \cdots & \frac{\partial x(t_1)}{\partial \phi_{25}} \\ \frac{\partial x(t_2)}{\partial \phi_1} & \frac{\partial x(t_2)}{\partial \phi_2} & \cdots & \frac{\partial x(t_2)}{\partial \phi_{25}} \\ \vdots & \vdots & \ddots & \vdots \\ \frac{\partial x(t_n)}{\partial \phi_1} & \frac{\partial x(t_n)}{\partial \phi_2} & \cdots & \frac{\partial x(t_n)}{\partial \phi_{25}} \end{bmatrix}. \tag{5.9}$$

The t_i, $i = 1,\ldots,n$ correspond to the times of the measured front location. We discuss the assumptions about Eq. (5.8), obtaining the covariance matrix of the input parameters, and approximating the sensitivity coefficients next.

Equation (5.8) assumes: 1) deviations in the input parameters from the mean value are random and described by $\mathrm{cov}(\phi)$ and 2) front location, x, is locally linear, i.e., a linear function of parameter deviation from the mean. Errors in input parameters can be correlated and no assumptions concerning the distribution of the input errors are required. Only when we want to specify an interval that puts bounds on the *output,* are we required to make statements about the *output* distribution. Estimates using Eq. (5.8) are only as good as the estimate of the covariance matrix describing input errors, $\mathrm{cov}(\phi)$, and the adequacy of the locally linear approximation.

The covariance matrix of the parameters, $\mathrm{cov}(\phi)$, is estimated using the data from calibrating the activation energies to the TGA experiments, (Appendix A) and from engineering estimates provided by Hobbs et al. (2003). The TGA experiments tested

small samples -- weighing 4-6 mg -- while the benchmark experiments tested samples that are orders of magnitude larger in mass and size. If the variability seen in the TGA experiments is mainly due to differences in the material composition, then we need some justification for expecting that the variability estimated from the TGA experiments is applicable to the larger benchmark samples. One option is to adjust the covariance matrix estimated from the TGA experiments to conditions for the benchmark experiments. Instead, however, as a worst case we will carry the full magnitude of the covariance matrix from the TGA to benchmark experiments. We also note that the activation energies are highly correlated and the covariance matrix has significant off-diagonal contributions as illustrated through the correlation matrix in Fig 5.2. The remaining parameters, outside of the chemistry activation energies, are assumed statistically independent of one another and the activation energies. The full covariance matrix is given in Table A.3, Appendix A.

The sensitivities in Eq. (5.9) are approximated using a central difference scheme

$$\frac{\partial x}{\partial \phi_i} \approx \frac{x(\phi_i + \delta\phi_i) - x(\alpha_i - \delta\phi_i)}{2\delta\phi_i}. \qquad (5.10)$$

The computer model is run twice to approximate the derivative for each parameter, ϕ_i, first with the parameter perturbed upward by $+\delta\phi_i$ and the second time perturbed downward, $-\delta\phi_i$. A relative perturbation in all parameters was used, $\delta\phi_i = 0.01\,\phi_i$. Approximating derivatives in this manner can be sensitive to numerical errors due to step size and numerical noise in the model results. Some indication of numerical noise is seen in the derivatives shown later in this section and the issue is discussed in Section 7.

Using the covariance of the model input errors, we can estimate uncertainty bounds on the model output. That is, we can specify a range that bounds a percentage of possible model outputs given that input errors, about the estimated values, are described by $\mathrm{cov}(\phi)$. These bounds are shown with the model results in Fig 5.8. The bound selected is one standard deviation, which if the output errors were normal would contain 68 percent of potential model outputs; two standard deviations would contain 95 percent of the potential outputs.

We can investigate the probability distribution of the front location using the calibration data. The 18 sets of activation energies provide data to study the distribution of the activation energies and the effect of these distributions on the front location. Hills et al. (2002) study histograms of 18 estimates of each of the 16 activation energies (Hills et al. (2002), Figure 3.1) and note that a significant number of the 16 activation energies do not appear to be normally distributed. To study the effect of non-normal activation energies on the distribution of the front location, a Monte Carlo approach is used. By sampling from the 18 sets of activation energies and assuming normal distributions on the other eight uncertain input parameters, they estimated the resulting distribution on the front location. The study indicated that the distribution on the front location is reasonably normal, even though the activation energies appeared non-normal, Hills et al. (2002).

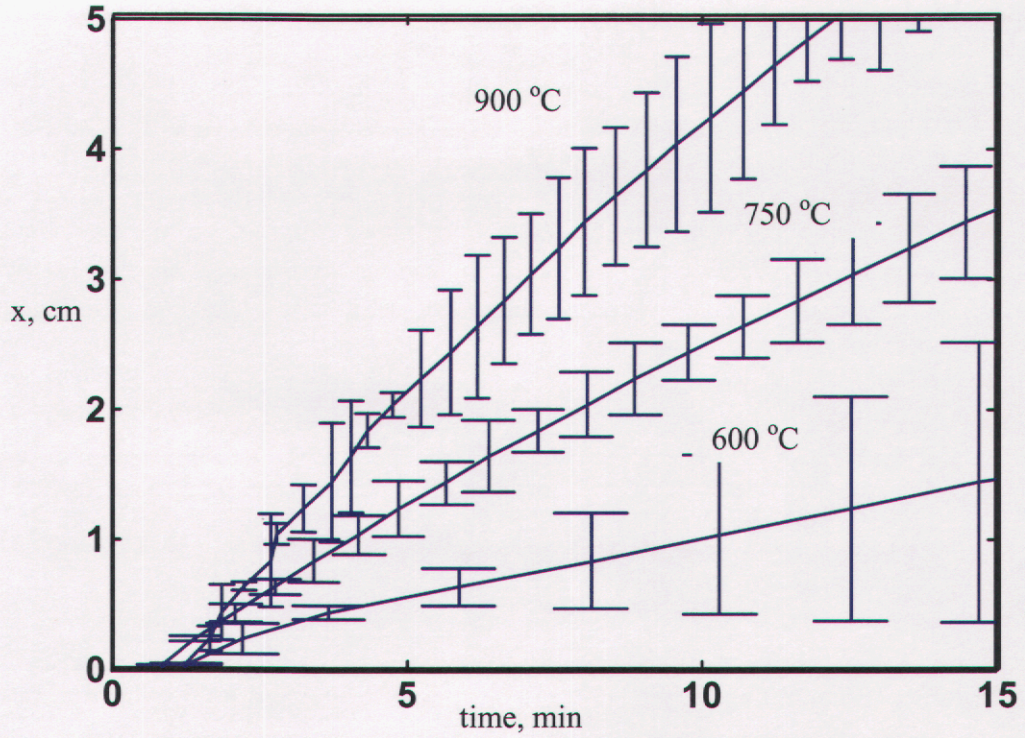

Figure 5.8. Model results and uncertainty for Experiments 1, 2, and 14; The uncertainty bars represent one standard deviation above and one standard deviation below the model results.

It is insightful to study the sensitivity coefficients and importance factors to identify main contributors to the model uncertainty. Scaled sensitivity coefficients, or partial derivatives with respect to the parameter multiplied by the parameter, are useful to understanding the dependence of the model on the parameters

$$\phi_i \frac{\partial x}{\partial \phi_i}. \qquad (5.11)$$

The scaled sensitivity coefficient can be used to rank the importance of parameters relative to their effect on the output. Importance factors, however, provide insight to the relative contribution of each parameter to the total uncertainty. The main contributors to the total variance can be identified through the importance factors. Importance factors are the gradient multiplied by the ratio of parameter variance to total variance

$$\gamma_i^2 \approx \left(\frac{\sigma_i}{\sigma_x} \frac{\partial x}{\partial \phi_i} \right)^2. \qquad (5.12)$$

The total variance, σ_x^2, are entries along the diagonal of covariance matrix for the front location, cov($\mathbf{x}_{model}$), (at a given time), which is calculated with Eq. (5.8). The importance factors have the relationship that

$$\sum_i \gamma_i^2 = 1. \qquad (5.13)$$

Consequently, the value of the importance factor for a given parameter is the fraction the parameter contributes to the total variance.

The scaled sensitivities and importance factors are plotted in Figure 5.9 for Exp 2 (750 C bottom heated). The top plots in the figure are data for the 17 parameters associated with the activation energies, E_1-E_{16} and σ_E, and the middle plot are data for thermophysical properties, ρ, c, h_r, ε, and T_o, and the bottom plot is for the remaining algorithm-like parameters, l_0, σ+1, and k_e, bridge population, lattice coordination number, and element death criterion, respectively. Note that activation energies have the largest sensitivities, but are minor contributors to the uncertainty in front location because uncertainty in the values is small. The small importance factors for the activation energies indicate their minor role in the uncertainty. The front location is less sensitive to thermophysical properties, but because the values have a larger relative uncertainty, the parameters contribute a combined 86 percent at (10 min) to the total variance in front location. While the ordering of main contributors does vary with time, thermophysical properties of density, specific heat, and emissivity (ρ, c, ε) are significant contributors.

The sensitivity coefficients in Fig. 5.9 do not vary smoothly with time, especially at early time. The non-smooth perturbations may be due to numerical effects. A possible explanation is the arbitrary nature of the element death process used in our calculation, Gartling et al. (1994). Further study is needed to identify the source of the noise.

Parameter and uncertainty dependencies for model results with a 900°C boundary temperature are similar to those for 750°C model. Results for a 600°C boundary temperature are markedly different, however. The sensitivity and uncertainty for a 600°C boundary temperature are dominated by the heat (enthalpy) of reaction, h_r; over 90 percent of the total variance is due to this single parameter.

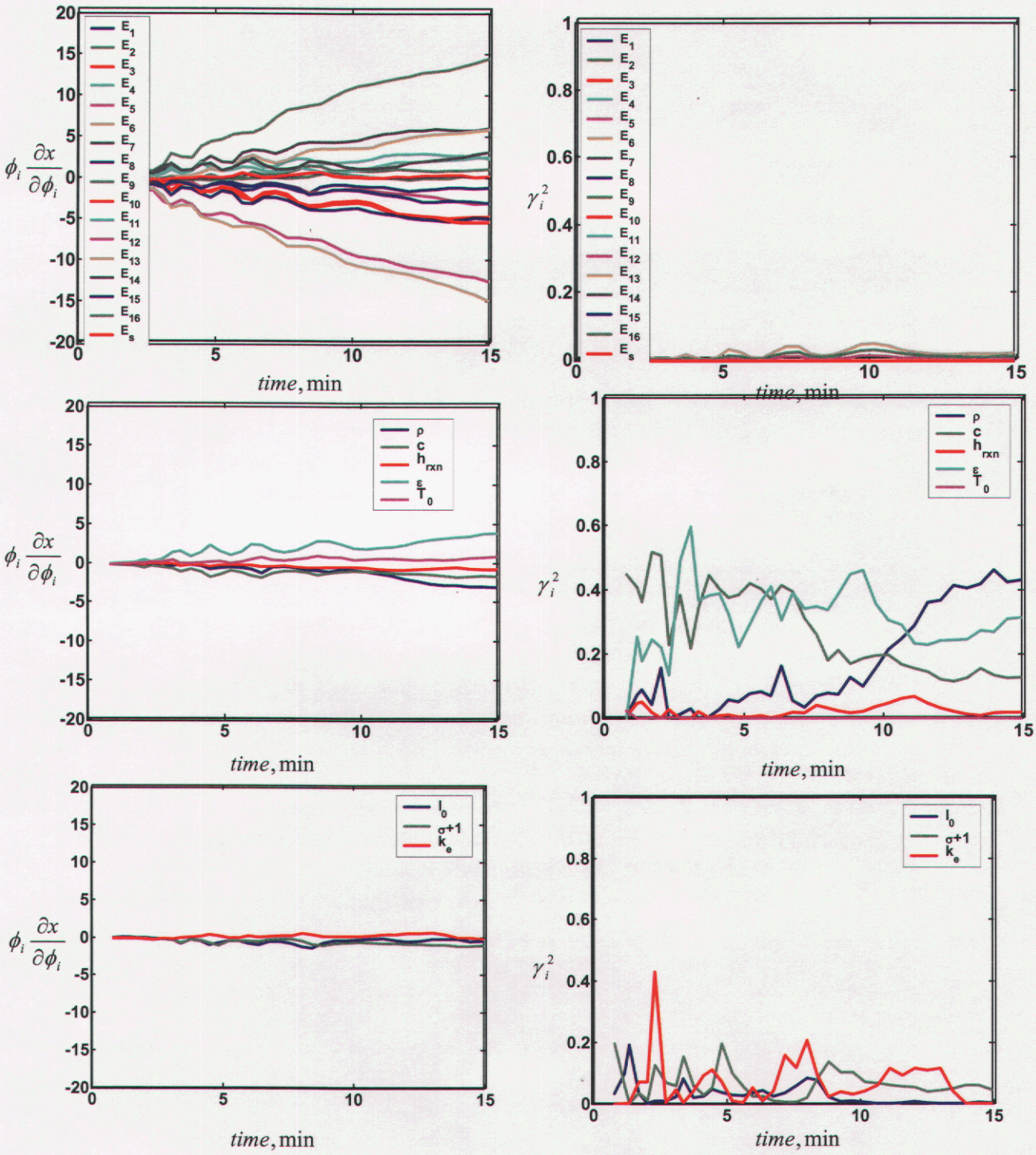

Figure 5.9 **Scaled sensitivity coefficients and importance factors for model results of 750 C experiment 2**

5.2.2 Solution Verification

It is important to assess convergence and numerical accuracy of the model results. Modeling thermal decomposition of foam is known to depend on discretization issues, Hobbs et al. (2003). The dependence is due to the discrete nature of removing material by element or group of elements, as is done with element death and steep gradients in regions where chemistry is occurring. Hobbs et al. (2003) has shown that an element thickness of 100 μm is required to obtain a grid independent velocity. Time step dependence was also studied in that reference. Because computational costs preclude meshing the foam with 100 μm elements, a correction was developed for the solution at larger characteristic element dimensions. The larger elements result in the front propagating at a slower rate than it would with the grid-independent size (100 μm). To compensate, a correction is added to the model to "bias correct" the numerical solution with larger element size to the grid-independent solution. Hobbs et al. (2003) discuss the bias correction factor and its implementation.

6.0 Metrics

In this section we provide an overview of metrics for assessing the accuracy of the model to represent the physical experiment and two metrics under present consideration are identified. The metrics are applied to quantify the differences between the experiments and model results and provide quantitative data to assess the accuracy of the model.

6.1 Introduction

Validation metrics are quantitative measures of a model's ability to represent nature (physical experiments). Trucano et al. (2001) describe a research project at Sandia National Laboratories concerning metrics. The project focused on case studies related to the thermal and structural dynamics applications. Analysis presented in subsequent sections resulted from work done as part of this project on the thermal case study.

For discussion purposes, we combine and repeat Eq. (1.6) and Eq. (1.7), the definition of the error between a mathematical model result, or model, and experimental measurement

$$e = \hat{D}(X,z) - S(\hat{\phi},\hat{z}) = \delta_D + S_p(\phi - \hat{\phi}, z - \hat{z}) + \delta_n + \varepsilon . \qquad (6.1)$$

As we discussed in Section 1.2, the difference between an experiment and mathematical model is a complex combination of contributors. In short, the measurement error, δ_D, error due to using estimated model parameters and measured boundary conditions to model the experiment, $S_p(\phi - \hat{\phi}, z - \hat{z})$, numerical error in solving the mathematical model, δ_n, and error due to the mathematical model approximating the physics, ε, all contribute to the total error, e.

Metrics, or measures, quantify the accuracy of a model to represent the physical world (experiments). A "valid" model has i) a magnitude of the error that makes the model useful for the application; e is "small" and ii) does not have "large" systematic errors; ε is not significant. We study metrics that address these two criteria. Acceptable limits for e and ε are application specific.

Philosophically, there are two views of characterizing and judging the error. The first view, we'll call *error estimation*, is that the validation process analyzes model results and experimental measurements to quantify the total error, e, between the two. Because we may expect the error to have a random nature, the mean and standard deviation of the error could be estimated. Statistical tests for bias and correlation (over X) can be conducted to "judge" the error. As Eq. (6.1) shows, the total error is a function of measurement error, error due to model inputs, numerical error in the model, and, finally, the approximation error of the model to the physical process. Clearly, the total error has many potential contributors. While we can estimate the total error, we are unlikely to have knowledge of what contributes to that error unless we can successfully study terms on the

right side of Eq. (6.1). Furthermore, it is not necessarily true that the total error is conservative because cancellation between various sources is likely to happen.

A second view, we will call *predictive testing*, is that the model result and experiment have errors associated with them that we can include in the mathematical model without using the specific validation data. We can often characterize the error associated with our ability to model the experiment, including model input error, $S_p(\phi-\hat{\phi}, z-\hat{z})$, and measurement error, δ_D, independent of the validation data. Then, the validation data is used to test (judge) whether there are additional errors outside of $S_p(\phi-\hat{\phi}, z-\hat{z})$ and δ_D, such as δ_n and ε in Eq. (6.1). This view assumes we can include the effect of input error in our mathematical model and estimate measurement error. Note that in the application we will need to address and model input error, hence the validation process can be used as a test of our modeling capability of the physics as well as the error. This desire to "test modeling capability" is a motivating reason for making validation experiments of relatively simple geometry, with controlled boundary conditions. If the outcome suggests the presence of numerical error or physics error (δ_n or ε) then additional analysis is required.

6.1.1 Metrics

In the remainder of this section we will quantitatively compare experimental results with model results for the TGA experiments and benchmark experiments. In the comparison, we will study two metrics. As discussed next, the two metrics focus on different aspects of error in Eq. (6.1).

The first metric looks to estimate statistical characteristics of the difference, *e*, and how it varies over experiments while relying solely on experimental data. This approach will quantify the total combined error and study its dependence on factors the model should capture. The outcome of this metric is a statistical model for *e* in Eq (6.1); for example, *e* can be represented as a random variable with an estimated mean and standard deviation. Statistically analyzing the prediction error is better suited to analyzing data that can be described by scalar value. There are not specific limitations to preclude multivariate data, but, since the approach relies solely on experimental data, requirements to characterize interactions, principally covariances, may be difficult. A final comment, this approach is an estimation process to statistically model the total error, *e,* and then possibly hold in reserve a subset of the validation experiments to test the estimated model.

The second metric, Hills and Trucano (2001) and (2002), provides a statistical test to identify deviations of the experiment and model that are not consistent with modeled uncertainty in both the experiment and math model. This metric relies on modeling the effect of errors and testing for deviations that are outside of this model. For example, given a model for $S_p(\phi-\hat{\phi}, z-\hat{z})$ and δ_D, using the differences *e* we can test for the presence of ε. The metric tests the mathematical model as well as our ability to model the errors in the model and experiment. The outcome of the metric is a probability that a

"valid model," i.e., ε=0, would result in the differences in *e*. Typically, vectors of data, for example transient data, are analyzed.

6.2 TGA Data

The TGA data available for assessing CPUF are shown in Fig. 6.1. Mass loss (solid fraction) as a function of temperature and pressure with model results overlaying all experimental data is plotted. In addition to mean model results, uncertainty limits for the model are provided. The limits represent bounds on the model results that would contain, with 95% probability, the true model result given uncertainty in the activation energies. Missing in this comparison are uncertainty estimates on the experimental measurement. Measurement uncertainty in solid fraction is discussed in Section 4.2.4.

We have decided not to quantitatively compare the isothermal experiments (Fig 4.2). The ramped thermal environment is more appropriate to evaluate the model for the intended application, where temperature is transient. Because we had sufficient experiments for a ramped thermal environment, we did not consider the isothermal experiments.

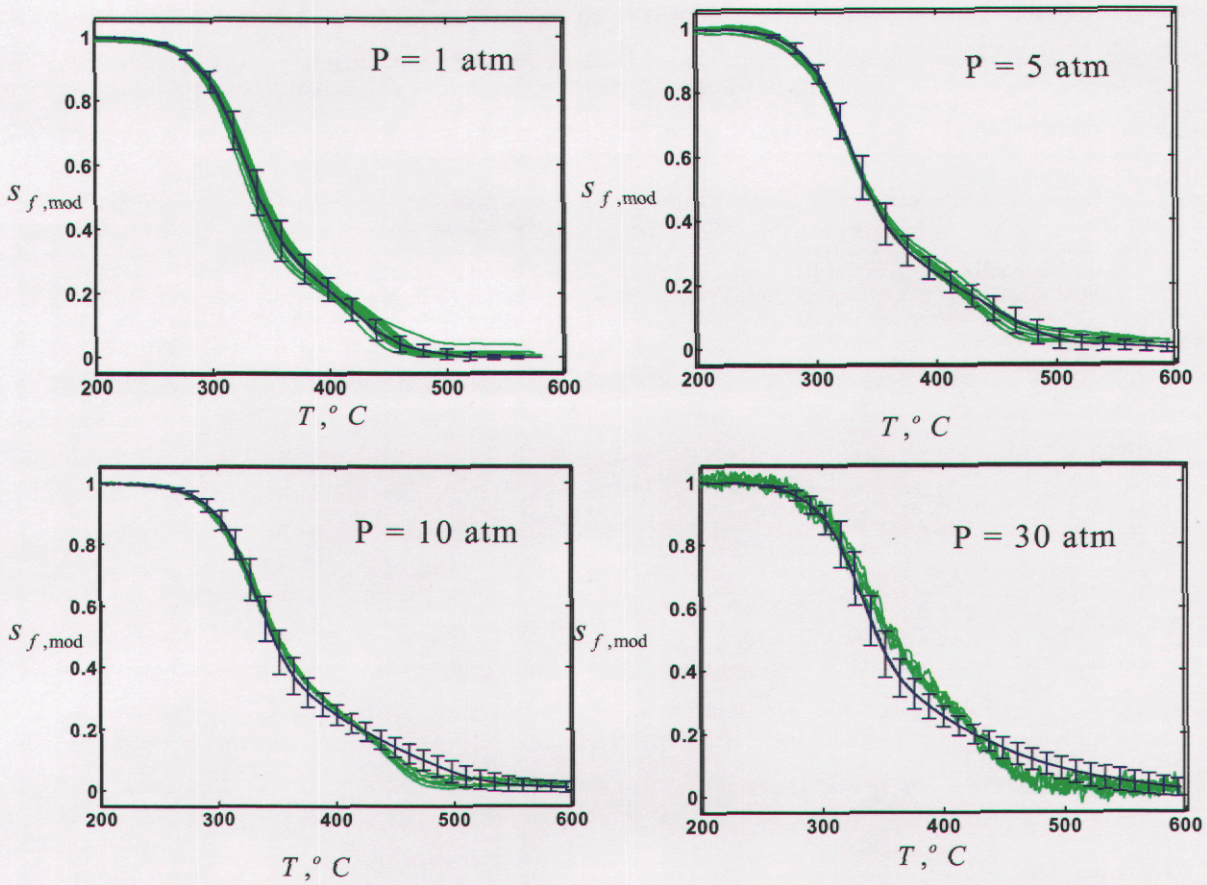

Figure 6.1 **Comparison of model predictions and experimental data for TGA data**

6.2.1 Choice of Comparison Variable

The chemistry model calculates the mass as a function of temperature. The temperature of the sample was ramped continuously at a rate of 20 °C/min for the experiments shown in Fig. 6.1. Because we are evaluating a fundamental physics model in this comparison, we expect that the model should capture the decomposition over the entire curve. Consequently, we will study the error at locations along the curve to understand the model's overall accuracy. Assessing the error over the curve will provide greater insight to the model's accuracy in predicting the physics.

We would also like to evaluate the model similarly to the way it is applied in the application. In the application, the chemistry model is coupled to the thermal diffusion and accounts for energy associated with chemical kinetics. The mass fraction, evaluated from the chemistry model, is monitored to evaluate when the decomposition is complete. When the mass fraction in an element reaches a prescribed level, say a couple of a percent, the element is assumed to be void of foam and no longer considered in the thermal diffusion. This process is called element death. Hence, another way to evaluate the model is to look at predicting the completion of decomposition. We would look at comparing data at the "tails" of the curves where solid fraction approaches zero in Fig 6.1.

6.2.2 Error Model Estimation

The model (CPUF) predicts the mass (loss) as a function of temperature. To evaluate the model we can observe the error in temperature to reach a specified mass fraction. This error is relevant if we need the model to predict the temperature at which mass reaches a specified value. Conversely, we can look at the error in mass fraction to reach a specified temperature. We study both errors in this subsection.

The relative error in temperature is defined as

$$e_T = \frac{T_{\exp}\big|_{s_f=m_o} - T_{cpuf}\big|_{s_f=m_o}}{T_{\exp}\big|_{s_f=m_o}} \qquad (6.2)$$

where m_o is the solid fraction value that the error is evaluated. Figure 6.2 and Tables 6.1-6.4 provide scatter plots and data indicating the error in the temperature when the solid fraction reaches values of 0.8, 0.6, 0.4, 0.2, and 0.1 at pressures from 1 to 30 atm.

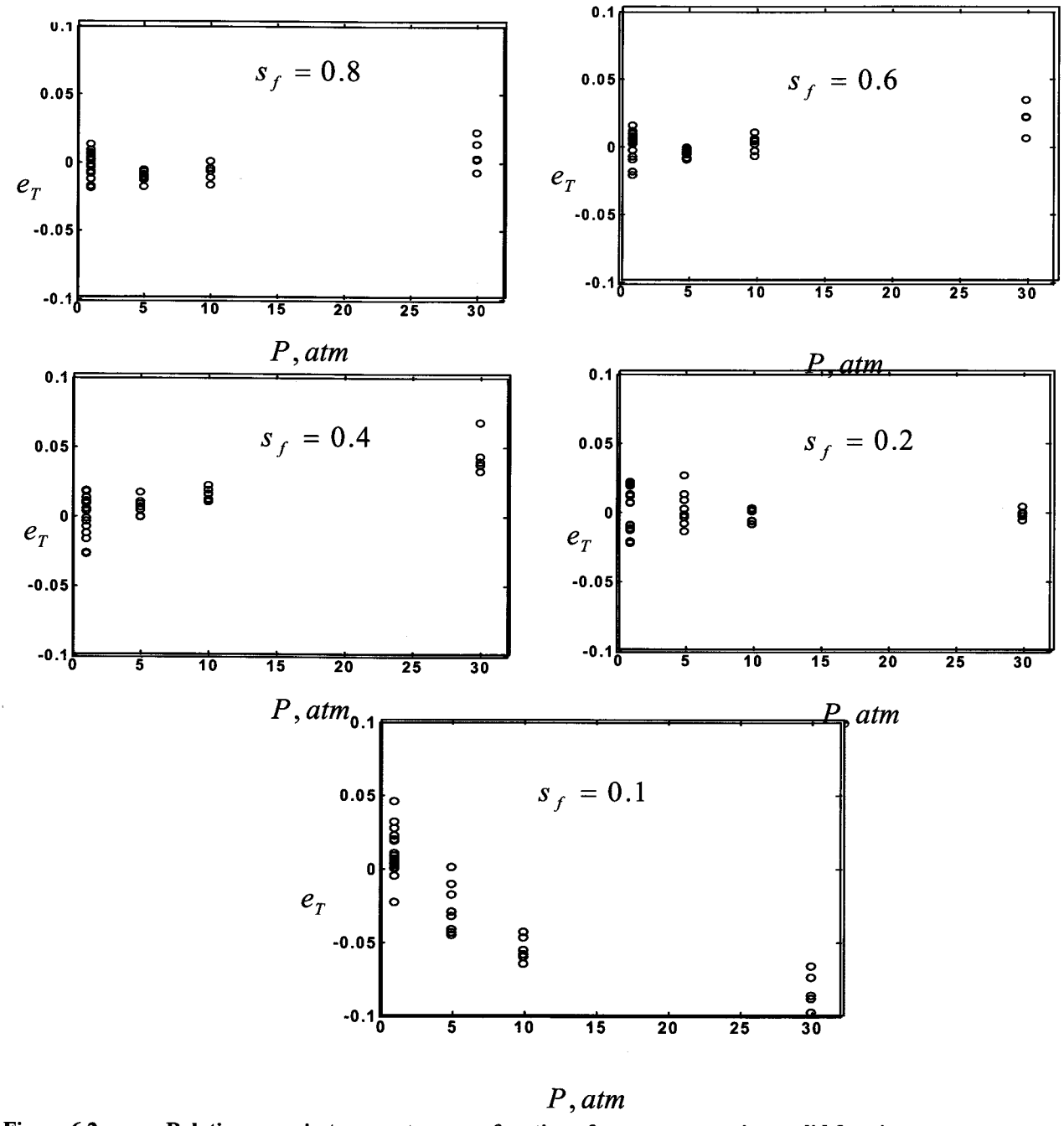

Figure 6.2 **Relative error in temperature as a function of pressure at various solid fractions**

Table 6.1 Temperature to reach a given solid fraction (ambient pressure, 20 °C/min)

Exp	Lab	$T\|_{s_f=0.8}$		$T\|_{s_f=0.6}$		$T\|_{s_f=0.4}$		$T\|_{s_f=0.2}$		$T\|_{s_f=0.1}$	
		Exp	Mod	Exp	Mod	Exp	Mod	Exp	Mod	Exp	Mod
1	SNL	307.9	308.5	330.4	330.8	354.4	354.5	401.0	405.4	427.0	436.3
2	SNL	305.1	308.5	328.9	330.8	353.7	354.5	414.7	405.4	451.0	436.3
3	SNL	310.9	308.5	333.9	330.8	358.8	354.5	410.8	405.4	439.4	436.3
4	SNL	311.1	308.5	333.8	330.8	358.2	354.5	410.8	405.5	439.4	436.4
5	SNL	308.5	308.6	332.3	330.9	356.1	354.5	411.3	405.4	445.5	436.3
6	SNL	309.4	308.5	333.3	330.8	358.2	354.4	414.3	405.4	445.2	436.4
7	SNL	309.6	308.5	333.4	330.8	358.3	354.5	408.7	405.5	434.6	436.3
8	SNL	309.8	308.5	334.5	330.8	361.6	354.5	415.1	405.4	457.7	436.3
9	SNL	310.0	308.5	332.8	330.8	356.8	354.4	408.8	405.4	438.3	436.4
10	SNL	309.5	308.5	332.3	330.8	356.2	354.5	411.3	405.5	441.4	436.4
11	SNL	311.7	308.4	335.1	330.8	359.7	354.4	413.8	405.4	449.0	436.4
12	SNL	313.1	308.5	336.6	330.8	361.3	354.5	413.7	405.4	446.7	436.3
13	SNL	310.8	308.5	331.9	330.8	352.3	354.4	400.8	405.4	436.8	436.4
14	SNL	311.1	308.5	332.2	330.8	352.3	354.5	401.3	405.4	439.1	436.3
15	BYU	306.7	308.4	328.2	330.9	349.2	354.5	401.9	405.4	440.6	436.3
16	BYU	303.6	308.5	324.7	331.0	346.0	354.6	397.6	405.5	437.7	436.3
17	BYU	306.3	308.4	328.8	330.7	350.6	354.3	402.2	405.4	439.6	436.3
18	BYU	303.4	308.5	325.2	330.7	345.5	354.5	396.9	405.3	437.1	436.4

Table 6.2 Error in temperature to reach a given solid fraction (ambient pressure, 20°C/min)

		e_T				
Exp	Lab	s_f=0.8	s_f=0.6	s_f=0.4	s_f=0.2	s_f=0.1
1	SNL	-0.0019	-0.0012	-0.0001	-0.0111	-0.0219
2	SNL	-0.0110	-0.0059	-0.0022	0.0224	0.0326
3	SNL	0.0078	0.0092	0.0120	0.0131	0.0069
4	SNL	0.0083	0.0090	0.0103	0.0130	0.0069
5	SNL	-0.0001	0.0044	0.0048	0.0143	0.0206
6	SNL	0.0028	0.0074	0.0106	0.0216	0.0199
7	SNL	0.0035	0.0078	0.0107	0.0079	-0.0039
8	SNL	0.0044	0.0112	0.0197	0.0233	0.0467
9	SNL	0.0049	0.0062	0.0067	0.0083	0.0045
10	SNL	0.0032	0.0045	0.0049	0.0141	0.0114
11	SNL	0.0105	0.0128	0.0145	0.0204	0.0281
12	SNL	0.0148	0.0172	0.0190	0.0200	0.0231
13	SNL	0.0074	0.0034	-0.0060	-0.0116	0.0010
14	SNL	0.0083	0.0042	-0.0062	-0.0103	0.0063
15	BYU	-0.0054	-0.0080	-0.0152	-0.0085	0.0096
16	BYU	-0.0161	-0.0195	-0.0247	-0.0197	0.0033
17	BYU	-0.0068	-0.0057	-0.0107	-0.0079	0.0076
18	BYU	-0.0171	-0.0169	-0.0258	-0.0209	0.0016

Table 6.3 Temperature to reach a given solid fraction (elevated pressure, 20 °C/min)

$T\|_{s_f=0.1}$

Exp	Pres (atm)	$T\|_{s_f=0.8}$		$T\|_{s_f=0.6}$		$T\|_{s_f=0.4}$		$T\|_{s_f=0.2}$			
		Exp	Mod	Exp	Mod	Exp	Mod	Exp	Mod	Exp	Mod
34	5	309.1	312.6	334.1	334.2	361.9	358.2	422.8	418.6	459.2	463.5
35	5	307.3	312.4	332.0	334.2	360.1	358.0	420.1	418.5	445.9	463.7
36	5	309.5	312.6	333.1	334.2	360.8	357.9	418.2	418.5	449.5	463.5
37	5	310.8	312.4	334.7	334.3	364.8	358.0	430.4	418.4	464.4	463.4
38	5	309.6	312.5	331.8	334.1	358.4	357.9	413.3	418.6	444.1	463.6
39	5	310.0	312.3	331.7	334.3	358.3	358.0	415.5	418.4	444.8	463.6
40	5	308.8	312.3	333.4	334.2	362.4	358.1	424.3	418.3	456.0	463.6
41	5	310.9	312.1	332.9	334.2	358.4	358.1	417.6	418.6	450.8	463.6
42	10	313.1	316.0	336.4	336.9	365.3	360.5	423.0	422.2	450.6	475.1
43	10	311.4	316.1	335.4	337.2	364.6	360.4	420.1	422.3	446.7	475.2
44	10	316.7	316.0	341.0	336.8	368.9	360.3	419.1	422.2	448.6	475.0
45	10	315.0	315.9	338.9	336.9	365.4	360.5	420.2	422.4	449.4	475.1
46	10	314.9	316.0	339.4	336.9	367.8	360.3	423.4	422.1	455.9	475.1
47	10	314.4	316.0	338.1	336.9	366.6	360.3	423.8	422.1	454.2	475.1
48	30	318.9	317.5	345.6	337.6	376.1	361.7	424.4	426.4	452.0	490.5
49	30	315.7	317.5	341.0	338.4	375.0	362.4	426.9	426.4	447.4	490.6
50	30	322.3	317.5	345.7	337.4	376.9	361.6	426.7	426.5	451.1	490.5
51	30	325.0	317.3	350.1	337.5	388.4	361.6	425.6	426.1	457.1	490.5
52	30	318.7	317.6	345.6	337.5	378.5	361.6	428.4	426.2	460.4	490.4

Table 6.4 Error in temperature to reach a given solid fraction (elevated pressure, 20°C/min)

Exp	Press (atm)	e_T				
		s_f=0.8	s_f=0.6	s_f=0.4	s_f=0.2	s_f=0.1
34	5	-0.0115	-0.0005	0.0102	0.0101	-0.0097
35	5	-0.0166	-0.0067	0.0058	0.0037	-0.0400
36	5	-0.0099	-0.0034	0.0079	-0.0007	-0.0313
37	5	-0.0052	0.0012	0.0187	0.0280	0.0021
38	5	-0.0093	-0.0069	0.0013	-0.0127	-0.0439
39	5	-0.0074	-0.0079	0.0006	-0.0072	-0.0422
40	5	-0.0113	-0.0023	0.0118	0.0141	-0.0167
41	5	-0.0039	-0.0040	0.0009	-0.0023	-0.0285
42	10	-0.0094	-0.0015	0.0132	0.0020	-0.0544
43	10	-0.0152	-0.0053	0.0117	-0.0051	-0.0638
44	10	0.0023	0.0121	0.0234	-0.0075	-0.0589
45	10	-0.0028	0.0059	0.0134	-0.0051	-0.0572
46	10	-0.0032	0.0074	0.0204	0.0032	-0.0419
47	10	-0.0049	0.0034	0.0173	0.0042	-0.0459
48	30	0.0045	0.0234	0.0383	-0.0047	-0.0852
49	30	-0.0056	0.0077	0.0337	0.0010	-0.0966
50	30	0.0151	0.0238	0.0405	0.0004	-0.0874
51	30	0.0237	0.0360	0.0688	-0.0013	-0.0729
52	30	0.0035	0.0234	0.0445	0.0053	-0.0652

Table 6.5 Statistics of error in temperature

Press	1 atm (N=18)		5 atm (N=8)		10 atm (N=6)		30 atm (N=5)	
sf	μ_{e_T}	σ_{e_T}	μ_{e_T}	σ_{e_T}	μ_{e_T}	σ_{e_T}	μ_{e_T}	σ_{e_T}
.8	.001	.009	-.0094	.004	-.0055	.006	.0082	.011
.6	.0022	.010	-.0038	.003	.0037	.006	.0228	.010
.4	.0012	.014	.0072	.006	.0166	.005	.0452	.014
.2	.0049	.016	.0041	.013	-.0014	.005	.0001	.004
.1	.0113	.015	-.0263	.017	-.0537	.008	-.0815	.012

The mean and standard deviation of the error at the various solid fractions and pressures are listed in Table 6.5. The mean and standard deviation are calculated as follows

$$\mu_{e_T} = \frac{1}{N}\sum_{i}^{N} e_T$$
$$\sigma_{e_T} = \left[\frac{1}{N-1}\sum_{i}^{N}(e_T - \mu_{e_T})^2\right]^{1/2} \qquad (6.3)$$

As discussed previously, we desire the error to be small (for the intended application) and not have significant systematic errors. The magnitudes of the errors are generally small. At ambient pressure (1 atm) the errors at various solid fractions have magnitudes less than 2 percent, except for a solid fraction of 0.1 where errors increase to over 3 percent. The mean error (Table 6.5) at ambient pressure is quite small, ranging from 0.1 to 1.1 percent depending on solid fraction. At higher pressures, the errors have larger magnitudes, particularly at solid fractions of 0.4 and 0.1 at 30 atm, where mean errors are 4.5 and 8 percent, respectively. The scatter in the error (standard deviation) does not appear to be greater at elevated pressures, and is nominally about 1 percent.

We can study a couple of statistics to test for systematic discrepancies in the error. First, we can look for a bias, that is, whether the mean error is different from zero. Because the error varies from experiment to experiment, we need to consider the scatter in the data relative to the discrepancy of the mean from zero. We can use the test statistic

$$T_e \equiv (\mu_{e_T} - 0)/(\sigma_{e_T}/\sqrt{N}). \qquad (6.4)$$

This statistic is a quantitative measure of the deviation of the mean value from, in this case, zero. It also provides a way to assess whether the bias is significant. Assuming the errors are normally distributed, we can calculate the probability that we would obtain an estimated mean value that deviates this much from zero (or more) by random chance. The Student's t-distribution is used to calculate this probability. Values of the statistic (Eq. 6.4) calculated using the data in Table 6.5, estimated mean and standard deviation, are listed in Table 6.6. Also given in Table 6.6 is the probability of a getting a value of T_e, or larger, by random chance. The smaller the probability, the stronger the evidence that the mean error is different from zero, or biased. The data indicate that it is probable that we could obtain the mean value seen for the ambient pressure data at all solid fractions except for the value seen at 0.1; there is only a 0.3 percent probability we would obtain a mean

value of .0113 (or larger) given that the true mean is 0. Similarly, at higher pressures, the probability is quite low that we would get the mean values seen given the true mean is zero. The conclusion is that the model appears to be biased (compared to the data) for low solid fractions at ambient pressure and at higher pressures.

In the preceding analysis, we have considered errors at various solid fractions and pressures independently, which is appropriate if we are interested in the ability to predict a specific mass fraction for a given pressure. We can also investigate the ability of the model to predict the effect of pressure on the decomposition. To assess this ability, we can study the dependence of the error on pressure. The effect is best demonstrated in Fig 5.1, where the TGA curve is shifted as a function of pressure. A statistic to quantify this effect is to look at the correlation structure of the error over pressure. The correlation coefficient is calculated as (Bethea et al., 1995)

$$r_\rho(e_T,P)=\frac{\sum_{i=1}^{N}\left(e_{T_i}-\bar{e}_T\right)\left(P_i-\bar{P}\right)}{\left[\left(\sum_{i=1}^{N}\left(e_{T_i}-\bar{e}_T\right)^2\right)\left(\sum_{i=1}^{N}\left(P_i-\bar{P}\right)^2\right)\right]^{1/2}} \qquad (6.5)$$

We tabulate the value of r_ρ^2 in next to last column of Table 6.6. We look at r_ρ^2 instead of r_ρ because r_ρ^2 is an indication of the proportion of variation in the error accounted for by linear relationship between the error and pressure. Again, assuming the errors are normally distributed we can calculate the probability that we would estimate a correlation this large (or larger) given that the "true" value is zero. This probability is also listed in the last column of Table 6.6. Interestingly, it is probable we could get correlation seen at solid fractions of 0.8 and 0.2, but highly improbable at solid fractions of 0.6, 0.4, and 0.1. The outcome suggests that the model systematically differs from the data at solid fractions of 0.6, 0.4, and 0.1 over the pressure range tested.

Table 6.6 Statistics of error in temperature

	T_e Statistic								r_ρ^2-statistic	
Press	**1 atm (N=18)**		**5 atm (N=8)**		**10 atm (N=6)**		**30 atm (N=5)**			
s_f	T_e	$Pr(t>T_e)$	T_e	$Pr(t>T_e)$	T_e	$Pr(t>T_e)$	T_e	$Pr(t>T_e)$	r_ρ^2	Pr
.8	.471	.322	6.60	.00015	2.25	.037	1.49	.105	.072	.109
.6	.933	.182	3.56	.0046	1.51	.096	4.56	.005	.388	$<10^{-4}$
.4	.365	.360	3.39	.0058	8.13	.00017	6.46	.001	.643	$<10^{-4}$
.2	1.29	.107	0.89	.202	0.686	.262	0.05	.481	.021	.395
.1	3.19	.003	4.36	.0017	16.44	$<10^{-4}$	13.58	$<10^{-4}$	.702	$<10^{-4}$

Table 6.7 Test statistics for error in solid fraction

Press (atm)	N	$\mu_{e_{sf}}$	$\sigma_{e_{sf}}$	T_e	Pr(t>T_e)
1	18	.0119	.0154	3.28	.0022
5	8	.0276	.0247	3.16	.008
10	6	.0542	.0189	7.02	.0004

Another comparison of the model to experimental data can be made similar to the way the model is used in the application. This comparison looks for the model's ability to predict the solid fraction at which decomposition is complete, i.e., can we identify the temperature at which the foam completes decomposition. We note that this temperature will likely be near the "tail" of the curve at ambient pressure, but adjusted to a higher solid fraction at higher pressures. Consequently, comparing the "tail" at elevated pressures where it is known that the decomposition produces liquids that dissolves and enhances the decomposition, although insightful for demonstration purposes, is not entirely relevant to assessing the model.

The process to evaluate a common temperature is shown in Fig 6.3, two tangent lines are drawn on the experiment curve (green line) on opposite sides of the "knee" in the curve. The intersection of the tangent lines defines the experimental temperature at which decomposition is assumed complete; call that temperature T_{burn}. Corresponding to this temperature is a solid fraction for the model and experiment. The value of this temperature is plotted as a function of pressure in Fig. 6.4. In this figure there doesn't appear to be much dependence on temperature (the r^2 is .0078). The error in the solid fraction (at T_{burn}) is defined as

$$e_{s_f} = s_{f\,\mathrm{mod}}\Big|_{T=T_{burn}} - s_{f\,\mathrm{exp}}\Big|_{T=T_{burn}} \qquad (6.6)$$

The error values are plotted in Fig. 6.5 and listed in Table 6.7. All values except one are positive at ambient pressure, suggesting a bias. Computing the T-statistic, Eq. (6.4), shows that it is unlikely that we would get the estimated mean given the model is unbiased (zero mean).

In this subsection we have looked at the error at various solid fractions separately, computing statistics of the error and the dependence on pressure. In the next sub section we study the solid fraction curve, looking at the error at different solid fractions jointly.

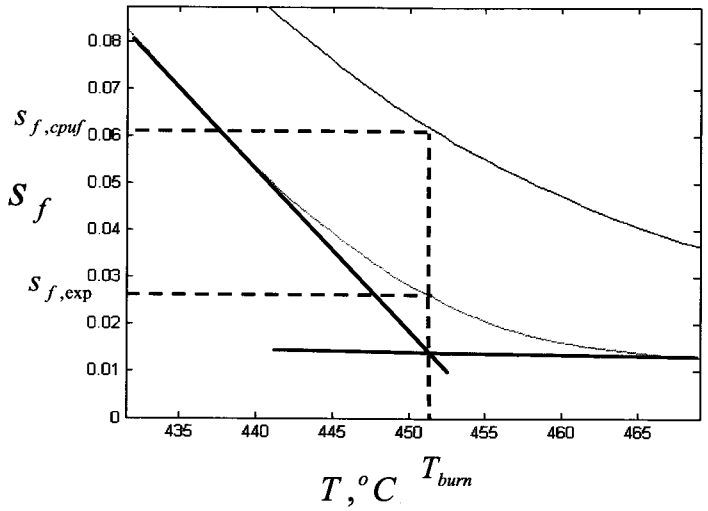

Figure 6.3 **Evaluating the element death (burnout) temperature**

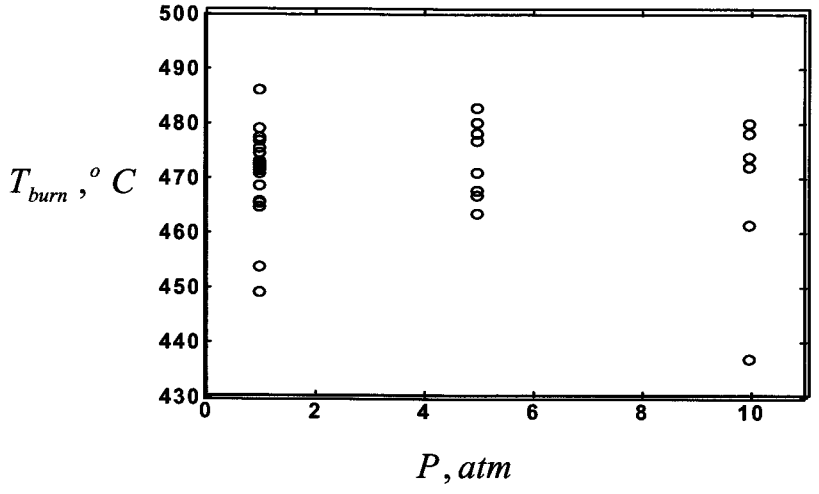

Figure 6.4 **Element death (burnout) temperature**

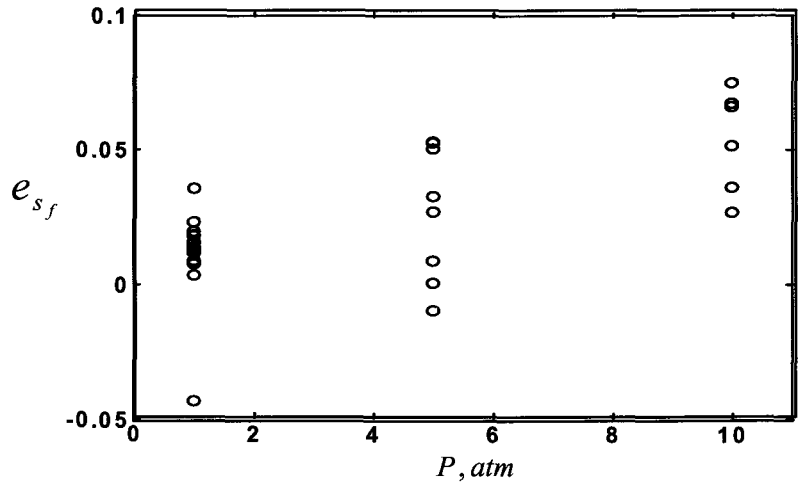

Figure 6.5 **Error (absolute) in solid fraction at "death" temperature as a function of pressure**

6.2.3 Predictive Testing

The foam model is essentially a constitutive relationship between mass and temperature (history) described by chemical kinetics. In this subsection we will study the model's ability to predict solid fraction over the range of the temperatures from the initiation to the completion of decomposition. The goal is to assess whether the systematic differences the model exhibited in the previous section could be due to model parametric uncertainty or measurement uncertainty.

Model predictions using the average activation energies are essentially the same for the eighteen experiments, the uncertainty in Figs. 5.4 and 5.5 represents the uncertainty for model results of all experiments at similar conditions (temperature and pressure). An overlay plot of the model predictions, including an uncertainty estimate, with experimental measurements is shown in Fig. 6.1. Although for validation we must proceed beyond the overlay plot or "vugraph norm," it is insightful to study the comparison for an overall fit of the model to the data. We note at ambient pressure that the experimental measurements are mostly within the model plus uncertainty. At higher pressure, the experimental data is consistently outside the model plus uncertainty at the "tail" of the curves where solid fraction approaches 0. We next consider a metric to compare model plus uncertainty to experimental measurement plus uncertainty.

A metric proposed by Hill and Trucano (1999) can be used to quantitatively assess the differences relative to the uncertainty in the differences. The statistic

$$r^2 = (s_{f,\exp} - s_{f,\mathrm{mod}})\,\mathrm{cov}^{-1}(s_{f,\exp} - s_{f,\mathrm{mod}})(s_{f,\exp} - s_{f,\mathrm{mod}})^T \qquad (6.7)$$

is used. The statistic involves the vector of differences and covariance of the differences. The statistic is a sum of the differences weighted by the inverse of the uncertainty (covariance) in the model and experiment. Differences with larger uncertainty are weighted less than differences with smaller uncertainty. Uncertainty in the differences has contributions from the model and experiment. Assuming the errors in the model and

experiment are independent the covariance for the difference between the experiment and model can be written as

$$\mathrm{cov}(s_{f,\mathrm{exp}} - s_{f,\mathrm{mod}}) = \mathrm{cov}(s_{f,\mathrm{exp}}) + \mathrm{cov}(s_{f,\mathrm{mod}}) \qquad (6.8)$$

Covariance of the model predictions comes from propagating the uncertainty in the activation energies through the model, Eq. (5.7). Assuming errors in experimentally measured solid fraction are independent, gives

$$\mathrm{cov}(s_{f,\mathrm{exp}}) = \sigma_s^2 \mathbf{I} \qquad (6.9)$$

where σ_s is the standard deviation of the measurement error and $\mathbf{I}$ is the identity matrix. We analyzed the TGA prior to the onset of decomposition and estimated the standard deviation in the solid fraction measurement to be 0.00125; see Section 4.2.4. Because we analyze data prior to the onset of decomposition, this estimate is expected to be a lower bound. An opinioned estimate of the measurement accuracy provided by the experimentalist suggested a factor of 4 to 6 increase in the lower bound. The two magnitudes of the experimental uncertainty for solid fraction used are σ_s=0.005 and 0.0075.

To evaluate the metric, data at discrete temperatures were used. In general, data at 24-28 equally spaced temperatures are used. Data collected during the initial time before decomposition started are not included. The comparison includes data beginning at the onset of decomposition (solid fraction near 0.99) and ending at completion of decomposition (solid fraction near 0.005).

The values of r^2 for the eighteen experiments at ambient pressure are listed in Table 6.8. Assuming the differences have a joint Normal distribution the r^2 statistic has a Chi-squared distribution. To assess the value of r^2 we calculate the probability that the math model would deviate from the experimental measurement as much or more simply by chance given that difference are described by $\mathrm{cov}(s_{f,\mathrm{exp}} - s_{f,\mathrm{mod}})$. In other words, what is the probability that the differences are consistent with model uncertainty and measurement uncertainty (consistent in the statistical sense that they come from the same population)? Using a threshold probability of 95 percent, we can calculate the maximum value of r^2 we expect to obtain given the differences are due to model and measurement uncertainty described by $\mathrm{cov}(s_{f,\mathrm{exp}} - s_{f,\mathrm{mod}})$; we define this value of r^2 as the critical value.

Two magnitudes of the experimental uncertainty are used to calculate the data listed in Table 6.8, σ_s=0.005 and 0.0075. At the lower measurement error (σ_s=0.005) threshold, it is improbable that the differences are described by $\mathrm{cov}(s_{f,\mathrm{exp}} - s_{f,\mathrm{mod}})$. Only two experiments (3 and 4) have a probability greater than .05 that the difference seen would happen by chance. If the measurement error is larger (σ_s=0.0075), only four experiments (2, 5, 8, 12) have a low probability of differences seen not being described by $\mathrm{cov}(s_{f,\mathrm{exp}} - s_{f,\mathrm{mod}})$.

We can gain some insight by looking at how the value of r^2 varies as more data is considered in the analysis. The value of r^2 calculated sequentially, i.e., consider the first data point, then first and second, then first, second and third, etc. until all data have been considered, are plotted in Fig 6.6 for the experiments 2, 5, 8, and 12, which all had low probability. The sequential analysis will indicate regions that contribute significantly to the total and will show where differences deviate from $\mathrm{cov}(s_{f,\mathrm{exp}} - s_{f,\mathrm{mod}})$. The sequential results show that significant contributions to r^2 are coming near the completing of decomposition. This outcome is an indication that there are additional errors, say unmodeled errors, outside of those we estimated with $\mathrm{cov}(s_{f,\mathrm{exp}} - s_{f,\mathrm{mod}})$. There are a couple of explanations for this outcome. First, the model is missing physics that the experiment contains. Second, model for the errors in the difference, $\mathrm{cov}(s_{f,\mathrm{exp}} - s_{f,\mathrm{mod}})$, is not an accurate estimate. We discuss the outcome of the test further after looking at data for higher pressure experiments.

Results for the r^2 metric applied to experiments at higher pressures is listed in Table 6.9 for two values of the experimental uncertainty, σ_s=0.01 and 0.015. At the lower value of measurement uncertainty, all outcomes have low probability (by chance) for 10 and 30 atm while some outcomes are probable for experiments at 5 atm. The situation is better if a larger measurement uncertainty is assumed. Only isolated outcomes have a low probability. As the sequential values of r^2 plotted in Fig 6.7 show, deviations in the tail contribute significantly to the total.

The preceding analysis considered comparing experiments to the model individually. Next, we will consider groups of two or more experiments. The same metric can be applied, but this requires us to decide how the errors between multiple experiments are related. One way to proceed is to assume independence between the errors from different experiments. Then the errors for multiple experiments can be modeled as a matrix with block diagonal contributions of the error from the single experiments

$$\mathrm{cov}(s_{f,\mathrm{exp}} - s_{f,\mathrm{mod}})\Big|_{\mathrm{exp}\,i,\mathrm{exp}\,j} = \begin{bmatrix} \mathrm{cov}(s_{f,\mathrm{exp}} - s_{f,\mathrm{mod}})\Big|_{\mathrm{exp}\,i} & 0 \\ 0 & \mathrm{cov}(s_{f,\mathrm{exp}} - s_{f,\mathrm{mod}})\Big|_{\mathrm{exp}\,j} \end{bmatrix}. \qquad (6.10)$$

where $\mathrm{cov}(s_{f,\mathrm{exp}} - s_{f,\mathrm{mod}})\Big|_i$ is the uncertainty due to model parameters and measurement uncertainty estimated from Eq. (6.8) using data for exp *i*. With this model for the uncertainty of multiple experiments, the probability is exceedingly small that the differences are represented by our estimate of $\mathrm{cov}(s_{f,\mathrm{exp}} - s_{f,\mathrm{mod}})\Big|_i$. A possible explanation is that the error, modeled as independent between experiments, is not independent. While the differences for a single experiment could be described by modeled error (model parameter uncertainty plus measurement uncertainty), the differences have a systematic dependence over multiple experiments that is not included in Eq. (6.10).

The outcome of the metrics studied here are directly dependent on an estimate for the measurement error. We mostly "pass" for individual experiments at ambient pressure

for measurement uncertainty σ_s=0.0075, but "fail" for σ_s=0.005. Without data to directly estimate statistics of the measurement error, we are only left to speculate on its effect.

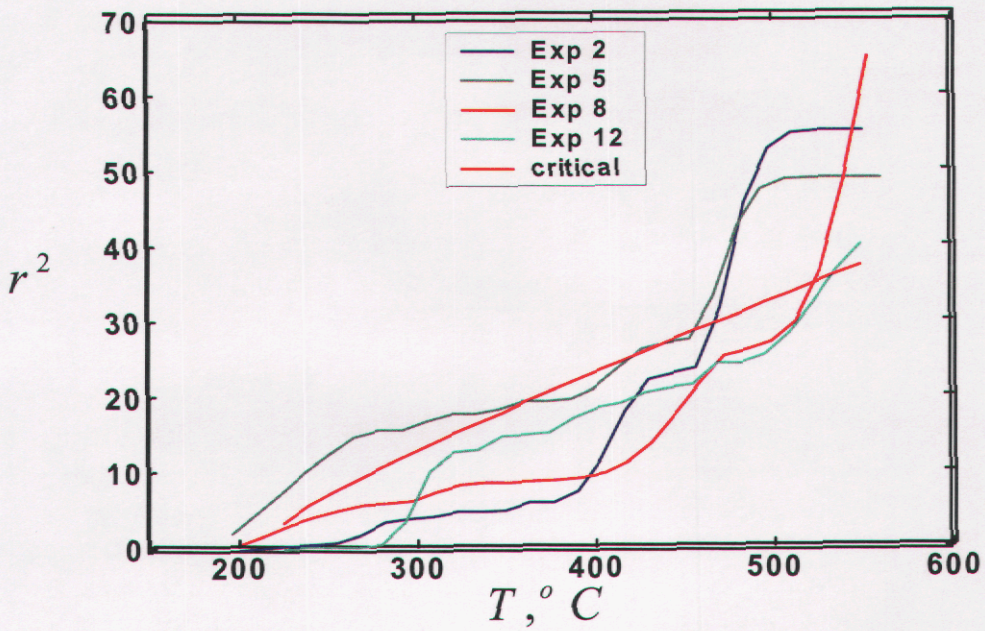

Figure 6.6 **r^2 statistic for comparing experiment and model, ambient pressure TGA**

Table 6.8 Statistical test of differences weighted by uncertainty

Exp	Heat Rate (C/m)	Pres (atm)	Lab	Df	$r^{2'}$ $\sigma_s = .005$	$Pr(r^2 > r^{2'})$ $\sigma_s = .005$	$r^{2'}$ $\sigma_s = .0075$	$Pr(r^2 > r^{2'})$ $\sigma_s = .0075$
1	20	1	SNL	28	41.7	.045	23.5	.709
2	20	1	SNL	27	113.3	10^{-12}	55.4	.001
3	20	1	SNL	28	33.1	.231	16.6	.957
4	20	1	SNL	28	29.2	.403	14.4	.984
5	20	1	SNL	28	107.7	10^{-11}	49.0	.008
6	20	1	SNL	26	49.1	.004	24.2	.567
7	20	1	SNL	28	68.1	.00003	32.8	.243
8	20	1	SNL	27	119.9	10^{-13}	65.2	0.0001
9	20	1	SNL	27	23.5	.656	11.2	.997
10	20	1	SNL	24	48.8	.002	22.4	.554
11	20	1	SNL	27	51.4	.003	25.9	.527
12	20	1	SNL	25	77.1	10^{-7}	40.2	0.028
13	20	1	SNL	26	42.9	.020	20.9	.747
14	20	1	SNL	26	52.0	.002	25.9	.470
15	20	1	BYU	28	45.4	.020	23.5	.707
16	20	1	BYU	28	33.9	.205	19.0	.897
17	20	1	BYU	28	52.7	.003	25.3	.610
18	20	1	BYU	28	47.0	.014	25.3	.614

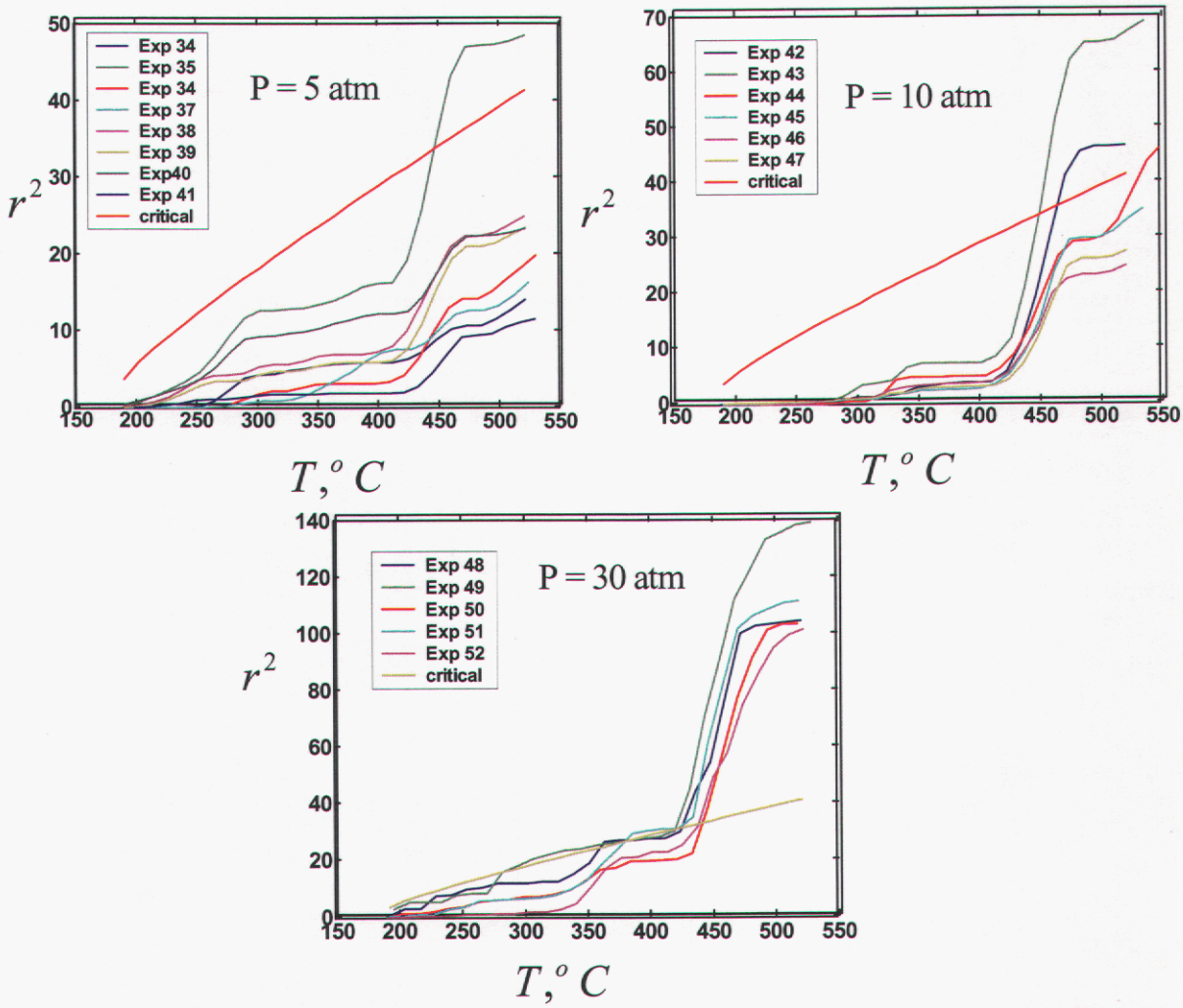

Figure 6.7 **r^2 statistic for comparing experiment and model, high pressure TGA**

Table 6.9 Statistical test of differences weighted by uncertainty

Exp	Heat Rate (C/m)	Press (atm)	Lab	Df	$r^{2'}$ $\sigma_s = .01$	$Pr(r^2 > r^{2'})$ $\sigma_s = .01$	$r^{2'}$ $\sigma_s = .015$	$Pr(r^2 > r^{2'})$ $\sigma_s = .015$
34	20	5	BYU	28	24.7	.645	14.1	.986
35	20	5	BYU	28	82.5	.0095	48.5	.010
36	20	5	BYU	28	36.6	.128	19.8	.870
37	20	5	BYU	28	30.4	.345	16.3	.960
38	20	5	BYU	28	46.6	.015	25.0	.629
39	20	5	BYU	28	44.1	.027	23.5	.710
40	20	5	BYU	28	40.9	.055	23.3	.717
41	20	5	BYU	28	22.1	.776	11.5	.997
42	20	10	BYU	28	75.9	.000002	46.5	.015
43	20	10	BYU	28	115.2	10^{-12}	68.7	.00003
44	20	10	BYU	28	87.9	10^{-08}	46.5	.015
45	20	10	BYU	28	62.1	.0002	35.1	.167
46	20	10	BYU	28	42.1	.043	25.0	.630
47	20	10	BYU	28	46.9	.014	27.5	.490
48	20	30	BYU	28	183.2	0	104.5	10^{-10}
49	20	30	BYU	28	240.5	0	139.0	0
50	20	30	BYU	28	177.8	0	103.3	10^{-09}
51	20	30	BYU	28	203.4	0	111.2	10^{-11}
52	20	30	BYU	28	165.7	0	101.6	10^{-09}

6.2.4 Summary of Metrics for TGA Experiments

The assessment shows that CPUF is an accurate representation of the experiments for ambient pressure conditions and solid fractions greater than 0.1. CPUF predicts the solid fraction at ambient pressure with errors in the temperature that have a mean less than 0.005 and standard deviation less then .016 for solid fractions greater than 0.1. The errors increase in magnitude at lower solid fractions; the mean and standard deviation are 0.0113 and 0.015 at a solid fraction of 0.1 and the mean error is (statistically) different from zero, meaning we have a bias.

Further analysis, based on metrics that assessed the error in solid fraction (differences between experiment and model) relative to the uncertainty, showed that differences were consistent with the uncertainty we estimated due to measurement and model uncertainty for most experiments considered individually. However, when the comparison was made for multiple experiments simultaneously, the differences were outside that estimated by model and measurement uncertainty, suggesting the presence of systematic errors between experiments. Possible systematic errors could be ...

The ambient pressure comparisons indicate that CPUF is biased, relative to the experimental data, in predicting the dependence of mass fraction on temperature at solid fractions less the 0.1. It is statistically probable that the uncertainty (due to model parameters and experimental measurements) is the source of the bias for a single experiment, but it is highly improbable that uncertainty is the source for multiple experiments. A similar bias (outside of the uncertainty) is seen at pressures greater than ambient. The bias demonstrates a dependence on pressure.

Because models only approximate the physical world, we should expect a bias. Deciding whether the bias is significant ultimately should be judged by the application requirements. In the absence of specific requirements, it is difficult for the analysts performing the validation to specify acceptance criteria. We do remark, however, that the error (in predicted temperature to reach a prescribed solid fraction) of CPUF relative to TGA experiments is relatively small at ambient pressure, mean value 0.011 and standard deviation of 0.015 at a solid fraction of 0.1. While the error increases in magnitude at higher pressures and demonstrates a dependence on the pressure, it is still less than 0.1. Based on engineering judgment, the model would appear to adequately represent the physics.

6.3 Benchmark Data

6.3.1 Choice of Prediction Variable

The model data and experimental measurements are plotted in Fig 6.8. Model data (connected symbols) and experimental measurements (symbols) are overlaid on the plots. Model uncertainty is omitted from this figure for clarity, but is shown in Fig. 5.8 for reference. Three plots are include in Fig 6.8. The first plot shows repeated experiments for a single boundary temperature, the second plot show the effect of orientation and the third plot shows the effect of boundary temperature. We consider the 9 experiments shown in Fig 6.8 to assess the model.

The nine experiments are plotted in groups to assess the repeatability of the experiment (Fig 6.8a), the effect of orientation (Fig. 6.8b), and the effect of boundary temperature (Fig 6.8c). A notable characteristic observed in Fig 6.8 is that the model results are consistently above the experimental measurements, indicating that the time for the experiment to recess a given distance is longer than the model predicts. The consistent offset could indicate evidence of a bias. We investigate this further in this section.

Data available to assess the model is front location as a function of time. A pertinent question is: What characteristic of the response do we need to predict for the application? Do we need to predict the dynamic response of front location, or characteristics of the response like the slope of the front location curve or a point on the front location curve? The answer to this question will focus the analysis to what is important for the application and not over work the problem. Unfortunately, in many validation activities at the single physics and simple coupled physics, Tier 1 and Tier 2 (Trucano et. al), respectively, the application requirements are loosely related to the variables that can be measured, predicted, and compared. We are in that position in this study. One can make a case that the time to uncover a component is important to predict in the application. However, the relationship between "time to expose a component in the application" and time-resolved front location, or another characteristic of that relationship, is sketchy, at best. In these cases, the way to proceed is understand the accuracy for variables that can be studied in the validation activity. Then, understand the relationship between the validation activities (and variables compared) and the system application (and variables we need to predict).

As a demonstration, we will study a representative scalar from the data, that being the slope or velocity of the front for one metric (Section 6.4.2). Because front location as a function of time is nearly linear it is reasonable to consider the slope, i.e., velocity, as a representative measure of performance. Then, a second study will assess based on the front location as a function of time curve (Section 6.4.3).

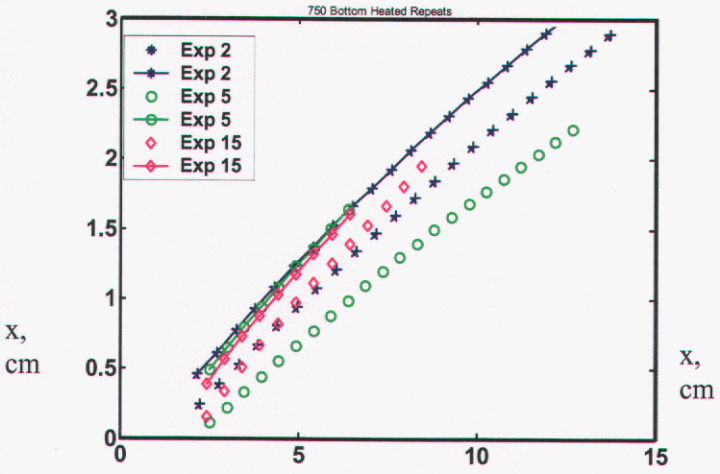

a) repeat experiments (750 °C)

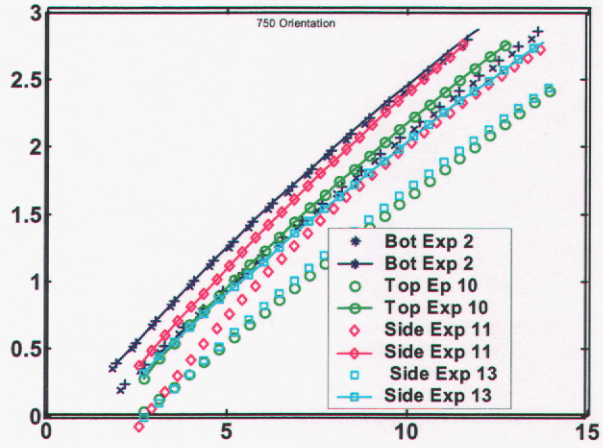

b) effect of orientation (750 °C)

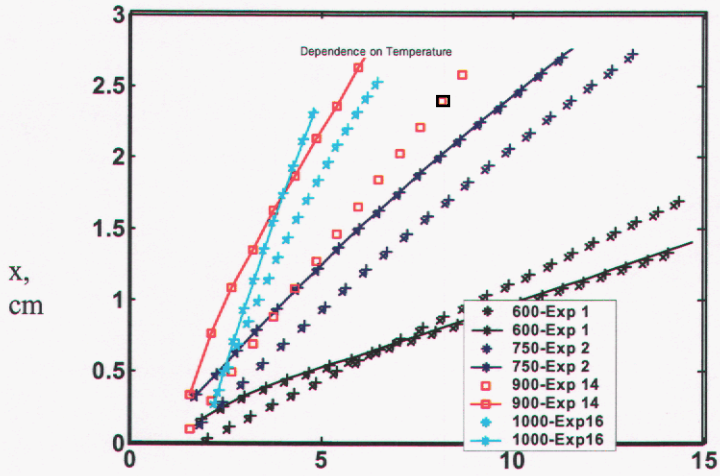

c) effect of BC temperature (bottom heated orientation)

Figure 6.8 Benchmark data (front location as a function of time) comparing experimental measurements with model predictions

6.3.2 Error Estimation

Two factors were explored in the experimental database:

1. Steady cup temperature (Temp): $600 \le T(^{o}C) \le 1000$,
2. Heating orientation (Orien): 1=Top, 2=Side, 3=Bottom

The relevant data are summarized in Table 6.10 and presented as a series of scatterplots in Figure 6.9. Here Vm is the measured recession velocity and Vp is the predicted recession velocity using the CPUF model with nominal values for the various parameters. The recession velocity is calculated from the time it takes the front to go from 1 cm to 2 cm of decomposition. Table 6.10 also provides some summary statistics for the last four columns. These statistics are defined by,

$$\text{Mean}: \bar{z} = \frac{\sum_{i-1}^{Ndata} z_i}{Ndata}$$

$$\text{Standard deviation}: S = \left[\frac{\sum_{i-1}^{Ndata} (z_i - \bar{z})^2}{Ndata - 1} \right]^{1/2} \qquad (6.11)$$

$$\text{Correlation coeffifient}: r_{\rho}(y;z) = \frac{\sum_{i=1}^{Ndata} (y_i - \bar{y})(z_i - \bar{z})}{\left[\left(\sum_{i=1}^{Ndata} (y_i - \bar{y})^2 \right) \left(\sum_{i=1}^{Ndata} (z_i - \bar{z})^2 \right) \right]^{1/2}},$$

and evaluated using built-in functions available with Microsoft Excel. Note from Figure 6.9 that the measured recession velocity is significantly dependent on the cup temperature (as indicated by the square of the correlation coefficient, r_{ρ}^2 (V_m;Temp). A useful model should be able to capture the observed dependence of recession velocity on cup temperature.

Table 6.10 Summary of information used for quantitative assessment of the Polyurethane foam model (CPUF)

Test #	Temp °C	Heating Orientation	Internal Components?	V_m (cm/min)	V_p (cm/min)	$e=\ln(V_m/V_p)$	e'
2	750	3	1	0.2323	0.2457	- 0.0561	0.073534
5	750	3	2	0.1958	0.2840	- 0.3719	0.238434
10	750	1	1	0.2110	0.2343	- 0.1047	0.005424
11	750	2	1	0.2582	0.2620	- 0.0146	-0.02632
13	750	2	1	0.2154	0.2279	- 0.0564	0.015476
15	750	3	2	0.2755	0.2840	- 0.0304	-0.10306
1	600	3	1	0.1307	0.0913	0.3588	-0.14687
14	900	3	1	0.3483	0.4498	- 0.2557	0.078757
16	1000	3	2	0.5578	0.7698	- 0.3221	-0.13537
			Mean:	0.269	0.317	-0.095	4.32E-17
			Standard deviation	0.123	0.193	0.216	0.122
			r_ρ^2(y;Temp)	0.895	0.930	0.591	1.85E-29
			r_ρ^2(y;Orien)	0.064	0.075	0.006	2.37E-30

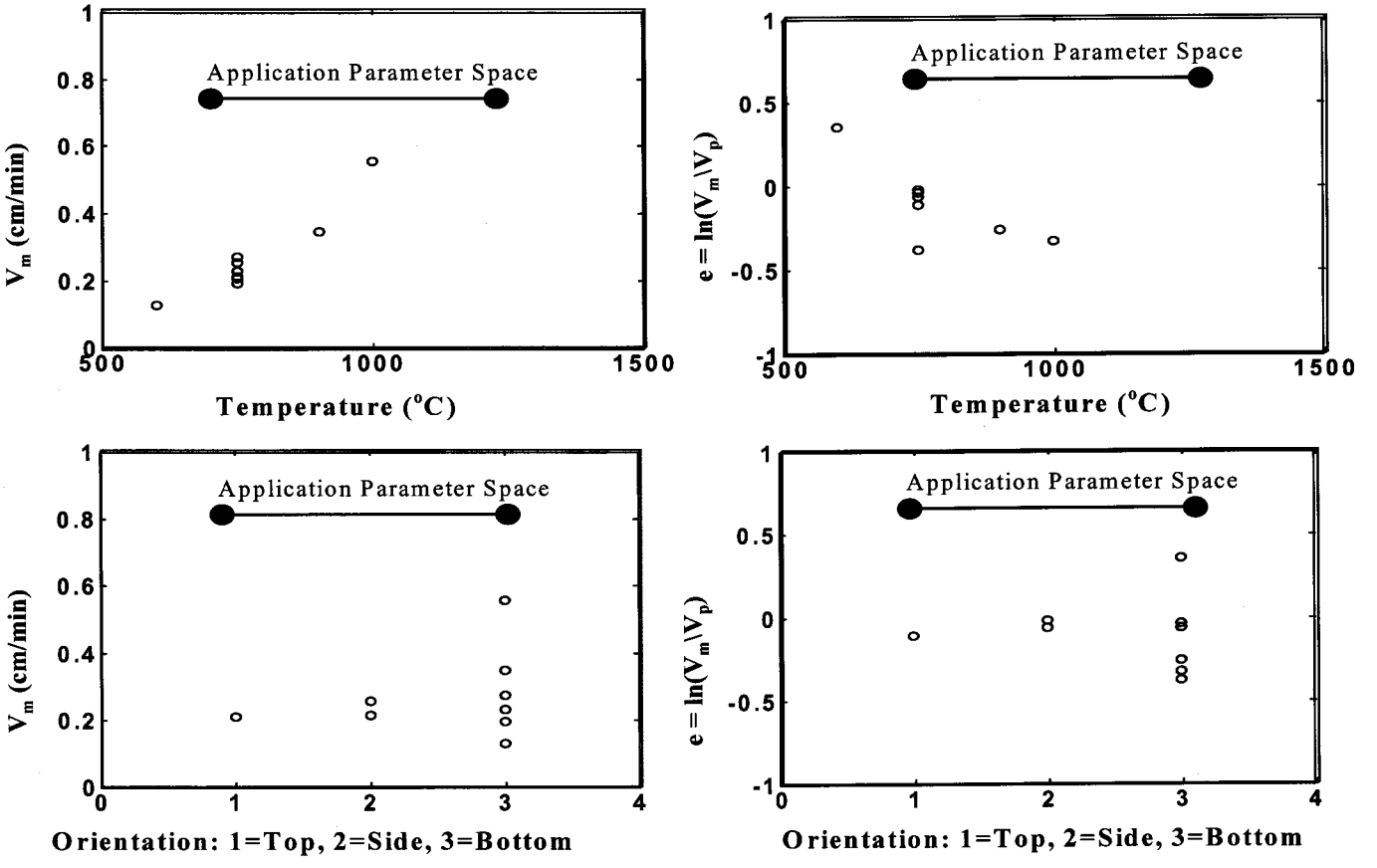

Figure 6.9 Scatterplots of measured recession velocity, Vm, and errors, $e=\ln(V_m/V_p)$, as a function of cup temperature and heating orientation.

The error[1], $e = \ln(V_m/V_p)$, in Table 6.10 is computed for each test within the database. Scatterplots of the errors are also shown in Figure 6.9. Qualitatively, a "valid" model is one in which the mean error ($\bar{e}$) is "small". Furthermore, a "valid" model must also capture all the effects (or absence of effects) of the factors explored in the database. To quantify these "association" effects, the square of the correlation coefficients,

$$r_\rho^2(e; \text{Temp})$$
$$r_\rho^2(e; \text{Orien})$$

are used as metrics. The statistic, r_ρ^2, measures the fraction of variability in e that can be explained by the variability in the tested parameter, assuming a linear association. Qualitatively then, for a model to be valid, it is expected that all the r_ρ^2s should also be "small".

In each scatterplot in Figure 6.9, the parameter space expected in the real weapon application is indicated. The application parameter space is straight forward with regard to orientation and embedded components. There are credible scenarios that heat the weapon from various orientations and the heating orientations of top, side, and bottom span the possibilities. With regards to embedded components, the application focus is on regions that have embedded components, but there are other heat transfer paths involving foam that do not have embedded components. Consequently, the database spans the application parameter space with regard heating orientation and embedded components. This should be a goal, although not always realizable, of good validation experiments.

Assessment of the application parameter space with regards to temperature is more complex. The experiments where conducted in such a way that the cup temperature was ramped from ambient to the target temperature over approximately 1.5 minutes and then held constant; consequently, foam recession occurs under conditions of predominately constant temperature (see Figure 6.1). In a weapon, foam recession occurs predominantly under conditions of a nearly constant temperature *ramp*. This is illustrated in Figure 6.10, which shows the predicted temperature response at two locations on the metal housing that immediately surrounds foam-embedded critical components in real weapon geometry, Romero (2002). The two locations approximately bound the spatial variation in the temperature response over the housing. Note that it takes approximately 30 minutes for the housing temperature to plateau at one location, and it still hasn't reached the temperature of the fire that radiates directly to the housing. The other location responds more rapidly, with the temperature reaching 900°C at 6 min then increases slowly toward the fire temperature. For simplicity, we have noted the range of credible fire temperatures on the scatterplot. An alternative perspective is to note that any given transient passes through a spectrum of temperatures that is not too different from what is noted on the scatterplots. Both these perspectives are oversimplifications, and we recommend that future testing be

[1] The measured velocities differ by a factor of ~5 (largest over the smallest). Here, we have opted to use logarithmetic errors, but we might just as well have used absolute errors ($e=V_m-V_p$).

performed under conditions of temperature ramps as opposed to constant temperature conditions.

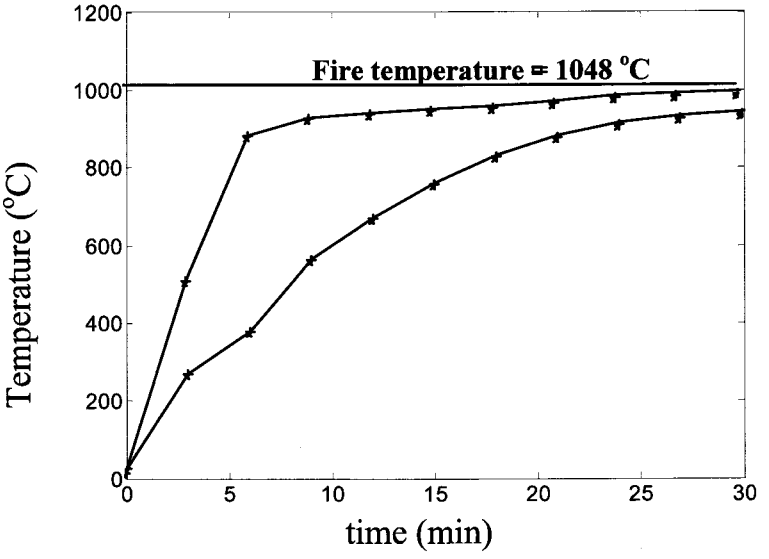

Figure 6.10 Temperature transient of metal housing surrounding foam-embedded critical components

The approach taken here to quantify validation judgments is in the spirit of Easterling (2002) and Rutherford and Dowding (2003), who applied their perspectives to the same application and data we are addressing here. Easterling focused more explicitly on characterizing bias, while Rutherford also addressed association effects. Rutherford did this by performing linear regression and examining the slope terms and their covariance. Here, we have chosen to focus on the r_ρ^2 statistic as a measure of association because we believe that it provides a useful, intuitive illustration as well as a framework for judging model validation in this application.

Table 6.10 suggests that mean error and some of the r_ρ^2 values may not be "small", but a discussion of how small is small enough will be deferred. These statistics are only estimates of true population values because they are based on a finite number of tests. Larger or smaller databases, as well as replicate databases of the same size, will yield different estimates of these statistics. Bootstrap techniques (Davison and Hinkly, 1997) can be used to estimate confidence intervals for these statistics. The bootstrap technique involves 4 steps:

1. Regression: The goal is to separate the errors (the e_i's) into two contributions. The first contribution captures any association with the factors explored as part of the database (x_i's) ensuring that the second contribution (the e'_i) more nearly represents random errors from factors not explored in the database. For the current problem, we have:

$$e_i = \left[\beta_0 + \sum_{j=1}^{Nfactors} \beta_j x_{i,j}\right] + e'_i \quad \text{for i = 1 to Ndata} \qquad (6.12)$$

where,

	β_0=-0.9654
x_1=Temp	β_1=0.0013
x_2=Orien	β_2=-0.0583

and the $\{e'_i\}$ are given in Table 6.10

2. Resampling: Compute a representative "sample" (index k),

$$^k e_i = \left[\beta_0 + \sum_{j=1}^{Nfactors} \beta_j x_{i,j}\right] + {}^k e'_i \quad \text{for i = 1 to Ndata} \qquad (6.13)$$

where members of the set $\{{}^k e'_i\}$ are chosen randomly, and with replacement, from the set $\{e'_i\}$.

3. Statistics: Compute the validation relevant statistics ($^k\bar{e}$ and each of the $^k r^2$'s) for the k^{th} "sample".

4. Confidence intervals: Repeat steps 2 and 3 a large number of times to generate "distributions" of the validation relevant statistics. In the current problem, the number of "samples" was taken to be $N_k=10^4$.

Steps 1 and 3 was accomplished with features available in Microsoft Excel, while Steps 2 and 4 were accomplished with the aid of commercially available software (@Risk, Palisade Corporation), which is an add-on to Microsoft Excel. The results are shown in Figure 6.11

With high (90 percent) confidence we can state the mean error is not zero. The initial reaction might then be to judge the model invalid. This "hypothesis testing" line of reasoning is flawed, however, because the standard error of the mean (one standard deviation of the distribution of the mean) is inversely proportional to the square root of the number of tests. With sufficient testing, it will always be concluded (with high confidence) that the mean error (or any other statistic of interest) is not zero.

All models are "wrong"; but some are more useful than others. *Validation* ideally should be judged in terms of usefulness of a model for a given application. Unfortunately, objective application-specific requirements are often not available; consequently, the validation analyst must establish acceptance criteria based on experience and judgment as to what *might* be useful in the application and apply those judgments within the constraints of the database. No application-specific requirements are available here:

consequently, it is judged that the mean error (bias) should not be greater than[2] +/-0.25. Furthermore, we judge that all the r_p^2s should also be less than 0.25. This implies that any correlation of errors with a tested factor is "secondary" and can reasonably be ignored. These acceptance limits are noted on each plot in Figure 6.11.

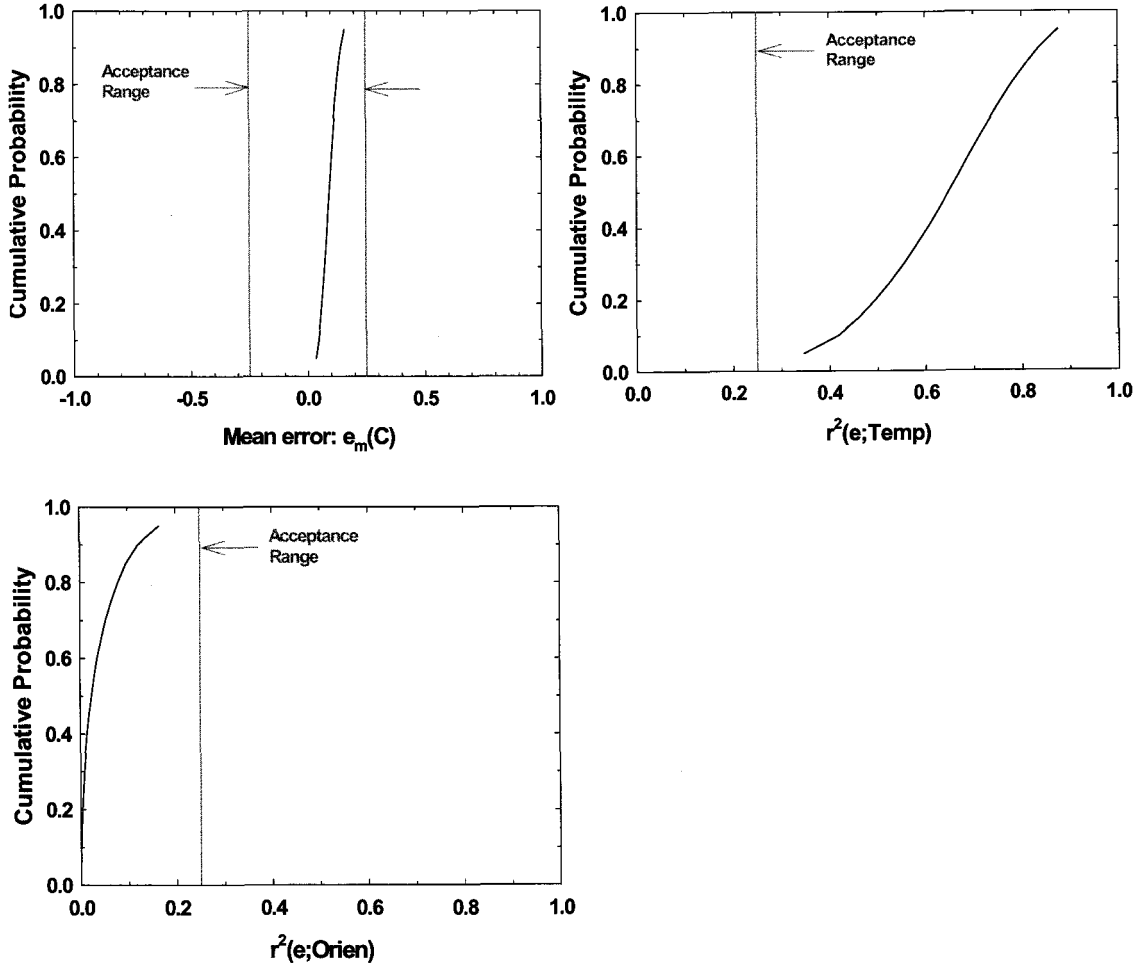

Figure 6.11 Distribution of important statistics supporting assessment of validation

Table 6.11 Quantitative assessment of model validation

[2] Note that the logarithmetic error is dimensionless and is approximately equal to the relative error [e~(VM-VP)/VP] when Vm/Vp is near unity. Consequently, the acceptance criteria is essentially equivalent to saying that the bias should be no more that +/-0.25.

	Acceptance Range		Distributional Values		
	Min	**Max**	**0.05**	**0.50**	**0.95**
Mean error	-0.25	0.25	0.035	0.093	0.161
r_ρ^2(e;Temp)	0	0.25	0.347	0.649	0.877
r_ρ^2(e;Orien)	0	0.25	0.000	0.023	0.166

Table 6.11 summarizes the graphical information in Figure 6.11 for the purpose of judging model validation. If we chose to judge validation based on "high confidence" then the 5th percentile and 95th percentile of the statistics $\bar{e}$ and r_ρ^2 should lie within the acceptance intervals. There are notable exceptions to this requirement. Clearly the model does not capture the effects of cup temperature or embedded components. This conclusion is not significantly changed even if validation is judged based on "nominal" (i.e. the 50 percentile of the statistic) values of $\bar{e}$ and all r_ρ^2s. Consequently, we would conclude that the model is *not* valid for the intended application. These conclusions would be more robust if a more formal (statistical design of experiments) approach were taken to define the test matrix.

It is outside the scope of this assessment to suggest improvements to the model. However, it is useful to briefly outline how the model *could* have been used in weapons assessments had there been no significant correlation of the errors with any of the factors explored in the database. There are two basic approaches. The first involves characterizing the distribution of errors and using this distribution directly in the weapons assessments. Here, we would like to say that[3]

$$\text{Reality} = \text{Predition} * e^{\text{error}}$$

so that any call to the model can be modified by a stochastic contribution. To be useful, we would like the error term to be represented by a probability distribution, such as a normal distribution, error = $N(\bar{e};S_{unit/unit})$ with a mean, $\bar{e}$ and a standard deviation, $S_{unit/unit}=sqrt(V_{unit/unit})$. Note that the variability embodied in the data (V_{data}) is comprised of three contributions,

$$V_{data} = V_{unit/unit} + V_{setup/setup} + V_{diagnostic}.$$

Here, $V_{unit/unit}$ represents the unit-to-unit variability. It reflects material property variabilities and manufacturing variabilities. $V_{setup/setup}$ represents the setup-to-setup variabilities of the experiment such as boundary conditions that cannot be applied in a precise and completely repeatable fashion from experiment to experiment. Lastly,

[3] Had we defined errors in absolute terms, e- Vm-Vp, then we would write: Reality = Prediction + Error

$V_{diagnostic}$ represents the variability of the diagnostic (in this case a thermocouple) from test to test.

The advantages of this approach are that it is a natural extension of the methodology used here to judge validation and that many factors can be captured (directly through testing) in the single error term. However, there are several disadvantages as well. The characterization of errors derived from data must be representative of the application parameter space; consequently, the approach may not be justifiable when significant extrapolation to the application parameter space is involved or when the database is not fully relevant to the application (e.g., constant temperature tests as opposed to application-relevant temperature ramp testing). Both the model *and* the error terms should be physics-based when significant extrapolation is required. In addition, the approach is only workable when the model is "separable" from all the other physics so that the stochastic modifier can be applied to the specific model.

The second approach for using a validated model in a weapon application is to characterize the sources of variability that contributed to the random distribution of errors characterized in the validation assessment. This involves a careful assessment of variability in the constitutive parameters, material properties, geometry, initial conditions, boundary conditions, and diagnostics. The advantages of this approach are two-fold: the separability constraint noted above is not an operable, and extrapolation is inherently physics based (eliminating sources of experimental variability that are not application-relevant and supplementing with additional sources of variability that might become important in the application parameter space). However, there are several drawbacks as well. It is difficult to establish conclusively that you understand what the dominant sources of variability are in the experiment. The variability study itself, can be computationally prohibitive. Lastly, some potentially dominant sources of variability (e.g., unit/unit variability) are very difficult or impossible to quantify because of the numerous intangibles associated with manufacturing.

6.3.3 Predictive Testing

In this section, we analyze the difference between the experiment and computer model over the whole curve of front location as a function of time, Hills et al. (2002). The effects of model uncertainty and experimental uncertainty are included in the analysis.

Model Validation: Single Data Sets

We measure the differences between the model results and the experimental observations in terms of a validation metric. Because we can approximate our model results as normally distributed, Hills et al. (2002), and because our measurement uncertainty is assumed to be normally distributed (see below), the difference between the two will also be normally distributed. This allows us to use the metric defined by Hills and Trucano (1999, 2001) for correlated, normally distributed differences to evaluate consistency between the experimental results and the model results. This metric is given by

$$r^2 = (\boldsymbol{x}_{model} - \boldsymbol{x}_{exp})^T \boldsymbol{cov}^{-1}(\boldsymbol{x}_{model} - \boldsymbol{x}_{exp})\ (\boldsymbol{x}_{model} - \boldsymbol{x}_{exp}) \qquad (6.14)$$

where

$$\boldsymbol{cov}(\boldsymbol{x}_{model} - \boldsymbol{x}_{exp}) = \boldsymbol{cov}(\boldsymbol{x}_{model}) + \boldsymbol{cov}(\boldsymbol{x}_{exp}) \qquad (6.15)$$

$\mathbf{cov}(\mathbf{x}_{model})$ was estimated from Eq. (5.8).

We do not have a good characterization for the uncertainty in the measurements. We will assume that the measurements are normally distributed, independent, with a variance given by

$$\boldsymbol{cov}(\boldsymbol{x}_{exp}) = (0.075)^2\, \boldsymbol{I} \qquad (6.16)$$

where **I** is the identity matrix of the appropriate size (number of measurements by number of measurements). If both the model results and the experimental observations are normally distributed, then r^2 is distributed as $\chi^2(df)$ (chi-square) where df is the degrees of freedom (number of measurements, or more strictly speaking, the rank of $\mathrm{cov}(\mathbf{x}_{model} - \mathbf{x}_{exp})$).

Results for applying the metric in Eq. (6.13) to experiments at the boundary temperatures of 600°C, 750°C, and 900°C are given in the first three rows of Table 6.12. The table lists the experiment number, boundary temperature, heating orientation, presence of a component, degrees of freedom, value of Eq. (6.13) for this experiment, and cumulative probability. The cumulative probability is based on the $\chi^2(df)$ distribution. Note that the 600°C experiment (exp 1, first row) shows a valid model would give this value for r^2 or larger 99.9 percent of the time. Clearly, we have no evidence to reject this model as valid for 600°C.

The probability that a valid model would give the value for r^2 or larger for the 750°C and 900°C cases, rows 2 and 3 of Table 6.12, respectively, is 0.20 and $<10^{-6}$, respectively. While we do not have sufficient evidence to reject the model at 750°C, we do for the 900°C case. It is very unlikely that by chance a valid model would result in a r^2 of 233 for 51 measurements.

These results are further illustrated in Figures 6.12 through 6.14. Figure 6.12 clearly illustrates that the model is not rejectable largely because there is considerable uncertainty in the validation exercise due to the model prediction uncertainty. This is illustrated by the large error bars. Note that the error bars actually include negative front locations at latter times. These results are clearly suspect, probably do to a failure of the locally linear approximation for the model. In contrast, the results for 750°C and 900°C shown in Figures 6.13 and 6.14 appear to be more reasonable. The uncertainty is not nearly as large and negative values for front location are not found within the uncertainty bars. The experimental data in Figure 6.13 are clearly within the error bars but the errors are correlated. While it would be dangerous to infer validity from this figure due to this correlation, the metric defined by Eq. (6.13) properly accounts for this correlation and the result in Table 6.11 indicates that there is not sufficient evidence to reject this model. This partially answers the question posed in a previous section - is the correlation in differences

due to parameter uncertainty, or due to a failure of the model to represent the physics (or both)? Because the 750°C results have a 0.20 significance, the correlation in the error does appear to be at least partially due to correlation induced by the model parameters.

Figure 6.14 illustrates the 900°C case where most of the experimental data lie outside the uncertainty bounds. This apparently poor agreement between experiment and prediction is consistent with the low probability for this result, as indicated in Table 6.11.

The results discussed above are for three similar experiments at different temperatures. Data was also provided for different experimental configurations for the 750°C case. These different configurations were summarized in Table 4.2. Here we repeat the above analysis for the remaining sets of 750°C data. We used linear interpolation of the sensitivity coefficients for experiment 2, to estimate sensitivity coefficients at the measurement times for experiments 5, 10, 11, 13, and 15. We start with evaluating model consistency using all of the data. Results are given in Table 6.12

Note that the differences between model results and experimental measurements for experiments 5, 11 and 13 have a low probability of being generated from a valid model, while the results from experiments 10 and 15 have a significantly higher probability. Inspection of the figures comparing the model and experiment data (Hills et al., 2002) indicates that for experiment 10, the model results and the experimental observations are shifted but have similar slopes. In contrast, the results for experiments 11 and 13 have different slopes at later times. The higher significance value for experiment 10 is due to the shift being consistent with the uncertainty in the parameters, whereas for experiments 11 and 13, the observed changes in slope are not consistent. This emphasizes the need to properly account for correlation between model results in developing metrics for time dependent models.

Table 6.12 Statistical test of differences weighted by uncertainty using all data

Exp	BC Temp (°C)	Heating Orien	Internal Comp	df	$r^{2'}$	$Pr(r^2 > r^{2'})$
1	600	Bottom	None	110	36.8	0.999
2	750	Bottom	None	79	89.3	0.200
14	900	Bottom	None	51	233.3	10^{-6}
5	750	Bottom	SS	9	23.8	0.0047
10	750	Top	None	100	111.3	0.207
11	750	Side	None	116	202.0	10^{-6}
13	750	Side	None	100	280.0	10^{-6}
15	750	Bottom	AL	9	8.58	0.477

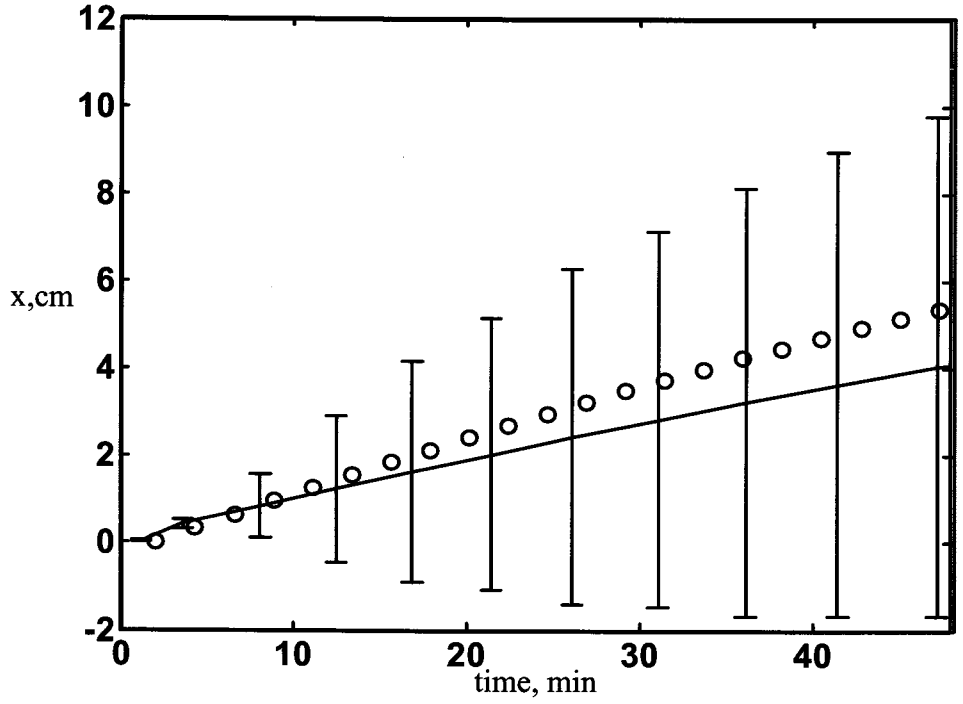

Figure 6.12 **Model results, experimental observations, and ± 1.96 σ model uncertainty bounds for 600 °C experiment.**

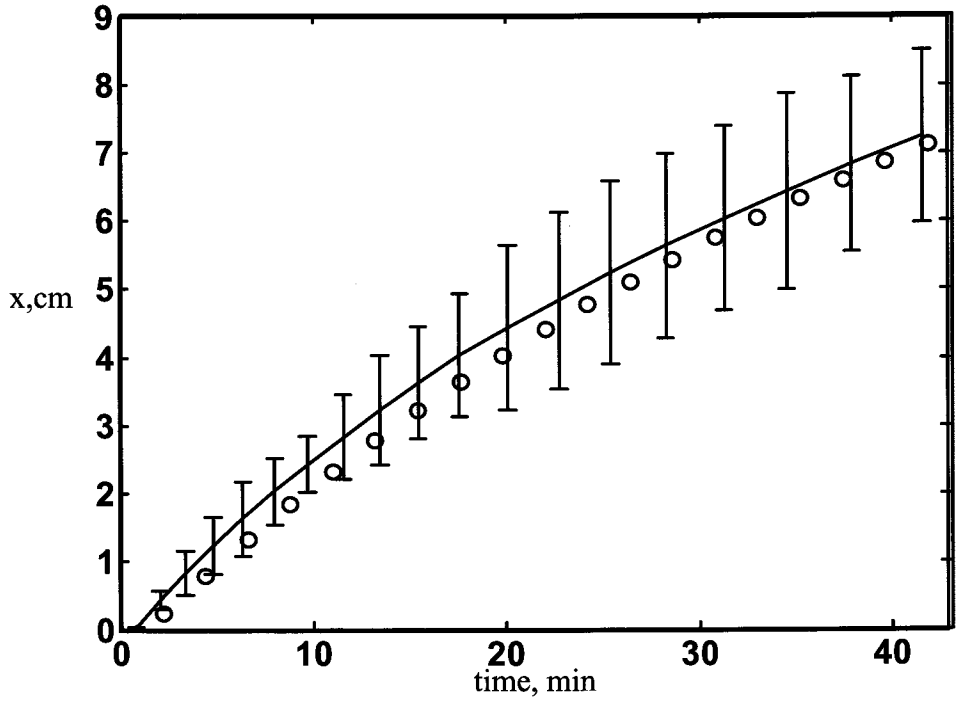

Figure 6.13 **Model results, experimental observations, and ± 1.96 σ model uncertainty bounds for 750 °C experiment.**

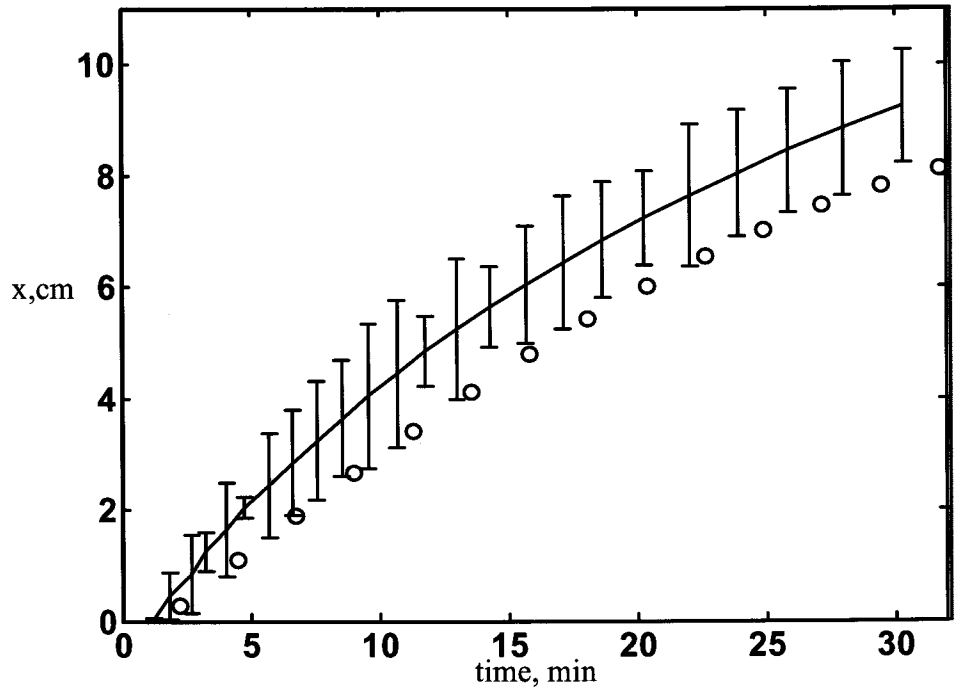

Figure 6.14 **Model results, experimental observations, and ± 1.96 σ model uncertainty bounds for 900 °C experiment.**

Model Validation: Multiple Data Sets

In the previous examples, we considered the data from the three experiments separately. Here we combine the data to look at the effect of the model over temperature. For this case, the model results vector and the sensitivity matrix are given by

$$\mathbf{x} = \begin{bmatrix} x_{600}(t_1) \\ x_{600}(t_2) \\ \vdots \\ x_{600}(t_{n_{600}}) \\ x_{750}(t_1) \\ x_{750}(t_2) \\ \vdots \\ x_{750}(t_{n_{750}}) \\ x_{900}(t_1) \\ x_{900}(t_2) \\ \vdots \\ x_{900}(t_{n_{900}}) \end{bmatrix}, \tag{6.17}$$

and

$$\nabla_{\alpha}\mathbf{x} = \begin{bmatrix} \frac{\partial x_{600}(t_1)}{\partial \phi_1} & \frac{\partial x_{600}(t_1)}{\partial \phi_2} & \cdots & \frac{\partial x_{600}(t_1)}{\partial \phi_{25}} \\ \frac{\partial x_{600}(t_2)}{\partial \phi_1} & \frac{\partial x_{600}(t_2)}{\partial \phi_2} & \cdots & \frac{\partial x_{600}(t_2)}{\partial \phi_{25}} \\ \vdots & \vdots & \ddots & \vdots \\ \frac{\partial x_{600}(t_{n_{600}})}{\partial \phi_1} & \frac{\partial x_{600}(t_{n_{600}})}{\partial \phi_2} & \cdots & \frac{\partial x_{600}(t_{n_{600}})}{\partial \phi_{25}} \\ \frac{\partial x_{750}(t_1)}{\partial \phi_1} & \frac{\partial x_{750}(t_1)}{\partial \phi_2} & \cdots & \frac{\partial x_{750}(t_1)}{\partial \phi_{25}} \\ \frac{\partial x_{750}(t_2)}{\partial \phi_1} & \frac{\partial x_{750}(t_2)}{\partial \phi_2} & \cdots & \frac{\partial x_{750}(t_2)}{\partial \phi_{25}} \\ \vdots & \vdots & \ddots & \vdots \\ \frac{\partial x_{750}(t_{n_{750}})}{\partial \phi_1} & \frac{\partial x_{750}(t_{n_{750}})}{\partial \phi_2} & \cdots & \frac{\partial x_{750}(t_{n_{750}})}{\partial \phi_{25}} \\ \frac{\partial x_{900}(t_1)}{\partial \phi_1} & \frac{\partial x_{900}(t_1)}{\partial \phi_2} & \cdots & \frac{\partial x_{900}(t_1)}{\partial \phi_{25}} \\ \frac{\partial x_{900}(t_2)}{\partial \phi_1} & \frac{\partial x_{900}(t_2)}{\partial \phi_2} & \cdots & \frac{\partial x_{900}(t_2)}{\partial \phi_{25}} \\ \vdots & \vdots & \ddots & \vdots \\ \frac{\partial x_{900}(t_{n_{900}})}{\partial \phi_1} & \frac{\partial x_{900}(t_{n_{900}})}{\partial \phi_2} & \cdots & \frac{\partial x_{900}(t_{n_{900}})}{\partial \phi_{25}} \end{bmatrix} \tag{6.18}$$

-

If we assume that the three experiments at the three temperatures are independent, and we have no reason to believe otherwise, then we can write the covariance matrix of all measurements in terms of the covariance matrix of the individual experiments as follows:

$$\mathbf{cov}(\mathbf{x}_{model} - \mathbf{x}_{exp}) =$$

$$\begin{bmatrix} \mathbf{cov}(\mathbf{x}_{model\,600} - \mathbf{x}_{exp\,600}) & \mathbf{0} & \mathbf{0} \\ \mathbf{0} & \mathbf{cov}(\mathbf{x}_{model\,750} - \mathbf{x}_{exp\,750}) & \mathbf{0} \\ \mathbf{0} & \mathbf{0} & \mathbf{cov}(\mathbf{x}_{model\,900} - \mathbf{x}_{exp\,900}) \end{bmatrix} \quad (6.19)$$

Using the covariance matrices for the model results, derived from Eq. (5.5), and the sensitivity matrices we find that our metric (Eq. (6.14)) gives the results listed in Table 6.13. Clearly, the model cannot represent the predicted front movement for all three temperatures. We can investigate whether it can represent the front movement for just the 600°C and 750°C temperatures by re-evaluating Eq. (6.14) for just these two temperatures. This result is consistent with that obtained previously. We do not have sufficient evidence (at the .05 significance level) to reject the model as valid.

Table 6.13 Statistical test of differences weighted by uncertainty using all data from multiple experiments

Exp	BC Temp (°C)	Heating Orien	Internal Comp	df	$r^{2'}$	$Pr(r^2 > r^{2'})$
1,2,14	600, 750, 900	Bottom	none	240	1068.3	10^{-6}
1,2	600, 750	Bottom	none	189	213.4	0.108

Model Validation: Application Parameter Space

In the previous analysis we considered the complete set of available measurement times. Our anticipated application will seldom have more than 2 cm thick foam surrounding the components. This suggests that we should re-evaluate whether the model is adequate for the first 2 cm of decomposition front motion. Repeating the above process using only those measurements for which the experimentally measured front has not moved past 2 cm, we obtain the results listed in Table 6.13.

We have significant statistical evidence to reject the model for the 900°C case. This is consistent with the results using all of the data. The data from experiments 5 and 15 were already restricted to less than the first 2 cm of movement, so the previous results are still valid. The interesting difference between these results and the results for the full data set is that the probabilities of a valid model giving these results (or worse) has increased from 0.207 to 0.697 for experiment 10, from 10^{-6} to 0.06 for experiment 11, and from less than 10^{-6} to 0.726 for experiment 13. In the case of experiment 10, the reduction of data allows for more uncertainty in the metric. In other words, the model is given a larger benefit of doubt. This is also true, in part, for experiments 11 and 13. In the previous case, the model was rejected. However, for the present case, the difference in slope at later times is not resolved by the model validation metric using the early time data, and the models are not rejected based on a .05 significance level.

Table 6.14 Statistical test of differences weighted by uncertainty using data only up to 2 cm of front propagation

Exp	BC Temp (°C)	Heating Orien	Internal Comp	df	$r^{2'}$	$Pr(r^2 > r^{2'})$
1	600	Bottom	None	26	9.67	0.998
2	750	Bottom	None	14	17.6	0.226
14	900	Bottom	None	9	72.6	10^{-6}
5	750	Bottom	SS	9	23.8	0.0047
10	750	Top	None	20	16.3	0.697
11	750	Side	None	18	27.9	0.064
13	750	Side	None	19	14.9	0.726
15	750	Bottom	AL	9	8.58	0.477

Model Validation: Ignoring Correlation

In the above analysis, we carefully accounted for correlation of the predicted differences between the model results and the experimental measurements. What effect would we see if we incorrectly ignore this correlation? This is easy to test. We simply set all off-diagonal terms in the covariance matrix for the differences to zero and re-evaluate the metric. Results while ignoring the correlation are shown in Table 6.15.

Note that if the model were valid, the probability of obtaining the 750°C (exp 2) results is very small. This is in contrast to the 0.226 fractional probability estimated in Table 6.11 for this case. This dramatic difference in the result is due to the correlation induced by model parameter uncertainty. Correlation of this type typically leads to bias in the differences between the measurements and the model results as illustrated by Figure 6.12. However, the results of the Table 6.11 clearly indicate that much of this correlation can be accounted for by uncertainty in the model parameters. Ignoring this correlation, as was done in evaluating the results of Table 6.15, results in the incorrect rejection of the model.

Table 6.15 Statistical test of differences weighted by uncertainty while ignoring correlation using data only up to 2 cm

Exp	BC Temp	Heating Orien	Internal Comp	df	$r^{2'}$	$Pr(r^2 > r^{2'})$
1	600	Bottom	None	26	19.3	0.825
2	750	Bottom	None	14	47.1	10^{-5}
14	900	Bottom	None	9	79.4	10^{-6}

6.3.4 Summary of Metrics for Benchmark Experiments

Comparing the model -- including mathematical models for thermal diffusion, enclosure radiation and thermal decomposition/material removal (CPUF/element death) --

to the benchmark experiments, had mixed results. We compared the velocity of the decomposing front, calculated as the slope of the time resolved front location, and the time resolved front location. Generally, the differences between the model and experiment are small for conditions of a 750°C boundary temperature. With the exception of Exp 5, the relative error in the front velocity is less than 0.1. Furthermore, there is a reasonable statistical probability that the differences in the measured and simulated front location (up to 2 cm) as a function of time are consistent with estimated experiment and model uncertainty.

The comparison is not as positive at other boundary temperatures. The model exhibited significantly larger discrepancies when compared to experiments with boundary temperatures of 600°C, 900°C, and 1000°C. The error in the front velocity ranged from -0.36 at 600°C to 0.26 and 0.32 at 900°C and 1000°C. In addition, it was statistically improbable that the differences in the front location between the experiment and model are due to experiment and model uncertainty at 900°C. The magnitude of the error, and the apparent under prediction of the model at lower boundary temperatures and over prediction at higher boundary temperatures, raise questions about the model's accuracy at boundary temperatures outside of 750°C. However, with only single experiments at boundary temperatures of 600°C, 900°C and 1000°C, we are restricted in our ability to assess the apparent temperature bias.

In the next section, we will discuss limitations on the overall process, how the conclusions are impacted by these limitations, and ways the process can be improved for this case and future studies.

7.0 Assessment and Prediction

After quantitatively comparing the computational model to experimental data, we need to assess the outcome of the metrics and the process. The ultimate goals to interpret what the metrics indicate about the accuracy of the model *for the intended application.* Achieving this goal is difficult because requirements for the intended application are difficult to relate to the validation activity when we have single-physics (Tier 1) and low-level physics coupling (Tier 2), Trucano et al. (2002). Furthermore, requirements for the application, if stated, are typically vague.

7.1 Assessment

We predicate our discussion of the assessment by putting into perspective conditions under which the experiments were run and our goals in this study. The experiments were conducted over two years prior to this study. At the time, work was just beginning on validation metrics and quantitative comparisons between experiments and math models. Hence, there was little guidance from the literature on conducting validation experiments, as Trucano et al. (2002) point out. Furthermore, applying the validation process provides guidance for specific changes that would help improve the process (the issue of hindsight versus foresight). Suggested improvements should not be interpreted as criticism of previous efforts. Finally, our goals were to demonstrate the methodology, assess what was learned, and provide guidance as to how we can improve future work.

Additional experiments were conducted, Hobbs et al. (2003), but not included as part of this analysis because quantitative data was not available in time to be analyzed and included in this report. The conclusions may be different had the additional data been included in the analysis. In the remainder of this subsection, we discuss the outcome of the validation study (for the data analyzed), limitations identified in the modeling and experimental work to support validation, and suggested improvements. The topics discussed are: 1) aligning validation activities with the intended application, 2) statistical experimental design, 3) parametric uncertainty, and 4) experimental uncertainty

7.2.1 Alignment with the Application

In recent years, information is becoming available concerning modeling needs for the application (thermal response in abnormal thermal environment), Tieszen et al. (2002). Requirements for the application are invaluable to setting the course of validation activities and experiments. During this validation exercise, several issues concerning alignment of validation work with the intended application have emerged. We discuss these issues next.

Foam thicknesses in the application are considerably less than the 6-10 cm of foam recession investigated in the experiments. While thicknesses of foam in the application vary, values in the range of 1-2 cm are anticipated. The experimental data collected can provide application relevant data by looking at an appropriate range of the

data (up to the time the front has recessed 2 cm). However, resources devoted to recessing beyond 2 cm are marginally useful to validation activities for the application.

Diagnostics to measure an application specific physical quantify would provide better alignment with the application. The diagnostic available for validation purposes was X-ray imagery. While thermocouples were also inserted into the foam, uncertainty concerns precluded using them for validation comparisons. Of interest for the application is the response of two components and the time to reach a given temperature ("thermal race"). By embedding objects that respond similar to weapon components, an application specific metric could be studied. Tests were conducted with objects embedded in the foam, but only a few of the total number conducted had embedded objects.

In a validation experiment we are often faced with competing goals. On one hand, we would like the experiment to be closely aligned with the application. On the other hand, doing so may confound the comparison to the point that due to extraneous issues we can't reach any conclusions about the accuracy of the model for the intended application. For example, instead of a cylindrical can we could use a container in the shape of a weapon component. If we do this we add geometric complexity and difficulties in modeling the boundary conditions, but the experiment maps more directly to the application. In the end, however, we would probably be unable to conclude whether the mathematical models or uncertainties in modeling the experiment (the geometry and boundary conditions) were the source of the errors. By using a cylindrical geometry, we remove the effect of geometry and boundary conditions errors and focus on the math model (approximation) errors.

This situation applies to the current validation experiments. The temperature of the plate on the surface of the foam filled can was ramped at rates of 300 to 500 °C/min then held at a fixed temperature of 600 °C to 1000 °C, depending on the experiment. In the application, temperature will ramp continuously until equilibrating with the outside temperature; roughly, 1000 °C for a hydrocarbon fuel fire. An alternative to ramping the temperature then holding it fixed is to follow a transient typical of the application. Depending on the location inside of the weapon, the foam temperature ramps at 100 to 450 °C/min during an initial transient; locations nearer the outer surface of the weapon heat more rapidly. After the initial transient, rate of increases reduces to 1 to 10 C/min over a longer time interval until reaching the surrounding temperature, Dobranich and Dempsey (1998).

7.2.2 Experimental Design

Because of limited coverage of the parameter space (see test matrix in Table 4.3) only the effect of temperature for a bottom heated orientation and the effect of orientation for 750 °C boundary temperature could be statistically studied. Assessing these effects was further limited because only a single experiment was conducted at points in the parameter space outside of 750 °C/bottom-heated. (The exception is 750 °C/side heated, which had two experiments.) Limited coverage of the parameter space means we cannot assess the combined effect of temperature and orientation, i.e., combination of 600/900

°C and top/side orientation. Lack of replication leaves us unable to discern whether errors are due to systematic or random effects.

The apparent bias in the model to predict the effect of temperature on foam decomposition is based on a collection of experiments with a boundary temperature of 750 °C and single experiments with boundary temperature of 600 °C, 900 °C, and 1000 °C. With only single a experiment it is impossible to separate random and systematic effects. Consequently, it is impossible to conclude whether the model has a systematic error that depends on temperature or a random error whose magnitude depends on temperature. Additional experiments are needed to separate these effects.

7.2.3 Parametric Uncertainty

The consistency test indicates whether there is evidence to suggest the contribution of ε or δ_n, Eq. (6.7), to e is significant. This test is based on estimating the effect of parametric uncertainty, $S_p(\phi - \hat{\phi}, z - \hat{z})$, and measurement uncertainty, δ_D, in Eq. (6.7) through the model. The outcome of the test is conditioned upon models for parametric error and measurement error. In this subsection we discuss issues associated with modeling parametric error. First, we will discuss the locally linear limitation of the first–order method used to propagate parametric uncertainty through the math model and numerical noise. Then, we discuss the importance of correlation in model results of a single experiment.

Limitations of the Locally Linear Model and Numerical Noise

We used a locally linear model to represent perturbations from the model of the non-linear CPUF/Coyote model. The use of a linear model can result in unrealistic uncertainty intervals for the model results if the uncertainty range in the parameters is large relative to the scale of linearity. As the results of the 600 °C case illustrate, the uncertainty intervals extended into negative front motion, which is non-physical. This suggests that either the parameter uncertainties were overestimated, or we need to use a more realistic model for the propagation of uncertainty for the 600 °C case. For cases where the parameters possess less uncertainty in the relevant model parameters, the range over which a locally linear model must be valid is smaller. We suspect that the small uncertainty bounds estimated for the 750 °C and 900 °C cases were due to decreased sensitivity to the model parameters with larger uncertainty.

For the 750 °C and 900 °C cases, we do not have clear evidence as to the validity of the locally linear model. The effect of uncertainty of the model parameters do not result in as much uncertainty in the model results, as suggested by the uncertainty bars. Thus, a possibility may exist that over this range of uncertainty, the local linear model is valid. We can test this by performing the sensitivity analysis using finite differences on the non-linear model. If the local linear approximation is valid, we would expect that the sensitivity of the model results to the model parameters should not change significantly if we broaden the nodal spacing of the parameter values used in our finite difference approximations to the sensitivity coefficients. However, this approach could fail if the numerical model is noisy.

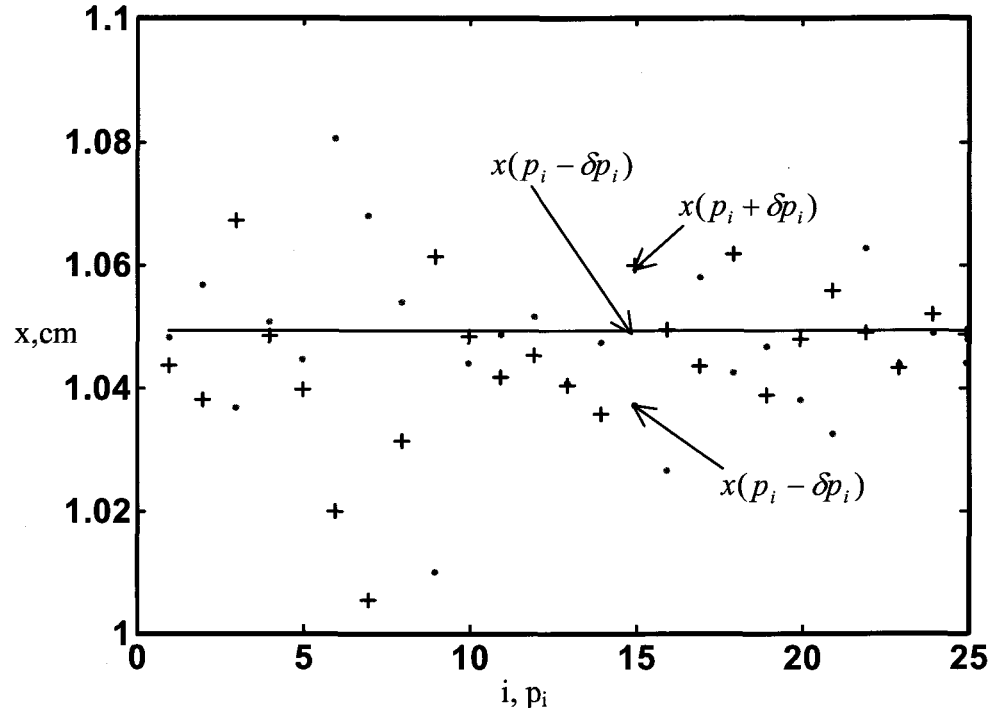

Figure 7.1 Results of perturbation analysis for 750 °C (exp 2), "+" are model results for positive perturbation in parameter p_i, "." is negative perturbation and solid line is model result at mean parameter values

Preliminary analysis indicates that numerical noise may be an issue with model (CPUF/Coyote). Numerical experiments indicate that the finite difference approximations of the sensitivity coefficients may be impacted by noise in the algorithm. Results of the perturbation analysis are shown in Figure 7.1 for the recession front at a location of 1.05 cm. Each of 25 uncertain parameters was perturbed independently upward and downward from its nominal value. The magnitude of the parameter perturbation was 1 percent of the nominal value. As shown in Fig 7.1, parameter 15, which is an activation energy, shows nearly a linear response. The effects of positive and negative perturbations equally shift the front location, upward and downward, respectively. For other parameters, however, results are nonlinear, for example, parameter 9. The negative perturbation changes the response (relative to the mean) a greater magnitude than the positive perturbation. In some cases, the relationship between the perturbation results suggests a complex dependence on the parameter. For example, a positive perturbation in parameter 16 has no effect while a negative perturbation has a significant effect. For other parameters the positive and negative perturbation both shift the result the same direction relative to the nominal value (parameter 14). There are two issues to address: are sensitivity coefficients affected by numerical noise and is a local linear approximation appropriate. These issues require further study. We can't answer the second question until the issue of numerical noise in the sensitivity coefficients is resolved.

If numerical noise is an issue, there are several possible approaches to address this problem. One is to use the model to build a representative surface and estimate the sensitivities from this surface. While this approach works well for models with a few parameters, this approach can be numerically expensive for models with 25 model parameters. Another possible approach is to develop model equations for the sensitivity derivatives directly. Unfortunately, if the model generates numerical noise, then a model for the sensitivity derivations will also generate numerical noise. This second approach is also invasive in the sense that the algorithm must be modified internally. In view of the sensitivity of the algorithm to noise (amplified when using finite differences to estimate derivatives), and the non-linearity of the problem, perhaps the most appropriate approach is to utilize a fully non-linear approach that requires fewer function evaluations than does a full Monte Carlo analysis. An example of such an approach is the maximum likelihood method presented by Hills and Trucano (2002). While this approach can be used to develop validation metrics, the metrics take on a slightly different meaning. In this approach, we search for the most likely model parameters, given the probability density functions for the parameters and for the measurements. We then ask - how probable are these parameters given that our model is valid? For models that are locally linear with normally distributed parameters, the maximum likelihood approach gives the same values for probability (significance) as does the metric used here. Another advantage of the maximum likelihood approach is that it does not require the estimation of a correlation matrix for the differences between model results and observation (see Hills and Trucano, 2002).

Importance of Correlation

Regardless of the suitability of the local linear model, one of the more important results found in this work was the effect of parameter-induced correlation in the model results. The early time results for experiment 2 clearly show that if we neglect the correlation in the differences between model results and experimental observations over time, which were induced by the model results dependence on the model parameters, we can greatly increase the chances of incorrectly rejecting a good model. Thus some method of estimating this correlation and accounting for it in our metrics must be used if we are to base our metrics on these differences (not required for the maximum likelihood method, Hills and Trucano, 2002).

There are several possible approaches to estimate this correlation. One is to use the model directly. We can either use a sensitivity analysis to propagate the parameter uncertainty through the model, or we can use a Monte Carlo analysis. Both of these approaches were used in Hills et al. (2002); only the sensitivity analysis was discussed in this report. The alternative is to perform the experiments, independently, and a sufficient number of times so that we can use the differences between model results and observations directly to estimate the correlation structure. For this method to work, our experiments must be designed so that adequate sampling of the model parameter space is obtained. For example, if the uncertainty is due to material properties induced by the variabilities in the manufacturing process, then we must reconstruct the test object multiple times using materials sampled from the manufacturing process. This may involve buying materials from the various suppliers. An alternative is to carefully

characterize the model parameters in the experiment so that there is little uncertainty. While this can be done for some material properties, it may be more difficult for others. For example, the modeling of a penetrator moving though geological media requires that we can characterize this media. This characterization will have very large uncertainties and there is little we can do about it.

7.2.5 Experimental uncertainty (include BC uncertainty)

As stressed in Section 1.2, when comparing experimental measurements with math models, experimental measurement error is one contributor to the difference. Measurement errors affect the values we compare to the models results and measured boundary/initial conditions can have an impact on the model results. In the benchmark experiments, we have measurement error in front location as a function of time and temperature measurements used as boundary conditions.

We had no quantitative estimate of the effect of measurement error in the front location. Front location was measured by digitizing the time resolved X-ray images and extracting, from the digitized image, the distance from the heated plate to the front. Distances were manually extracted from the image, which required a subjective identification of the front. By extracting the distance from time-resolved images, we get front location as a function of time. The "raw" distance data was smoothed by fitting a function to the data. Points at discrete times were taken from the fit and used as the measured front location as a function of time.

The temperature of the heated plate was measured with two thermocouples inserted from the outer radius of the plate towards the center at two locations across the plate's thickness and separated by 30 degrees around the circumference. When inserted, the thermocouples junctions were at nominally the same radial location, separated by about 0.25 inches across the plate thickness, and about 0.25 inches in the circumferential direction. The thermocouple nearer to the heated lamps was used to control the lamps to provide the desired temperature history. The other thermocouple was to be used for the boundary condition in the model. The thickness of plate between the thermocouple (nearer to the foam) and foam was included in the model and its surface was prescribed to be equal to the thermocouple measurements.

The model results for some experiments used the wrong thermocouple for the boundary condition. The thermocouple nearer to the heated lamps was used for the boundary temperature. Hobbs et al. (2003) discuss this effect. This is potentially important because the model is sensitive to the boundary temperature. We can see the sensitivity of the model to measured temperature in results for exp 11 and 13 in Table 6.1. The experiments were nominally a repeat for 750 °C, side orientation. The model results, which use identical information for all parameters and only differ through the boundary conditions, show the front velocity for exp 13 is 15 percent less than the value for exp 11. The boundary conditions used for these two model results are shown in Figure 7.2. (The data are shifted in time to align the curves.) We see that the measured temperature for the two experiments are consistent through the transient but have an

offset at equilibrium that ranges from 6-10 °C. This modest difference in temperature results in the 15 percent change in velocity. Note that the velocities measured in the experiments are consistent with the model.

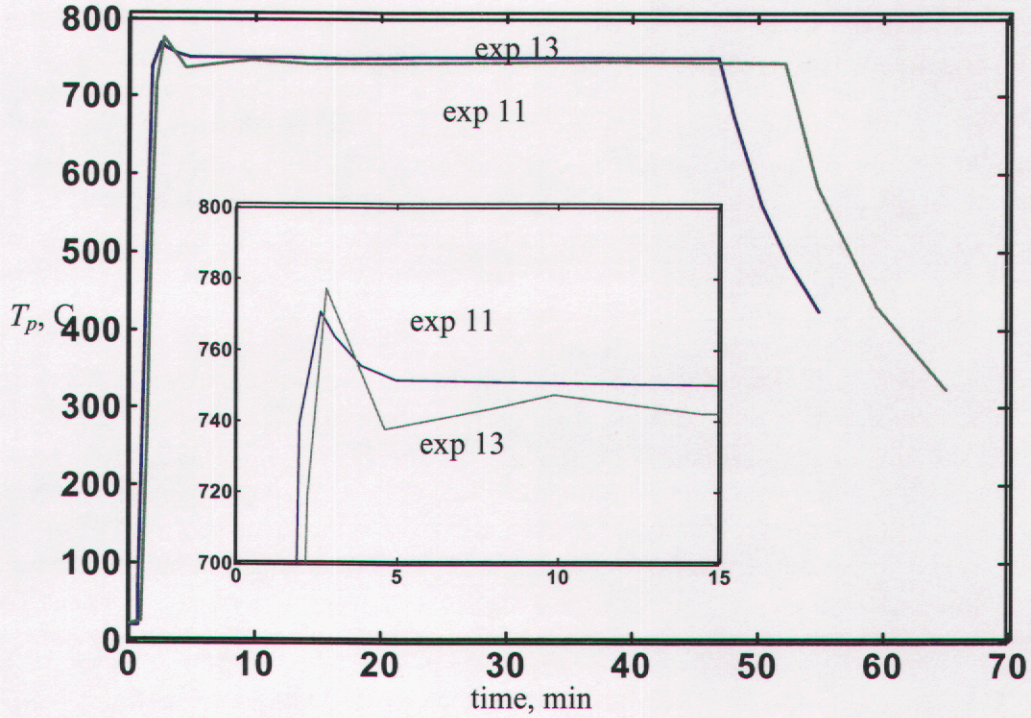

Figure 7.2 **Measure plate temperatures for the experiments 11 and 13**

Hobbs et al. (2003) document which model results were generated using the wrong thermocouple as the boundary condition. A more important issue, however, is the fact that thermocouples demonstrate differences that are not consistent with heating rate or orientation. In some experiments the two thermocouples vary by over 10 °C at equilibrium, while other experiments show less than a 2 °C difference. The differences may be caused by installation issues. At any rate, this is a potentially important uncertainty that was not considered in the analysis. The case (exp 5) that demonstrated the largest deviation between the model and experiment had the largest discrepancy between the thermocouples (for the experiments studied in this report). The issue warrants further study and indicates we need to carefully measure and define boundary conditions for use in validation.

7.3 Prediction

Validation activities aim to quantify the accuracy of the computational model for the intended application. Conceptually, validation activities should support prediction expressed as (Trucano et al., 2002)

$$\text{Best Estimate Plus Uncertainty } (Be+U). \qquad (7.1)$$

Trucano et al. (2002) argue that modeling results should be presented as our best estimate of the physical process bounded with an uncertainty in that estimate. Validation activities should ideally support both aspects: "best estimate" and "uncertainty". The difficulty, however, is the inference from the conditions that the validation experiments were conducted to the conditions expected for the application. The inference is discussed in Easterling (2001a) and Easterling and Berger (2002) and is conceptually represented as shown in Fig. 7.3, which is a reproduction from Easterling (2001a).

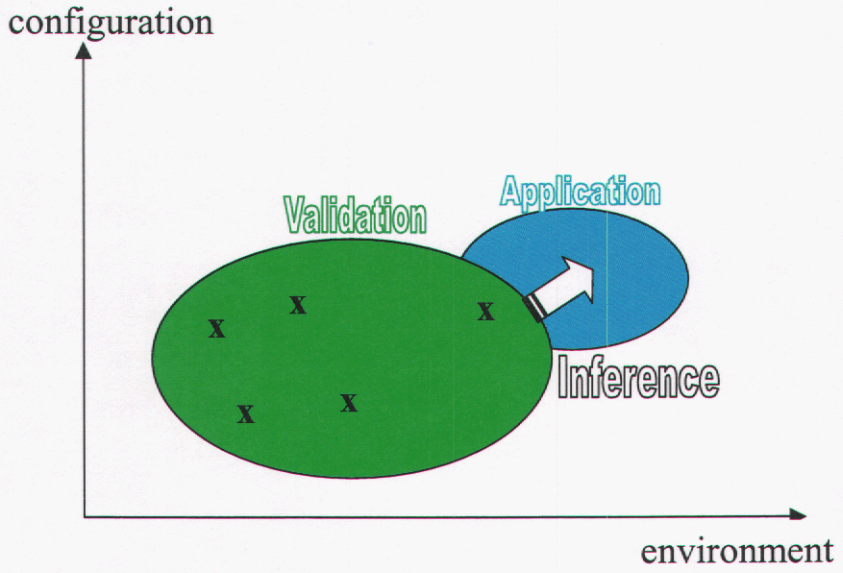

Figure 7.3 Inference associated with validation process

We compare the model to experiments in the region identified with the ellipse label validation in Fig 7.3. We are interested in whether the model is accurate for the region identified as application. The axes in Fig. 7.3 are identified as configuration and environment. In the situation depicted, we are extrapolating from the validation region to the application region. In some instances, we may only be interpolating.

There are potentially two inferences to be made between the validation space and application space. The first inference is the computational model to calculate the best estimate. The second inference is a model for the uncertainty associated with the best estimate. For the application we can write the "best estimate" plus "uncertainty" as follows

$$S^A(\phi^A, z^A, X) = \overbrace{S^A(\hat{\phi}^A, \hat{z}^A, X^A)}^{BE} + \overbrace{S_p^A(\hat{\phi}^A - \phi^A, z^A - \hat{z}^A) + \varepsilon^A(\phi^A, z^A, X^A)}^{U}. \quad (7.2)$$

The model prediction for the application is $S^A(\phi^A, z^A)$, which can be, and likely is, different from the physical quantity studied in the validation, which is $S(\phi, z)$. The uncertainty in applying this model (for the application) is composed of that due to parameter/boundary condition uncertainty, $S_P^A(\hat{\phi}^A - \phi^A, z^A - \hat{z}^A)$, as well as errors due to

the model approximating the physical world, $\varepsilon^A(\phi^A, z^A, X^A)$. This is the point that Easterling and Berger (2002) stress. The uncertainty, or error, in a computational model is due to uncertainty associated with inputs in the model and uncertainty due to the model approximating the physical world.

For the application, we will need to infer the mathematical model to provide the best estimate, $S^A(\hat{\phi}^A, \hat{z}^A)$ in Eq. (7.2) and the uncertainty in this best estimate. The uncertainty has a contribution due to parameter/boundary condition uncertainty and uncertainty due to the model approximating the physical world. One approach to quantifying the uncertainty for the application is to infer it from the validation experiments. That is, use a model for the uncertainty estimated from the validation data as the uncertainty for the application

$$S_p^A(\hat{\phi}^A - \phi^A, z^A - \hat{z}^A) + \varepsilon^A(\phi^A, z^A, X^A) \approx e(\hat{\phi} - \phi, z - \hat{z}, X). \qquad (7.3)$$

We estimate a model for the total error, *e,* from the validation experiments and infer its value to the application the model. Notice that in Eq. (7.3) we infer that the total error estimated from the validation experiments, Eq. (1.2) models the error in the application. This inference assumes: 1) we have a direct linking variable between the application and validation, 2) the validation experiments have spanned the application space, 3) there is not significant cancellation in the errors that contribute to the total error *e* and 4) we are not extrapolating too far. Mathematically, we can write these conditions as

$$\begin{aligned} S^A &= f(S) \\ \left(\hat{\phi}^A - \phi^A, z^A - \hat{z}^A\right) &\approx (\hat{\phi} - \phi, z - \hat{z}) \\ S_p^A(\hat{\phi}^A - \phi^A, z^A - \hat{z}^A) &\approx S_p(\hat{\phi} - \phi, z - \hat{z}) \\ \varepsilon^A(\phi^A, z^A, X^A) &\approx f(\varepsilon(\phi, z, X)) \end{aligned} \qquad (7.4)$$

In relation to the foam model, the conditions in Eq. (7.4) require, 1) a relationship between front location or velocity and an application variable, like thermal response of critical components, 2) the validation experiments were conducted to span the uncertainty/variability in the chemistry and thermophysical parameters and boundary conditions expected in the application, 3) the model's dependence on chemistry and thermophysical parameters and boundary conditions for the validation experiments is similar to that for the application, and 4) the approximation error in front location or velocity can be related to the application.

The point of the previous discussion is to indicate that the inference of uncertainty/error from the validation experiments to the application space has many implicit assumptions. Studying the validation experiments only indicates how the model performed in the validation region. It is from investigating the errors that contribute to the model's accuracy that we get data to infer what the model's accuracy will be in an application.

The validation process indicated the appearance of a bias with respect to model the effect of temperature on the foam decomposition. A potential reaction to bias is to make bias-corrected predictions at temperatures between 600 C and 1000 C. That is, bias-correct the model to agree with the data. The danger of doing this is that we may be correcting the model for the wrong reasons, for example an experimental bias. One should be cautious when few data points are available. Easterling (2002) estimated a bias correction to compensate the model to more closely align with the benchmark experiments. Easterling (2002) estimated a correction to the velocity, which is difficult to infer to the application because the correction is for a model output.

8.0 Summary and Recommendations

By way of example, we have documented a methodology for assessing the validation status of a computational model. We methodically worked through the process, covering steps to identifying the requirements/planning of the computational model, collecting experimental data to assess the model, applying the computational modeling to simulate the experiments, comparing the experimental measurements and model results with quantitative metrics, and assessing the process.

In the report, we highlighted the application of model uncertainty, validation metrics, and statistical inference as part of the validation process to specifically assess the accuracy of a computational model. We suggested specific metrics for assessing a model's accuracy relative to experimental data and demonstrate that how the metrics can be applied. The report used previously collected experimental data, not allowing the concerns or needs of the validation analyst to be addressed prior to collecting the data.

In this section we collect the lessons learned from applying the validation process to the foam decomposition and make recommendations for future activities. Four main lessons are taken from this study.

1. Validation experiments need a clearly defined target application. Without requirements to specify what prediction is needed from the model and the accuracy of the prediction, we can only speculate on model's performance relative to the accuracy needed for the intended application. Furthermore, the validation exercise may not investigate the model's performance for quantities of interest for the application.
2. Validation experiments should be performed in the parameter range anticipated for the intended application. The size of materials and test conditions should be selected to map directly to the intended application.
3. Validation experiments should be designed to provide/investigate responses that are meaningful to the application. Validation means data, and carefully managing the data collected and experimental procedures can greatly improve the outcome of the validation.
    a. Use statistical design to define the experimental test matrix. The main goals are to efficiently coverage the parameter space and data to assess the experimental variability.
    b. The effect of uncertainty on the measured response needs to be estimated. Quantifying measurement errors is challenging, and may require additional experiments. Considering this issue during the experimental design phase may suggest ways to reduce the effect.
    c. Uncertainty in measured boundary and initial conditions need to be estimated. Large uncertainty in the boundary/initial conditions can significantly
4. The computational model should be used to study the effect of uncertainty prior to conducing the experiments to understand the important parameters/boundary conditions needed to model the experiment.

9.0 References

Bentz J., and J. Pantuso, (1999), "Letter Report for the Thermal Degradation of Polyurethane Foam at Radiant Heat Facility," memorandum, Sandia National Laboratories, Albuquerque, NM, November 1999.

Bethea, R. M., B. S. Duran, and T. L. Boullion, Statistical Methods for Engineers and Scientists, 3rd edition, 1995, Marcel Dekker, New York.

Blackwell B. (2002A), "Calore Verification: Steady Conduction in Cylindrical Shell Geometry," Calore Web page, http://www.engsci.sandia.gov/calore/verification/model_eqns/index.html

Blackwell, B. (2002B), "Calore Verification using a Spherical Shell," Calore Web page, http://www.engsci.sandia.gov/calore/verification/model_eqns/index.html

Blackwell, B. (2002C), "Verification of Steady Heat Conduction in a Rectangular Cross Section Bar," Calore Web page, http://www.engsci.sandia.gov/calore/verification/model_eqns/index.html

Blackwell, B. (2002D), "Verification of Unsteady Heat Conduction," Calore Web page

Boucheron, E. A.,"W80 NSafE Thermal Analyses," Memorandum to Todd Jones, Sandia National Laboratories, Albuquerque, NM, August 30, 1995.

Bova, S. W, M. W. Glass, K. J. Dowding, R. R. Lober and R. J. Cochran, (2002A), "Calore, A Computational Heat Transfer Program, Volume 1: Theory Manual," SAND02-xxxx, Sandia National Laboratories, Albuquerque, New Mexico, 2002

Bova, S. W., M. W. Glass, K. J. Dowding, R. R. Lober and R. J. Cochran, (2002B), "Calore Verification Plan," draft plan, version 0.0.1, http://www.engsci.sandia.gov/calore/verification/plan.pdf

Calore, 2002, http://www.engsci.sandia.gov/calore/

Clayton, D., 2002, "Modeling Flow Effects During Polymer Decomposition Using Percolation Lattice Statistics," PhD Dissertation, Brigham Young University, Provo, UT (In progress)

Copps, K. and J. Stewart, (2002), "Verification Studies in Calore," memorandum dated August 22, 2002, Sandia National Laboratories, Albuquerque, NM., http://www.engsci.sandia.gov/calore/verification/error_norms.pdf

Dobranich D., and Walter Gill, (1999), "Thermal Simulations and Experiments for the W76 AF&F Assembly – An Integrated Approach," Sandia National Laboratories, SAND99-1925.

Dobranich, D., and J. F. Dempsey, (1998), "The Thermal Response of the W76 Warhead in Abnormal Thermal Environments," SAND98-1506, Sandia National Laboratories, Albuquerque, NM, July 1998.

Dowding, K. (2002A), "Error Norms for Verification of Steady Heat Conduction in a Rectangular Cross Section Bar," Calore Web page, http://www.engsci.sandia.gov/calore/verification/model_eqns/index.html

Dowding, K. (2002B), "Solution Verification for Isothermal Chemistry," Calore Web page, http://www.engsci.sandia.gov/calore/verification/model_eqns/index.html

Easterling, R. G., (2001a), "Measuring the Predictive Capability of Computational Models: Principles and Methods, Issues, and Illustrations," Sandia National Laboratories, SAND2001-0243.

Easterling, R. G., (2001b), "Measuring Predictive Capability of Computational Models: Foam Case Study," internal memorandum, Sandia National Laboratories, July 2001

Easterling, R. G., (2002), "Measuring Predictive Capability of Computational Models:
Foam Degradation Case Study," submitted to VV&A Foundations 2002, Laural MD, Octorber 22-22, 2002.

Easterling, R. G., and Berger, J., (2002), "Statistical Foundations for the Validation of Computer Models, V&V Foundations," submitted to VV&A Foundations 2002, Laural MD, Octorber 22-22, 2002.

Edwards, H. C., J. R. Stewart, and J. D. Zepper, (2002), "Mathematical Abstractions of the SIERRA Computational Mechanics Framework," Fifth World Congress on Computational Mechanics, Eds. H. A. Mang, F. G. Rammerstorfer, J. Eberhardsteiner, July 7-12, 2002, Vienna, Austria

Eldred, M. S., A. A. Giunta, B. G. van Bloemen Waanders, S. F. Wojtkiewicz, W. E. Hart, and M. P. Alleva (2001) "DAKOTA, A Multilevel Parallel Object-Oriented Framework for Design Optimization, Parameter Estimation, Uncertainty Quantification, and Sensitivity Analysis, Version 3.0 Users Manual", SAND2001-3796, Sandia National Laboratories, Albuquerque.

Erickson, J. N. Castaneda, T. A. Ulibarri, D. K. Derzon, and A. M. Renlund, (2000), "Thermal Decomposition Chemistry of Rigid Polyurethane (RPU) Foams," draft SAND report, Sandia National Laboratories, Albuquerque, NM.

Gartling, D.K., Hogan, R.E., and Glass, M.W. (1994), "Coyote - A Finite Element Computer Program for Nonlinear Heat Conduction Problems Part I – Theoretical Background," Report number SAND94-1173, Sandia National Laboratories, Albuquerque.

Glass, M. W., (1995), "Chaparral – A Library Package for Solving Large Enclosure Radiation Heat Transfer Problems, SAND95-2049, Sandia National Laboratories, Albuquerque, NM.

Hahn, G. J., and Meeker, W. Q., (1991), *Statistical Intervals*, John Wiley & Sons, Inc., New York.

Hills, R. G. and T. G. Trucano (1999), "Statistical Validation of Engineering and Scientific Models: Background," SAND99-1256, Sandia National Laboratories, Albuquerque.

Hills, R. G., and T. Trucano, (2001), "Statistical Validation of Engineering and Scientific Models with Applications to CTH," Sandia National Laboratories, SAND2001-0312.

Hills, R. G. and T. G. Trucano (2002), "Statistical Validation of Engineering and Scientific Models: A Maximum Likelihood Based Metric," SAND2002-1783, Sandia National Laboratories, Albuquerque.

Hills, R. G., I. H. Leslie, K. J. Dowding, (2002), "Statistical Validation of Engineering and Scientific Models: Application to the Abnormal Thermal Environment," in preparation

Hobbs M. L., K. L. Erickson, T. Y. Chu, T. T. Borek, K. R. Thompson, K. J. Dowding, D. Clayton, and T. H. Fletcher, (2003), "CPUF – Chemical structure-based

PolyUrethane decomposition model," SAND report, Sandia National Laboratories, Albuquerque, in preparation.
Kennedy, M. C. and O'Hagan, A., (2001), "Bayesian Calibration of Computer Models," J
McMasters, R.L., Z. Zhou, K. J. Dowding, C. Somertom, J. V. Beck, (2002), "Exact Solution for Nonlinear Thermal Diffusion and its Use for Verification," *AIAA Journal of Thermophysics and Heat Transfer*, Vol. 16, No. 2.
Romero, V. J., R. R. Lober, D. D. Dobranich, S. R. Tieszen, R. J. Cochran, T. Y. Chu, and W. C. Moffatt, (2000), "Calore Verification and Validation Plan for Weapon-in-a-Fire Simulations, " Version 1.2, SAND report in preparation, Albuquerque NM.
Romero, V. J., (2002), personal communication
Tieszen, S. R., T. Y. Chu, D. Dobranich, V. J. Romero, T. G. Trucano, J. T. Nakos, W. C. Moffat, T. F. Hendrickson, K. B. Sobolik, S. N. Kempka, and M. Pilch, (2002), "Integrated Modeling and Simulation Validation Plan for W76-1 Abnormal Thermal Environment Qualification Version 1.0." SAND2002-????, Albuquerque NM.
Trucano, T. G., R. G. Easterling, K. J. Dowding, T. L. Paez, A. Uribina, V. J. Romero, B. M. Rutherford, and R. G. Hills, (2001), "Description of the Sandia Validation Metrics Project," SAND2001-1339, Sandia National Laboratories, Albuquerque, NM, August 2001.
Trucano, T. G., M. Pilch, and W. L. Oberkampf, (2002), "General Concepts for Experimental Validation of ASCI Code Applications," report SAND2002-0341, Sandia National Laboratories, Albuquerque, NM, March 2002.
Trucano, T., (2002), "On the Role of Code Comparisons in V&V," internal memorandum, Sandia National Laboratories, Albuquerque, NM, April 2002.
U.S. Department of Energy Defense Programs (2000), "Accelerated Strategic Computing Initiative (ASCI) Program Plan," DOE/DP-99-000010592.
Young, T. R., (1980), "CHEMEQ – A subroutine for Solving Stiff Ordinary Differential Equations," Report 4091, Naval Research Laboratory, Washington, D.C., February 26, 1980.
Zoeller,T. and T. Voth, (2000), "Heat Conduction with Chemistry Using Calore," memorandum, Sandia National Laboratories, Albuquerque, NM. Calore Web page, http://www.engsci.sandia.gov/calore/verification/model_eqns/index.html

Appendices

Appendix A: Model parameters

Appendix B: Measurements, Predictions, and Sensitivities

Appendix C: Code (Coyote) Input file

Appendix A: Model Parameters

The 18 sets of estimated parameters for each of the 18 TGA experiments performed at atmospheric conditions are listed in Table A.1.

Table A.1. Activation Energies for Each of the 18 TGA Experiments

Experiment	E_1	E_2	E_3	E_4	E_5	E_6	E_7	E_8	E_9
1	50256	50301	49533	50164	49711	49373	50368	49336	51838
2	50078	50692	49374	50369	50295	49466	50375	49279	51469
3	50067	50478	49411	50347	50009	49645	50337	49354	51473
4	50041	50418	49422	50332	49956	49685	50318	49387	51508
5	50386	50654	49436	50461	50011	49292	50534	49138	51575
6	50319	50650	49386	50495	49971	49354	50496	49182	51549
7	50073	50400	49453	50275	49916	49587	50348	49359	51627
8	50077	50417	49447	50297	49915	49590	50354	49353	51597
9	49964	50431	49393	50336	49931	49634	50326	49372	51513
10	49957	50417	49411	50310	49968	49672	50315	49386	51477
11	50084	50366	49434	50284	49822	49609	50324	49378	51608
12	50943	50875	49055	50703	50185	50033	50422	49232	51378
13	50078	50428	49422	50323	49896	49568	50359	49339	51610
14	50016	50436	49413	50324	49929	49594	50343	49355	51549
15	50318	50772	49306	50561	50062	49316	50475	49158	51352
16	50408	50937	49253	50667	50118	49173	50533	49057	51308
17	50350	50666	49343	50456	49977	49337	50414	49212	51478
18	50346	50868	49232	50644	50049	49215	50513	49091	51329

Experiment	E_{10}	E_{11}	E_{12}	E_{13}	E_{14}	E_{15}	E_{16}	σ_E
1	49662	50279	49920	50360	51137	49714	49712	3547
2	49887	50176	50032	50093	51227	49686	49621	3549
3	49765	50228	50474	50231	50926	49528	49687	3511
4	49718	50248	49952	50284	50844	49501	49680	3546
5	49747	50235	49968	50229	51022	49601	49870	3509
6	49740	50241	50463	50235	50983	49598	49811	3510
7	49698	50258	49943	50305	50944	49514	49710	3511
8	49700	50257	49943	50303	50933	49503	49717	3511
9	49713	50250	49951	50286	50966	49464	49692	3546
10	49728	50244	49955	50273	50958	49462	49693	3511
11	49700	50259	49941	50309	50982	49526	49706	3546
12	50208	49649	50061	49814	51729	50177	49568	3520
13	49700	50255	49942	50301	50946	49504	49715	3511
14	49715	50249	49951	50284	50965	49470	49712	3511
15	49870	50177	50526	50102	51145	49608	49813	3511
16	49913	50160	50551	50036	51286	49694	49855	3511
17	49897	50163	50539	50089	51207	49734	49749	3513
18	49877	50174	50530	50090	51266	49658	49829	3512

An estimate of the covariance matrix for the 18 sets of nonlinear least squares estimates of the activation energies and the associate distribution parameter is provided in Table A.2.

Table A.2. Estimate covariance matrix of chemistry parameters from TGA data

Parameter	E_1	E_2	E_3	E_4	E_5	E_6	E_7	E_8	E_9
E_1	57033	34871	-19923	27988	12901	-150	12093	-17301	-11420
E_2	34871	39613	-17955	29033	20257	-14903	12732	-19661	-20711
E_3	-19923	-17955	11518	-14683	-9709	-3361	-3963	6775	10931
E_4	27988	29033	-14683	22994	13565	-7076	9262	-14109	-16177
E_5	12901	20257	-9709	13565	17161	-27	4145	-7194	-12931
E_6	-150	-14903	-3361	-7076	-27	44541	-11212	15785	2928
E_7	12093	12732	-3963	9262	4145	-11212	6140	-8437	-4598
E_8	-17301	-19661	6775	-14109	-7194	15785	-8437	12164	8264
E_9	-11420	-20711	10931	-16177	-12931	2928	-4598	8264	16274
E_{10}	26307	21631	-13386	16461	13047	4569	4483	-7880	-11709
E_{11}	-28291	-16793	13232	-14156	-10404	-13675	-2617	4623	8466
E_{12}	23626	36888	-13300	27138	13121	-31514	13350	-21321	-22174
E_{13}	-26810	-24242	13904	-18182	-14290	-1381	-5623	9570	13230
E_{14}	43554	31114	-19082	22864	15782	2868	7531	-12682	-12740
E_{15}	37080	21160	-13720	15899	10479	6163	5240	-8376	-6542
E_{16}	1435	5392	681	3960	-1053	-14349	4614	-6001	-1759
σ_E	-914	-1107	414	-1002	-282	728	-575	750	677

Parameter	E_{10}	E_{11}	E_{12}	E_{13}	E_{14}	E_{15}	E_{16}	σ_E
E_1	26307	-28291	23626	-26810	43554	37080	1435	-914
E_2	21631	-16793	36888	-24242	31114	21160	5392	-1107
E_3	-13386	13232	-13300	13904	-19082	-13720	681	414
E_4	16461	-14156	27138	-18182	22864	15899	3960	-1002
E_5	13047	-10404	13121	-14290	15782	10479	-1053	-282
E_6	4569	-13675	-31514	-1381	2868	6163	-14349	728
E_7	4483	-2617	13350	-5623	7531	5240	4614	-575
E_8	-7880	4623	-21321	9570	-12682	-8376	-6001	750
E_9	-11709	8466	-22174	13230	-12740	-6542	-1759	677
E_{10}	17610	-17314	14754	-18046	25783	19770	-2096	-310
E_{11}	-17314	20000	-5024	16867	-26089	-21579	4490	193
E_{12}	14754	-5024	72800	-18421	17195	10366	10996	-1939
E_{13}	-18046	16867	-18421	18854	-26091	-19493	941	430
$E1_4$	25783	-26089	17195	-26091	43786	33473	-2815	-107
E_{15}	19770	-21579	10366	-19493	33473	28432	-3374	35
E_{16}	-2096	4490	10996	941	-2815	-3374	6244	-611
σ_E	-310	193	-1939	430	-107	35	-611	267

An estimate of the full covariance matrix for chemistry parameters (activation energies and the associate distribution parameter), thermophysical properties of polyurethane foam, and algorithmic constants for CPUF, are provided in Table A.3. Only chemistry parameters have off-diagonal nonzero entries.

Table A.3. Full covariance matrix for chemistry parameters, thermophysical properties, and algorithm parameters

Parameter	E_1	E_2	E_3	E_4	E_5	E_6	E_7	E_8	E_9
E_1	57033	34871	-19923	27988	12901	-150	12093	-17301	-11420
E_2	34871	39613	-17955	29033	20257	-14903	12732	-19661	-20711
E_3	-19923	-17955	11518	-14683	-9709	-3361	-3963	6775	10931
E_4	27988	29033	-14683	22994	13565	-7076	9262	-14109	-16177
E_5	12901	20257	-9709	13565	17161	-27	4145	-7194	-12931
E_6	-150	-14903	-3361	-7076	-27	44541	-11212	15785	2928
E_7	12093	12732	-3963	9262	4145	-11212	6140	-8437	-4598
E_8	-17301	-19661	6775	-14109	-7194	15785	-8437	12164	8264
E_9	-11420	-20711	10931	-16177	-12931	2928	-4598	8264	16274
E_{10}	26307	21631	-13386	16461	13047	4569	4483	-7880	-11709
E_{11}	-28291	-16793	13232	-14156	-10404	-13675	-2617	4623	8466
E_{12}	23626	36888	-13300	27138	13121	-31514	13350	-21321	-22174
E_{13}	-26810	-24242	13904	-18182	-14290	-1381	-5623	9570	13230
E_{14}	43554	31114	-19082	22864	15782	2868	7531	-12682	-12740
E_{15}	37080	21160	-13720	15899	10479	6163	5240	-8376	-6542
E_{16}	1435	5392	681	3960	-1053	-14349	4614	-6001	-1759
σ_E	-914	-1107	414	-1002	-282	728	-575	750	677
T_i	0	0	0	0	0	0	0	0	0
I_0	0	0	0	0	0	0	0	0	0
ρ	0	0	0	0	0	0	0	0	0
c	0	0	0	0	0	0	0	0	0
h_r	0	0	0	0	0	0	0	0	0
ε	0	0	0	0	0	0	0	0	0
$\sigma+1$	0	0	0	0	0	0	0	0	0
k_e	0	0	0	0	0	0	0	0	0

Table A.3. Covariance Matrix, continued

Parameter	E_{10}	E_{11}	E_{12}	E_{13}	E_{14}	E_{15}	E_{16}	σ_E	T_i
E_1	26307	-28291	23626	-26810	43554	37080	1435	-914	0
E_2	21631	-16793	36888	-24242	31114	21160	5392	-1107	0
E_3	-13386	13232	-13300	13904	-19082	-13720	681	414	0
E_4	16461	-14156	27138	-18182	22864	15899	3960	-1002	0
E_5	13047	-10404	13121	-14290	15782	10479	-1053	-282	0
E_6	4569	-13675	-31514	-1381	2868	6163	-14349	728	0
E_7	4483	-2617	13350	-5623	7531	5240	4614	-575	0
E_8	-7880	4623	-21321	9570	-12682	-8376	-6001	750	0
E_9	-11709	8466	-22174	13230	-12740	-6542	-1759	677	0
E_{10}	17610	-17314	14754	-18046	25783	19770	-2096	-310	0
E_{11}	-17314	20000	-5024	16867	-26089	-21579	4490	193	0
E_{12}	14754	-5024	72800	-18421	17195	10366	10996	-1939	0
E_{13}	-18046	16867	-18421	18854	-26091	-19493	941	430	0
E_{14}	25783	-26089	17195	-26091	43786	33473	-2815	-107	0
E_{15}	19770	-21579	10366	-19493	33473	28432	-3374	35	0
E_{16}	-2096	4490	10996	941	-2815	-3374	6244	-611	0
σ_E	-310	193	-1939	430	-107	35	-611	267	0
T_i	0	0	0	0	0	0	0	0	9
I_0	0	0	0	0	0	0	0	0	0
ρ	0	0	0	0	0	0	0	0	0
c	0	0	0	0	0	0	0	0	0
h_r	0	0	0	0	0	0	0	0	0
ε	0	0	0	0	0	0	0	0	0
$\sigma+1$	0	0	0	0	0	0	0	0	0
k_e	0	0	0	0	0	0	0	0	0

Table A.3. Covariance Matrix, continued

Parameter	l_0	ρ	c	h_r	ε	$\sigma+1$	k_e
E_1	0	0	0	0	0	0	0
E_2	0	0	0	0	0	0	0
E_3	0	0	0	0	0	0	0
E_4	0	0	0	0	0	0	0
E_5	0	0	0	0	0	0	0
E_6	0	0	0	0	0	0	0
E_7	0	0	0	0	0	0	0
E_8	0	0	0	0	0	0	0
E_9	0	0	0	0	0	0	0
E_{10}	0	0	0	0	0	0	0
E_{11}	0	0	0	0	0	0	0
E_{12}	0	0	0	0	0	0	0
E_{13}	0	0	0	0	0	0	0
E_{14}	0	0	0	0	0	0	0
E_{15}	0	0	0	0	0	0	0
E_{16}	0	0	0	0	0	0	0
σ_E	0	0	0	0	0	0	0
T_i	0	0	0	0	0	0	0
l_0	0.0025	0	0	0	0	0	0
ρ	0	0.001325	0	0	0	0	0
c	0	0	0.01	0	0	0	0
h_r	0	0	0	4.2436	0	0	0
ε	0	0	0	0	0.0025	0	0
$\sigma+1$	0	0	0	0	0	0.0784	0
k_e	0	0	0	0	0	0	4.76E-05

(Page left blank)

Appendix B: Measurements, Predictions, and Sensitivities

Table B1 contains the measured and predicted front location as a function of time for Experiment 1 at 600C. The model predictions are based on the mean values of the parameters tabulated in Table A.2. Table B1 also contains the sensitivities the corresponding predictions with respect to these model parameters. Note that p1 refers to parameter 1, etc. Tables B2 and B3 contain the corresponding data for 750C and 900C experiments 2 and 14. Tables B4 through B9 contain model predictions vs. experimental observations for 5 other experiments performed at 750C. Sensitivity matrices were not generated directly for these predictions. Linear interpolation over time of the sensitivities listed in Table B2 was used for the other experiments.

Table B.1. Measured, Predicted Measurements and Sensitivity Matrix, Experiment 1: 600 C

Time, min	2.089286	2.655252	3.221218	3.787185	4.353151	4.919118	5.485084	6.05105
x_{exp}, cm	0.042367	0.122609	0.20253	0.282128	0.361403	0.440355	0.518981	0.597282
x_{model}, cm	0.228102	0.313119	0.390635	0.45937	0.513394	0.565608	0.614018	0.662914
$E_1 dx/dE_1$, cm	-0.90662	-0.90666	-0.98995	-1.12497	-1.0054	-0.81016	-0.45589	-0.20488
$E_2 dx/dE_2$, cm	0.443187	0.439944	0.398681	0.398612	0.487506	0.574013	0.655503	0.730268
$E_3 dx/dE_3$, cm	-0.26539	-0.20872	-0.25193	-0.29704	-0.30946	-0.30641	-0.27089	-0.22712
$E_4 dx/dE_4$, cm	-0.15427	-0.13466	0.063404	0.199237	0.165624	0.155409	0.194371	0.287174
$E_5 dx/dE_5$, cm	-1.72046	-1.68564	-1.56506	-1.69749	-1.44304	-1.13424	-0.71121	-0.22051
$E_6 dx/dE_6$, cm	-0.18968	-0.18691	-0.14539	-0.12136	-0.13343	-0.15621	-0.20155	-0.24974
$E_7 dx/dE_7$, cm	0.194824	0.195101	0.249078	0.351886	0.309577	0.258857	0.190463	0.175969
$E_8 dx/dE_8$, cm	-0.03746	-0.0213	-0.04838	-0.0884	-0.03282	0.004242	0.002407	-0.0291
$E_9 dx/dE_9$, cm	0.629601	0.535463	0.189326	0.024327	-0.04669	-0.17333	-0.41684	-0.7148
$E_{10} dx/dE_{10}$, cm	0.270871	0.266619	0.239615	0.269971	0.165717	0.025354	-0.1909	-0.4226
$E_{11} dx/dE_{11}$, cm	-0.03629	-0.02549	-0.02612	-0.05212	0.003789	0.068409	0.151329	0.228576
$E_{12} dx/dE_{12}$, cm	0.23038	0.218908	0.269936	0.36563	0.226432	0.089441	-0.04291	-0.19861
$E_{13} dx/dE_{13}$, cm	0.196467	0.199658	0.202717	0.203789	0.20152	0.287698	0.559768	0.865074
$E_{14} dx/dE_{14}$, cm	1.453014	1.489289	1.637115	1.808796	1.659794	1.52929	1.437663	1.413567
$E_{15} dx/dE_{15}$, cm	-0.31819	-0.32822	-0.40319	-0.47509	-0.55265	-0.65023	-0.78984	-0.96353
$E_{16} dx/dE_{16}$, cm	-0.4393	-0.34417	-0.19058	-0.15749	-0.15212	-0.12382	-0.04732	0.04248
$\sigma_E dx/d\sigma_E$, cm	0.022868	0.073112	0.091525	0.110422	0.075119	0.016268	-0.09208	-0.17883
$T_i dx/dT_i$, cm	-0.16223	-0.11514	-0.01015	0.050667	0.028436	0.024372	0.058488	0.107465
$I_0 dx/dI_0$, cm	0.094225	0.087423	0.099368	0.137024	0.113696	0.071806	-0.0091	-0.10009
$\rho dx/d\rho$, cm	-0.37468	-0.29906	-0.31499	-0.40091	-0.37686	-0.35075	-0.32033	-0.26153
$c dx/dc$, cm	0.019439	-0.00023	0.036879	0.09117	0.044961	-0.04723	-0.23604	-0.36932
$h_r dx/dh_r$, cm	0.631903	0.477031	0.064368	-0.11337	-0.23505	-0.41614	-0.72213	-1.08193
$\varepsilon dx/d\varepsilon$, cm	0.09236	0.149225	0.171023	0.183494	0.299879	0.448074	0.663123	0.822388
$(\sigma+1)dx/d(\sigma+1)$, cm	-0.53394	-0.42816	-0.33036	-0.29721	-0.36582	-0.48061	-0.69243	-0.94614
$k_e dx/dk_e$, cm	0	0	5.21E-05	-0.00795	-0.05452	-0.06648	-0.00569	0.058471

Table B.1. Continued

Time, min	6.617017	7.182983	7.74895	8.314916	8.880882	9.446849	10.01282	10.57878
x_{exp}, cm	0.675255	0.752901	0.830218	0.907206	0.983862	1.060187	1.13618	1.211838
x_{model}, cm	0.713215	0.763621	0.814311	0.864902	0.915261	0.966576	1.02002	1.072899
$E_1 dx/dE_1$, cm	-0.25282	-0.2454	-0.08727	0.034872	0.071379	0.073447	-0.00108	-0.01698
$E_2 dx/dE_2$, cm	0.785566	0.8482	0.9308	0.985863	0.975407	0.919709	0.763383	0.643739
$E_3 dx/dE_3$, cm	-0.15948	-0.11741	-0.14492	-0.15578	-0.12702	-0.08887	-0.02982	-0.07804
$E_4 dx/dE_4$, cm	0.535858	0.757534	0.905712	1.025877	1.079393	1.155905	1.283566	1.362519
$E_5 dx/dE_5$, cm	0.466144	1.16218	1.883764	2.578382	3.208841	3.80362	4.319038	4.81945
$E_6 dx/dE_6$, cm	-0.30623	-0.34804	-0.34994	-0.33513	-0.28058	-0.24018	-0.23127	-0.21354
$E_7 dx/dE_7$, cm	0.317526	0.442827	0.523891	0.557506	0.47823	0.459619	0.575939	0.776137
$E_8 dx/dE_8$, cm	-0.14651	-0.26839	-0.40241	-0.52656	-0.62722	-0.69744	-0.69999	-0.75104
$E_9 dx/dE_9$, cm	-1.1704	-1.60263	-1.97126	-2.366	-2.82283	-3.2906	-3.78272	-4.23212
$E_{10} dx/dE_{10}$, cm	-0.69899	-0.93737	-1.0723	-1.22534	-1.42149	-1.64542	-1.93112	-2.10261
$E_{11} dx/dE_{11}$, cm	0.289399	0.341404	0.36941	0.394845	0.414162	0.453304	0.536543	0.648348
$E_{12} dx/dE_{12}$, cm	-0.42191	-0.61958	-0.74749	-0.9019	-1.11938	-1.3277	-1.51568	-1.67138
$E_{13} dx/dE_{13}$, cm	1.266606	1.646666	1.968292	2.281183	2.573291	2.816784	2.952146	3.091978
$E_{14} dx/dE_{14}$, cm	1.584979	1.742515	1.86229	2.013301	2.238629	2.457755	2.663086	2.805954
$E_{15} dx/dE_{15}$, cm	-1.23586	-1.42958	-1.40939	-1.42291	-1.51667	-1.58491	-1.59644	-1.65192
$E_{16} dx/dE_{16}$, cm	0.170788	0.292351	0.395557	0.450826	0.392047	0.367872	0.420663	0.521283
$\sigma_E dx/d\sigma_E$, cm	-0.20306	-0.19314	-0.09024	0.029737	0.190365	0.317945	0.372017	0.423009
$T_i dx/dT_i$, cm	0.199463	0.256069	0.216356	0.197565	0.228552	0.191901	0.00481	-0.14657
$I_0 dx/dI_0$, cm	-0.22028	-0.3344	-0.43198	-0.50846	-0.53473	-0.54432	-0.51682	-0.44709
$\rho dx/d\rho$, cm	-0.12057	-0.04975	-0.16978	-0.26056	-0.28176	-0.26166	-0.14968	-0.1152
$c dx/dc$, cm	-0.34177	-0.3476	-0.44421	-0.50709	-0.4897	-0.48891	-0.52506	-0.58792
$h_r dx/dh_r$, cm	-1.5975	-2.11326	-2.62954	-3.15876	-3.71875	-4.33083	-5.05877	-5.75678
$\varepsilon dx/d\varepsilon$, cm	0.820146	0.805491	0.757051	0.760734	0.888428	1.012404	1.128112	1.231265
$(\sigma+1)dx/d(\sigma+1)$, cm	-1.32111	-1.64685	-1.83864	-2.00894	-2.12809	-2.26458	-2.43966	-2.5726
$k_e dx/dk_e$, cm	0.13238	0.195135	0.227537	0.240666	0.20794	0.192746	0.216548	0.232448

Table B.1. Continued

Time, min	11.14475	11.71071	12.27668	12.84265	13.40861	13.97458	14.54055	15.10651
x_{exp}, cm	1.287163	1.362151	1.436804	1.511119	1.585096	1.658733	1.73203	1.804986
x_{model}, cm	1.125057	1.175889	1.225505	1.277046	1.330463	1.382405	1.433494	1.483973
$E_1 dx/dE_1$, cm	0.04203	0.158728	0.3283	0.458851	0.551351	0.555256	0.508077	0.62952
$E_2 dx/dE_2$, cm	0.570959	0.613024	0.760344	0.954975	1.195736	1.384122	1.542305	1.595163
$E_3 dx/dE_3$, cm	-0.26335	-0.42463	-0.56392	-0.77579	-1.05846	-1.23213	-1.34294	-1.32257
$E_4 dx/dE_4$, cm	1.379236	1.491162	1.69035	1.791286	1.796415	1.74815	1.669099	1.634798
$E_5 dx/dE_5$, cm	5.300709	5.754563	6.183315	6.644344	7.136839	7.724356	8.366659	8.844898
$E_6 dx/dE_6$, cm	-0.18454	-0.22828	-0.33868	-0.32958	-0.20395	-0.11895	-0.05738	-0.05242
$E_7 dx/dE_7$, cm	1.083518	1.402744	1.732834	2.033866	2.306558	2.54855	2.772838	2.951183
$E_8 dx/dE_8$, cm	-0.86405	-0.94479	-0.99596	-1.05508	-1.12194	-1.16941	-1.2057	-1.17774
$E_9 dx/dE_9$, cm	-4.62696	-4.99535	-5.33951	-5.69989	-6.07607	-6.41691	-6.73737	-7.09222
$E_{10} dx/dE_{10}$, cm	-2.12815	-2.2091	-2.34083	-2.49538	-2.67219	-2.91397	-3.19323	-3.40493
$E_{11} dx/dE_{11}$, cm	0.796658	0.934049	1.061438	1.212948	1.387977	1.594565	1.819348	2.058317
$E_{12} dx/dE_{12}$, cm	-1.78584	-1.80733	-1.74361	-1.75206	-1.83088	-1.98759	-2.18923	-2.43905
$E_{13} dx/dE_{13}$, cm	3.237528	3.459036	3.750168	3.961271	4.094334	4.182699	4.245289	4.315477
$E_{14} dx/dE_{14}$, cm	2.869014	2.978236	3.129768	3.28304	3.438004	3.651723	3.899319	4.119288
$E_{15} dx/dE_{15}$, cm	-1.76358	-1.92362	-2.128	-2.25762	-2.31433	-2.32479	-2.30859	-2.30355
$E_{16} dx/dE_{16}$, cm	0.683021	0.830923	0.966149	1.103075	1.241656	1.387561	1.537688	1.553668
$\sigma_E dx/d\sigma_E$, cm	0.470065	0.541905	0.63646	0.663306	0.624127	0.509549	0.351495	0.247601
$T_i dx/dT_i$, cm	-0.25231	-0.29952	-0.29308	-0.1639	0.084946	0.15517	0.122395	0.228869
$I_0 dx/dI_0$, cm	-0.3234	-0.25283	-0.23093	-0.26502	-0.35369	-0.40256	-0.42848	-0.36937
$\rho dx/d\rho$, cm	-0.17975	-0.34961	-0.61599	-0.84714	-1.04392	-1.13795	-1.17274	-1.25626
$c dx/dc$, cm	-0.6849	-0.81417	-0.97302	-1.01064	-0.93003	-0.77874	-0.58672	-0.57556
$h_r dx/dh_r$, cm	-6.41659	-7.00523	-7.52866	-8.05139	-8.57343	-9.13215	-9.71201	-10.2914
$\varepsilon dx/d\varepsilon$, cm	1.318381	1.358932	1.356808	1.362557	1.375981	1.341952	1.280563	1.290361
$(\sigma+1) dx/d(\sigma+1)$, cm	-2.65172	-2.77864	-2.94938	-3.11938	-3.28867	-3.38412	-3.43699	-3.52879
$k_e dx/dk_e$, cm	0.238253	0.315343	0.457768	0.59383	0.723683	0.812642	0.878019	0.917642

Table B.1. Continued

Time, min	15.67248	16.23845	16.80441	17.37038	17.93634	18.50231	19.06828	19.63424
x_{exp}, cm	1.877599	1.94987	2.021796	2.093378	2.164613	2.235502	2.306042	2.376234
x_{model}, cm	1.534161	1.585989	1.638573	1.689341	1.739604	1.789861	1.840115	1.889958
E_1dx/dE_1, cm	0.831445	0.964159	1.064956	1.071682	1.052291	0.992237	0.92158	0.921809
E_2dx/dE_2, cm	1.597753	1.539001	1.451964	1.385156	1.323966	1.336024	1.367182	1.48856
E_3dx/dE_3, cm	-1.23959	-1.24421	-1.28922	-1.35505	-1.42665	-1.54339	-1.6719	-1.76111
E_4dx/dE_4, cm	1.621855	1.641706	1.67668	1.730643	1.789878	1.81007	1.820081	1.857892
E_5dx/dE_5, cm	9.244847	9.805684	10.4407	10.99961	11.53737	11.96625	12.36673	12.82238
E_6dx/dE_6, cm	-0.07448	-0.10677	-0.14379	-0.14896	-0.14529	-0.14925	-0.15519	-0.12025
E_7dx/dE_7, cm	3.107604	3.260784	3.412467	3.512333	3.59781	3.7223	3.856963	4.052328
E_8dx/dE_8, cm	-1.11911	-1.02488	-0.91423	-0.87379	-0.85284	-0.80217	-0.74377	-0.7155
E_9dx/dE_9, cm	-7.4635	-7.87483	-8.30463	-8.58727	-8.82905	-9.05966	-9.28735	-9.60094
$E_{10}dx/dE_{10}$, cm	-3.58439	-3.72235	-3.84116	-3.99745	-4.16414	-4.31239	-4.45584	-4.56964
$E_{11}dx/dE_{11}$, cm	2.304063	2.430313	2.501459	2.479503	2.431698	2.487209	2.569662	2.658931
$E_{12}dx/dE_{12}$, cm	-2.71188	-2.95729	-3.19005	-3.21906	-3.1915	-3.12221	-3.04203	-3.02821
$E_{13}dx/dE_{13}$, cm	4.389294	4.545199	4.738955	4.95671	5.181124	5.428625	5.682145	5.869525
$E_{14}dx/dE_{14}$, cm	4.326077	4.524921	4.720096	4.853825	4.97049	5.043473	5.105066	5.165069
$E_{15}dx/dE_{15}$, cm	-2.30384	-2.42827	-2.60994	-2.73971	-2.85506	-2.87961	-2.88048	-2.97668
$E_{16}dx/dE_{16}$, cm	1.505623	1.556701	1.653487	1.780115	1.915026	1.923267	1.898476	1.952562
$\sigma_E dx/d\sigma_E$, cm	0.169555	0.14242	0.138762	0.099468	0.050282	-0.06049	-0.18732	-0.31562
$T_i dx/dT_i$, cm	0.401808	0.53747	0.655941	0.82533	1.008851	1.11728	1.206125	1.130817
$l_0 dx/dl_0$, cm	-0.26966	-0.11987	0.053032	0.102027	0.116621	0.144956	0.176876	0.283234
$\rho dx/d\rho$, cm	-1.36305	-1.42632	-1.46953	-1.44844	-1.40949	-1.25535	-1.07116	-0.89774
$c dx/dc$, cm	-0.65074	-0.71629	-0.77738	-0.75992	-0.72065	-0.71788	-0.72464	-0.83767
$h_r dx/dh_r$, cm	-10.8707	-11.3545	-11.7942	-12.1961	-12.5874	-12.89	-13.1696	-13.4488
$\varepsilon dx/d\varepsilon$, cm	1.334135	1.365649	1.39151	1.446566	1.509726	1.605951	1.710798	1.836485
$(\sigma+1)dx/d(\sigma+1)$, cm	-3.63917	-3.79198	-3.96435	-4.12461	-4.28151	-4.42913	-4.57433	-4.6569
$k_e dx/dk_e$, cm	0.944974	1.079342	1.263065	1.336686	1.379736	1.408315	1.433121	1.374044

Table B.1. Continued

Time, min	20.20021	20.76618	21.33214	21.89811	22.46408	23.03004	23.59601	24.16197
x_{exp}, cm	2.446076	2.515567	2.584706	2.653492	2.721925	2.790003	2.857726	2.925092
x_{model}, cm	1.9397	1.987904	2.035704	2.085113	2.135208	2.18433	2.233044	2.280755
$E_1 dx/dE_1$, cm	0.939394	0.960714	0.983008	0.991945	0.995181	0.983095	0.964587	1.05191
$E_2 dx/dE_2$, cm	1.632033	1.687894	1.720876	1.709128	1.678295	1.693004	1.726798	1.772059
$E_3 dx/dE_3$, cm	-1.84069	-1.98611	-2.14872	-2.39079	-2.66675	-2.80531	-2.88629	-2.83108
$E_4 dx/dE_4$, cm	1.902511	2.012293	2.13909	2.266089	2.393174	2.526201	2.661721	2.819686
$E_5 dx/dE_5$, cm	13.29155	13.6906	14.07134	14.48314	14.90819	15.24987	15.55663	15.91307
$E_6 dx/dE_6$, cm	-0.0753	-0.05507	-0.04129	-0.13116	-0.26525	-0.33873	-0.38681	-0.41812
$E_7 dx/dE_7$, cm	4.262559	4.457584	4.648633	4.847902	5.050675	5.242554	5.429872	5.53237
$E_8 dx/dE_8$, cm	-0.69461	-0.68639	-0.68147	-0.64769	-0.60161	-0.64091	-0.71599	-0.76731
$E_9 dx/dE_9$, cm	-9.93558	-10.2329	-10.5205	-10.8688	-11.243	-11.6196	-11.9971	-12.3597
$E_{10} dx/dE_{10}$, cm	-4.67619	-4.83271	-5.00227	-5.15478	-5.30002	-5.39244	-5.46272	-5.49035
$E_{11} dx/dE_{11}$, cm	2.74987	2.809894	2.861844	2.939871	3.029025	3.085251	3.127682	3.216761
$E_{12} dx/dE_{12}$, cm	-3.03065	-3.05222	-3.0788	-3.07076	-3.04795	-2.95214	-2.82572	-2.79625
$E_{13} dx/dE_{13}$, cm	6.040714	6.195833	6.346755	6.454578	6.544012	6.604286	6.652343	6.700508
$E_{14} dx/dE_{14}$, cm	5.224686	5.32864	5.444169	5.619451	5.820225	6.00241	6.176809	6.286817
$E_{15} dx/dE_{15}$, cm	-3.09622	-3.22831	-3.36368	-3.38305	-3.35293	-3.28613	-3.20394	-3.19383
$E_{16} dx/dE_{16}$, cm	2.025962	2.082486	2.134604	2.16939	2.196782	2.269183	2.360445	2.473152
$\sigma_E dx/d\sigma_E$, cm	-0.44429	-0.4378	-0.39602	-0.35264	-0.30859	-0.31892	-0.35205	-0.34393
$T_i dx/dT_i$, cm	1.015314	0.936541	0.867361	0.809933	0.757519	0.717451	0.682555	0.665822
$I_0 dx/dI_0$, cm	0.407822	0.392801	0.341326	0.25735	0.159509	0.171329	0.2291	0.247734
$\rho dx/d\rho$, cm	-0.72695	-0.64779	-0.59256	-0.55558	-0.52639	-0.50985	-0.49861	-0.58021
$c dx/dc$, cm	-0.97672	-1.0057	-1.00594	-1.06083	-1.13905	-1.23586	-1.34048	-1.41997
$h_r dx/dh_r$, cm	-13.7279	-14.1713	-14.6577	-15.1832	-15.7256	-16.2227	-16.701	-17.0845
$\varepsilon dx/d\varepsilon$, cm	1.967278	2.043851	2.106264	2.13189	2.141818	2.161311	2.184811	2.211034
$(\sigma+1)dx/d(\sigma+1)$, cm	-4.72414	-4.82953	-4.94488	-5.09057	-5.24921	-5.37646	-5.49057	-5.57391
$k_e dx/dk_e$, cm	1.294426	1.304442	1.337865	1.406696	1.490635	1.467699	1.39998	1.347371

Table B.1. Continued

Time, min	24.72794	25.29391	25.85987	26.42584	26.99181	27.55777	28.12374	28.68971
x_{exp}, cm	2.992101	3.058751	3.125042	3.190972	3.256541	3.321748	3.386592	3.451071
x_{model}, cm	2.327931	2.375348	2.422976	2.47025	2.517059	2.563437	2.608795	2.65417
$E_1 dx/dE_1$, cm	1.195738	1.224144	1.151097	1.044876	0.895144	0.819633	0.920425	0.999114
$E_2 dx/dE_2$, cm	1.823443	1.975895	2.217182	2.390414	2.47438	2.553092	2.619328	2.677147
$E_3 dx/dE_3$, cm	-2.70315	-2.6361	-2.62257	-2.67582	-2.81665	-2.93209	-2.98723	-3.04871
$E_4 dx/dE_4$, cm	2.989637	3.079662	3.099432	3.134211	3.188673	3.233274	3.254451	3.277075
$E_5 dx/dE_5$, cm	16.29605	16.68247	17.07192	17.42552	17.73207	18.02736	18.29592	18.56988
$E_6 dx/dE_6$, cm	-0.44048	-0.45979	-0.47644	-0.49267	-0.50836	-0.51436	-0.49733	-0.4923
$E_7 dx/dE_7$, cm	5.589585	5.60214	5.57544	5.556858	5.548924	5.563957	5.633549	5.70804
$E_8 dx/dE_8$, cm	-0.80595	-0.9017	-1.04765	-1.13739	-1.15338	-1.15931	-1.14135	-1.13555
$E_9 dx/dE_9$, cm	-12.7142	-13.0732	-13.436	-13.7506	-14.0019	-14.2533	-14.5049	-14.7549
$E_{10} dx/dE_{10}$, cm	-5.49521	-5.50781	-5.52722	-5.58151	-5.68154	-5.79528	-5.94161	-6.08559
$E_{11} dx/dE_{11}$, cm	3.330747	3.467067	3.623014	3.727698	3.765141	3.789555	3.783024	3.774807
$E_{12} dx/dE_{12}$, cm	-2.81853	-2.88653	-2.99469	-3.12748	-3.29256	-3.44714	-3.57676	-3.7115
$E_{13} dx/dE_{13}$, cm	6.748731	6.809005	6.879871	6.966768	7.074691	7.225176	7.476774	7.730583
$E_{14} dx/dE_{14}$, cm	6.362449	6.417475	6.454386	6.518681	6.61889	6.732122	6.876295	7.01028
$E_{15} dx/dE_{15}$, cm	-3.22219	-3.21699	-3.18229	-3.2321	-3.39275	-3.56472	-3.76357	-3.95513
$E_{16} dx/dE_{16}$, cm	2.597309	2.711962	2.818257	2.897888	2.942544	2.941135	2.830299	2.722261
$\sigma_E dx/d\sigma_E$, cm	-0.31379	-0.38189	-0.53634	-0.62585	-0.63019	-0.62696	-0.60577	-0.57897
$T_i dx/dT_i$, cm	0.658787	0.636299	0.600229	0.533573	0.426804	0.338165	0.29259	0.249412
$I_0 dx/dI_0$, cm	0.245473	0.206139	0.13422	0.065512	0.001017	-0.035	-0.00337	0.031675
$\rho dx/d\rho$, cm	-0.71138	-0.8726	-1.06023	-1.16025	-1.14535	-1.10558	-1.00671	-0.92694
$c dx/dc$, cm	-1.48604	-1.50593	-1.48523	-1.39274	-1.20609	-1.08649	-1.12613	-1.17013
$h_r dx/dh_r$, cm	-17.4175	-17.7528	-18.0904	-18.4084	-18.7008	-18.9892	-19.2681	-19.5376
$\varepsilon dx/d\varepsilon$, cm	2.238712	2.283586	2.343573	2.474799	2.69946	2.87034	2.91348	2.93295
$(\sigma+1)dx/d(\sigma+1)$, cm	-5.64083	-5.76459	-5.93831	-6.03509	-6.03095	-6.0235	-6.00822	-6.00074
$k_e dx/dk_e$, cm	1.302827	1.28033	1.27721	1.274217	1.27139	1.312749	1.459072	1.606207

Table B.1. Continued

Time, min	29.25567	29.82164	30.38761	30.95357	31.51954	32.0855	32.65147	33.21744
x_{exp}, cm	3.515185	3.578933	3.642314	3.705327	3.767972	3.830246	3.892149	3.95368
x_{model}, cm	2.699716	2.745263	2.790113	2.834881	2.880079	2.925494	2.970958	3.01648
$E_1 dx/dE_1$, cm	0.858462	0.717808	0.787144	0.880853	0.994861	1.119216	1.249238	1.385898
$E_2 dx/dE_2$, cm	2.651445	2.625743	2.731464	2.852436	2.974614	3.097402	3.177199	3.206606
$E_3 dx/dE_3$, cm	-3.17301	-3.29732	-3.39374	-3.48692	-3.59348	-3.70686	-3.78728	-3.82905
$E_4 dx/dE_4$, cm	3.314054	3.351034	3.393028	3.435602	3.517335	3.619033	3.740724	3.885847
$E_5 dx/dE_5$, cm	18.89741	19.22494	19.58741	19.95392	20.3205	20.68708	21.03565	21.36309
$E_6 dx/dE_6$, cm	-0.60634	-0.72038	-0.7037	-0.67186	-0.72595	-0.82386	-0.9267	-1.03532
$E_7 dx/dE_7$, cm	5.831147	5.954257	6.132791	6.317756	6.432199	6.51068	6.541277	6.515748
$E_8 dx/dE_8$, cm	-1.2505	-1.36545	-1.42647	-1.48124	-1.48502	-1.46279	-1.46808	-1.50565
$E_9 dx/dE_9$, cm	-14.9894	-15.2239	-15.4599	-15.696	-15.9396	-16.187	-16.45	-16.7311
$E_{10} dx/dE_{10}$, cm	-6.20627	-6.32696	-6.52025	-6.72197	-6.97007	-7.24183	-7.46514	-7.63167
$E_{11} dx/dE_{11}$, cm	3.749866	3.724924	3.848053	3.988365	4.125583	4.261219	4.368068	4.441176
$E_{12} dx/dE_{12}$, cm	-3.89712	-4.08275	-4.24596	-4.40657	-4.52307	-4.61707	-4.68572	-4.72465
$E_{13} dx/dE_{13}$, cm	8.00633	8.282082	8.425102	8.552714	8.686675	8.823868	8.926847	8.989722
$E_{14} dx/dE_{14}$, cm	7.043155	7.076031	7.074885	7.069791	7.030496	6.973764	6.979741	7.059217
$E_{15} dx/dE_{15}$, cm	-4.07441	-4.19369	-4.30401	-4.41329	-4.48517	-4.53799	-4.57219	-4.58459
$E_{16} dx/dE_{16}$, cm	2.641976	2.56169	2.538266	2.521442	2.547325	2.594983	2.599013	2.551907
$\sigma_E dx/d\sigma_E$, cm	-0.49657	-0.41417	-0.2505	-0.0774	0.120923	0.332103	0.416327	0.351751
$T_i dx/dT_i$, cm	0.230034	0.210655	0.246292	0.288314	0.255967	0.185701	0.126158	0.079185
$I_0 dx/dI_0$, cm	0.100577	0.169479	0.146854	0.113605	0.121965	0.151541	0.191056	0.242218
$\rho dx/d\rho$, cm	-1.03681	-1.14667	-1.28458	-1.42573	-1.51739	-1.5838	-1.60674	-1.57872
$c dx/dc$, cm	-1.25731	-1.34448	-1.35501	-1.35664	-1.49032	-1.69133	-1.80832	-1.82683
$h_r dx/dh_r$, cm	-19.7133	-19.889	-20.1341	-20.3873	-20.6624	-20.9487	-21.2706	-21.6342
$\varepsilon dx/d\varepsilon$, cm	2.717529	2.502104	2.355073	2.215982	2.15133	2.124635	2.091309	2.050212
$(\sigma+1) dx/d(\sigma+1)$, cm	-6.07071	-6.14069	-6.18055	-6.2169	-6.28197	-6.36168	-6.44978	-6.54773
$k_e dx/dk_e$, cm	1.761402	1.9166	2.015554	2.107978	2.092159	2.021148	1.948419	1.873677

Table B.1. Continued

Time, min	33.7834	34.34937	34.91534	35.4813	36.04727	36.61324	37.1792	37.74517
x_{exp}, cm	4.014839	4.075624	4.136034	4.196068	4.255726	4.315006	4.373907	4.43243
x_{model}, cm	3.061507	3.105157	3.148808	3.192168	3.235521	3.278185	3.320503	3.363002
$E_1 dx/dE_1$, cm	1.481488	1.46236	1.443233	1.438215	1.433594	1.428837	1.424013	1.395604
$E_2 dx/dE_2$, cm	3.250548	3.335094	3.419641	3.479711	3.539096	3.536349	3.502443	3.463495
$E_3 dx/dE_3$, cm	-3.86684	-3.89346	-3.92008	-3.98467	-4.05032	-4.05399	-4.02656	-3.98514
$E_4 dx/dE_4$, cm	4.006279	4.057752	4.109224	4.192081	4.275821	4.364897	4.456646	4.540081
$E_5 dx/dE_5$, cm	21.69045	22.0176	22.34476	22.67784	23.0111	23.33097	23.64412	23.93604
$E_6 dx/dE_6$, cm	-1.11422	-1.11012	-1.10601	-1.13239	-1.15963	-1.18557	-1.21086	-1.20989
$E_7 dx/dE_7$, cm	6.496413	6.494374	6.492336	6.514304	6.536947	6.570989	6.610747	6.651543
$E_8 dx/dE_8$, cm	-1.55593	-1.64175	-1.72758	-1.73226	-1.73466	-1.75606	-1.78698	-1.79278
$E_9 dx/dE_9$, cm	-16.9906	-17.1892	-17.3878	-17.6378	-17.8893	-18.0976	-18.2841	-18.4754
$E_{10} dx/dE_{10}$, cm	-7.8016	-7.981	-8.16041	-8.34493	-8.52959	-8.57161	-8.54208	-8.53384
$E_{11} dx/dE_{11}$, cm	4.51513	4.591453	4.667775	4.61912	4.566953	4.473962	4.360499	4.258365
$E_{12} dx/dE_{12}$, cm	-4.7473	-4.72447	-4.70163	-4.70866	-4.71651	-4.74529	-4.78456	-4.81809
$E_{13} dx/dE_{13}$, cm	9.053374	9.119203	9.185032	9.348442	9.514596	9.62412	9.705243	9.794156
$E_{14} dx/dE_{14}$, cm	7.183131	7.431183	7.679234	7.911721	8.143776	8.359801	8.567786	8.752355
$E_{15} dx/dE_{15}$, cm	-4.60695	-4.65716	-4.70737	-4.69862	-4.68822	-4.70665	-4.73954	-4.78381
$E_{16} dx/dE_{16}$, cm	2.529992	2.578439	2.626887	2.619178	2.609892	2.567656	2.508897	2.447059
$\sigma_E dx/d\sigma_E$, cm	0.292494	0.248092	0.20369	0.221755	0.241574	0.262762	0.284636	0.291256
$T_i dx/dT_i$, cm	0.050662	0.073672	0.096682	0.147589	0.19928	0.311584	0.454283	0.587892
$I_0 dx/dI_0$, cm	0.266055	0.213567	0.161079	0.184035	0.209111	0.316313	0.464698	0.571328
$\rho dx/d\rho$, cm	-1.5691	-1.61089	-1.65269	-1.82181	-1.99452	-2.09284	-2.15386	-2.21441
$c dx/dc$, cm	-1.86641	-1.96486	-2.0633	-2.17657	-2.29027	-2.3748	-2.4447	-2.52036
$h_r dx/dh_r$, cm	-22.0159	-22.4479	-22.8799	-23.1827	-23.482	-23.7139	-23.9122	-24.1367
$\varepsilon dx/d\varepsilon$, cm	2.002335	1.935515	1.868695	1.818398	1.768564	1.820439	1.923319	2.011051
$(\sigma+1)dx/d(\sigma+1)$, cm	-6.63796	-6.70666	-6.77536	-6.80248	-6.82843	-6.83535	-6.83272	-6.8492
$k_e dx/dk_e$, cm	1.800407	1.731243	1.662079	1.647978	1.635423	1.612823	1.585185	1.57247

Table B.1. Continued

Time, min	38.31113	38.8771	39.44307	40.00903	40.575	41.14097	41.70693	42.2729
x_{exp}, cm	4.490571	4.548331	4.605709	4.662704	4.719314	4.775539	4.831377	4.886829
x_{model}, cm	3.405917	3.448832	3.491618	3.5344	3.57705	3.619623	3.661353	3.700984
$E_1 dx/dE_1$, cm	1.312938	1.230269	1.172742	1.11592	1.022595	0.908323	0.80426	0.725618
$E_2 dx/dE_2$, cm	3.412946	3.362396	3.351002	3.340705	3.345471	3.358881	3.378069	3.411649
$E_3 dx/dE_3$, cm	-3.9115	-3.83786	-3.82371	-3.81122	-3.81081	-3.81733	-3.81684	-3.79887
$E_4 dx/dE_4$, cm	4.60438	4.66868	4.745056	4.821768	4.872603	4.908586	4.936936	4.946277
$E_5 dx/dE_5$, cm	24.17911	24.42219	24.72779	25.03513	25.33752	25.63707	25.9122	26.12652
$E_6 dx/dE_6$, cm	-1.14852	-1.08715	-0.98076	-0.87311	-0.8061	-0.76242	-0.7277	-0.71528
$E_7 dx/dE_7$, cm	6.694723	6.737905	6.798274	6.859122	6.937714	7.026488	7.117095	7.212273
$E_8 dx/dE_8$, cm	-1.74075	-1.68872	-1.62645	-1.5639	-1.57114	-1.61843	-1.67282	-1.74491
$E_9 dx/dE_9$, cm	-18.6775	-18.8796	-19.1295	-19.3807	-19.5743	-19.7347	-19.884	-20.0054
$E_{10} dx/dE_{10}$, cm	-8.57459	-8.61533	-8.69625	-8.77829	-8.7968	-8.77884	-8.80019	-8.91944
$E_{11} dx/dE_{11}$, cm	4.182303	4.10624	4.078242	4.051589	4.094807	4.178123	4.281512	4.434908
$E_{12} dx/dE_{12}$, cm	-4.83843	-4.85878	-4.86878	-4.8785	-4.91265	-4.96083	-5.00464	-5.03757
$E_{13} dx/dE_{13}$, cm	9.900984	10.00781	10.13147	10.2556	10.35602	10.44284	10.52759	10.60722
$E_{14} dx/dE_{14}$, cm	8.883043	9.013734	9.11846	9.222458	9.303976	9.372592	9.428291	9.451824
$E_{15} dx/dE_{15}$, cm	-4.85429	-4.92476	-5.01002	-5.09568	-5.15824	-5.20752	-5.2473	-5.26338
$E_{16} dx/dE_{16}$, cm	2.378138	2.309215	2.403083	2.501503	2.653404	2.835997	3.007325	3.150607
$\sigma_E dx/d\sigma_E$, cm	0.262781	0.234306	0.134374	0.032446	-0.11361	-0.28498	-0.42549	-0.48916
$T_i dx/dT_i$, cm	0.700578	0.813267	0.875506	0.936334	0.964109	0.972914	0.968731	0.932198
$I_0 dx/dI_0$, cm	0.581887	0.592447	0.550577	0.507243	0.481251	0.465214	0.458626	0.475572
$\rho dx/d\rho$, cm	-2.2739	-2.33339	-2.44668	-2.56148	-2.62562	-2.6607	-2.66935	-2.61222
$c dx/dc$, cm	-2.60928	-2.6982	-2.67921	-2.6572	-2.60409	-2.53312	-2.45017	-2.3374
$h_r dx/dh_r$, cm	-24.4215	-24.7064	-24.9031	-25.0974	-25.3078	-25.5273	-25.7452	-25.9588
$\varepsilon dx/d\varepsilon$, cm	2.063931	2.116811	2.067247	2.014818	2.007396	2.025805	2.05482	2.110256
$(\sigma+1) dx/d(\sigma+1)$, cm	-6.90963	-6.97006	-7.03564	-7.10136	-7.09163	-7.0386	-6.99374	-6.96924
$k_e dx/dk_e$, cm	1.594091	1.615712	1.612355	1.608299	1.631249	1.669697	1.696684	1.695126

Table B.1. Continued

Time, min	42.83887	43.40483	43.9708	44.53676	45.10273	45.6687	46.23466	46.80063
x_{exp}, cm	4.941892	4.996567	5.050851	5.104744	5.158246	5.211354	5.264069	5.316388
x_{model}, cm	3.740615	3.779708	3.818636	3.857765	3.897732	3.937699	3.977281	4.016694
$E_1 dx/dE_1$, cm	0.646976	0.602361	0.568304	0.562233	0.67222	0.782206	0.807759	0.795769
$E_2 dx/dE_2$, cm	3.445228	3.490737	3.53995	3.581935	3.593953	3.605971	3.65798	3.727772
$E_3 dx/dE_3$, cm	-3.78091	-3.79135	-3.81061	-3.84076	-3.91606	-3.99135	-4.04263	-4.08323
$E_4 dx/dE_4$, cm	4.955618	4.986092	5.023124	5.057932	5.083523	5.109113	5.086146	5.041585
$E_5 dx/dE_5$, cm	26.34085	26.61994	26.91914	27.21497	27.4969	27.77883	27.99789	28.189
$E_6 dx/dE_6$, cm	-0.70287	-0.67237	-0.63625	-0.62622	-0.72436	-0.82249	-0.88734	-0.93741
$E_7 dx/dE_7$, cm	7.307451	7.38058	7.44687	7.505271	7.530962	7.556653	7.649067	7.771152
$E_8 dx/dE_8$, cm	-1.81701	-1.87573	-1.93029	-1.97357	-1.97	-1.96643	-1.982	-2.00609
$E_9 dx/dE_9$, cm	-20.1268	-20.2659	-20.4106	-20.5586	-20.7205	-20.8825	-21.0545	-21.231
$E_{10} dx/dE_{10}$, cm	-9.03868	-9.05283	-9.03437	-9.03191	-9.09582	-9.15974	-9.25554	-9.36551
$E_{11} dx/dE_{11}$, cm	4.588304	4.708936	4.819406	4.927447	5.025429	5.123412	5.201206	5.270025
$E_{12} dx/dE_{12}$, cm	-5.0705	-5.08239	-5.08775	-5.08394	-5.0421	-5.00027	-4.90101	-4.77622
$E_{13} dx/dE_{13}$, cm	10.68684	10.7385	10.78147	10.85197	11.03657	11.22118	11.38486	11.53924
$E_{14} dx/dE_{14}$, cm	9.475357	9.579303	9.708205	9.850362	10.04751	10.24465	10.39764	10.531
$E_{15} dx/dE_{15}$, cm	-5.27947	-5.30357	-5.33015	-5.3487	-5.3339	-5.31911	-5.29934	-5.27735
$E_{16} dx/dE_{16}$, cm	3.293889	3.388434	3.467858	3.541277	3.589796	3.638316	3.673599	3.702997
$\sigma_E dx/d\sigma_E$, cm	-0.55282	-0.6084	-0.66146	-0.70064	-0.6822	-0.66376	-0.64727	-0.63164
$T_i dx/dT_i$, cm	0.895664	0.944732	1.020364	1.065909	0.986691	0.907473	0.92342	0.981684
$I_0 dx/dI_0$, cm	0.492519	0.375724	0.217425	0.073466	-0.01104	-0.09554	-0.16152	-0.21927
$\rho dx/d\rho$, cm	-2.55509	-2.48605	-2.41331	-2.35313	-2.34507	-2.33701	-2.32389	-2.30853
$c dx/dc$, cm	-2.22462	-2.16506	-2.12202	-2.08788	-2.09065	-2.09343	-2.09138	-2.0872
$h_r dx/dh_r$, cm	-26.1723	-26.3812	-26.5887	-26.7966	-27.0069	-27.2171	-27.4489	-27.6903
$\varepsilon dx/d\varepsilon$, cm	2.165692	2.220266	2.274574	2.310255	2.268694	2.227132	2.217777	2.222744
$(\sigma+1)dx/d(\sigma+1)$, cm	-6.94473	-6.98504	-7.04546	-7.10065	-7.13415	-7.16766	-7.21499	-7.26846
$k_e dx/dk_e$, cm	1.693569	1.653688	1.601914	1.546861	1.478206	1.409551	1.356823	1.311175

Table B.1. Continued

Time, min	47.3666	47.93256	48.49853	49.0645	49.63046	50.19643	50.76239	51.32836
x_{exp}, cm	5.368312	5.41984	5.470969	5.5217	5.572031	5.621962	5.671491	5.720618
x_{model}, cm	4.056263	4.096677	4.137092	4.175915	4.213991	4.252061	4.290014	4.327968
$E_1 dx/dE_1$, cm	0.781989	0.75845	0.73491	0.6855	0.623951	0.562072	0.49446	0.426846
$E_2 dx/dE_2$, cm	3.798347	3.873186	3.948026	4.010429	4.066995	4.123509	4.179115	4.234721
$E_3 dx/dE_3$, cm	-4.11288	-4.08282	-4.05275	-4.05576	-4.07428	-4.09077	-4.07192	-4.05306
$E_4 dx/dE_4$, cm	4.999552	4.971298	4.943044	4.912785	4.881586	4.848468	4.781943	4.715418
$E_5 dx/dE_5$, cm	28.37673	28.54598	28.71524	28.93153	29.16988	29.40425	29.56904	29.73384
$E_6 dx/dE_6$, cm	-0.9825	-1.00054	-1.01858	-0.92836	-0.78733	-0.64558	-0.49135	-0.33711
$E_7 dx/dE_7$, cm	7.903716	8.09342	8.283128	8.40398	8.492518	8.582597	8.699489	8.816384
$E_8 dx/dE_8$, cm	-2.02548	-2.01927	-2.01306	-1.93387	-1.82042	-1.70512	-1.55763	-1.41013
$E_9 dx/dE_9$, cm	-21.4165	-21.6513	-21.8861	-22.115	-22.3412	-22.5654	-22.7558	-22.9461
$E_{10} dx/dE_{10}$, cm	-9.47	-9.54455	-9.6191	-9.66083	-9.68715	-9.71514	-9.7721	-9.82905
$E_{11} dx/dE_{11}$, cm	5.325607	5.309005	5.292403	5.2849	5.281667	5.278247	5.271552	5.264856
$E_{12} dx/dE_{12}$, cm	-4.66106	-4.59849	-4.53592	-4.55807	-4.61999	-4.68444	-4.79307	-4.9017
$E_{13} dx/dE_{13}$, cm	11.67914	11.74004	11.80095	11.77909	11.7184	11.66376	11.71458	11.7654
$E_{14} dx/dE_{14}$, cm	10.65221	10.70713	10.76206	10.83508	10.9166	10.99632	11.04464	11.09295
$E_{15} dx/dE_{15}$, cm	-5.2549	-5.22991	-5.20491	-5.19006	-5.17997	-5.17449	-5.2494	-5.32431
$E_{16} dx/dE_{16}$, cm	3.722495	3.688002	3.653507	3.60561	3.551425	3.503879	3.572005	3.640133
$\sigma_E dx/d\sigma_E$, cm	-0.61351	-0.58171	-0.54991	-0.55276	-0.57187	-0.59034	-0.59762	-0.60491
$T_i dx/dT_i$, cm	1.024486	0.982968	0.941448	0.941428	0.960882	0.979747	0.988351	0.996955
$I_0 dx/dI_0$, cm	-0.25334	-0.15825	-0.06316	0.011765	0.077218	0.139076	0.138307	0.137538
$\rho dx/d\rho$, cm	-2.28165	-2.19199	-2.10234	-2.10019	-2.13912	-2.18122	-2.27862	-2.37602
$c dx/dc$, cm	-2.08727	-2.11059	-2.13391	-2.19662	-2.27781	-2.35557	-2.37348	-2.39139
$h_r dx/dh_r$, cm	-27.9253	-28.1252	-28.3251	-28.4872	-28.6315	-28.7803	-29.0068	-29.2333
$\varepsilon dx/d\varepsilon$, cm	2.238023	2.309548	2.381075	2.389185	2.367535	2.349472	2.393901	2.438329
$(\sigma+1)dx/d(\sigma+1)$, cm	-7.34202	-7.52513	-7.70824	-7.81573	-7.88773	-7.96277	-8.09077	-8.21877
$k_e dx/dk_e$, cm	1.282292	1.344837	1.407383	1.518568	1.652576	1.784972	1.889241	1.993512

Table B.1. Continued

Time, min	51.89433	52.46029	53.02626	53.59223	54.15819	54.72416	55.29013	55.85609
x_{exp}, cm	5.769341	5.81766	5.865573	5.91308	5.96018	6.006872	6.053154	6.099027
x_{model}, cm	4.365605	4.402803	4.440001	4.477213	4.51443	4.551686	4.589757	4.627828
$E_1 dx/dE_1$, cm	0.386544	0.384034	0.381525	0.373693	0.363906	0.356701	0.405236	0.453769
$E_2 dx/dE_2$, cm	4.318489	4.441222	4.563957	4.642412	4.704587	4.763992	4.763573	4.763154
$E_3 dx/dE_3$, cm	-4.04244	-4.04322	-4.04399	-4.06194	-4.0862	-4.11229	-4.17797	-4.24365
$E_4 dx/dE_4$, cm	4.657453	4.611336	4.565217	4.536987	4.515335	4.494409	4.489189	4.48397
$E_5 dx/dE_5$, cm	29.88409	30.0142	30.14432	30.32584	30.52626	30.7266	30.92533	31.12406
$E_6 dx/dE_6$, cm	-0.23818	-0.2158	-0.19341	-0.22886	-0.28557	-0.34169	-0.38514	-0.42858
$E_7 dx/dE_7$, cm	8.892965	8.913762	8.934559	8.964402	8.99757	9.029927	9.044775	9.059623
$E_8 dx/dE_8$, cm	-1.32428	-1.32373	-1.32318	-1.36486	-1.42208	-1.47705	-1.48358	-1.49011
$E_9 dx/dE_9$, cm	-23.1573	-23.3974	-23.6375	-23.8712	-24.1027	-24.3318	-24.5096	-24.6875
$E_{10} dx/dE_{10}$, cm	-9.90578	-10.0099	-10.114	-10.2403	-10.3749	-10.5064	-10.571	-10.6356
$E_{11} dx/dE_{11}$, cm	5.248257	5.217952	5.187647	5.201994	5.232758	5.262299	5.26544	5.268581
$E_{12} dx/dE_{12}$, cm	-4.99727	-5.07475	-5.15223	-5.21423	-5.27053	-5.32602	-5.36407	-5.40211
$E_{13} dx/dE_{13}$, cm	11.84585	11.9673	12.08875	12.16456	12.22359	12.28094	12.30218	12.32343
$E_{14} dx/dE_{14}$, cm	11.10607	11.07047	11.03487	11.06574	11.12104	11.17795	11.26932	11.36069
$E_{15} dx/dE_{15}$, cm	-5.40537	-5.49491	-5.58446	-5.6213	-5.63877	-5.65747	-5.70283	-5.7482
$E_{16} dx/dE_{16}$, cm	3.72324	3.827073	3.930908	3.960611	3.96306	3.964083	3.93433	3.904578
$\sigma_E dx/d\sigma_E$, cm	-0.61888	-0.64211	-0.66533	-0.74473	-0.84476	-0.94697	-1.09596	-1.24494
$T_i dx/dT_i$, cm	0.997799	0.987903	0.978007	0.979668	0.985577	0.995686	1.096432	1.197177
$I_0 dx/dI_0$, cm	0.118168	0.073063	0.027956	0.036249	0.064173	0.092892	0.138758	0.184624
$\rho dx/d\rho$, cm	-2.4625	-2.53387	-2.60524	-2.62881	-2.63482	-2.6355	-2.52119	-2.40687
$c dx/dc$, cm	-2.39359	-2.37407	-2.35456	-2.32644	-2.29516	-2.2654	-2.26856	-2.27172
$h_r dx/dh_r$, cm	-29.4492	-29.6504	-29.8515	-29.9989	-30.1264	-30.2528	-30.3537	-30.4546
$\varepsilon dx/d\varepsilon$, cm	2.521949	2.659796	2.797644	2.902896	2.996162	3.086317	3.109282	3.132246
$(\sigma+1)dx/d(\sigma+1)$, cm	-8.32849	-8.41292	-8.49734	-8.55518	-8.60324	-8.65154	-8.70518	-8.75881
$k_e dx/dk_e$, cm	2.007489	1.896525	1.785559	1.760805	1.767746	1.773282	1.748494	1.723706

Table B.1. Continued

Time, min	56.42206	56.98803	57.55399	58.11996	58.68592	59.25189	59.81786	60.38382
x_{exp}, cm	6.144488	6.189537	6.234173	6.278396	6.322203	6.365594	6.408569	6.451126
x_{model}, cm	4.665663	4.70317	4.740675	4.777502	4.814103	4.850675	4.88575	4.920824
$E_1 dx/dE_1$, cm	0.473748	0.453906	0.434063	0.437385	0.448371	0.458331	0.415983	0.373636
$E_2 dx/dE_2$, cm	4.750538	4.720911	4.691286	4.640594	4.582933	4.525986	4.505488	4.48499
$E_3 dx/dE_3$, cm	-4.32442	-4.42624	-4.52806	-4.68613	-4.86283	-5.03768	-5.11864	-5.1996
$E_4 dx/dE_4$, cm	4.487899	4.504585	4.521271	4.56214	4.61101	4.661245	4.781019	4.900791
$E_5 dx/dE_5$, cm	31.31246	31.48645	31.66044	31.7639	31.84402	31.92392	31.99274	32.06156
$E_6 dx/dE_6$, cm	-0.47031	-0.50967	-0.54902	-0.58135	-0.61136	-0.64101	-0.65219	-0.66337
$E_7 dx/dE_7$, cm	9.094628	9.157744	9.220858	9.309226	9.405948	9.501319	9.527773	9.554226
$E_8 dx/dE_8$, cm	-1.48499	-1.46364	-1.44228	-1.38589	-1.3179	-1.25152	-1.26701	-1.28251
$E_9 dx/dE_9$, cm	-24.8372	-24.9475	-25.0579	-25.1049	-25.1309	-25.1557	-25.1144	-25.0731
$E_{10} dx/dE_{10}$, cm	-10.7055	-10.7829	-10.8604	-10.9675	-11.0845	-11.1985	-11.1633	-11.1282
$E_{11} dx/dE_{11}$, cm	5.268206	5.262929	5.257652	5.299655	5.357302	5.414518	5.449776	5.485033
$E_{12} dx/dE_{12}$, cm	-5.44702	-5.50151	-5.556	-5.58344	-5.60192	-5.62023	-5.62951	-5.63879
$E_{13} dx/dE_{13}$, cm	12.35464	12.39976	12.44488	12.47499	12.50014	12.52588	12.58218	12.63847
$E_{14} dx/dE_{14}$, cm	11.47539	11.62264	11.76989	11.97566	12.2008	12.42362	12.52839	12.63315
$E_{15} dx/dE_{15}$, cm	-5.8346	-5.97823	-6.12186	-6.24908	-6.37086	-6.49218	-6.59011	-6.68803
$E_{16} dx/dE_{16}$, cm	3.894394	3.911501	3.928607	3.909792	3.879091	3.846981	3.743078	3.639177
$\sigma_E dx/d\sigma_E$, cm	-1.34316	-1.37057	-1.39798	-1.36792	-1.31885	-1.26936	-1.19829	-1.12721
$T_i dx/dT_i$, cm	1.259973	1.269844	1.279716	1.258158	1.226202	1.193031	1.097965	1.002901
$I_0 dx/dI_0$, cm	0.23568	0.293974	0.352267	0.393584	0.429284	0.461726	0.328109	0.194495
$\rho dx/d\rho$, cm	-2.30005	-2.20367	-2.10729	-2.02047	-1.93681	-1.85533	-1.88492	-1.91451
$c dx/dc$, cm	-2.29577	-2.34896	-2.40215	-2.47733	-2.5598	-2.64122	-2.66922	-2.69721
$h_r dx/dh_r$, cm	-30.579	-30.7359	-30.8929	-31.0927	-31.3067	-31.5194	-31.663	-31.8067
$\varepsilon dx/d\varepsilon$, cm	3.150131	3.160933	3.171735	3.21424	3.267234	3.320676	3.396877	3.473076
$(\sigma+1)dx/d(\sigma+1)$, cm	-8.77838	-8.75044	-8.7225	-8.67757	-8.62703	-8.57782	-8.59646	-8.6151
$k_e dx/dk_e$, cm	1.706708	1.700571	1.694436	1.644587	1.580275	1.51641	1.475366	1.434322

Table B.1. Continued

Time, min	60.94979	61.51576	62.08172	62.64769	63.21366	63.77962
x_{exp}, cm	6.493264	6.534982	6.57628	6.617156	6.657609	6.697639
x_{model}, cm	4.955834	4.990522	5.02521	5.059518	5.092878	5.126236
$E_1 dx/dE_1$, cm	0.361055	0.495687	0.630316	0.750976	0.836643	0.922308
$E_2 dx/dE_2$, cm	4.462115	4.427479	4.392843	4.346896	4.272619	4.198343
$E_3 dx/dE_3$, cm	-5.28008	-5.35815	-5.43621	-5.51059	-5.57573	-5.64087
$E_4 dx/dE_4$, cm	5.020575	5.140412	5.260247	5.367374	5.442669	5.517962
$E_5 dx/dE_5$, cm	32.13376	32.2227	32.31164	32.41951	32.5748	32.73008
$E_6 dx/dE_6$, cm	-0.67822	-0.71118	-0.74415	-0.78229	-0.83338	-0.88447
$E_7 dx/dE_7$, cm	9.573979	9.560597	9.547214	9.499733	9.366847	9.233964
$E_8 dx/dE_8$, cm	-1.29222	-1.2733	-1.25439	-1.20813	-1.09339	-0.97865
$E_9 dx/dE_9$, cm	-25.0442	-25.0765	-25.1087	-25.1829	-25.362	-25.541
$E_{10} dx/dE_{10}$, cm	-11.0847	-11.0005	-10.9162	-10.8734	-10.9342	-10.9951
$E_{11} dx/dE_{11}$, cm	5.521388	5.563177	5.604965	5.652484	5.714355	5.776225
$E_{12} dx/dE_{12}$, cm	-5.65885	-5.7322	-5.80555	-5.8648	-5.88875	-5.9127
$E_{13} dx/dE_{13}$, cm	12.70272	12.8063	12.90988	12.9863	12.99471	13.00311
$E_{14} dx/dE_{14}$, cm	12.7128	12.66819	12.62358	12.56895	12.48922	12.4095
$E_{15} dx/dE_{15}$, cm	-6.7652	-6.73967	-6.71414	-6.6887	-6.6635	-6.63831
$E_{16} dx/dE_{16}$, cm	3.539301	3.459334	3.379369	3.316469	3.296313	3.276158
$\sigma_E dx/d\sigma_E$, cm	-1.04987	-0.94153	-0.83319	-0.71424	-0.56871	-0.42318
$T_i dx/dT_i$, cm	0.924947	0.931621	0.938295	0.959284	1.016126	1.072967
$I_0 dx/dI_0$, cm	0.058574	-0.08874	-0.23606	-0.31114	-0.20529	-0.09944
$\rho dx/d\rho$, cm	-1.93663	-1.92177	-1.90691	-1.92323	-2.01766	-2.11209
$c dx/dc$, cm	-2.71793	-2.70265	-2.68736	-2.66741	-2.63574	-2.60408
$h_r dx/dh_r$, cm	-31.9347	-31.985	-32.0353	-32.0828	-32.123	-32.1632
$\varepsilon dx/d\varepsilon$, cm	3.53417	3.520555	3.50694	3.503038	3.523464	3.543889
$(\sigma+1)dx/d(\sigma+1)$, cm	-8.64267	-8.71445	-8.78622	-8.85565	-8.91921	-8.98276
$k_e dx/dk_e$, cm	1.395697	1.369043	1.342389	1.324776	1.32981	1.334844

Table B.2. Measured, Predicted Measurements and Sensitivity Matrix, Experiment 2: 750 C

Time, min	2.25	2.802101	3.354202	3.906303	4.458403	5.010504	5.562605	6.114706
x_{exp}, cm	0.253504	0.397054	0.538829	0.678847	0.817126	0.953686	1.088542	1.221715
x_{model}, cm	0.502354	0.655016	0.819475	0.973063	1.126577	1.282418	1.417811	1.572104
$E_1 dx/dE_1$, cm	-0.82622	-0.15743	-0.23347	-0.09466	-0.91097	-0.61382	-0.62349	-1.28714
$E_2 dx/dE_2$, cm	0.126543	0.02402	0.309816	0.144865	-0.06644	-0.0782	0.108216	0.404319
$E_3 dx/dE_3$, cm	-0.07686	-0.31583	-1.06862	-0.58	-1.0619	-1.31305	-1.06032	-1.87521
$E_4 dx/dE_4$, cm	0.698814	0.620826	1.380878	0.969342	1.919512	1.385282	1.245762	2.318534
$E_5 dx/dE_5$, cm	-0.93503	-1.38903	-2.98553	-2.65092	-3.918	-4.20613	-4.30393	-5.16879
$E_6 dx/dE_6$, cm	-0.78869	-1.13353	-3.01928	-3.10513	-4.17156	-4.91547	-5.52853	-5.67793
$E_7 dx/dE_7$, cm	0.611798	0.637851	1.688658	1.099042	1.862234	2.559313	2.009072	3.298595
$E_8 dx/dE_8$, cm	-0.67736	-0.62279	-1.64508	-1.02477	-1.59344	-1.94527	-1.59942	-2.88471
$E_9 dx/dE_9$, cm	0.865901	1.04191	2.69349	2.665789	3.621718	4.663045	5.232172	5.589809
$E_{10} dx/dE_{10}$, cm	0.008529	-0.32023	-0.7302	-0.4863	-1.42087	-1.18276	-1.19269	-2.24605
$E_{11} dx/dE_{11}$, cm	0.357801	0.41399	0.987483	0.73012	1.731762	1.151334	1.094041	1.500589
$E_{12} dx/dE_{12}$, cm	0.115255	-0.15389	-0.48722	-0.28859	-0.76007	-0.57984	-0.3638	-0.63928
$E_{13} dx/dE_{13}$, cm	-0.20605	0.127356	0.337876	0.351171	0.761637	1.238302	1.303674	2.579893
$E_{14} dx/dE_{14}$, cm	1.196081	0.796971	1.786111	1.054149	1.575747	1.602202	1.258522	2.089329
$E_{15} dx/dE_{15}$, cm	-0.2	-0.26697	-0.55739	-0.48233	-1.04547	-0.49651	-0.33322	-0.78062
$E_{16} dx/dE_{16}$, cm	0.093937	0.002819	0.200908	-0.01505	0.136036	0.412933	0.073297	0.068815
$\sigma_E dx/d\sigma_E$, cm	-0.10783	-0.06099	-0.01315	0.126841	0.270457	0.232385	0.305462	0.743886
$T_i dx/dT_i$, cm	0.196423	0.312073	0.246929	0.146336	0.248743	0.314608	0.243989	0.687757
$I_0 dx/dI_0$, cm	-0.03724	-0.10475	-0.60486	-0.25295	-0.77425	-0.55492	-0.39357	-0.75691
$\rho dx/d\rho$, cm	0.134435	0.05813	-0.0987	-0.11284	-0.54657	-0.45189	-0.44248	-0.75566
$c dx/dc$, cm	-0.36466	-0.38014	-0.85062	-0.73391	-1.46847	-1.18208	-0.98756	-1.55933
$h_r dx/dh_r$, cm	0.035184	0.02292	-0.1597	-0.08169	-0.25267	-0.1323	-0.1407	-0.17415
$\varepsilon dx/d\varepsilon$, cm	0.406939	0.710209	1.572665	1.107617	2.201279	1.471311	1.449774	2.503407
$(\sigma+1)dx/d(\sigma+1)$, cm	-0.13306	-0.16248	-0.54415	-0.2439	-0.52242	-0.7784	-0.39977	-0.38749
$k_e dx/dk_e$, cm	-0.1385	-0.02505	-0.01118	0.136512	0.407009	0.226385	0.056449	0.259672

Table B.2. Continued

Time, min	6.666807	7.218908	7.771008	8.323109	8.87521	9.427311	9.979412	10.53151
x_{exp}, cm	1.353222	1.483082	1.611312	1.737931	1.862957	1.986408	2.108302	2.228658
x_{model}, cm	1.712439	1.842727	1.975219	2.113724	2.245315	2.367427	2.489362	2.610101
$E_1 dx/dE_1$, cm	-0.92	-0.75542	-1.08344	-1.5546	-0.95489	-0.64692	-0.72358	-0.8605
$E_2 dx/dE_2$, cm	0.71809	0.602213	0.914111	1.537016	1.610734	1.036626	1.052672	1.01925
$E_3 dx/dE_3$, cm	-2.15069	-1.5979	-2.25128	-3.19127	-3.19676	-2.92585	-2.81672	-2.9378
$E_4 dx/dE_4$, cm	1.61857	1.588455	2.268476	2.447696	1.936723	1.93916	2.144198	2.321628
$E_5 dx/dE_5$, cm	-5.47107	-6.18347	-7.02384	-7.13673	-7.28659	-8.07404	-8.95993	-9.40652
$E_6 dx/dE_6$, cm	-5.92802	-7.05058	-8.04379	-8.04072	-8.40849	-9.23004	-10.1598	-10.6484
$E_7 dx/dE_7$, cm	3.486685	3.145768	3.756177	4.371756	4.465068	4.497185	4.660124	4.982273
$E_8 dx/dE_8$, cm	-2.43548	-2.15334	-2.62845	-3.40442	-3.66222	-3.71007	-3.51935	-3.71322
$E_9 dx/dE_9$, cm	6.031756	7.354714	8.436843	8.812894	9.166589	10.14862	10.94579	11.43716
$E_{10} dx/dE_{10}$, cm	-1.90957	-1.45601	-2.03055	-2.95679	-3.02638	-2.67373	-2.55667	-2.66771
$E_{11} dx/dE_{11}$, cm	1.137738	0.912969	1.144509	1.305541	0.947593	0.858607	0.9687	1.298607
$E_{12} dx/dE_{12}$, cm	-0.52877	-0.47911	-0.80905	-1.36527	-1.60348	-1.28423	-1.13881	-1.26048
$E_{13} dx/dE_{13}$, cm	2.55835	2.019227	2.49918	3.331026	3.65291	3.724167	3.792898	3.871809
$E_{14} dx/dE_{14}$, cm	2.030947	1.246394	1.332452	1.933896	2.207423	1.842501	1.434084	1.350735
$E_{15} dx/dE_{15}$, cm	-0.64393	-0.50585	-0.86424	-1.56621	-1.6463	-1.25111	-1.25785	-1.47918
$E_{16} dx/dE_{16}$, cm	0.177208	0.179428	0.187304	0.260756	0.659325	0.762937	0.525125	0.332559
$\sigma_E dx/d\sigma_E$, cm	0.302175	0.302851	0.474244	0.751929	0.87306	0.40027	0.271196	0.21784
$T_i dx/dT_i$, cm	0.678019	0.477489	0.691784	0.986124	0.93028	0.80679	0.5768	0.702485
$l_0 dx/dl_0$, cm	-0.60264	-0.47146	-0.79949	-1.23824	-0.66121	-0.30987	-0.27381	-0.15239
$\rho dx/d\rho$, cm	-0.68301	-0.31175	-0.53753	-0.77647	-0.97185	-0.75818	-0.90086	-1.12208
$c dx/dc$, cm	-1.36689	-0.92231	-0.96352	-1.25968	-1.13397	-0.99459	-0.9435	-0.97766
$h_r dx/dh_r$, cm	-0.26451	-0.22524	-0.38784	-0.46695	-0.38017	-0.35615	-0.43278	-0.54977
$\varepsilon dx/d\varepsilon$, cm	2.030795	1.537835	1.868153	2.72673	2.917282	2.440779	1.973278	2.01227
$(\sigma+1)dx/d(\sigma+1)$, cm	-0.27372	-0.13036	-0.19533	-0.66995	-0.997	-0.73364	-0.63678	-0.60326
$k_e dx/dk_e$, cm	0.169233	0.326925	0.393627	0.51796	0.225653	0.233181	0.206691	0.277193

Table B.2. Continued

Time, min	11.08361	11.63571	12.18782	12.73992	13.29202	13.84412	14.39622	14.94832
x_{exp}, cm	2.347494	2.464827	2.580677	2.695062	2.807998	2.919506	3.029603	3.138307
x_{model}, cm	2.728935	2.847009	2.963253	3.078735	3.195286	3.311612	3.426081	3.535011
$E_1 dx/dE_1$, cm	-0.91752	-1.1356	-1.34888	-1.24014	-1.09071	-0.95404	-1.02525	-1.01076
$E_2 dx/dE_2$, cm	1.078177	1.230085	1.122709	1.035093	0.998755	1.065065	1.136417	1.214737
$E_3 dx/dE_3$, cm	-3.52218	-4.16482	-4.3496	-4.43454	-4.54895	-4.55934	-4.46113	-4.46718
$E_4 dx/dE_4$, cm	2.753966	2.984686	3.02748	3.100848	2.962836	2.874798	2.800029	2.546867
$E_5 dx/dE_5$, cm	-9.65729	-10.1488	-10.587	-10.8606	-11.1643	-11.4797	-11.7281	-12.2188
$E_6 dx/dE_6$, cm	-10.9144	-11.1454	-11.4725	-12.0152	-12.5698	-13.1809	-13.8126	-14.5591
$E_7 dx/dE_7$, cm	5.389987	5.691106	5.91828	5.981974	6.016659	5.920172	5.939386	6.104922
$E_8 dx/dE_8$, cm	-4.06924	-4.3114	-4.66921	-4.84219	-4.97189	-4.93338	-4.67987	-4.6804
$E_9 dx/dE_9$, cm	11.80834	12.19086	12.53621	12.9269	13.1386	13.48874	14.00963	14.55274
$E_{10} dx/dE_{10}$, cm	-3.24943	-4.04681	-4.25631	-4.4166	-4.73295	-5.09095	-5.18259	-5.17882
$E_{11} dx/dE_{11}$, cm	1.680617	2.108786	2.109067	2.190863	2.31734	2.402487	2.570513	2.673298
$E_{12} dx/dE_{12}$, cm	-1.42496	-1.66644	-1.80174	-1.97139	-2.25466	-2.5814	-2.85688	-2.89458
$E_{13} dx/dE_{13}$, cm	4.256875	4.716118	5.061478	5.373916	5.5183	5.639475	5.801531	5.952122
$E_{14} dx/dE_{14}$, cm	1.400711	1.588077	1.995143	2.216892	2.412693	2.605818	2.914816	3.226596
$E_{15} dx/dE_{15}$, cm	-1.8013	-1.98477	-2.33455	-2.68303	-2.64654	-2.57901	-2.68668	-2.80036
$E_{16} dx/dE_{16}$, cm	0.232543	0.093354	0.016013	0.122718	0.092353	0.256646	0.339513	0.342958
$\sigma_E dx/d\sigma_E$, cm	0.213204	0.399805	0.337465	0.457684	0.50764	0.545343	0.346401	0.381046
$T_i dx/dT_i$, cm	0.741948	0.643896	0.534861	0.615363	0.592035	0.735212	0.872305	0.998137
$I_0 dx/dI_0$, cm	-0.03761	-0.28046	-0.44345	-0.29706	-0.12106	-0.13545	-0.3785	-0.40729
$\rho dx/d\rho$, cm	-1.4495	-1.90724	-2.21069	-2.55323	-2.66626	-2.78748	-2.82955	-2.90131
$c dx/dc$, cm	-1.08542	-1.21212	-1.25945	-1.36987	-1.54728	-1.5744	-1.53441	-1.58466
$h_r dx/dh_r$, cm	-0.71163	-0.69424	-0.63749	-0.5601	-0.44937	-0.49726	-0.60565	-0.62467
$\varepsilon dx/d\varepsilon$, cm	2.159668	2.438117	2.850186	3.152166	3.378777	3.476386	3.761885	3.960061
$(\sigma+1) dx/d(\sigma+1)$, cm	-0.68064	-0.75686	-0.82228	-0.79473	-0.89281	-0.99049	-1.05345	-0.96147
$k_e dx/dk_e$, cm	0.459114	0.506464	0.63855	0.692242	0.604031	0.177543	0.033798	-0.06649

Table B.2. Continued

Time, min	15.50042	16.05252	16.60462	17.15672	17.70882	18.26092	18.81303	19.36513
x_{exp}, cm	3.245636	3.351609	3.456244	3.559558	3.661571	3.762301	3.861765	3.959981
x_{model}, cm	3.641371	3.747001	3.847336	3.951125	4.050957	4.146641	4.23967	4.324909
$E_1 dx/dE_1$, cm	-0.70809	-0.82884	-0.94689	-1.02607	-0.79181	-0.41975	-1.10852	-1.5855
$E_2 dx/dE_2$, cm	1.520782	1.821679	2.109086	2.270656	2.295058	2.396847	2.821654	3.184761
$E_3 dx/dE_3$, cm	-4.54918	-4.5967	-4.52369	-4.61676	-4.57685	-4.2044	-3.92651	-3.919
$E_4 dx/dE_4$, cm	2.411747	2.355754	2.394364	2.579722	2.269798	1.931505	1.929207	2.228868
$E_5 dx/dE_5$, cm	-12.8676	-13.0122	-13.1223	-13.0534	-13.3733	-14.3351	-15.1032	-15.3418
$E_6 dx/dE_6$, cm	-15.3136	-15.8097	-16.1461	-17.0243	-17.5463	-17.8219	-18.3443	-18.9517
$E_7 dx/dE_7$, cm	6.34403	6.485722	6.278007	6.619968	6.622982	6.06406	5.666203	5.682243
$E_8 dx/dE_8$, cm	-4.95075	-5.25952	-5.25452	-5.38872	-5.47605	-5.39117	-5.40429	-5.56007
$E_9 dx/dE_9$, cm	14.94108	15.28537	15.52121	16.04974	16.9821	17.57238	18.18465	18.56914
$E_{10} dx/dE_{10}$, cm	-5.24302	-5.38885	-5.52158	-5.62105	-5.72768	-5.79854	-5.73709	-5.77735
$E_{11} dx/dE_{11}$, cm	2.949967	3.070172	3.17105	3.529682	3.983655	4.283234	4.777646	4.865893
$E_{12} dx/dE_{12}$, cm	-3.11403	-3.35762	-3.50277	-3.51202	-3.48406	-3.66259	-3.88265	-4.15451
$E_{13} dx/dE_{13}$, cm	5.923275	5.940842	6.118565	6.270004	6.097458	5.772159	5.780754	6.055115
$E_{14} dx/dE_{14}$, cm	3.45673	3.504634	3.360558	3.594327	3.877627	3.853343	3.684619	3.973149
$E_{15} dx/dE_{15}$, cm	-2.86369	-2.79333	-2.55713	-2.46921	-2.59088	-3.03288	-3.39303	-3.29171
$E_{16} dx/dE_{16}$, cm	0.496883	0.666563	0.771407	0.841018	0.947552	1.260427	1.663851	1.52739
$\sigma_E dx/d\sigma_E$, cm	0.507116	0.63502	0.651533	0.657826	0.44394	0.484843	0.495815	0.528257
$T_i dx/dT_i$, cm	0.839469	0.656176	0.602164	0.869627	1.128312	0.74845	0.485772	0.131037
$I_0 dx/dI_0$, cm	-0.47931	-0.40488	-0.36459	-0.14564	-0.02485	-0.10456	0.002934	-0.09795
$\rho dx/d\rho$, cm	-2.90687	-2.91907	-3.14689	-3.19332	-2.91517	-2.30504	-2.549	-2.93957
$c dx/dc$, cm	-1.35132	-1.43853	-1.70505	-2.04836	-2.00512	-1.95228	-2.30727	-2.25143
$h_r dx/dh_r$, cm	-0.56245	-0.53748	-0.38405	-0.44913	-0.31089	-0.35072	-0.93793	-1.48827
$\varepsilon dx/d\varepsilon$, cm	3.739223	3.572521	3.587927	3.550775	3.522847	4.200667	4.700608	4.746553
$(\sigma+1)dx/d(\sigma+1)$, cm	-0.91921	-0.62036	-0.69785	-0.79107	-0.96359	-1.17267	-1.50854	-1.58872
$k_e dx/dk_e$, cm	0.047541	0.303688	0.431198	0.246582	0.578771	0.820702	1.463015	1.715572

Table B.2. Continued

Time, min	19.91723	20.46933	21.02143	21.57353	22.12563	22.67773	23.22983	23.78193
x_{exp}, cm	4.056969	4.152746	4.24733	4.34074	4.432994	4.52411	4.614106	4.703001
x_{model}, cm	4.40827	4.4927	4.577122	4.658768	4.742041	4.822895	4.902116	4.983031
$E_1 dx/dE_1$, cm	-1.79747	-1.78752	-1.71595	-1.77984	-1.92769	-1.9619	-2.1591	-2.2002
$E_2 dx/dE_2$, cm	3.400523	3.424878	3.355932	3.344546	3.122549	3.049239	3.203193	3.514087
$E_3 dx/dE_3$, cm	-3.86943	-3.88613	-4.07267	-4.38955	-4.6153	-4.77037	-4.89827	-5.10418
$E_4 dx/dE_4$, cm	2.431496	2.569659	2.77904	3.076658	2.774418	2.710759	2.903408	3.119686
$E_5 dx/dE_5$, cm	-15.6226	-15.8726	-16.1302	-16.5514	-16.9176	-16.9573	-17.1288	-17.3894
$E_6 dx/dE_6$, cm	-19.4386	-19.7976	-20.1082	-20.4922	-21.0706	-21.5851	-21.7985	-21.8487
$E_7 dx/dE_7$, cm	6.013851	6.367887	6.644333	6.957784	7.361192	7.638145	7.831325	7.92522
$E_8 dx/dE_8$, cm	-6.00122	-6.27877	-6.27802	-6.30981	-6.58077	-6.60497	-6.58653	-6.53364
$E_9 dx/dE_9$, cm	18.76355	19.0009	19.46173	20.12036	20.57395	20.74355	21.1266	21.51524
$E_{10} dx/dE_{10}$, cm	-6.12192	-6.33589	-6.24668	-6.09943	-6.24605	-6.52244	-6.81965	-7.1456
$E_{11} dx/dE_{11}$, cm	4.572365	4.195445	3.931275	3.760922	3.442386	3.534046	3.722827	3.84292
$E_{12} dx/dE_{12}$, cm	-4.41006	-4.60958	-4.72621	-4.75362	-4.63384	-4.64209	-4.75925	-4.8771
$E_{13} dx/dE_{13}$, cm	6.275332	6.335021	6.51004	7.159895	7.74338	7.586479	7.577627	7.813982
$E_{14} dx/dE_{14}$, cm	4.292453	4.682212	5.099109	5.3732	5.382985	5.371841	5.601931	5.986299
$E_{15} dx/dE_{15}$, cm	-3.20264	-3.18658	-3.25455	-3.38665	-3.38251	-3.42607	-3.63247	-3.9161
$E_{16} dx/dE_{16}$, cm	1.31333	1.296985	1.483235	1.636817	1.540104	1.584496	1.521398	1.259308
$\sigma_E dx/d\sigma_E$, cm	0.631753	0.692489	0.707239	0.762762	0.712829	1.062007	1.202516	1.138868
$T_i dx/dT_i$, cm	-0.05504	-0.25883	-0.42476	-0.31502	-0.13161	0.152153	0.367987	0.486754
$l_0 dx/dl_0$, cm	-0.15765	-0.17348	-0.21024	-0.29918	-0.21639	-0.49729	-0.54376	-0.46683
$\rho dx/d\rho$, cm	-2.95821	-2.80642	-2.7731	-2.98261	-3.12427	-2.88721	-2.77825	-2.76214
$c dx/dc$, cm	-2.3054	-2.65386	-3.06852	-3.13097	-2.95508	-3.05643	-3.04539	-2.95672
$h_r dx/dh_r$, cm	-1.46538	-1.04	-0.60354	-0.51429	-0.76538	-0.73538	-0.80345	-0.89795
$\varepsilon dx/d\varepsilon$, cm	4.499406	4.234851	4.140538	4.184488	3.936868	3.967215	4.297778	4.626047
$(\sigma+1) dx/d(\sigma+1)$, cm	-1.50272	-1.45629	-1.50372	-1.52217	-1.35412	-1.17768	-1.17757	-1.13569
$k_e dx/dk_e$, cm	1.767179	1.920087	2.214601	2.400499	2.095803	2.082061	2.125356	2.064337

Table B.2. Continued

Time, min	24.33403	24.88613	25.43824	25.99034	26.54244	27.09454	27.64664	28.19874
x_{exp}, cm	4.790812	4.877557	4.963256	5.047927	5.131586	5.214253	5.295946	5.376683
x_{model}, cm	5.067549	5.151504	5.232697	5.314086	5.392766	5.469622	5.547536	5.62103
$E_1 dx/dE_1$, cm	-1.85129	-1.47995	-1.42011	-1.11935	-0.76463	-0.49486	-0.45095	-0.59149
$E_2 dx/dE_2$, cm	3.865099	4.067504	3.945723	3.81961	3.828698	3.959431	4.131964	4.214743
$E_3 dx/dE_3$, cm	-5.427	-5.67135	-5.90013	-6.01329	-5.98459	-5.88104	-5.81425	-5.73279
$E_4 dx/dE_4$, cm	3.210719	3.379858	3.509287	3.523925	3.543886	3.613469	3.745136	3.726741
$E_5 dx/dE_5$, cm	-17.5784	-17.4731	-17.5879	-17.6793	-17.8369	-18.1348	-18.6793	-18.9477
$E_6 dx/dE_6$, cm	-21.874	-21.8917	-22.1709	-22.6257	-23.1108	-23.543	-23.8583	-24.1579
$E_7 dx/dE_7$, cm	7.890606	7.751044	7.890517	7.809909	7.694358	7.623235	7.626313	7.690578
$E_8 dx/dE_8$, cm	-6.38879	-6.05311	-5.89069	-5.89665	-5.96322	-6.05542	-6.18852	-6.11793
$E_9 dx/dE_9$, cm	21.6854	21.73184	22.13359	22.74964	23.11716	23.27018	23.50439	23.53872
$E_{10} dx/dE_{10}$, cm	-7.43279	-7.42254	-7.31173	-7.42791	-7.49768	-7.49294	-7.51968	-7.59757
$E_{11} dx/dE_{11}$, cm	3.831153	3.889312	4.027583	4.097604	4.140434	4.130159	3.982519	3.712057
$E_{12} dx/dE_{12}$, cm	-4.88397	-4.75163	-4.57805	-4.62388	-4.84044	-5.10684	-5.26042	-5.25319
$E_{13} dx/dE_{13}$, cm	8.251929	8.675789	8.839271	8.846008	8.834909	8.855572	8.912917	8.971213
$E_{14} dx/dE_{14}$, cm	6.350739	6.454863	6.463104	6.504081	6.657633	6.887904	7.103056	6.961813
$E_{15} dx/dE_{15}$, cm	-4.16757	-4.30796	-4.16143	-3.82901	-3.5163	-3.30789	-3.24524	-3.27689
$E_{16} dx/dE_{16}$, cm	0.874296	0.84025	1.115188	1.192057	1.307157	1.493794	1.677655	1.659881
$\sigma_E dx/d\sigma_E$, cm	0.986174	0.952045	0.905179	0.656757	0.354627	0.016537	-0.43044	-0.56544
$T_i dx/dT_i$, cm	0.578987	0.90382	0.917913	0.901541	0.826622	0.736329	0.718236	0.820305
$I_0 dx/dI_0$, cm	-0.47833	-0.7317	-0.7161	-0.71386	-0.66839	-0.60253	-0.58587	-0.87354
$\rho dx/d\rho$, cm	-2.74612	-2.68839	-2.81206	-2.81132	-2.89549	-3.05375	-3.15412	-3.01588
$c dx/dc$, cm	-2.90684	-3.0412	-3.32822	-3.6035	-3.81603	-3.91744	-3.82832	-3.76483
$h_r dx/dh_r$, cm	-0.87282	-0.62426	-0.5229	-0.52022	-0.58705	-0.69493	-0.82446	-0.82674
$\varepsilon dx/d\varepsilon$, cm	4.700007	4.636012	4.537882	4.502397	4.639535	4.878808	5.056733	5.115568
$(\sigma+1) dx/d(\sigma+1)$, cm	-0.89896	-0.70424	-0.56997	-0.425	-0.44035	-0.54169	-0.51601	-0.52055
$k_e dx/dk_e$, cm	1.909995	2.094977	2.09643	1.881334	1.862531	1.989578	1.952483	1.780136

Table B.2. Continued

Time, min	28.75084	29.30294	29.85504	30.40714	30.95924	31.51134	32.06345	32.61555
x_{exp}, cm	5.456483	5.535362	5.613341	5.690436	5.766666	5.84205	5.916604	5.990349
x_{model}, cm	5.695479	5.769529	5.84063	5.912083	5.985022	6.058712	6.126514	6.195322
$E_1 dx/dE_1$, cm	-0.67166	-0.64747	-0.46212	-0.52142	-0.55944	-0.53777	-0.55849	-0.52693
$E_2 dx/dE_2$, cm	4.325372	4.412851	4.386131	4.456439	4.500763	4.49696	4.478437	4.425298
$E_3 dx/dE_3$, cm	-5.51194	-5.23077	-5.02978	-5.0336	-5.10508	-5.20327	-5.20253	-5.21042
$E_4 dx/dE_4$, cm	3.734508	3.741758	3.694092	3.748632	3.701737	3.522094	3.337517	3.215056
$E_5 dx/dE_5$, cm	-19.3888	-19.8976	-20.272	-20.5307	-20.7201	-20.835	-20.8406	-21.0613
$E_6 dx/dE_6$, cm	-24.3717	-24.5572	-24.815	-24.9116	-25.1042	-25.3898	-25.3852	-25.466
$E_7 dx/dE_7$, cm	7.820268	8.034659	8.363388	8.372105	8.386609	8.454564	8.468836	8.464412
$E_8 dx/dE_8$, cm	-6.08495	-6.06638	-6.00956	-6.02215	-6.03944	-6.06503	-6.19177	-6.22521
$E_9 dx/dE_9$, cm	23.70128	23.89591	23.94291	24.08885	24.17196	24.18733	24.33934	24.59046
$E_{10} dx/dE_{10}$, cm	-7.71891	-7.90265	-8.17915	-8.35605	-8.47728	-8.56889	-8.77005	-8.9834
$E_{11} dx/dE_{11}$, cm	3.5168	3.462824	3.64539	3.76168	3.829025	3.868839	4.019657	4.164161
$E_{12} dx/dE_{12}$, cm	-5.24216	-5.21212	-5.12941	-4.99341	-4.86662	-4.77041	-4.74915	-4.75904
$E_{13} dx/dE_{13}$, cm	8.83467	8.67626	8.796044	8.998556	9.120046	9.130614	9.105351	9.162221
$E_{14} dx/dE_{14}$, cm	6.929167	6.932514	6.82363	6.880346	6.983901	7.100614	7.140414	7.209655
$E_{15} dx/dE_{15}$, cm	-3.30872	-3.31666	-3.26657	-3.22076	-3.23519	-3.322	-3.44349	-3.51723
$E_{16} dx/dE_{16}$, cm	1.490999	1.274099	1.179542	1.284	1.349691	1.350863	1.442565	1.405283
$\sigma_E dx/d\sigma_E$, cm	-0.67625	-0.69688	-0.50351	-0.25735	-0.14484	-0.20231	-0.32806	-0.44394
$T_i dx/dT_i$, cm	0.999756	1.158572	1.13626	1.174897	1.153308	1.069239	1.093356	0.945948
$I_0 dx/dI_0$, cm	-0.96208	-0.92316	-0.90805	-1.00031	-1.01097	-0.91989	-0.88835	-0.77723
$\rho dx/d\rho$, cm	-2.98684	-3.01746	-3.00393	-2.93601	-2.89462	-2.90653	-3.01371	-3.10839
$c dx/dc$, cm	-3.63524	-3.52191	-3.56692	-3.71005	-3.91833	-4.13571	-4.02998	-3.91842
$h_r dx/dh_r$, cm	-0.92258	-1.09051	-1.28037	-1.3897	-1.54003	-1.72561	-1.74292	-1.71507
$\varepsilon dx/d\varepsilon$, cm	5.147166	5.110544	4.934015	4.809388	4.762676	4.79637	4.839173	4.897559
$(\sigma+1)dx/d(\sigma+1)$, cm	-0.46332	-0.3519	-0.2056	-0.25418	-0.41921	-0.63962	-0.57034	-0.42762
$k_e dx/dk_e$, cm	1.543532	1.280379	1.050275	1.07069	1.184981	1.384126	1.731203	1.915075

Table B.2. Continued

Time, min	33.16765	33.71975	34.27185	34.82395	35.37605	35.92815	36.48025	37.03235
x_{exp}, cm	6.063301	6.13548	6.206902	6.277588	6.347553	6.416818	6.4854	6.553316
x_{model}, cm	6.263949	6.32991	6.397285	6.465953	6.536953	6.602788	6.667217	6.730992
$E_1 dx/dE_1$, cm	-0.4595	-0.3616	-0.24123	-0.07344	0.224046	0.519763	0.741643	0.764937
$E_2 dx/dE_2$, cm	4.357682	4.30449	4.293297	4.26475	4.112852	4.011655	3.952835	3.977746
$E_3 dx/dE_3$, cm	-5.21117	-5.16824	-5.15864	-5.18402	-5.27966	-5.18711	-5.08297	-5.06206
$E_4 dx/dE_4$, cm	3.132172	3.074113	3.217576	3.426363	3.556024	3.59244	3.656008	3.849763
$E_5 dx/dE_5$, cm	-21.3435	-21.4296	-21.4572	-21.4986	-21.6756	-21.7898	-21.9109	-22.0889
$E_6 dx/dE_6$, cm	-25.6652	-26.1373	-26.4781	-26.6677	-26.5337	-26.6895	-26.9512	-27.3231
$E_7 dx/dE_7$, cm	8.534341	8.918476	9.042019	8.996018	8.758791	8.949483	9.160613	9.166512
$E_8 dx/dE_8$, cm	-6.2077	-6.18457	-6.37376	-6.65099	-6.91114	-7.02503	-7.11922	-7.24922
$E_9 dx/dE_9$, cm	24.83018	24.8315	25.04965	25.36599	25.69352	26.14306	26.5991	26.99839
$E_{10} dx/dE_{10}$, cm	-9.14374	-9.08231	-9.12084	-9.21299	-9.33911	-9.52656	-9.69196	-9.76043
$E_{11} dx/dE_{11}$, cm	4.332171	4.600306	4.856776	5.104574	5.340076	5.456535	5.537983	5.597224
$E_{12} dx/dE_{12}$, cm	-4.76864	-4.7156	-4.64269	-4.56567	-4.50448	-4.56549	-4.62811	-4.62069
$E_{13} dx/dE_{13}$, cm	9.298285	9.567337	9.836858	10.08419	10.25423	10.44823	10.65172	10.86626
$E_{14} dx/dE_{14}$, cm	7.288945	7.347512	7.323919	7.33522	7.591084	7.73931	7.84061	7.880539
$E_{15} dx/dE_{15}$, cm	-3.52289	-3.36907	-3.38813	-3.51092	-3.73043	-3.94852	-4.20238	-4.55385
$E_{16} dx/dE_{16}$, cm	1.295489	1.170214	1.326503	1.555213	1.608321	1.579112	1.618547	1.893717
$\sigma_E dx/d\sigma_E$, cm	-0.5245	-0.49283	-0.52374	-0.53255	-0.3705	-0.40945	-0.46859	-0.45994
$T_i dx/dT_i$, cm	0.804387	1.023612	1.2175	1.307094	1.0751	1.052081	1.132589	1.365833
$I_0 dx/dI_0$, cm	-0.61247	-0.40501	-0.42588	-0.51431	-0.49083	-0.33238	-0.16252	-0.04397
$\rho dx/d\rho$, cm	-3.18726	-3.2318	-3.3539	-3.45767	-3.38096	-3.27078	-3.23704	-3.43034
$c dx/dc$, cm	-3.84314	-3.91458	-3.88894	-3.8172	-3.73314	-3.48301	-3.24123	-3.12313
$h_r dx/dh_r$, cm	-1.64671	-1.51655	-1.43364	-1.36699	-1.28502	-1.05068	-0.77775	-0.49324
$\varepsilon dx/d\varepsilon$, cm	4.95134	4.957158	4.885303	4.79465	4.756509	4.69497	4.669101	4.753928
$(\sigma+1)dx/d(\sigma+1)$, cm	-0.28347	-0.27913	-0.28357	-0.25044	-0.0744	-0.13841	-0.22144	-0.20978
$k_e dx/dk_e$, cm	1.990404	1.983517	1.912257	1.777177	1.519161	1.602706	1.678457	1.525206

Table B.2. Continued

Time, min	37.58445	38.13655	38.68866	39.24076	39.79286	40.34496	40.89706	41.44916
x_{exp}, cm	6.620587	6.687229	6.753261	6.818701	6.883567	6.947877	7.011651	7.074905
x_{model}, cm	6.794373	6.857612	6.921051	6.982524	7.042346	7.101904	7.161119	7.219051
$E_1 dx/dE_1$, cm	0.644072	0.503263	0.665071	0.796017	0.901062	1.019933	1.089921	0.945544
$E_2 dx/dE_2$, cm	3.964901	3.923226	3.787689	3.772287	3.857719	4.020972	4.174497	4.238988
$E_3 dx/dE_3$, cm	-5.07364	-5.12433	-5.36071	-5.42585	-5.34727	-5.29648	-5.27548	-5.36278
$E_4 dx/dE_4$, cm	4.025448	4.169899	4.141554	4.03143	3.852663	3.957162	4.088354	4.156947
$E_5 dx/dE_5$, cm	-22.0887	-22.0394	-22.184	-22.3354	-22.4925	-22.8272	-23.1622	-23.389
$E_6 dx/dE_6$, cm	-27.5472	-27.7081	-27.8655	-28.0377	-28.2223	-28.3587	-28.4724	-28.5205
$E_7 dx/dE_7$, cm	8.927389	8.635808	8.722459	8.789427	8.839875	8.742408	8.612125	8.435047
$E_8 dx/dE_8$, cm	-7.2842	-7.26726	-7.16535	-7.24116	-7.46614	-7.61035	-7.73218	-7.80973
$E_9 dx/dE_9$, cm	27.3547	27.69262	28.02948	28.35353	28.66682	28.96154	29.25197	29.53578
$E_{10} dx/dE_{10}$, cm	-9.94615	-10.146	-10.0845	-10.1338	-10.2761	-10.3325	-10.3775	-10.4281
$E_{11} dx/dE_{11}$, cm	5.732232	5.884947	5.931594	5.947322	5.937098	6.034849	6.134469	6.175259
$E_{12} dx/dE_{12}$, cm	-4.66342	-4.72116	-4.73282	-4.73588	-4.73173	-4.70859	-4.70321	-4.78433
$E_{13} dx/dE_{13}$, cm	10.80622	10.64959	10.6395	10.78552	11.06255	11.15011	11.17883	11.07687
$E_{14} dx/dE_{14}$, cm	7.732326	7.508076	7.312037	7.189299	7.128083	7.272401	7.48749	7.873583
$E_{15} dx/dE_{15}$, cm	-4.81395	-5.03014	-5.20879	-5.39322	-5.58248	-5.58559	-5.56306	-5.54765
$E_{16} dx/dE_{16}$, cm	1.954773	1.937627	2.013691	2.194008	2.461832	2.501348	2.486247	2.382228
$\sigma_E dx/d\sigma_E$, cm	-0.32891	-0.15952	-0.08988	-0.09736	-0.16957	-0.39373	-0.61962	-0.75897
$T_i dx/dT_i$, cm	1.427301	1.411125	1.360412	1.335797	1.333087	1.331391	1.33624	1.368022
$I_0 dx/dI_0$, cm	-0.12088	-0.23896	-0.05035	0.058334	0.099939	-0.03657	-0.18966	-0.30259
$\rho dx/d\rho$, cm	-3.51919	-3.54219	-3.40749	-3.4274	-3.57709	-3.75778	-3.92933	-4.04321
$c dx/dc$, cm	-3.17047	-3.24263	-2.98171	-2.77224	-2.60595	-2.41423	-2.25357	-2.23938
$h_r dx/dh_r$, cm	-0.43236	-0.49216	-0.74067	-0.91626	-1.03066	-0.97554	-0.89951	-0.84013
$\varepsilon dx/d\varepsilon$, cm	4.908361	5.086699	5.223613	5.287401	5.289812	5.236389	5.158354	5.011182
$(\sigma+1) dx/d(\sigma+1)$, cm	-0.06677	0.108214	0.108774	-0.02785	-0.27962	-0.55638	-0.76761	-0.68746
$k_e dx/dk_e$, cm	1.36267	1.243018	1.466761	1.603576	1.66743	1.626769	1.535605	1.296365

Table B.2. Continued

Time, min	42.00126	42.55336	43.10546	43.65756	44.20966	44.76176	45.31387
x_{exp}, cm	7.137658	7.199929	7.261734	7.323094	7.384026	7.444547	7.504677
x_{model}, cm	7.276362	7.332959	7.370523	7.399889	7.429254	7.466652	7.523384
$E_1 dx/dE_1$, cm	0.923347	1.04128	1.040513	0.988606	0.9367	0.875376	0.791386
$E_2 dx/dE_2$, cm	4.245396	4.185189	4.151924	4.130267	4.10861	4.069653	3.989058
$E_3 dx/dE_3$, cm	-5.46178	-5.57422	-5.73941	-5.92733	-6.11524	-6.27785	-6.37956
$E_4 dx/dE_4$, cm	4.270169	4.434576	4.547877	4.639159	4.730442	4.743597	4.568716
$E_5 dx/dE_5$, cm	-23.5663	-23.6871	-23.716	-23.7053	-23.6947	-23.7002	-23.7446
$E_6 dx/dE_6$, cm	-28.5225	-28.4717	-28.4441	-28.4264	-28.4088	-28.3857	-28.3496
$E_7 dx/dE_7$, cm	8.235627	8.010582	7.914635	7.874308	7.83398	7.812919	7.83823
$E_8 dx/dE_8$, cm	-7.86899	-7.9073	-8.00593	-8.13056	-8.25519	-8.31098	-8.20109
$E_9 dx/dE_9$, cm	29.81826	30.09921	30.19864	30.21987	30.2411	30.27772	30.35136
$E_{10} dx/dE_{10}$, cm	-10.5172	-10.6506	-10.6918	-10.6932	-10.6946	-10.6795	-10.6247
$E_{11} dx/dE_{11}$, cm	6.15248	6.056792	6.036177	6.047906	6.059634	6.060995	6.037404
$E_{12} dx/dE_{12}$, cm	-4.91329	-5.09709	-5.12195	-5.07833	-5.0347	-5.02294	-5.08787
$E_{13} dx/dE_{13}$, cm	11.0365	11.06678	11.12446	11.19394	11.26342	11.34028	11.43492
$E_{14} dx/dE_{14}$, cm	8.170264	8.364396	8.407696	8.386012	8.364329	8.353553	8.369031
$E_{15} dx/dE_{15}$, cm	-5.50281	-5.42422	-5.43349	-5.4806	-5.52771	-5.56886	-5.59565
$E_{16} dx/dE_{16}$, cm	2.28213	2.186527	2.16643	2.178863	2.191296	2.232945	2.34491
$\sigma_E dx/d\sigma_E$, cm	-0.89389	-1.02371	-0.99734	-0.90369	-0.81003	-0.70437	-0.56982
$T_i dx/dT_i$, cm	1.359055	1.303352	1.360041	1.465152	1.570263	1.671929	1.765307
$I_0 dx/dI_0$, cm	-0.31612	-0.21565	-0.15223	-0.10479	-0.05734	-0.04778	-0.12944
$\rho dx/d\rho$, cm	-4.0265	-3.85999	-3.79091	-3.76379	-3.73668	-3.6736	-3.52398
$c dx/dc$, cm	-2.24203	-2.26401	-2.20182	-2.10337	-2.00491	-1.9203	-1.86898
$h_r dx/dh_r$, cm	-0.79823	-0.77639	-0.69094	-0.57808	-0.46523	-0.3648	-0.29427
$\varepsilon dx/d\varepsilon$, cm	4.871738	4.741158	4.629912	4.526995	4.424078	4.40377	4.582288
$(\sigma+1) dx/d(\sigma+1)$, cm	-0.6495	-0.65995	-0.65268	-0.63777	-0.62286	-0.57791	-0.46063
$k_e dx/dk_e$, cm	1.124375	1.029513	1.102282	1.247271	1.39226	1.526861	1.63646

Table B.3. Measured, Predicted Measurements and Sensitivity Matrix, Experiment 14: 900 C

Time, min	2.214286	2.782353	3.35042	3.918487	4.486555	5.054622	5.622689	6.190756
x_{exp}, cm	0.298222	0.504217	0.709126	0.912882	1.11542	1.316676	1.516583	1.715077
x_{model}, cm	0.5434	0.992914	1.325844	1.59787	1.887928	2.135274	2.411162	2.644188
$E_1 dx/dE_1$, cm	-1.9189	-0.2017	-0.62201	-0.45837	-0.71564	-0.7537	-0.31279	-0.21375
$E_2 dx/dE_2$, cm	-0.44511	0.101533	0.073005	0.06651	0.514302	0.847502	1.115974	1.286602
$E_3 dx/dE_3$, cm	0.697195	-0.16302	-0.77708	-0.90687	-1.3565	-1.78587	-1.85411	-2.75922
$E_4 dx/dE_4$, cm	2.119004	0.391796	0.892012	1.110903	1.19472	1.547578	2.0938	2.655144
$E_5 dx/dE_5$, cm	-1.27239	-2.3153	-3.75937	-4.7115	-4.87995	-5.17268	-5.35834	-5.70431
$E_6 dx/dE_6$, cm	0.907319	-2.05102	-3.50785	-4.7637	-5.07856	-5.51171	-6.14519	-6.07378
$E_7 dx/dE_7$, cm	2.415342	1.025904	2.478279	2.68438	3.062366	3.540535	3.619948	4.073259
$E_8 dx/dE_8$, cm	-2.3498	-1.11812	-1.6843	-1.49558	-1.65591	-2.24898	-2.51908	-3.42334
$E_9 dx/dE_9$, cm	0.479973	1.921687	3.46442	4.492667	4.927506	5.638875	6.094063	6.242323
$E_{10} dx/dE_{10}$, cm	1.526717	0.018716	-0.70007	-0.9929	-1.45825	-1.65122	-2.19951	-2.87102
$E_{11} dx/dE_{11}$, cm	0.437606	0.020493	0.385883	0.776164	1.201559	1.990285	1.676975	2.572746
$E_{12} dx/dE_{12}$, cm	2.310495	0.169003	0.017913	-0.06066	0.223872	-0.60303	-0.99219	-1.66513
$E_{13} dx/dE_{13}$, cm	-1.16079	0.16767	0.44803	0.534405	1.362899	2.029279	2.721568	3.575971
$E_{14} dx/dE_{14}$, cm	1.546462	0.144628	0.498282	0.798557	0.957723	1.057147	1.607853	1.415538
$E_{15} dx/dE_{15}$, cm	-0.54255	-0.05112	-0.54548	-0.79945	-1.14897	-1.52615	-1.14269	-2.03262
$E_{16} dx/dE_{16}$, cm	-1.37055	-0.18524	-0.48745	-0.35925	-0.04014	0.380203	0.354336	0.562183
$\sigma_E dx/d\sigma_E$, cm	-0.48024	-0.04732	-0.4673	-0.52279	-0.20757	-0.19771	0.09495	0.304454
$T_i dx/dT_i$, cm	-0.09633	-0.0995	-0.05186	0.014676	0.125733	0.445314	0.439463	0.746823
$I_0 dx/dI_0$, cm	-1.0256	-0.09045	0.114326	0.046065	0.324047	0.361286	-0.04407	-0.30252
$\rho dx/d\rho$, cm	-0.40928	-0.27105	-1.20387	-1.41112	-1.41193	-1.51503	-1.72972	-2.51604
$c dx/dc$, cm	-1.53311	0.027384	-0.24035	-0.52121	-0.77062	-0.97119	-1.6719	-2.06439
$h_r dx/dh_r$, cm	-1.19279	-0.1672	-0.70423	-1.12012	-1.34112	-1.34021	-1.32991	-2.3453
$\varepsilon dx/d\varepsilon$, cm	-2.52275	-0.00968	-0.02002	-0.00893	0.421877	0.782523	0.930633	1.427099
$(\sigma+1) dx/d(\sigma+1)$, cm	-1.11975	-0.13945	-0.95083	-0.92436	-1.15382	-2.11976	-1.32069	-2.05687
$k_e dx/dk_e$, cm	1.390692	0.21783	0.320698	0.61466	0.706994	0.77767	1.029976	1.279294

Table B.3. Continued

Time, min	6.758824	7.326891	7.894958	8.463025	9.031092	9.59916	10.16723	10.73529
x_{exp}, cm	1.912092	2.107562	2.301422	2.493608	2.684053	2.872692	3.05946	3.244292
x_{model}, cm	2.923416	3.165487	3.395995	3.615535	3.833245	4.048696	4.25102	4.459299
E_1dx/dE_1, cm	0.13727	0.327972	0.290657	0.436671	0.355059	0.378936	0.28346	0.202281
E_2dx/dE_2, cm	0.627471	0.536714	1.069663	1.310149	1.508619	2.397044	2.015616	2.428921
E_3dx/dE_3, cm	-1.36748	-1.16037	-2.17797	-2.80866	-3.1916	-3.8161	-4.01359	-3.61288
E_4dx/dE_4, cm	1.865011	2.216949	2.740822	2.563122	2.434011	2.764425	3.090989	3.795844
E_5dx/dE_5, cm	-7.80475	-8.29242	-8.17733	-8.66318	-9.18148	-8.79388	-9.92896	-10.8003
E_6dx/dE_6, cm	-8.58425	-9.2214	-9.72904	-10.281	-11.188	-12.0055	-12.0507	-11.8917
E_7dx/dE_7, cm	3.685772	3.434358	3.824653	4.221422	4.569625	4.832295	4.808351	5.12792
E_8dx/dE_8, cm	-2.17427	-2.84496	-3.28332	-3.45786	-3.5693	-3.86682	-4.38582	-4.46243
E_9dx/dE_9, cm	8.522628	9.143615	8.888907	9.031474	9.610956	10.46581	11.09258	11.54039
$E_{10}dx/dE_{10}$, cm	-1.58477	-1.57363	-2.00608	-2.44629	-2.80998	-3.64896	-3.90782	-3.63706
$E_{11}dx/dE_{11}$, cm	0.685081	0.449427	0.945443	1.048682	1.268382	1.847022	1.947359	1.493135
$E_{12}dx/dE_{12}$, cm	-1.26784	-1.36705	-2.29872	-2.58939	-3.09298	-3.44038	-3.33964	-2.82925
$E_{13}dx/dE_{13}$, cm	3.180259	3.997474	4.34371	5.054637	5.208246	5.044744	5.081224	5.222211
$E_{14}dx/dE_{14}$, cm	1.615292	1.84858	1.960117	1.8086	2.030441	3.01057	3.5657	3.659209
$E_{15}dx/dE_{15}$, cm	-0.78664	-0.62517	-0.90478	-1.32322	-1.55547	-2.00798	-1.76559	-1.88808
$E_{16}dx/dE_{16}$, cm	0.66044	0.541764	0.941667	0.957994	1.482642	2.302871	2.283371	1.705663
$\sigma_E dx/d\sigma_E$, cm	0.104889	0.022009	-0.07659	-0.13784	-0.05943	0.005846	-0.11934	-0.07404
$T_i dx/dT_i$, cm	0.429561	0.125684	0.260962	0.686678	1.08494	1.098448	1.720718	1.535321
$I_0 dx/dI_0$, cm	-0.61826	-0.76247	-1.34012	-1.74522	-1.39462	-1.68258	-2.25863	-1.88066
$\rho dx/d\rho$, cm	-1.26289	-1.25306	-1.74637	-1.79584	-2.26076	-2.98344	-3.66324	-3.31876
$c dx/dc$, cm	-1.23058	-1.10394	-1.48191	-1.73767	-2.47385	-3.33035	-3.62152	-3.0744
$h_r dx/dh_r$, cm	-1.17909	-1.33967	-2.33135	-2.59589	-3.02401	-3.4279	-3.29373	-2.91078
$\varepsilon dx/d\varepsilon$, cm	0.659776	0.687702	0.873713	1.143105	1.256817	1.399734	1.818683	2.023612
$(\sigma+1)dx/d(\sigma+1)$, cm	-0.98231	-0.85922	-1.3527	-2.01736	-2.35895	-2.69313	-2.64857	-2.22314
$k_e dx/dk_e$, cm	0.440107	0.530156	0.821741	0.648798	0.742733	0.792797	0.965776	0.971051

Table B.3. Continued

Time, min	11.30336	11.87143	12.4395	13.00756	13.57563	14.1437	14.71176	15.27983
x_{exp}, cm	3.427122	3.607884	3.786514	3.962946	4.137114	4.308954	4.4784	4.645386
x_{model}, cm	4.66651	4.866385	5.065202	5.236712	5.415069	5.602992	5.754568	5.937426
$E_1 dx/dE_1$, cm	0.171972	-0.05021	-0.07785	-0.51268	-0.31143	-0.2475	-0.15444	0.083636
$E_2 dx/dE_2$, cm	1.885126	1.342265	1.29361	2.771813	2.275145	2.15004	3.102726	1.970944
$E_3 dx/dE_3$, cm	-2.95626	-2.71201	-2.7669	-3.73384	-3.23634	-3.26121	-3.80311	-3.23758
$E_4 dx/dE_4$, cm	3.31899	2.739066	2.400607	3.308139	3.315301	2.912625	3.840191	3.055902
$E_5 dx/dE_5$, cm	-10.7186	-10.8066	-11.1225	-12.5133	-11.7588	-12.3434	-12.3844	-12.1333
$E_6 dx/dE_6$, cm	-11.8883	-12.5245	-13.8796	-14.1328	-14.4824	-15.0301	-15.6347	-15.6853
$E_7 dx/dE_7$, cm	5.176222	5.040082	4.793927	4.926545	5.076899	5.227774	5.511105	5.534236
$E_8 dx/dE_8$, cm	-4.09415	-3.63166	-3.66171	-4.32232	-4.33352	-4.5424	-4.69293	-4.42809
$E_9 dx/dE_9$, cm	11.7075	12.07067	13.11957	13.49372	13.51828	14.51469	14.55486	15.10696
$E_{10} dx/dE_{10}$, cm	-3.12352	-3.0589	-3.81631	-4.46862	-4.27381	-4.54401	-4.67424	-4.52676
$E_{11} dx/dE_{11}$, cm	1.051609	0.89602	0.788518	1.951096	1.168249	1.447536	2.164895	1.545443
$E_{12} dx/dE_{12}$, cm	-2.02391	-2.00427	-2.2286	-3.33667	-2.15408	-2.70125	-2.98471	-2.33912
$E_{13} dx/dE_{13}$, cm	5.354364	5.673768	5.634523	5.491218	6.074634	6.330482	6.305962	7.176797
$E_{14} dx/dE_{14}$, cm	3.066387	2.533905	1.90619	3.114494	2.983995	2.655581	3.589151	2.956803
$E_{15} dx/dE_{15}$, cm	-1.46149	-0.96382	-0.85643	-1.98479	-2.04436	-1.64459	-2.57933	-1.20016
$E_{16} dx/dE_{16}$, cm	1.061908	0.875516	0.849455	2.074729	1.540385	1.87037	1.952809	1.62731
$\sigma_E dx/d\sigma_E$, cm	-0.07554	-0.12975	-0.10352	-0.12504	-0.16157	-0.09122	-0.20173	-0.14127
$T_i dx/dT_i$, cm	0.795471	0.636402	0.794919	1.488483	0.995981	1.331884	1.114116	0.816242
$I_0 dx/dI_0$, cm	-1.27763	-0.6763	-0.71935	-1.3019	-0.92482	-0.87513	-1.00178	-0.52173
$\rho dx/d\rho$, cm	-2.556	-2.1279	-2.05392	-2.99362	-2.55551	-2.35229	-3.01844	-1.98256
$c dx/dc$, cm	-2.41786	-2.11194	-1.92029	-3.03349	-2.28109	-2.5745	-2.97895	-2.03793
$h_r dx/dh_r$, cm	-2.03617	-1.29888	-1.50417	-2.66127	-2.02857	-2.16613	-2.07029	-1.46718
$\varepsilon dx/d\varepsilon$, cm	1.333378	0.937717	0.74979	2.113833	1.370264	1.357308	1.780036	1.264845
$(\sigma+1)dx/d(\sigma+1)$, cm	-1.61796	-1.38006	-1.27525	-2.48742	-1.80781	-2.1651	-2.67022	-1.87927
$k_e dx/dk_e$, cm	0.523327	0.364962	0.368254	0.886758	0.412012	0.306941	0.235667	0.030011

Table B.3. Continued

Time, min	15.8479	16.41597	16.98403	17.5521	18.12017	18.68824	19.2563	19.82437
x_{exp}, cm	4.809848	4.971719	5.130936	5.287431	5.44114	5.591997	5.739938	5.884896
x_{model}, cm	6.088978	6.259603	6.40189	6.563117	6.708421	6.845016	6.991633	7.135527
$E_1 dx/dE_1$, cm	0.148192	0.389173	0.45705	0.919246	0.407995	0.356745	0.627714	0.287678
$E_2 dx/dE_2$, cm	3.08822	1.904499	2.866633	2.823274	2.407408	3.258886	3.251669	2.65379
$E_3 dx/dE_3$, cm	-3.93	-3.09405	-3.7078	-3.94895	-3.21684	-3.81688	-3.97865	-3.80183
$E_4 dx/dE_4$, cm	4.080886	3.301959	3.944178	3.863603	3.424483	4.071759	3.894235	3.553858
$E_5 dx/dE_5$, cm	-13.0997	-13.1606	-13.248	-14.2871	-14.0876	-14.2227	-14.6557	-14.6692
$E_6 dx/dE_6$, cm	-16.422	-16.2826	-17.4199	-17.1583	-17.217	-18.2269	-18.3619	-18.1911
$E_7 dx/dE_7$, cm	5.525173	5.50844	5.614532	5.472103	5.787878	6.113002	5.719082	5.753733
$E_8 dx/dE_8$, cm	-4.7698	-5.04152	-5.20754	-5.09861	-5.23949	-5.2334	-5.15931	-5.25197
$E_9 dx/dE_9$, cm	15.38407	15.50113	16.39404	16.32372	16.18235	17.19186	17.87946	17.68987
$E_{10} dx/dE_{10}$, cm	-4.8259	-4.97628	-5.00504	-5.06888	-5.19805	-5.36541	-5.28403	-5.63421
$E_{11} dx/dE_{11}$, cm	2.476895	1.938645	2.136636	2.970488	2.225821	2.636521	3.392491	3.089492
$E_{12} dx/dE_{12}$, cm	-2.99769	-2.54013	-3.02463	-3.46627	-2.65397	-3.14943	-3.68872	-3.40627
$E_{13} dx/dE_{13}$, cm	6.399096	7.12383	7.011218	6.560332	7.607487	7.514124	6.857201	7.206368
$E_{14} dx/dE_{14}$, cm	4.01364	3.759529	3.986163	4.38087	4.22683	4.209298	4.424624	4.333046
$E_{15} dx/dE_{15}$, cm	-2.13864	-1.42213	-2.09519	-2.51267	-1.65373	-2.31829	-3.01851	-2.56267
$E_{16} dx/dE_{16}$, cm	2.222915	1.546111	1.587548	2.210682	1.158044	1.313649	2.251334	1.981216
$\sigma_E dx/d\sigma_E$, cm	-0.16739	-0.12338	-0.31422	-0.21084	-0.1155	-0.03804	0.037341	0.010046
$T_i dx/dT_i$, cm	1.362503	0.833116	1.068248	1.582927	0.908202	1.281132	1.783187	1.037354
$I_0 dx/dI_0$, cm	-0.82985	-0.37997	-0.68478	-0.75559	-0.438	-0.6694	-0.87333	-0.37645
$\rho dx/d\rho$, cm	-3.22366	-2.41108	-3.04862	-3.15503	-2.54638	-3.32977	-3.47098	-2.86574
$c dx/dc$, cm	-3.11032	-2.36954	-2.70522	-3.28417	-2.31905	-2.73978	-3.15662	-2.70087
$h_r dx/dh_r$, cm	-2.34138	-1.77893	-1.99448	-2.42206	-1.35817	-1.6088	-2.25496	-1.84255
$\varepsilon dx/d\varepsilon$, cm	1.942366	1.3359	1.58614	2.24782	1.285798	1.549338	2.055649	1.442803
$(\sigma+1)dx/d(\sigma+1)$, cm	-2.42147	-2.10728	-2.19473	-2.87646	-1.75583	-1.99231	-2.47902	-1.65102
$k_e dx/dk_e$, cm	0.064846	0.008621	0.094329	0.289404	0.106832	-0.0385	-0.1115	-0.00699

Table B.3. Continued

Time, min	20.39244	20.9605	21.52857	22.09664	22.66471	23.23277	23.80084	24.36891
x_{exp}, cm	6.026806	6.165604	6.301223	6.433599	6.562665	6.688357	6.810609	6.929356
x_{model}, cm	7.264977	7.391414	7.518341	7.649233	7.775583	7.90111	8.021268	8.137651
$E_1 dx/dE_1$, cm	0.096657	0.085784	-0.11636	-0.15986	-0.01439	-0.10844	-0.09833	0.19343
$E_2 dx/dE_2$, cm	2.649779	3.193503	3.456034	3.548248	3.447766	3.429891	3.327136	3.05739
$E_3 dx/dE_3$, cm	-3.401	-3.71008	-4.2297	-4.33937	-4.34429	-4.35849	-4.3555	-4.38892
$E_4 dx/dE_4$, cm	3.814387	4.260842	4.450023	4.480751	4.389859	4.452974	4.616662	4.702141
$E_5 dx/dE_5$, cm	-14.7	-14.832	-15.0718	-15.2757	-15.4399	-15.6613	-15.9504	-16.2889
$E_6 dx/dE_6$, cm	-18.562	-19.2898	-19.5611	-19.7545	-19.9382	-20.1226	-20.3638	-20.5389
$E_7 dx/dE_7$, cm	6.050987	6.327171	6.184581	5.875105	5.857674	5.975458	6.145636	6.25971
$E_8 dx/dE_8$, cm	-5.55373	-5.6633	-5.68639	-5.79648	-5.98301	-6.16039	-6.2237	-6.15171
$E_9 dx/dE_9$, cm	17.77462	18.68756	19.24247	19.55174	19.71758	19.95731	20.31312	20.61452
$E_{10} dx/dE_{10}$, cm	-6.12966	-6.3126	-6.20244	-6.31521	-6.46758	-6.51972	-6.58094	-6.66431
$E_{11} dx/dE_{11}$, cm	2.622662	2.638333	3.134339	3.623189	3.635602	3.538772	3.462622	3.522739
$E_{12} dx/dE_{12}$, cm	-2.7715	-2.88961	-3.53485	-3.9451	-4.06556	-4.16736	-4.1149	-4.05048
$E_{13} dx/dE_{13}$, cm	7.953897	7.978336	7.734193	7.430162	7.631544	7.885022	8.319038	8.270453
$E_{14} dx/dE_{14}$, cm	4.250919	4.380533	4.530212	4.569148	4.612628	4.780568	4.945388	5.116181
$E_{15} dx/dE_{15}$, cm	-1.99769	-2.10058	-2.50489	-2.73247	-2.81222	-2.56491	-2.36231	-2.40705
$E_{16} dx/dE_{16}$, cm	1.294126	1.378233	1.468606	1.487506	1.891737	1.981906	1.872978	1.860233
$\sigma_E dx/d\sigma_E$, cm	-0.05419	-0.13264	-0.28069	-0.24795	-0.20383	-0.22726	-0.29871	-0.49862
$T_i dx/dT_i$, cm	0.75885	0.953954	1.233968	1.43649	1.323548	1.005877	0.946478	0.841701
$I_0 dx/dI_0$, cm	-0.31144	-0.22193	-0.25996	-0.32427	-0.17588	-0.24848	-0.32214	-0.26378
$\rho dx/d\rho$, cm	-2.34117	-2.64234	-3.28161	-3.76012	-3.84817	-3.73599	-3.51814	-3.2189
$c dx/dc$, cm	-2.45887	-2.70276	-3.20792	-3.43823	-3.37903	-3.30766	-3.22404	-3.2562
$h_r dx/dh_r$, cm	-1.64962	-1.79487	-2.1025	-2.47656	-2.42429	-2.32382	-2.03592	-1.9788
$\varepsilon dx/d\varepsilon$, cm	1.30888	1.608951	2.059945	2.314998	2.306777	1.93975	1.701239	1.632915
$(\sigma+1)dx/d(\sigma+1)$, cm	-1.47244	-1.84399	-2.32117	-2.34996	-2.12853	-2.04951	-1.91293	-1.58468
$k_e dx/dk_e$, cm	-0.00438	0.128484	0.246688	0.433445	0.493913	0.58156	0.587428	0.502855

Table B.3. Continued

Time, min	24.93697	25.50504	26.07311	26.64118	27.20924	27.77731	28.34538	28.91345
x_{exp}, cm	7.044532	7.156073	7.263912	7.367985	7.468226	7.564569	7.65695	7.745303
x_{model}, cm	8.249387	8.365596	8.48051	8.587835	8.695457	8.802397	8.907861	9.012855
$E_1 dx/dE_1$, cm	0.412451	0.365345	0.315953	0.222733	0.142189	0.230497	0.196664	-0.23017
$E_2 dx/dE_2$, cm	3.017283	3.21861	3.29861	3.372874	3.527788	3.773911	3.869865	3.906307
$E_3 dx/dE_3$, cm	-4.46969	-4.46638	-4.44196	-4.42452	-4.43873	-4.36769	-4.21642	-4.17652
$E_4 dx/dE_4$, cm	4.851186	4.901274	4.897566	4.989461	5.135255	5.24113	5.34354	5.539812
$E_5 dx/dE_5$, cm	-16.5647	-16.7073	-16.736	-16.8713	-16.9746	-16.8868	-16.6576	-16.5718
$E_6 dx/dE_6$, cm	-20.6732	-20.8729	-21.061	-21.1401	-21.2218	-21.2952	-21.2724	-21.3774
$E_7 dx/dE_7$, cm	6.233104	6.210576	6.228528	6.272382	6.469242	6.849137	7.162866	7.362321
$E_8 dx/dE_8$, cm	-6.16161	-6.16719	-6.25509	-6.42967	-6.52033	-6.53035	-6.48775	-6.54545
$E_9 dx/dE_9$, cm	20.77082	20.96766	21.25801	21.60472	21.66462	21.35497	21.26326	21.60992
$E_{10} dx/dE_{10}$, cm	-6.74171	-6.77798	-6.86257	-7.0232	-7.15583	-7.33031	-7.48014	-7.79401
$E_{11} dx/dE_{11}$, cm	3.618561	3.680044	3.62432	3.538196	3.365037	3.173742	3.316314	3.568742
$E_{12} dx/dE_{12}$, cm	-4.0671	-4.21289	-4.34598	-4.35142	-4.38852	-4.45084	-4.31503	-4.07632
$E_{13} dx/dE_{13}$, cm	8.418054	8.297974	8.278206	8.235867	8.236634	8.349015	8.40953	8.227034
$E_{14} dx/dE_{14}$, cm	5.326143	5.435492	5.443808	5.418235	5.347861	5.359372	5.385938	5.136074
$E_{15} dx/dE_{15}$, cm	-2.38638	-2.51968	-2.75413	-2.88639	-2.84175	-3.01432	-3.34475	-3.3499
$E_{16} dx/dE_{16}$, cm	1.91228	1.894945	1.978854	2.055647	2.043879	1.914323	1.741341	1.86915
$\sigma_E dx/d\sigma_E$, cm	-0.79191	-0.78134	-0.60596	-0.49848	-0.63707	-0.52885	-0.31839	-0.19825
$T_i dx/dT_i$, cm	0.937337	0.69483	0.656071	1.083958	1.291988	1.308546	1.365888	1.317687
$I_0 dx/dI_0$, cm	-0.34166	-0.09101	-0.23792	-0.21531	-0.18104	-0.20681	-0.09774	0.024495
$\rho dx/d\rho$, cm	-3.11756	-3.12898	-3.16021	-3.14438	-3.21081	-3.40088	-3.3236	-3.11913
$c dx/dc$, cm	-3.34688	-3.42181	-3.40144	-3.37242	-3.39625	-3.44558	-3.54282	-3.37601
$h_r dx/dh_r$, cm	-1.92672	-1.65669	-1.83421	-1.94813	-1.88168	-1.79974	-1.81173	-1.69622
$\varepsilon dx/d\varepsilon$, cm	1.687509	1.688295	1.951705	2.217256	2.365347	2.37395	2.273271	2.259784
$(\sigma+1)dx/d(\sigma+1)$, cm	-1.33805	-1.39809	-1.62884	-1.80173	-1.99505	-2.11557	-2.1605	-2.01784
$k_e dx/dk_e$, cm	0.446199	0.589043	0.548756	0.588229	0.608091	0.590928	0.625893	0.528863

Table B.3. Continued

Time, min	29.48151	30.04958	30.61765
x_{exp}, cm	7.829562	7.909662	7.985539
x_{model}, cm	9.108291	9.1993	9.28756
$E_1 dx/dE_1$, cm	-0.33328	-0.08459	0.065572
$E_2 dx/dE_2$, cm	3.761135	3.485675	3.295742
$E_3 dx/dE_3$, cm	-4.09323	-3.96944	-3.98441
$E_4 dx/dE_4$, cm	5.646932	5.583677	5.521636
$E_5 dx/dE_5$, cm	-16.6521	-16.6491	-16.6825
$E_6 dx/dE_6$, cm	-21.5057	-21.509	-21.6084
$E_7 dx/dE_7$, cm	7.50423	7.387726	7.209115
$E_8 dx/dE_8$, cm	-6.91955	-7.07581	-6.87732
$E_9 dx/dE_9$, cm	22.19791	22.5442	22.67137
$E_{10} dx/dE_{10}$, cm	-8.2096	-8.35578	-8.1345
$E_{11} dx/dE_{11}$, cm	3.463585	3.362359	3.437422
$E_{12} dx/dE_{12}$, cm	-4.01613	-4.14386	-4.3309
$E_{13} dx/dE_{13}$, cm	8.245147	8.501917	8.70393
$E_{14} dx/dE_{14}$, cm	4.922691	5.012813	5.209026
$E_{15} dx/dE_{15}$, cm	-3.00423	-2.88532	-2.92571
$E_{16} dx/dE_{16}$, cm	2.006919	2.169408	2.336054
$\sigma_E dx/d\sigma_E$, cm	-0.28244	-0.39864	-0.41792
$T_i dx/dT_i$, cm	1.095674	1.021508	1.214915
$I_0 dx/dI_0$, cm	0.064298	0.13211	0.191985
$\rho dx/d\rho$, cm	-2.97259	-2.93552	-3.02631
$c dx/dc$, cm	-3.01171	-2.76309	-2.84082
$h_r dx/dh_r$, cm	-1.56685	-1.61783	-1.87969
$\varepsilon dx/d\varepsilon$, cm	2.443925	2.488458	2.498337
$(\sigma+1) dx/d(\sigma+1)$, cm	-1.79466	-1.701	-1.861
$k_e dx/dk_e$, cm	0.451476	0.443468	0.657851

Table B.4. Experimental Observations and Model Predictions, Experiment 5: 750 C

Time min	x_{exp} cm	x_{model} cm
2.664286	0.177264	0.5604
3.157395	0.286209	0.7180
3.650504	0.396682	0.8676
4.143613	0.507982	1.0144
4.636723	0.619478	1.1553
5.129832	0.730614	1.3028
5.622941	0.840907	1.4335
6.116050	0.949948	1.5726
6.609160	1.057399	1.7145
7.102269	1.162997	
7.595378	1.266552	
8.088487	1.367947	
8.581597	1.467139	
9.074706	1.564156	
9.567815	1.659102	
10.06092	1.752153	
10.55403	1.843558	
11.04714	1.933639	
11.54025	2.022792	
12.03336	2.111486	
12.52647	2.200263	
13.01958	2.289738	

Table B.5. Experimental Observations and Model Predictions, Experiment 10: 750 C

Time min	x_{exp} cm	x_{model} cm	Time min	x_{exp} cm	x_{model} cm	Time min	x_{exp} cm	x_{model} cm
3.250000	0.211467	0.462752	21.419610	3.837919	4.435099	39.589220	6.156223	6.859669
3.672549	0.306731	0.618998	21.842160	3.907493	4.499496	40.011760	6.195462	6.906297
4.095098	0.401670	0.733462	22.264710	3.976299	4.563402	40.434310	6.234177	6.953038
4.517647	0.496269	0.868584	22.687250	4.044336	4.627892	40.856860	6.272384	7.001468
4.940196	0.590508	0.977375	23.109800	4.111602	4.692888	41.279410	6.310095	7.049898
5.362745	0.684371	1.085648	23.532350	4.178095	4.757724	41.701960	6.347325	7.096639
5.785294	0.777840	1.208928	23.954900	4.243815	4.819600	42.124510	6.384090	7.143376
6.207843	0.870899	1.321337	24.377450	4.308760	4.882767	42.547060	6.420404	7.190471
6.630392	0.963531	1.423611	24.800000	4.372931	4.947180	42.969610	6.456284	7.237625
7.052941	1.055721	1.528889	25.222550	4.436327	5.011696	43.392160	6.491745	7.282959
7.475490	1.147453	1.644091	25.645100	4.498949	5.074687	43.814710	6.526804	7.327645
7.898039	1.238712	1.752545	26.067650	4.560798	5.135442	44.237250	6.561478	7.372330
8.320588	1.329483	1.850765	26.490200	4.621875	5.197834	44.659800	6.595784	7.417016
8.743137	1.419751	1.947950	26.912750	4.682182	5.260059	45.082350	6.629739	7.461393
9.165686	1.509503	2.042499	27.335290	4.741720	5.318966	45.504900	6.663362	7.504901
9.588235	1.598725	2.140751	27.757840	4.800493	5.378421	45.927450	6.696671	7.548410
10.010780	1.687404	2.246650	28.180390	4.858502	5.438485	46.350000	6.729685	7.591067
10.433330	1.775526	2.342418	28.602940	4.915750	5.496430	46.772550	6.762422	7.633693
10.855880	1.863080	2.434140	29.025490	4.972242	5.553740	47.195100	6.794902	7.674389
11.278430	1.950052	2.525953	29.448040	5.027980	5.609215	47.617650	6.827145	7.713891
11.700980	2.036432	2.617970	29.870590	5.082970	5.664665	48.040200	6.859171	7.753120
12.123530	2.122207	2.708686	30.293140	5.137215	5.720045	48.462750	6.891001	7.789456
12.546080	2.207367	2.797930	30.715690	5.190721	5.776015	48.885290	6.922655	7.825791
12.968630	2.291900	2.885909	31.138240	5.243492	5.832679	49.307840	6.954155	7.860064
13.391180	2.375798	2.972619	31.560780	5.295536	5.888511	49.730390	6.985523	7.890225
13.813730	2.459049	3.058279	31.983330	5.346857	5.943979	50.152940	7.016780	7.920385
14.236270	2.541644	3.143952	32.405880	5.397462	5.995920	50.575490	7.047949	7.950446
14.658820	2.623574	3.228749	32.828430	5.447357	6.047431	50.998040	7.079053	7.975175
15.081370	2.704830	3.313416	33.250980	5.496551	6.102174	51.420590	7.110115	7.999905
15.503920	2.785403	3.397471	33.673530	5.545050	6.156537	51.843140	7.141158	8.024634
15.926470	2.865286	3.480334	34.096080	5.592863	6.207190	52.265690	7.172207	8.049363
16.349020	2.944471	3.561866	34.518630	5.639997	6.257890	52.688240	7.203285	8.069117
16.771570	3.022950	3.642969	34.941180	5.686462	6.308842	53.110780	7.234418	8.088741
17.194120	3.100716	3.722310	35.363730	5.732266	6.360259	53.533330	7.265630	8.108365
17.616670	3.177763	3.799822	35.786270	5.777419	6.413623	53.955880	7.296947	8.127989
18.039220	3.254085	3.877654	36.208820	5.821930	6.465313	54.378430	7.328394	8.147614
18.461760	3.329676	3.957074	36.631370	5.865810	6.513412	54.800980	7.359998	8.156834
18.884310	3.404529	4.029878	37.053920	5.909069	6.561335	55.223530	7.391785	8.164621
19.306860	3.478641	4.097812	37.476470	5.951719	6.608701	55.646080	7.423782	8.172407
19.729410	3.552006	4.164559	37.899020	5.993769	6.656374	56.068630	7.456016	8.180194
20.151960	3.624621	4.233830	38.321570	6.035233	6.706138	56.491180	7.488515	8.187981
20.574510	3.696480	4.301463	38.744120	6.076121	6.756206	57.083330	7.510000	8.198893
20.997060	3.767580	4.368461	39.166670	6.116447	6.808528			

Table B.6. Experimental Observations and Model Predictions, Experiment 11: 750 C

Time min	x_{exp} cm	x_{model} cm	Time min	x_{exp} cm	x_{model} cm	Time min	x_{exp} cm	x_{model} cm
3.107143	0.107880	0.564231	18.789500	3.655411	4.261981	34.471850	6.036890	6.393603
3.471849	0.238878	0.678055	19.154200	3.710835	4.324962	34.836550	6.095296	6.437314
3.836555	0.366319	0.791946	19.518910	3.765905	4.384391	35.201260	6.153733	6.477108
4.201261	0.490311	0.902934	19.883610	3.820663	4.440122	35.565970	6.212177	6.513286
4.565966	0.610957	1.009561	20.248320	3.875147	4.492186	35.930670	6.270603	6.557682
4.930672	0.728362	1.108646	20.613030	3.929397	4.544542	36.295380	6.328982	6.596931
5.295378	0.842627	1.215311	20.977730	3.983448	4.601678	36.660080	6.387285	6.636691
5.660084	0.953853	1.319626	21.342440	4.037335	4.659091	37.024790	6.445482	6.679256
6.024790	1.062138	1.418907	21.707140	4.091091	4.715874	37.389500	6.503540	6.718996
6.389496	1.167581	1.527950	22.071850	4.144749	4.770851	37.754200	6.561425	6.758114
6.754202	1.270276	1.626845	22.436550	4.198338	4.818950	38.118910	6.619104	6.796396
7.118908	1.370318	1.721149	22.801260	4.251887	4.873343	38.483610	6.676538	6.833723
7.483613	1.467799	1.815522	23.165970	4.305425	4.929527	38.848320	6.733689	6.871484
7.848319	1.562812	1.918725	23.530670	4.358975	4.986024	39.213030	6.790518	6.912119
8.213025	1.655446	2.015085	23.895380	4.412563	5.038014	39.577730	6.846983	6.954325
8.577731	1.745789	2.105549	24.260080	4.466211	5.087380	39.942440	6.903041	6.989720
8.942437	1.833927	2.192739	24.624790	4.519940	5.137192	40.307140	6.958649	7.031483
9.307143	1.919947	2.284406	24.989500	4.573771	5.192076	40.671850	7.013760	7.070456
9.671849	2.003930	2.378103	25.354200	4.627720	5.246077	41.036550	7.068326	7.101522
10.036550	2.085961	2.472036	25.718910	4.681805	5.294278	41.401260	7.122299	7.138843
10.401260	2.166118	2.556821	26.083610	4.736041	5.339757	41.765970	7.175628	7.173421
10.765970	2.244482	2.639900	26.448320	4.790441	5.389254	42.130670	7.228261	7.206085
11.130670	2.321130	2.722326	26.813030	4.845017	5.441265	42.495380	7.280146	7.239914
11.495380	2.396137	2.804817	27.177730	4.899780	5.490601	42.860080	7.331225	7.274936
11.860080	2.469579	2.891343	27.542440	4.954739	5.535779	43.224790	7.381444	7.309461
12.224790	2.541528	2.975044	27.907140	5.009900	5.584408	43.589500	7.430744	7.343541
12.589500	2.612055	3.056942	28.271850	5.065271	5.634203	43.954200	7.479065	7.380028
12.954200	2.681232	3.139371	28.636550	5.120855	5.682780	44.318910	7.526346	7.413229
13.318910	2.749125	3.216683	29.001260	5.176655	5.728484	44.683610	7.572525	7.445950
13.683610	2.815802	3.292778	29.365970	5.232673	5.774563	45.048320	7.617537	7.478473
14.048320	2.881328	3.368334	29.730670	5.288908	5.820953	45.413030	7.661317	7.509001
14.413030	2.945768	3.442903	30.095380	5.345359	5.867392	45.777730	7.703797	7.546166
14.777730	3.009183	3.515259	30.460080	5.402023	5.912791	46.142440	7.744908	7.583605
15.142440	3.071634	3.585151	30.824790	5.458894	5.956121	46.507140	7.784581	7.616196
15.507140	3.133180	3.652138	31.189500	5.515966	6.000528	46.871850	7.822743	7.655705
15.871850	3.193880	3.720888	31.554200	5.573232	6.046066	47.236550	7.859322	7.689368
16.236550	3.253788	3.789182	31.918910	5.630682	6.087063	47.601260	7.894241	7.719085
16.601260	3.312961	3.856800	32.283610	5.688306	6.131996	47.965970	7.927426	7.750063
16.965970	3.371451	3.923391	32.648320	5.746091	6.177298	48.330670	7.958798	7.773606
17.330670	3.429310	3.993717	33.013030	5.804023	6.220858	48.695380	7.988277	7.795571
17.695380	3.486587	4.063972	33.377730	5.862086	6.265345	49.060080	8.015782	7.817632
18.060080	3.543332	4.132809	33.742440	5.920265	6.309955	49.424790	8.041232	7.840057
18.424790	3.599592	4.196924	34.107140	5.978539	6.353425	54.583330	8.110000	7.962355

Table B.7. Experimental Observations and Model Predictions, Experiment 13: 750 C

Time min	x_{exp} cm	x_{model} cm	Time min	x_{exp} cm	x_{model} cm	Time min	x_{exp} cm	x_{model} cm
3.250000	0.166095	0.515853	20.534310	3.684020	4.136970	37.818630	6.455077	6.351333
3.671569	0.278535	0.633931	20.955880	3.754613	4.199354	38.240200	6.518637	6.399250
4.093137	0.388914	0.759698	21.377450	3.824945	4.261810	38.661760	6.581787	6.447165
4.514706	0.497299	0.884654	21.799020	3.895034	4.321974	39.083330	6.644499	6.493070
4.936275	0.603758	0.987219	22.220590	3.964900	4.382947	39.504900	6.706746	6.538848
5.357843	0.708353	1.097024	22.642160	4.034560	4.444625	39.926470	6.768495	6.583003
5.779412	0.811150	1.215115	23.063730	4.104030	4.510756	40.348040	6.829716	6.626634
6.200980	0.912210	1.319329	23.485290	4.173324	4.575273	40.769610	6.890376	6.670603
6.622549	1.011595	1.415574	23.906860	4.242457	4.636861	41.191180	6.950442	6.714960
7.044118	1.109364	1.511619	24.328430	4.311441	4.697478	41.612750	7.009878	6.759281
7.465686	1.205577	1.609392	24.750000	4.380288	4.757393	42.034310	7.068649	6.803465
7.887255	1.300292	1.711835	25.171570	4.449007	4.814370	42.455880	7.126717	6.847650
8.308824	1.393564	1.816466	25.593140	4.517608	4.870825	42.877450	7.184045	6.888854
8.730392	1.485450	1.915120	26.014710	4.586099	4.926412	43.299020	7.240591	6.929891
9.151961	1.576003	2.010094	26.436270	4.654487	4.981618	43.720590	7.296317	6.970794
9.573529	1.665278	2.103382	26.857840	4.722778	5.036546	44.142160	7.351179	7.011569
9.995098	1.753325	2.196175	27.279410	4.790975	5.092093	44.563730	7.405136	7.052341
10.416670	1.840196	2.289112	27.700980	4.859082	5.147842	44.985290	7.458142	7.093072
10.838240	1.925940	2.381225	28.122550	4.927102	5.201875	45.406860	7.510153	7.133803
11.259800	2.010607	2.472323	28.544120	4.995036	5.255542	45.828430	7.561122	7.174262
11.681370	2.094242	2.563105	28.965690	5.062882	5.306753	46.250000	7.611001	7.214542
12.102940	2.176893	2.651510	29.387250	5.130641	5.358800	46.671570	7.659742	7.254695
12.524510	2.258604	2.738253	29.808820	5.198309	5.415394	47.093140	7.707295	7.293911
12.946080	2.339420	2.822794	30.230390	5.265883	5.470857	47.514710	7.753608	7.333127
13.367650	2.419382	2.905700	30.651960	5.333358	5.524540	47.936270	7.798630	7.373225
13.789220	2.498533	2.988236	31.073530	5.400728	5.576470	48.357840	7.842306	7.413992
14.210780	2.576914	3.070400	31.495100	5.467987	5.626818	48.779410	7.884583	7.454676
14.632350	2.654562	3.150650	31.916670	5.535125	5.676942	49.200980	7.925405	7.494738
15.053920	2.731517	3.232413	32.338240	5.602134	5.726873	49.622550	7.964714	7.534800
15.475490	2.807814	3.309267	32.759800	5.669003	5.775952	50.044120	8.002453	7.574098
15.897060	2.883491	3.385340	33.181370	5.735720	5.824297	50.465690	8.038563	7.612931
16.318630	2.958582	3.462370	33.602940	5.802272	5.871709	50.887250	8.072983	7.651676
16.740200	3.033119	3.540992	34.024510	5.868646	5.918061	51.308820	8.105651	7.688594
17.161760	3.107136	3.614079	34.446080	5.934825	5.964478	51.730390	8.136505	7.725512
17.583330	3.180663	3.683099	34.867650	6.000795	6.011039	52.151960	8.165482	7.762458
18.004900	3.253731	3.748815	35.289220	6.066536	6.058405	52.573530	8.192515	7.799457
18.426470	3.326368	3.812675	35.710780	6.132032	6.109890	52.995100	8.217539	7.836457
18.848040	3.398602	3.879009	36.132350	6.197261	6.160133	53.416670	8.240487	7.864386
19.269610	3.470460	3.948875	36.553920	6.262202	6.205990	53.838240	8.261291	7.887084
19.691180	3.541966	4.014019	36.975490	6.326835	6.252003	54.259800	8.279879	7.909781
20.112750	3.613145	4.076868	37.397060	6.391134	6.301693	54.681370	8.296183	7.932479

Table B.8. Experimental Observations and Model Predictions, Experiment 15: 750 C

Time min	x_{exp} cm	x_{model} cm
2.571429	0.220588	0.4588
3.083473	0.403602	0.6336
3.595518	0.575666	0.7998
4.107563	0.738318	0.9483
4.619608	0.893088	1.1029
5.131653	1.041499	1.2448
5.643697	1.18507	1.3940
6.155742	1.32531	1.5335
6.667787	1.463722	1.6811
7.179832	1.601804	
7.691877	1.741045	
8.203922	1.882929	
8.715966	2.028931	

Table B.9. Experimental Observations and Model Predictions, Experiment 16: 1000 C

Time min	x_{exp} cm	x_{model} cm	Time min	x_{exp} cm	x_{model} cm
3	0.576731	0.5279	4.863636	1.679489	2.0385
3.045455	0.604704	0.5675	4.909091	1.704032	2.0722
3.090909	0.632748	0.607	4.954546	1.728444	2.106
3.136364	0.660843	0.6466	5	1.752726	2.1399
3.181818	0.688974	0.6862	5.045455	1.776878	2.1743
3.227273	0.717124	0.7249	5.090909	1.800901	2.2087
3.272727	0.74528	0.7635	5.136364	1.824794	2.2431
3.318182	0.773429	0.802	5.181818	1.848558	2.2775
3.363636	0.801559	0.8406	5.227273	1.872194	2.3119
3.409091	0.829658	0.8792	5.272727	1.895701	2.3463
3.454546	0.857718	0.9177	5.318182	1.919082	2.3792
3.5	0.885729	0.9561	5.363636	1.942336	2.4112
3.545455	0.913683	0.9939	5.409091	1.965463	2.4431
3.590909	0.941571	1.0317	5.454546	1.988465	2.4751
3.636364	0.969388	1.0696	5.5	2.011342	2.5071
3.681818	0.997127	1.1074	5.545455	2.034095	2.5391
3.727273	1.024782	1.1452	5.590909	2.056725	2.5712
3.772727	1.052348	1.183	5.636364	2.079231	2.6048
3.818182	1.07982	1.2202	5.681818	2.101616	2.6385
3.863636	1.107193	1.257	5.727273	2.123879	2.6722
3.909091	1.134465	1.2937	5.772727	2.146022	2.7059
3.954546	1.16163	1.3305	5.818182	2.168046	2.7395
4	1.188686	1.3673	5.863636	2.18995	2.7732
4.045455	1.21563	1.404	5.909091	2.211736	
4.090909	1.242459	1.4408	5.954546	2.233405	
4.136364	1.269171	1.4778	6	2.254957	
4.181818	1.295763	1.5149	6.045455	2.276393	
4.227273	1.322235	1.5519	6.090909	2.297715	
4.272727	1.348584	1.5889	6.136364	2.318922	
4.318182	1.374808	1.6259	6.181818	2.340016	
4.363636	1.400907	1.6629	6.227273	2.360998	
4.409091	1.42688	1.6986	6.272727	2.381869	
4.454546	1.452724	1.7327	6.318182	2.402628	
4.5	1.478441	1.7668	6.363636	2.423278	
4.545455	1.504028	1.801	6.409091	2.443818	
4.590909	1.529485	1.8351	6.454546	2.46425	
4.636364	1.554812	1.8692	6.5	2.484575	
4.681818	1.580009	1.9034	6.545455	2.504793	
4.727273	1.605075	1.9372	6.590909	2.524906	
4.772727	1.630011	1.9709	6.636364	2.544913	
4.818182	1.654815	2.0047	6.681818	2.564817	

Appendix C: Code (Coyote) Input files

Table C.1 Input file Coyote for analysis of Experiment 2 (750 C boundary temperature)

```
TITLE
  MAVEN FY2000 test #2
END
$
$ MATERIAL DEFINITIONS
$
MATERIAL, INERT_FOAM, ISOTROPIC          $ Nonreactive foam
 DENSITY=0.364                    $ 22.7 lb/ft^3 divided by 62.4
 COND=VFUNC,5                      $ cal/cm-s-K
 SPECIFIC HEAT=VFUNC,6                  $ cal/g-K
 INIT TEMP=300.0                  $ K
 EMIS=0.8                       $ Emissivity
END
MATERIAL, CPUF_FOAM, ISOTROPIC           $ CPUF model:  16 eqns. 15 species + SF
 DENSITY=0.364                    $ 22.7 lb/ft^3 divided by 62.4
$ COND=VFUNC,5                      $ cal/cm-s-K
 COND=USER                        $ cal/cm-s-K (BIAS Correction needed of 1-mm elements)
 SPECIFIC HEAT=VFUNC,6                  $ cal/g-K
 INIT TEMP=300.0                  $ K
 EMIS=0.8                       $ Emissivity
 REACT MIX=16,16,USER,USER $ 15 species (+1 aux. variables), 16 rxns, rxn rates, species
 SPEC= BTDI,BTAC,BTDA,CHAR,BADIP,DTDI,DTAC,DTDA,DADIP,*
    TDI,TAC,TDA,CPN,CO2,H2O,SF
 SPEC PHASE=COND,COND,COND,COND,COND,COND,COND,COND,COND,*
       COND,GAS,GAS,GAS,GAS,GAS,COND,COND
 FRAC COND=0.0          $ Fraction condensed not used
 CHEM ACT TEMP=450.
 INIT CONC=0.78,0.,0.,0.,0.22,0.,0.,0.,0.,0.,0.,0.,0.,0.,1.,1.
 MIN CONC= 1.E-12,1.E-12,1.E-12,1.E-12,1.E-12,1.E-12,1.E-12,1.E-12,1.E-12,*
       1.E-12,1.E-12,1.E-12,1.E-12,1.E-12,1.E-12,1.E-12,1.E-12
 STERIC COEF= 0.,0.,0.,0.,*
         0.,0.,0.,0.,*
         0.,0.,0.,0.,*
         0.,0.,0.,0.
 PREEXP FACT= 3.E15,3.E15,3.E15,3.E15,*
         3.E15,3.E15,3.E15,3.E15,*
         3.E15,3.E15,3.E15,3.E15,*
         3.E15,3.E15,3.E15,3.E15 $ 1/s
 ACTIVATION ENERGY= 50200, 50600, 49400, 50400,   *
              50000, 49500, 50400, 49300,   *
              51600, 49800, 50200, 50100,   *
              50200, 51100, 49600, 49700    $ cal/mol
 ENERGY REL=     -20.6,20.6,-20.6,20.6,0.,-20.6,20.6,-20.6,0.,-20.6,*
              20.6,-20.6,0.,-20.6,20.6,-20.6      $ volumetric heat release, cal/cc
$      Rxn-->1 2 3 4 5 6 7 8 9 0 1 2 3 4 5 6   CPUF MECHANISM (B's are bridges, D's are danglers)
 CONC EXP, 1= 1 0 0 0 1 0 0 0 0 0 0 0 0 0 0 0      $ BTDI :  rxn [1]  BTDI      --> DTDI
 CONC EXP, 2= 0 0 0 0 0 1 0 0 1 0 0 0 0 0 0 0      $ BTAC :  rxn [2]  DTDI      --> BTDI
 CONC EXP, 3= 0 0 0 0 0 0 0 0 0 0 1 0 0 1 0 0 0    $ BTDA :  rxn [3]  DTDI      --> TDI
```

```
 CONC EXP, 4= 0 0 0 0 0 0 0 0 0 0 0 0 0 0 0 0     $ CHAR :  rxn [4]  TDI       --> DTDI
 CONC EXP, 5= 0 0 0 0 0 0 0 0 0 0 0 0 0 0 1 0 0   $ BADIP:  rxn [5]  BTDI + H2O  --> BTAC + CO2
 CONC EXP, 6= 0 1 1 0 0 0 0 0 0 0 0 0 0 0 0 0 0   $ DTDI :  rxn [6]  BTAC       --> DTAC
 CONC EXP, 7= 0 0 0 0 0 0 0 1 1 0 0 0 0 0 0 0 0   $ DTAC :  rxn [7]  DTAC       --> BTAC
 CONC EXP, 8= 0 0 0 0 0 0 0 0 0 0 0 1 1 0 0 0 0   $ DTDA :  rxn [8]  DTAC       --> TAC
 CONC EXP, 9= 0 0 0 0 0 0 0 0 0 0 0 0 0 0 0 1 1   $ DADIP:  rxn [9]  BTAC + H2O  --> BTDA + CO2
 CONC EXP,10= 0 0 0 1 0 0 0 0 0 0 0 0 0 0 0 0 0    $ TDI  :  rxn [10] BTDA       --> DTDA
 CONC EXP,11= 0 0 0 0 0 0 0 0 0 0 0 0 0 0 0 0 0    $ CO2  :  rxn [11] DTDA       --> BTDA
 CONC EXP,12= 0 0 0 0 0 0 0 0 0 0 0 0 0 0 0 0 0    $ TAC  :  rxn [12] DTDA       --> TDA
 CONC EXP,13= 0 0 0 0 0 0 0 0 0 0 0 0 0 0 0 0 0    $ TDA  :  rxn [13] BTDA       --> CHAR
 CONC EXP,14= 0 0 0 0 0 0 0 0 0 0 0 0 0 0 0 0 0    $ CPN  :  rxn [14] BADIP      --> DADIP
 CONC EXP,15= 0 0 0 0 1 0 0 0 1 0 0 0 0 0 0 0 1    $ H2O  :  rxn [15] DADIP      --> BADIP
 CONC EXP,16= 0 0 0 0 0 0 0 0 0 0 0 0 0 0 0 0 0    $ SF   :  rxn [16] DADIP + H2O --> CPN + CO2
$      Rxn--> 1  2  3  4  5  6  7  8  9  0  1  2  3  4  5  6          CPUF RATE EQUATIONS
 STO COEF, 1= -1  1  0  0 -1  0  0  0  0  0  0  0  0  0  0  0 $ BTDI :  dBTDI/dt  = -r1 +r2 -r5
 STO COEF, 2=  0  0  0  0  1 -1  1  0 -1  0  0  0  0  0  0  0 $ BTAC :  dBTAC/dt  = +r5 -r6 +r7 -r9
 STO COEF, 3=  0  0  0  0  0  0  0  0  1 -1  1  0 -1  0  0  0 $ BTDA :  dBTDA/dt  = +r9 -r10 +r11 -r13
 STO COEF, 4=  0  0  0  0  0  0  0  0  0  0  0  0  0  1  0  0 $ CHAR :  dCHAR/dt  = +r13
 STO COEF, 5=  0  0  0  0  0  0  0  0  0  0  0  0  0 -1  1  0 $ BADIP:  dBADIP/dt = -r14 +r15
 STO COEF, 6=  1 -1 -1  1  0  0  0  0  0  0  0  0  0  0  0  0 $ DTDI :  dDTDI/dt  = +r1 -r2 -r3 +r4
 STO COEF, 7=  0  0  0  0  0  1 -1 -1  0  0  0  0  0  0  0  0 $ DTAC :  dDTAC/dt  = +r6 -r7 -r8
 STO COEF, 8=  0  0  0  0  0  0  0  0  0  1 -1 -1  0  0  0  0 $ DTDA :  dDTDA/dt  = +r10 -r11 -r12
 STO COEF, 9=  0  0  0  0  0  0  0  0  0  0  0  0  0  1 -1 -1 $ DADIP:  dDADIP/dt = +r14 -r15 -r16
 STO COEF,10=  0  0  1 -1  0  0  0  0  0  0  0  0  0  0  0  0 $ TDI  :  dTDI/dt   = +r3 -r4
 STO COEF,11=  0  0  0  0  0  0  0  1  0  0  0  0  0  0  0  0 $ CO2  :  dTAC/dt   = +r8
 STO COEF,12=  0  0  0  0  0  0  0  0  0  0  0  1  0  0  0  0 $ TAC  :  dTDA/dt   = +r12
 STO COEF,13=  0  0  0  0  0  0  0  0  0  0  0  0  0  0  0  1 $ TDA  :  dCPN/dt   = +r16
 STO COEF,14=  0  0  0  0  1  0  0  0  1  0  0  0  0  0  0  1 $ CPN  :  dCO2/dt   = +r5 +r9 +r16
 STO COEF,15=  0  0  0  0 -1  0  0  0 -1  0  0  0  0  0  0 -1 $ H2O  :  dH2O/dt   = -r5 -r9 -r16
 STO COEF,16=  0  0  0  0  0  0  0  0  0  0  0  0  0  0  0  0 $ SF   :  dSF/dt    = 0.
END
USER CONSTANTS
 USER REAL=1, 2.8  $ sig+1 average coordination number
 USER REAL=2, 0.78  $ l0   init. urethane bridge population (note: ladip0 set to 1-l0)
 USER REAL=3, 0.82  $ TMP  site wt. frc. TMP (note: DEG = 1-TMP)
 USER REAL=4, 45.  $ pc(2) critical pressure for 2-mer
 USER REAL=5, 45.  $ pc(3) critical pressure for 3-mer
 USER REAL=6, 45.  $ pc(4) critical pressure for 1-mer (TMP fraction)
 USER REAL=7, 1.   $ press system pressure,atm
 USER REAL=8, 3520. $ standard deviation of act. energy
 USER REAL=9, 0.0  $ scaling of temperature bcs
END
MATERIAL, 304SS, ISOTROPIC     $ Cup bottom
 DENSITY=7.9              $ g/cc, Touloukian, vol 3, pg
 COND=VFUNC,10            $ cal/cm-s-K
 SPECIFIC HEAT=VFUNC,11     $ cal/g-K
 INIT TEMP=300.0          $ K
 EMIS=0.8               $ Emissivity, Touloukian, vol 3, pg 236
END
MATERIAL, 321SS, ISOTROPIC     $ Cup sides
 DENSITY=7.9              $ g/cc, Touloukian, vol 3, pg
 COND=VFUNC,10            $ cal/cm-s-K
 SPECIFIC HEAT=VFUNC,11     $ cal/g-K
 INIT TEMP=300.0          $ K
```

```
  EMIS=0.8              $ Emissivity, Touloukian, vol 3, pg 236
END
$
PROBLEM DEFINITION
  GEOM=AXI
  ELEMENT BLOCK=10, 304SS     $ cup bottom plate
  ELEMENT BLOCK=20, 321SS     $ cup sides
  ELEMENT BLOCK=30, CPUF_FOAM  $ reacting foam
  ELEMENT BLOCK=40, INERT_FOAM $ slug
$
$ Node Set and Side Set definitions for BC's
$
$ NODE=100: Node set on cup bottom next to foam (T BC)
$ NODE=200: Node set on cup side (T BC)
$ SIDE=300: Side set for exposed foam & cup sides (rad BC)
$ SIDE=400: Side set for exposed foam & cup sides (conv BC)
$ SIDE=500: Side set for enclosure radiation
$
  BCTYPE=TEMP,NODE=100,TFUN,1  $ Temperature on cup bottom next to foam
  BCTYPE=TEMP,NODE=200,USER,1  $ Temperature on cup side next to foam
  BCTYPE=RAD,  SIDE=300, COEF=1.0,1.0,TREF=300.0,1.0     $ exposed foam
  BCTYPE=CONV, SIDE=400, COEF=3.0E-04,1.0,TREF=300.0,1.0 $ exposed foam
  BCTYPE=ENCL RAD, SIDE=500, 1
  BCTYPE=ENCL RAD, BLOCK=30, 1
$mlh changed to the following line ENCLOSURE=1,FULL,,,,DYNAMIC
  RADIATION ENCLOSURE=1,FULL,DYN,,,,,
  VIEWFACTOR SHADING=1,BLOCKING
  DEATH,30,SF,0.036,CMIN
  SIGMA=1.3543E-12
  GAS CONSTANT=1.987
$  SPECIAL OUTPUT=24,0.05,0.81,0.05,1.51,0.05,2.02,0.05,2.79,0.05,3.34,*
$               0.05,4.11,0.05,4.55,0.05,5.24,0.05,5.95,0.05,6.57,*
$               0.05,7.12,0.05,7.86,0.05,8.51,0.05,9.23,0.05,9.84,*
$              0.05,10.35,2.34,0.73,2.34,1.40,2.34,2.73,2.34,4.08,*
$               2.34,5.25,2.34,6.61,2.34,7.95,2.34,15.02
END
SOLUTION,1,TRANSIENT
  RADIATION SOLUTION=1,GAUSS
  VIEWFACTOR COMPUTATION=1,HEMI,1.E-3,1.E-6,8,NONE
  VIEWFACTOR ADAPTIVE=1,0,25,UNI,100000,HAL,5.E-5
  VIEWFACTOR HEMICUBE=1,400,5,5
$  VIEWFACTOR COMPUTATION=1,HEMI,1.E-4,1.E-6,8,200,5,5.0,CALC,16,1000,UNI,0,NONE
  INT METH=EULER
  MATR SOL=CG
  INT TOL=1.E-4    $ DEFAULT VALUE is 1.E-2
  CONV TOL=1.E-7
  TIME STEP OPTION=AUTO
  TIME STEP=0.5
  MAXIMUM TEMPERATURE STEP=5.
  INIT TIME=0.
  FINAL TIME=3300.0
  CHEMISTRY STEP MULT = 1.E4
  NUM TIME STEP=50000000
  MAX MATRIX ITER=1000
```

```
END

TIME FUNCTION=1  $ Temperature history cup bottom
  0.0  300.0   $ t(s), T (K)   test 2 (cup plate T=750C, no component)
 34.8  300.5
 39.8  402.2
 64.8  937.7
 89.8  1045.4
139.8  1024.5
199.8  1024.7
254.8  1023.8
334.8  1023.9
499.8  1023.1
879.8  1023.5
1079.8  1023.5
1499.8  1023.3
2419.8  1023.4
2794.8  1024.0
2909.8   912.2
3044.8   816.7
3306.8   700.4
END
VAR FUNCTION=5    $ Rigid Polyurethane conductivity (cal/s-cm-K)
  100.0   1.4E-04 $ Hobbs memo dated 5/20/97
  296.0   1.4E-04
  323.0   1.5E-04
  373.0   1.6E-04
  423.0   1.8E-04
  473.0   2.0E-04
  523.0   2.2E-04
 3500.0   1.3E-03 $ linearly extrapolated value
END
VAR FUNCTION=6    $ Rigid polyurethane specific heat, cal/g-K
  100.0   0.303   $ Hobbs memo dated 5/20/97
  296.0   0.303
  323.0   0.324
  373.0   0.358
  423.0   0.440
  473.0   0.475
  523.0   0.526
 3500.0   0.526   $ extrapolated value
END
VAR FUNCTION=10   $ Conductivity of 303 SS,
   50., 0.0300   $ cal/cm-s-K
  200., 0.0300   $ Touloukian, Vol. 3, pg 176
  300., 0.0325
  400., 0.0375
  600., 0.0450
  750., 0.0500
 1100., 0.0625
 2000., 0.0900   $ Extrapolated value
END
VAR FUNCTION=11   $ AISI-304 stainless steel specific heat
 50.0   0.096    $ cal/g-K
```

```
 200.0  0.096   $ Obtained from Dobranich, 9113
 300.0  0.114
 400.0  0.123
 600.0  0.133
 800.0  0.139
1000.0  0.146
1300.0  0.153
3400.0  0.153
END
$
POST
$
  NOD DATA=TEMP,TDOT
  CHEM DATA=SF
  ELEMENT DATA=STATUS
  OUTPUT TIME STEP=30
$  OUTPUT FREQ =1
$  GLOBAL DATA = TP1,TP2,TP3,TP4,TP5,TP6,TP7,TP8,TP9,TP10,TP11,TP12,TP13,TP14,*
$            TP15,TP16,TP17,TP18,TP19,TP20,TP21,TP22,TP23,TP24
END
EXIT
```

Table C.2 User subroutine for temperature boundary condition

```
      SUBROUTINE USRT (TEMPBC, XNODE, YNODE, ZNODE, IDNSET, TIME,
     *                 KSTEP, RCONST, ICONST)
C
C     ***************************************************************
C
C     Version: $Id: USRT.F,v 1.2 1997/04/27 12:21:41 rehogan Exp $
C
C     DESCRIPTION:
C       USER SUBROUTINE TO EVALUATE A TEMPERATURE AT A NODE
C
C     PARAMETERS:
C       TEMPBC    (REAL) - Temperature at the node (output)
C       XNODE,    (REAL) - Coordinates for the node (input)
C       YNODE,
C       ZNODE
C       IDNSET (INTEGER) - Boundary condition node set id (input)
C       TIME      (REAL) - Current time (input)
C       KSTEP  (INTEGER) - Current iteration/time step number (input)
C       RCONST    (REAL) - User constants (input)
C       ICONST (INTEGER) - User constants (input)
C
C     CALLED BY: BCNODE
C
C     ***************************************************************
C
      DIMENSION RCONST(*), ICONST(*)
C
C     ***************************************************************
C
C     USER SUPPLIED FORTRAN CODE TO EVALUATE A TEMPERATURE
C
C-----------------------------------------------------------------C
C Program to interpolate temperatures along the cup wall
C-----------------------------------------------------------------C
C. . .VARIABLE DECLARATIONS. . . . . .
      parameter (npt = 18)
      dimension z(8),ts(npt)
      dimension t0(npt),t1(npt),t2(npt),t3(npt)
      dimension t4(npt),t5(npt),t6(npt),t7(npt)
C. . .COMMON BLOCK AREA. . . . . .
C. . .DATA STATEMENTS. . . . . .
C z distance from bottom plate TC to CUP TC's
      data z/ 0.0, 0.48, 1.11, 2.38, 3.65, 4.92, 6.83,16.51/
C ts time in s
      data ts/ 0., 34.8, 39.8, 64.8, 89.8, 139.8, 199.8, 254.8,
     & 334.8, 499.8, 879.8, 1079.8, 1499.8, 2419.8, 2794.8,
     & 2909.8, 3044.8, 3306.8/
C t0 thermocouple 0 (bottom plate thermal couple)
      data t0/ 300.0, 300.5, 402.2, 937.7, 1045.4, 1024.5, 1024.7,
     & 1023.8, 1023.9, 1023.1, 1023.5, 1023.5, 1023.3, 1023.4, 1024.0,
     & 912.2, 816.7, 700.4/
```

```
C t1 thermocouple 1
      data t1/ 300.0, 300.6, 301.3, 507.2, 703.5, 822.2, 856.2,
     & 870.2, 879.2, 891.5, 891.8, 894.6, 898.6, 899.2, 900.9,
     & 849.6, 777.0, 669.0/
C t2 thermocouple 2
      data t2/ 300.0, 301.2, 301.3, 382.2, 541.8, 678.3, 739.2,
     & 768.3, 794.0, 824.5, 835.0, 838.0, 845.3, 847.4, 850.0,
     & 812.3, 750.9, 648.3/
C t3 thermocouple 3
      data t3/ 300.0, 302.6, 302.7, 313.0, 383.2, 509.6, 580.9,
     & 619.5, 661.5, 721.6, 790.0, 795.1, 813.2, 817.9, 819.2,
     & 784.7, 722.9, 624.4/
C t4 thermocouple 4
      data t4/ 300.0, 304.1, 304.2, 307.4, 340.3, 437.3, 500.2,
     & 542.1, 582.3, 624.2, 727.9, 741.4, 772.9, 783.4, 783.8,
     & 756.0, 696.7, 604.0/
C t5 thermocouple 5
      data t5/ 300.0, 305.9, 306.1, 309.6, 333.3, 407.3, 462.2,
     & 504.8, 530.2, 566.0, 655.4, 664.2, 714.2, 740.3, 739.1,
     & 720.0, 666.3, 579.9/
C t6 thermocouple 6
      data t6/ 300.0, 309.0, 310.3, 318.1, 329.4, 376.5, 404.3,
     & 466.2, 457.9, 471.6, 534.8, 534.2, 571.3, 640.0, 644.1,
     & 636.6, 595.6, 527.4/
C t7 thermocouple 7 (This is the assumed temperature at the top of the cup)
      data t7/ 300., 300., 300., 300., 300., 300., 300., 300., 300.,
     & 300., 300., 300., 300., 300., 300., 300.,300.,300./
      save
C. . .EXECUTABLE STATEMENTS. . . . . .
C YNODE  = Coordinate of Y node <--- input from COYOTE
C TIME   = Current time        <--- input from COYOTE
C TEMPBC = Temperature at node  <--- this is what we return
C-----------------------------------------------------------------------C
C Check to see if ynode is within interpolation range (z is tc location)
      if (ynode.lt.z(8).and.ynode.gt.z(1)) then
C       determine which two tc's the node is between
        if (ynode.le.z(2)) then
C          node is between 0 and 1
           temp1 = tfun(time,npt,ts,t0)
           temp2 = tfun(time,npt,ts,t1)
           fac = (ynode-z(1))/(z(2)-z(1))
           tempbc = fac*temp2+(1.-fac)*temp1
           tempbc = tempbc + (tempbc-300)*RCONST(9)
        elseif (ynode.le.z(3)) then
C          node is between 1 and 2
           temp1 = tfun(time,npt,ts,t1)
           temp2 = tfun(time,npt,ts,t2)
           fac = (ynode-z(2))/(z(3)-z(2))
           tempbc = fac*temp2+(1.-fac)*temp1
           tempbc = tempbc + (tempbc-300)*RCONST(9)
        elseif (ynode.le.z(4)) then
C          node is between 2 and 3
           temp1 = tfun(time,npt,ts,t2)
           temp2 = tfun(time,npt,ts,t3)
```

```
        fac = (ynode-z(3))/(z(4)-z(3))
        tempbc = fac*temp2+(1.-fac)*temp1
        tempbc = tempbc + (tempbc-300)*RCONST(9)
      elseif (ynode.le.z(5)) then
C       node is between 3 and 4
        temp1 = tfun(time,npt,ts,t3)
        temp2 = tfun(time,npt,ts,t4)
        fac = (ynode-z(4))/(z(5)-z(4))
        tempbc = fac*temp2+(1.-fac)*temp1
        tempbc = tempbc + (tempbc-300)*RCONST(9)
      elseif (ynode.le.z(6)) then
C       node is between 4 and 5
        temp1 = tfun(time,npt,ts,t4)
        temp2 = tfun(time,npt,ts,t5)
        fac = (ynode-z(5))/(z(6)-z(5))
        tempbc = fac*temp2+(1.-fac)*temp1
        tempbc = tempbc + (tempbc-300)*RCONST(9)
      elseif (ynode.le.z(7)) then
C       node is between 5 and 6
        temp1 = tfun(time,npt,ts,t5)
        temp2 = tfun(time,npt,ts,t6)
        fac = (ynode-z(6))/(z(7)-z(6))
        tempbc = fac*temp2+(1.-fac)*temp1
        tempbc = tempbc + (tempbc-300)*RCONST(9)
      else
C       node is between 7 and 8
        temp1 = tfun(time,npt,ts,t6)
        temp2 = tfun(time,npt,ts,t7)
        fac = (ynode-z(7))/(z(8)-z(7))
        tempbc = fac*temp2+(1.-fac)*temp1
        tempbc = tempbc + (tempbc-300)*RCONST(9)
      endif
    elseif (ynode.le.z(1)) then
C     get tempbc from t0
      tempbc = tfun(time,npt,ts,t0)
      tempbc = tempbc + (tempbc-300)*RCONST(9)
    else
C     get tempbc from t7
      tempbc = tfun(time,npt,ts,t7)
      tempbc = tempbc + (tempbc-300)*RCONST(9)
    endif
    RETURN
    END
    function tfun(time,nfp,timpts,tmppts)
C-----------------------------------------------------------------------C
C Linear interpolation of temperature
c  input
c     time   - Time for temperature BC function
c     nfp    - Number of function points
c     timpts - Array containing function times
c     tmppts - Array containing function temperatures
c
c  output
c     return tfun - temperature at time
```

```
C-----------------------------------------------------------------------C
C. . .VARIABLE DECLARATIONS. . . . . .
      dimension timpts(*),tmppts(*)
      do 10 i=2,nfp
        if (timpts(i).ge.time) then
          dtdt = (tmppts(i)-tmppts(i-1))/(timpts(i)-timpts(i-1))
          tfun = tmppts(i-1) + dtdt*(time-timpts(i-1))
          return
        endif
10    continue
      if (time.le.timpts(1)) then
       tfun = tmppts(1)
       return
      endif
      if (time.ge.timpts(nfp)) then
        tfun = tmppts(nfp)
        return
      endif
      stop
      end
```

Table C.3 User subroutine for thermal conductivity of foam

```
      SUBROUTINE USRCON (COND11, COND22, COND33, TEMP, TDOT, SPEC,
     *                   XIP, YIP, ZIP, NAME, NUMIPT, MXSPEC, NSPEC,
     *                   TIME, KSTEP, KELM, RCONST, ICONST)
C
C     ****************************************************************
C
C     DESCRIPTION: (see detailed description below)
C       USER SUBROUTINE TO EVALUATE THE CONDUCTIVITY FOR A MATERIAL AT
C       THE ELEMENT INTEGRATION POINTS
C
C     PARAMETERS:
C       COND11   (REAL) - Principle thermal conductivity component in
C                         the 11 direction evaluated at the element
C                         integration points(output)
C       COND22   (REAL) - Principle thermal conductivity component in
C                         the 22 direction evaluated at the element
C                         integration points(output)
C       COND33   (REAL) - Principle thermal conductivity component in
C                         the 33 direction evaluated at the element
C                         integration points(output)
C       TEMP     (REAL) - Temperatures at the element integration
C                         points (input)
C       TDOT     (REAL) - Temperature rates at the element integration
C                         points (input)
C       SPEC     (REAL) - Chemical species at the element integration
C                         points (input)
C       XIP      (REAL) - Coordinates for the element integration
C       YIP                points (input)
C       ZIP
C       NAME (CHARACTER) - Material name (input)
C       NUMIPT (INTEGER) - Number of element integration points (input)
C       MXSPEC (INTEGER) - Maximum number of chemical species (input)
C       NSPEC  (INTEGER) - Number of chemical species (input)
C       TIME     (REAL) - Current time (input)
C       KSTEP  (INTEGER) - Current iteration/time step number (input)
C       RCONST   (REAL) - User constants (input)
C       ICONST (INTEGER) - User constants (input)
C**MLH  KELM   (INTEGER) - Current element number
C         To add KELM to the argument list I had to modify the call arguments
C         in the following routines:
C           ELFLX2.F, ELFLX3.F, ELMKF2.F, ELMKF3.F, ELMKFB.F, and ELMKFS.F
C
C     CALLED BY: ELMKF2, ELMKF3
C
C     ****************************************************************
C
      CHARACTER*20 NAME
C
      DIMENSION COND11(*), COND22(*), COND33(*)
      DIMENSION TEMP(*), TDOT(*), SPEC(MXSPEC,*)
      DIMENSION XIP(*), YIP(*), ZIP(*)
```

```
      DIMENSION RCONST(*), ICONST(*)
C
C     ****************************************************************
C
C     USER SUPPLIED FORTRAN CODE TO EVALUATE THE CONDUCTIVITY TENSOR,
C     COND11,COND22,COND33
C
C     Comment-out the following call when this subroutine is populated
C
cmlh  CALL ERROR('USRCON','Attempting to use an empty user subroutine',
cmlh *         ' ',0,' ',0,' ',0.0,' ',0.0,
cmlh *         'User failed to provide user subroutine',' ',' ',1)
C234567890123456789012345678901234567890123456789012345678901234567890123456789012
C-----------------------------------------------------------------------C
C     DESCRIPTION:
C       USER SUBROUTINE TO IMPLEMENT A DISCRETIZATION BIAS CORRECTION
C       BASED ON EXTRAPOLATING CONDUCTIVITY PAST 250 C.
C       THE MEASURED CONDUCTIVITY IS:
C          T, K   T, C    k, cal/s-cm-K
C         ------  ------  -------------
C          100.0  -173     1.4E-04
C          296.0    23     1.4E-04
C          323.0    50     1.5E-04
C          373.0   100     1.6E-04
C          423.0   150     1.8E-04
C          473.0   200     2.0E-04
C          523.0   250     2.2E-04
C         3500.0  3227     1.3E-03 linearly extrapolated value*
C         * The extrapolated number is to be multiplied by bias where
C          bias = 1.57 + 0.538(dT/dt) -0.00812*(dT/dt)^2
C          (See mlhobbs research notebook 1999 page 130)
C     NOTES:
C        1. dT/dt is the temperature gradient (tdot) when the
C           integration point reaches 523 K.
C        2. bias is calculated at the time the integration point
C           reaches 523 K.  After this time, bias is not changed.
C        3. The bias correction increases the value of the
C           extrapolated conductivity to increase the foam
C           decomposition rate so that the decomposition front velocity
C           calculated with 1-mm sized elements is the same as the
C           decomposition front velocity calculated with 50-um elements.
C           Thus, this routine should be used with elements that are
C           approximately 1-mm in dimension.
C-----------------------------------------------------------------------C
C. . .VARIABLE DECLARATIONS. . . . . . . . . . . . . . . . . . . . . . C
      parameter (npt = 8, numel=4689)
      dimension tk(npt),cond(npt)
      dimension bias(numel)
C. . .COMMON BLOCK AREA (NONE) . . . . . . . . . . . . . . . . . . . . C
C. . .DATA STATEMENTS. . . . . . . . . . . . . . . . . . . . . . . . . C
C tk, temperatures in K at which the thermal conductivity were measured
      data tk/100.,296.,323.,373.,423.,473.,523.,3500./
      data cond/1.4E-04,1.4E-04,1.5E-04,1.6E-04,
     &          1.8E-04,2.0E-04,2.2E-04,1.3E-03/
```

```
      data one/1.E0/
      data icount/1/
      save
C. . .EXECUTABLE STATEMENTS. . . . . C
      if (icount.eq.1) then
C       initialize bias array
        do i = 1,numel
          bias(i) = one
        enddo
        icount = 0
      endif
      if (bias(kelm).eq.one) then
C       this element has not been bias corrected,
C       check to see if bias correction needed
        thi = temp(1)
        ihi = 1
        do ipt = 2,numipt
          if (thi.le.temp(ipt)) then
            thi = temp(ipt)
            ihi = ipt
          endif
        enddo
C       bias correct if the element exceeds 523 K
        if(thi.ge.523.) then
C         set bias for mild boundary conditions where tdot <= 1.6
          bias(kelm) = 1.01
          if (tdot(ihi).ge.1.6) bias(kelm) =
     &              1.57+0.538*tdot(ihi)-0.00812*tdot(ihi)*tdot(ihi)
          if (tdot(ihi).ge.33.) bias(kelm) = 10.5
        endif
      endif
      cond(8) = bias(kelm)*1.3E-03
      do ipt = 1,numipt
        cond11(ipt) = cfun(temp(ipt),npt,tk,cond)
        cond22(ipt) = cond11(ipt)
        cond33(ipt) = cond11(ipt)
C-----------------------------------------------------------------C
C The following "enddo" finishes loading integ. pts for this element
C-----------------------------------------------------------------C
      enddo
C
      RETURN
      END
      function cfun(t,nfp,tpts,cpts)
C-----------------------------------------------------------------C
C Linear interpolation of temperature
c  input
c       t   - Temperature to interpolate conductivity
c       nfp  - Number of function points
c       tpts - Array containing measured temperatures
c       cpts - Array containing measured conductivities
c
c  output
c       return cfun - thermal conductivity at t
```

```
C-----------------------------------------------------------------------C
C. . .VARIABLE DECLARATIONS. . . . . .
      dimension tpts(*),cpts(*)
      do 10 i=2,nfp
        if (tpts(i).ge.t) then
          dcdt = (cpts(i)-cpts(i-1))/(tpts(i)-tpts(i-1))
          cfun = cpts(i-1) + dcdt*(t-tpts(i-1))
          return
        endif
10    continue
      if (t.le.tpts(1)) then
       cfun = cpts(1)
       return
      endif
      if (t.ge.tpts(nfp)) then
        cfun = cpts(nfp)
        return
      endif
      stop
      end
```

Table C.2 User subroutine for reaction rates.

```
      SUBROUTINE USRRR (RRATES, AK, TEMP, TEMPR, SPEC, SPCNAM, NAME,
     *                  NUMIPT, MXSPEC, MXREAC, NSPEC, NREAC, STERIC,
     *                  PREX, AENRGY, AMUSP, RCONST, ICONST)
C
C     ****************************************************************
C
C     Version: $Id: USRRR.F,v 1.4 1998/11/05 20:58:35 dkgartl Exp $
C
C     DESCRIPTION:
C      USER SUBROUTINE TO EVALUATE THE CHEMICAL REACTION RATES FOR
C      A MATERIAL AT THE ELEMENT INTEGRATION POINTS
C
C     PARAMETERS:
C      RRATES    (REAL) - Reaction rates evaluated at the element
C                 integration points (output)
C      AK       (REAL) - Kinetic Coefficients (output)
C      TEMP      (REAL) - Temperatures at the element integration
C                 points (input)
C      TEMPR     (REAL) - Temperature rates at the element
C                 integration points (input)
C      SPEC      (REAL) - Chemical species at the element integration
C                 points (input)
C      SPCNAM(CHARACTER) - Species names (input)
C      NAME  (CHARACTER) - Material name (input)
C      NUMIPT  (INTEGER) - Number of element integration points (input)
C      MXSPEC  (INTEGER) - Maximum number of chemical species (input)
C      MXREAC  (INTEGER) - Maximum number of chemical reactions (input)
C      NSPEC   (INTEGER) - Number of chemical species (input)
C      NREAC   (INTEGER) - Number of chemical reactions (input)
C      STERIC    (REAL) - Steric coefficients (input)
C      PREX      (REAL) - Pre-exponential factors (input)
C      AENRGY    (REAL) - Activation energy (input)
C      AMUSP     (REAL) - Exponents for reactive species (input)
C      RCONST    (REAL) - User constants
C      ICONST  (INTEGER) - User constants
C
C     CALLED BY: CHEMDF
C
C     ****************************************************************
C
      CHARACTER*40 NAME,SPCNAM
C
      DIMENSION RRATES(MXREAC,*), AK(MXREAC,*)
      DIMENSION TEMP(*), TEMPR(*), SPEC(MXSPEC,*), SPCNAM(MXSPEC,*)
      DIMENSION STERIC(*), PREX(*)
      DIMENSION AENRGY(*), AMUSP(MXSPEC,*)
      DIMENSION RCONST(*), ICONST(*)
      data icount/1/
c     data es,badip0/3970.,0.22/
      save
C     I am using the user defined reaction rates to implement distributed
```

```
C    activation energies.
C. . .extract species index and read CPUF specific parameters
     if (icount.eq.1) then
       badip0 = 1.-rconst(2)
       icount = icount+1
C       divide the activation energy standard deviation by the gas constant
       es = rconst(8)/1.987
       do i = 1, nspec
         if(spcnam(i,1)(1:5).eq.'BADIP') index = i
       end do
     end if
     DO 40 KPT=1,NUMIPT
     DO 40 KRC=1,NREAC
     fx = 1.-spec(index,kpt)/badip0
     call inverf(fx,x)
     AK(KRC,KPT)=EXP(STERIC(KRC)*ALOG(TEMP(KPT))+PREX(KRC)-
    *          ((AENRGY(KRC)+x*es)/TEMP(KPT)))
   40 CONTINUE
C
C    DEFINE CONCENTRATION MULTIPLIERS
C
     DO 60 KPT=1,NUMIPT
     DO 60 KRC=1,NREAC
     RRATES(KRC,KPT)=AK(KRC,KPT)
     DO 50 KSP=1,NSPEC
     IF (AMUSP(KSP,KRC).NE.0) RRATES(KRC,KPT)=
    &       RRATES(KRC,KPT)*SPEC(KSP,KPT)**AMUSP(KSP,KRC)
   50 CONTINUE
   60 CONTINUE
     RETURN
     END
     subroutine inverf(y,x)
C-----------------------------------------------------------------------C
c  this program calculates the inverse of the area under the normal curve.
c  if y=area(x), then given y, this program will calculate x.
c  A table lookup is performed.
C-----------------------------------------------------------------------C
C. . .VARIABLE DECLARATIONS. . . . . .
     dimension xx(18),yy(18)
C. . .COMMON BLOCK AREA. . . . . .
C    none
C. . .DATA STATEMENTS. . . . . .
     data xx/3.4,3.2,3.,2.8,2.6,2.4,2.2,2.,1.8,1.6,1.4,
    &       1.2,1.,.8,.6,.4,.2,0./
     data yy/.9997,.9993,.9987,.9974,.9953,.9918,.9861,.9772,.9641,
    &       .9452,.9192,.8849,.8413,.7881,.7257,.6554,.5793,.5/
     save
     fac = 1.
c  check to see if y is within range
     if(y.lt.0.0228)then
       x = -2.0
       return
     elseif(y.lt.0.5)then
       yp = 1.-y
```

```
      fac = -1.
    elseif(y.gt.0.9997)then
      x = 3.5
      return
    else
      yp = y
    endif
c  search for range
    do 10 i=17,1,-1
      if(yp.le.yy(i+1))then
        x = xx(i) + (yp-yy(i))*(xx(i+1)-xx(i))/(yy(i+1)-yy(i))
        x = fac*x
        return
      endif
10    continue
    return
    end
```

External Distribution

M. A. Adams
Jet Propulsion Laboratory
4800 Oak Grove Drive, MS 97
Pasadena, CA 91109

M. Aivazis
Center for Advanced Computing
Research
California Institute of Technology
1200 E. California Blvd./MS 158-79
Pasadena, CA 91125

Charles E. Anderson
Southwest Research Institute
P. O. Drawer 28510
San Antonio, TX 78284-0510

Bilal Ayyub (2)
Department of Civil Engineering
University of Maryland
College Park, MD 20742-3021

Ivo Babuska
TICAM
Mail Code C0200
University of Texas at Austin
Austin, TX 78712-1085

Osman Balci
Department of Computer Science
Virginia Tech
Blacksburg, VA 24061

S. L. Barson
Boeing Company
Rocketdyne Propulsion & Power
MS IB-39
P. O. Box 7922
6633 Canoga Avenue
Canoga Park, CA 91309-7922

Steven Batill (2)
Dept. of Aerospace & Mechanical Engr.
University of Notre Dame
Notre Dame, IN 46556

Ted Belytschko (2)
Department of Mechanical Engineering
Northwestern University
2145 Sheridan Road
Evanston, IL 60208

John Benek
AFRL/VAAC
2210 Eighth St.
Wright-Patterson AFB, OH 45433

James Berger
Inst. of Statistics and Decision Science
Duke University
Box 90251
Durham, NC 27708-0251

Jay Boris (2)
Laboratory for Computational Physics
and Fluid Dynamics
Naval Research Laboratory
Code 6400
4555 Overlook Ave, SW
Washington, DC 20375-5344

Pavel A. Bouzinov
ADINA R&D, Inc.
71 Elton Avenue
Watertown, MA 02472

John A. Cafeo
General Motors R&D Center
Mail Code 480-106-256
30500 Mound Road
Box 9055
Warren, MI 48090-9055

James C. Cavendish
General Motors R&D Center
Mail Code 480-106-359
30500 Mound Road
Box 9055
Warren, MI 48090-9055

Chun-Hung Chen (2)
Department of Systems Engineering &
Operations Research
George Mason University
4400 University Drive, MS 4A6
Fairfax, VA 22030

Wei Chen
Department of Mechanical Engineering
Northwestern University
2145 Sheridan Road, Tech B224
Evanston, IL 60208-3111

Kyeongjae Cho (2)
Dept. of Mechanical Engineering
MC 4040
Stanford University
Stanford, CA 94305-4040

Harry Clark
Rocket Test Operations
AEDC
1103 Avenue B
Arnold AFB, TN 37389-1400

Hugh Coleman
Department of Mechanical &
Aero. Engineering
University of Alabama/Huntsville
Huntsville, AL 35899

Raymond Cosner (2)
Boeing-Phantom Works
MC S106-7126
P. O. Box 516
St. Louis, MO 63166-0516

Thomas A. Cruse
398 Shadow Place
Pagosa Springs, CO 81147-7610

Phillip Cuniff
U.S. Army Soldier Systems Center
Kansas Street
Natick, MA 01750-5019

Department of Energy (5)
Attn: Kevin Greenaugh, NA-115
D. Kusnezov, NA-114
Jamileh Soudah, NA-114
K. Sturgess, NA-115
J. Van Fleet, NA-113
Forrestal Building
1000 Independence Ave., SW
Washington, DC 20585

Prof. Urmila Diwekar (2)
University of Illinois at Chicago
Chemical Engineering Dept.
810 S. Clinton St.
209 CHB, M/C 110
Chicago, IL 60607

David Dolling
Department of Aerospace Engineering
& Engineering Mechanics
University of Texas at Austin
Austin, TX 78712-1085

Robert G. Easterling
51 Avenida Del Sol
Cedar Crest, NM 87008

Isaac Elishakoff
Dept. of Mechanical Engineering
Florida Atlantic University
777 Glades Road
Boca Raton, FL 33431-0991

Ashley Emery
Dept. of Mechanical Engineering
Box 352600
University of Washington
Seattle, WA 98195-2600

Scott Ferson
Applied Biomathematics
100 North Country Road
Setauket, New York 11733-1345

Joseph E. Flaherty (2)
Dept. of Computer Science
Rensselaer Polytechnic Institute
Troy, NY 12181

John Fortna
ANSYS, Inc.
275 Technology Drive
Canonsburg, PA 15317

Marc Garbey
Dept. of Computer Science
Univ. of Houston
501 Philipp G. Hoffman Hall
Houston, Texas 77204-3010

Roger Ghanem
Dept. of Civil Engineering
Johns Hopkins University
Baltimore, MD 21218

Mike Giltrud
Defense Threat Reduction Agency
DTRA/CPWS
6801 Telegraph Road
Alexandria, VA 22310-3398

James Glimm (2)
Dept. of Applied Math & Statistics
P138A
State University of New York
Stony Brook, NY 11794-3600

James Gran
SRI International
Poulter Laboratory AH253
333 Ravenswood Avenue
Menlo Park, CA 94025

Bernard Grossman (2)
The National Institute of Aerospace
144 Research Drive
Hampton, VA 23666

Sami Habchi
CFD Research Corp.
Cummings Research Park
215 Wynn Drive
Huntsville, AL 35805

Raphael Haftka (2)
Dept. of Aerospace and Mechanical
Engineering and Engr. Science
P. O. Box 116250
University of Florida
Gainesville, FL 32611-6250

Achintya Haldar (2)
Dept. of Civil Engineering
& Engineering Mechanics
University of Arizona
Tucson, AZ 85721

Tim Hasselman
ACTA
2790 Skypark Dr., Suite 310
Torrance, CA 90505-5345

G. L. Havskjold
Boeing - Rocketdyne Propulsion & Power
MS GB-09
P. O. Box 7922
6633 Canoga Avenue
Canoga Park, CA 91309-7922

George Hazelrigg
Division of Design, Manufacturing
& Innovation
Room 508N
4201 Wilson Blvd.
Arlington, VA 22230

David Higdon
Inst. of Statistics and Decision Science
Duke University
Box 90251
Durham, NC 27708-0251

Richard Hills (2)
Mechanical Engineering Dept.
New Mexico State University
P. O. Box 30001/Dept. 3450
Las Cruces, NM 88003-8001

F. Owen Hoffman (2)
SENES
102 Donner Drive
Oak Ridge, TN 37830

Luc Huyse
Southwest Research Institute
6220 Culebra Road
P. O. Drawer 28510
San Antonio, TX 78284-0510

George Ivy
Northrop Grumman Information
Technology
222 West Sixth St.
P.O. Box 471
San Pedro, CA 90733-0471

Rima Izem
Sience and Technology Policy Intern
Board of Mathematical Sciences and their
Applications
500 5th Street, NW
Washington, DC 20001

Ralph Jones (2)
Sverdrup Tech. Inc./AEDC Group
1099 Avenue C
Arnold AFB, TN 37389-9013

Leo Kadanoff (2)
Research Institutes Building
University of Chicago
5640 South Ellis Ave.
Chicago, IL 60637

George Karniadakis (2)
Division of Applied Mathematics
Brown University
192 George St., Box F
Providence, RI 02912

Alan Karr
Inst. of Statistics and Decision Science
Duke University
Box 90251
Durham, NC 27708-0251

J. J. Keremes
Boeing Company
Rocketdyne Propulsion & Power
MS AC-15
P. O. Box 7922
6633 Canoga Avenue
Canoga Park, CA 91309-7922

K. D. Kimsey
U.S. Army Research Laboratory
Weapons & Materials Research
Directorate
AMSRL-WM-TC 309 120A
Aberdeen Proving Gd, MD 21005-5066

B. A. Kovac
Boeing - Rocketdyne Propulsion & Power
MS AC-15
P. O. Box 7922
6633 Canoga Avenue
Canoga Park, CA 91309-7922

Chris Layne
AEDC
Mail Stop 6200
760 Fourth Street
Arnold AFB, TN 37389-6200

W. K. Liu (2)
Northwestern University
Dept. of Mechanical Engineering
2145 Sheridan Road
Evanston, IL 60108-3111

Robert Lust
General Motors, R&D and Planning
MC 480-106-256
30500 Mound Road
Warren, MI 48090-9055

Sankaran Mahadevan (2)
Dept. of Civil &
Environmental Engineering
Vanderbilt University
Box 6077, Station B
Nashville, TN 37235

Hans Mair
Institute for Defense Analysis
Operational Evaluation Division
4850 Mark Center Drive
Alexandria VA 22311-1882

W. McDonald
NDM Solutions
1420 Aldenham Lane
Reston, VA 20190-3901

Gregory McRae (2)
Dept. of Chemical Engineering
Massachusetts Institute of Technology
Cambridge, MA 02139

Michael Mendenhall (2)
Nielsen Engineering & Research, Inc.
605 Ellis St., Suite 200
Mountain View, CA 94043

Juan Meza
High Performance Computing Research
Lawrence Berkeley National Laboratory
One Cyclotron Road, MS: 50B-2239
Berkeley, CA 94720

Dr. John G. Michopoulos
Naval Research Laboratory,
Special Projects Group, Code 6303
Computational Mutliphysics Systems Lab
Washington DC 20375, USA

Sue Minkoff (2)
Dept. of Mathematics and Statistics
University of Maryland
1000 Hilltop Circle
Baltimore, MD 21250

Max Morris (2)
Department of Statistics
Iowa State University
304A Snedecor-Hall
Ames, IW 50011-1210

R. Namburu
U.S. Army Research Laboratory
AMSRL-CI-H
Aberdeen Proving Gd, MD 21005-5067

NASA/Ames Research Center (2)
Attn: Unmeel Mehta, MS 229-3
David Thompson, MS 269-1
Moffett Field, CA 94035-1000

NASA/Glen Research Center (2)
Attn: John Slater, MS 86-7
Chris Steffen, MS 5-11
21000 Brookpark Road
Cleveland, OH 44135

NASA/Langley Research Center (7)
Attn: Dick DeLoach, MS 236
Michael Hemsch, MS 286
Tianshu Liu, MS 238
Jim Luckring, MS 286
Joe Morrison, MS 128
Ahmed Noor, MS 369
Sharon Padula, MS 159
Hampton, VA 23681-0001

C. Needham
Applied Research Associates, Inc.
4300 San Mateo Blvd., Suite A-220
Albuquerque, NM 87110

A. Needleman
Division of Engineering, Box D
Brown University
Providence, RI 02912

Robert Nelson
Dept. of Aerospace & Mechanical Engr.
University of Notre Dame
Notre Dame, IN 46556

Dick Neumann
8311 SE Millihanna Rd.
Olalla, WA 98359

Efstratios Nikolaidis (2)
MIME Dept.
4035 Nitschke Hall
University of Toledo
Toledo, OH 43606-3390

D. L. O'Connor
Boeing Company
Rocketdyne Propulsion & Power
MS AC-15
P. O. Box 7922
6633 Canoga Avenue
Canoga Park, CA 91309-7922

Tinsley Oden (2)
TICAM
Mail Code C0200
University of Texas at Austin
Austin, TX 78712-1085

Michael Ortiz (2)
Graduate Aeronautical Laboratories
California Institute of Technology
1200 E. California Blvd./MS 105-50
Pasadena, CA 91125

Dale Pace
Applied Physics Laboratory
Johns Hopkins University
111000 Johns Hopkins Road
Laurel, MD 20723-6099

Alex Pang
Computer Science Department
University of California
Santa Cruz, CA 95064

Chris L. Pettit
AFRL/VASD
2130 Eighth Street
Wright-Patterson AFB, OH 45433-7532

Allan Pifko
2 George Court
Melville, NY 11747

Joseph Powers
Dept. of Aerospace and Mechanical Engr.
University of Notre Dame
Notre Dame, IN 46556-5637

Cary Presser (2)
Process Measurements Div.
National Institute of Standards
and Technology
Bldg. 221, Room B312
Gaithersburg, MD 20899

Gerald R. Prichard
Principal Systems Analyst
Dynetics, Inc.
1000 Explorer Blvd.
Huntsville, AL 35806

Thomas A. Pucik
Pucik Consulting Services
13243 Warren Avenue
Los Angles, CA 90066-1750

P. Radovitzky
Graduate Aeronautical Laboratories
California Institute of Technology
1200 E. California Blvd./MS 105-50
Pasadena, CA 91125

W. Rafaniello
DOW Chemical Company
1776 Building
Midland, MI 48674

J. N. Reddy
Dept. of Mechanical Engineering
Texas A&M University
ENPH Building, Room 210
College Station, TX 77843-3123

John Renaud (2)
Dept. of Aerospace & Mechanical Engr.
University of Notre Dame
Notre Dame, IN 46556

Grant Reinman
Pratt & Whitney
400 Main Street, M/S 162-01
East Hartford, CT 06108

Patrick J. Roache
1215 Apache Drive
Socorro, NM 87801

A. J. Rosakis
Graduate Aeronautical Laboratories
California Institute of Technology
1200 E. California Blvd./MS 105-50
Pasadena, CA 91125

Tim Ross (2)
Dept. of Civil Engineering
University of New Mexico
Albuquerque, NM 87131

Chris Roy (2)
Dept. of Aerospace Engineering
211 Aerospace Engineering Bldg.
Auburn University, AL 36849-5338

J. Sacks
Inst. of Statistics and Decision Science
Duke University
Box 90251
Durham, NC 27708-0251

Sunil Saigal (2)
Carnegie Mellon University
Department of Civil and
Environmental Engineering
Pittsburgh, PA 15213

Larry Sanders
DTRA/ASC
8725 John J. Kingman Rd
MS 6201
Ft. Belvoir, VA 22060-6201

Len Schwer
Schwer Engineering & Consulting
6122 Aaron Court
Windsor, CA 95492

Paul Senseny
Factory Mutual Research Corporation
1151 Boston-Providence Turnpike
P.O. Box 9102
Norwood, MA 02062

E. Sevin
Logicon RDA, Inc.
1782 Kenton Circle
Lyndhurst, OH 44124

Mark Shephard (2)
Rensselaer Polytechnic Institute
Scientific Computation Research Center
Troy, NY 12180-3950

Tom I-P. Shih
Dept. of Mechanical Engineering
2452 Engineering Building
East Lansing, MI 48824-1226

T. P. Shivananda
Bldg. SB2/Rm. 1011
TRW/Ballistic Missiles Division
P. O. Box 1310
San Bernardino, CA 92402-1310

Y.-C. Shu
Graduate Aeronautical Laboratories
California Institute of Technology
1200 E. California Blvd./MS 105-50
Pasadena, CA 91125

Don Simons
Northrop Grumman Information Tech.
222 W. Sixth St.
P.O. Box 471
San Pedro, CA 90733-0471

Munir M. Sindir
Boeing - Rocketdyne Propulsion & Power
MS GB-11
P. O. Box 7922
6633 Canoga Avenue
Canoga Park, CA 91309-7922

Ashok Singhal (2)
CFD Research Corp.
Cummings Research Park
215 Wynn Drive
Huntsville, AL 35805

R. Singleton
Engineering Sciences Directorate
Army Research Office
4300 S. Miami Blvd.
P.O. Box 1221
Research Triangle Park, NC 27709-2211

W. E. Snowden
DARPA
7120 Laketree Drive
Fairfax Station, VA 22039

Bill Spencer (2)
Dept. of Civil Engineering
and Geological Sciences
University of Notre Dame
Notre Dame, IN 46556-0767

G. R. Srinivasan
Org. L2-70, Bldg. 157
Lockheed Martin Space & Strategic Missiles
1111 Lockheed Martin Way
Sunnyvale, CA 94089

Fred Stern
Professor Mechanical Engineering
Iowa Institute of Hydraulic Research
The University of Iowa
Iowa City Iowa 52242

D. E. Stevenson (2)
Computer Science Department
Clemson University
442 Edwards Hall, Box 341906
Clemson, SC 29631-1906

Tim Swafford
Sverdrup Tech. Inc./AEDC Group
1099 Avenue C
Arnold AFB, TN 37389-9013

Kenneth Tatum
Sverdrup Tech. Inc./AEDC Group
740 Fourth Ave.
Arnold AFB, TN 37389-6001

Ben Thacker
Southwest Research Institute
6220 Culebra Road
P. O. Drawer 28510
San Antonio, TX 78284-0510

Fulvio Tonon (2)
Geology and Geophysics Dept.
East Room 719
University of Utah
135 South 1460
Salt Lake City, UT 84112

Robert W. Walters (2)
Aerospace and Ocean Engineering
Virginia Tech
215 Randolph Hall, MS 203
Blacksburg, VA 24061-0203

Leonard Wesley
Intellex Inc.
5932 Killarney Circle
San Jose, CA 95138

Justin Y-T Wu
8540 Colonnade Center Drive, Ste 301
Raleigh, NC 27615

Ren-Jye Yang
Ford Research Laboratory
MD2115-SRL
P.O.Box 2053
Dearborn, MI 4812

Simone Youngblood (2)
DOD/DMSO
Technical Director for VV&A
1901 N. Beauregard St., Suite 504
Alexandria, VA 22311

M. A. Zikry
North Carolina State University
Mechanical & Aerospace Engineering
2412 Broughton Hall, Box 7910
Raleigh, NC 27695

Foreign Distribution

Yakov Ben-Haim (2)
Department of Mechanical Engineering
Technion-Israel Institute of Technology
Haifa 32000
ISRAEL

Gert de Cooman (2)
Universiteit Gent
Onderzoeksgroep, SYSTeMS
Technologiepark - Zwijnaarde 9
9052 Zwijnaarde
BELGIUM

Graham de Vahl Davis
CFD Research Laboratory
University of NSW
Sydney, NSW 2052
AUSTRALIA

Luis Eca (2)
Instituto Superior Tecnico
Department of Mechanical Engineering
Av. Rovisco Pais
1096 Lisboa CODEX
PORTUGAL

Charles Hirsch (2)
Department of Fluid Mechanics
Vrije Universiteit Brussel
Pleinlaan, 2
B-1050 Brussels
BELGIUM

Igor Kozin (2)
Systems Analysis Department
Riso National Laboratory
P. O. Box 49
DK-4000 Roskilde
DENMARK

Nina Nikolova - Jeliazkova
Institute of Parallel Processing
Bulgarian Academy of Sciences
25a "acad. G. Bonchev" str.
Sofia 1113
Bulgaria

K. Papoulia
Inst. Eng. Seismology & Earthquake Engineering
P.O. Box 53, Finikas GR-55105
Thessaloniki
GREECE

Dominique Pelletier
Genie Mecanique
Ecole Polytechnique de Montreal
C.P. 6079, Succursale Centre-ville
Montreal, H3C 3A7
CANADA

Vincent Sacksteder
Via Eurialo 28, Int. 13
00181 Rome
Italy

Lev Utkin
Institute of Statistics
Munich University
Ludwigstr. 33
80539, Munich
GERMANY

Malcolm Wallace
Computational Dynamics Ltd.
200 Shepherds Bush Road
London W6 7NY
UNITED KINGDOM

Department of Energy Laboratories

Los Alamos National Laboratory (53)
Mail Station 5000
P.O. Box 1663
Los Alamos, NM 87545
Attn: Peter Adams, MS B220
Mark C. Anderson, MS T080
Cuauhtemoc Aviles-Ramos, MS P946
Robert Benjamin, MS P940
Jane M. Booker, MS P946
Terrence Bott, MS K557
Jerry S. Brock, MS F663
D. Cagliostro, MS F645
Katherine Campbell, MS F600
David L. Crane, MS P946
John F. Davis, MS B295
Helen S. Deaven, MS B295
Barbara DeVolder, MS B259
Scott Doebling, MS P946
S. Eisenhawer, MS K557
Dawn Flicker, MS F664
George T. Gray, MS G755
Ken Hanson, MS B250
Alexandra Heath, MS F663
R. Henninger, MS D413
Kathleen Holian, MS B295
Darryl Holm, MS B284
James Hyman, MS B284
Valen Johnson, MS F600
Cliff Joslyn, MS B265
James Kamm, MS D413
S. Keller-McNulty, MS F600
Joseph Kindel, MS B259
Ken Koch, MS F652
Douglas Kothe, MS B250
Jeanette Lagrange, MS D445
Len Margolin, MS D413
Harry Martz, MS F600
Mike McKay, MS F600
Kelly McLenithan, MS F664
Mark P. Miller, MS P946
John D. Morrison, MS F602
Karen I. Pao, MS B256
James Peery, MS F652
M. Peterson-Schnell, MS B295
Douglas Post, MS F661 X-DO
William Rider, MS D413
Tom Seed, MS F663
Kari Sentz, MS F600
David Sharp, MS B213
Richard N. Silver, MS D429
Ronald E. Smith, MS J576
Christine Treml, MS J570
David Tubbs, MS B220
Daniel Weeks, MS B295
Morgan White, MS F663
Alyson G. Wilson, MS F600

Lawrence Livermore National Laboratory (23)
7000 East Ave.
P.O. Box 808
Livermore, CA 94550
Attn: Thomas F. Adams, MS L-095
Steven Ashby, MS L-561
John Bolstad, MS L-023
Peter N. Brown, MS L-561
T. Scott Carman, MS L-031
R. Christensen, MS L-160
Evi Dube, MS L-095
Henry Hsieh, MS L-229
Richard Klein, MS L-023
Roger Logan, MS L-125
C. F. McMillan, MS L-098
C. Mailhiot, MS L-055
J. F. McEnerney, MS L-023
M. J. Murphy, MS L-282
Daniel Nikkel, MS L-342
Cynthia Nitta, MS L-096
Peter Raboin, MS L-125
Edward Russell, MS L-631
Kambiz Salari, MS L-228
David D. Sam, MS L-125
Peter Terrill, MS L-125
Charles Tong, MS L-560
Carol Woodward, MS L-561

Argonne National Laboratory
Attn: Paul Hovland
Mike Minkoff
MCS Division
Bldg. 221, Rm. C-236
9700 S. Cass Ave.
Argonne, IL 60439

Sandia Internal Distribution

1 MS 0511 1021 K. D. Meeks
1 MS 1152 1642 M. L. Kiefer
1 MS 1186 1674 R. J. Lawrence
1 MS 0525 1734 P. V. Plunkett
1 MS 0525 1734 R. B. Heath
1 MS 0525 1734 S. D. Wix
1 MS 0429 2100 J. S. Rottler
1 MS 0437 2100 R. C. Hartwig
1 MS 0447 2111 P. Davis
1 MS 0447 2111 P. D. Hoover
1 MS 0479 2113 J. O. Harrison
1 MS 0487 2115 P. A. Sena
1 MS 0453 2130 H. J. Abeyta
1 MS 0481 2132 M. A. Rosenthal
1 MS 0427 2134 R. A. Paulsen
1 MS 0509 2300 M. W. Callahan
1 MS 1138 2345 G. K. Froehlich
1 MS 0512 2500 T. E. Blejwas
1 MS 0437 2830 J. M. McGlaun
1 MS 0647 2912 D. R. Olson
1 MS 0634 2951 K. V. Chavez
1 MS 0768 4140 A. L. Camp
1 MS 0757 4142 R. D. Waters
1 MS 0759 4145 G. D. Wyss
1 MS 1115 4200 D. S. Miyoshi
1 MS 0670 5526 J. R. Weatherby
1 MS 0576 5536 M. T. McCornack
1 MS 0735 6115 S. C. James
1 MS 0751 6117 R. M. Brannon
1 MS 0751 6117 L. S. Costin
1 MS 0751 6117 A. F. Fossum
1 MS 0708 6214 P. S. Veers
1 MS 1138 6221 G. E. Barr
1 MS 1138 6222 S. M. DeLand
1 MS 1138 6222 P. G. Kaplan
1 MS 1138 6223 L. M. Claussen
1 MS 1138 6223 A. L. Hodges
1 MS 1137 6224 G. D. Valdez
1 MS 0490 6252 J. A. Cooper
1 MS 1395 6820 M. J. Chavez
1 MS 1395 6821 J. W. Garner
1 MS 1395 6821 E. R. Giambalvo
1 MS 0778 6851 P. N. Swift
1 MS 0778 6851 B. W. Arnold
1 MS 0778 6851 R. J. MacKinnon
1 MS 0776 6852 T. Hadgu
1 MS 0776 6852 M. K. Knowles
1 MS 0776 6852 J. S. Stein
1 MS 1399 6853 M. G. Marietta
1 MS 0776 6853 R. P. Rechard
1 MS 1399 6853 P. Vaughn
1 MS 0748 6861 D. G. Robinson
1 MS 0727 6870 D. A. Powers
1 MS 1146 6871 P. J. Griffin
1 MS 1379 6957 A. Johnson
1 MS 9001 8000 P. E. Nielan
1 MS 9004 8100 R. H. Stulen
1 MS 9007 8200 D. R. Henson
1 MS 9202 8205 R. M. Zurn
1 MS 9014 8242 A. R. Ortega
1 MS 9042 8752 C. D. Moen
1 MS 9409 8754 J. R. Garcia
1 MS 9409 8754 W. A. Kawahara
1 MS 9161 8763 E. P. Chen
1 MS 9405 8763 R. E. Jones
1 MS 9161 8763 P. A. Klein
1 MS 9405 8763 R. A. Regueiro
1 MS 9042 8774 J. J. Dike
1 MS 9003 8900 K. E. Washington
1 MS 9003 8940 C. M. Hartwig
1 MS 9003 8960 J. L. Handrock
1 MS 9217 8962 P. D. Hough
1 MS 9217 8962 K. R. Long
1 MS 9217 8962 M. L. Martinez-Canales
1 MS 0384 9100 T. C. Bickel
1 MS 1393 9100 T.Y. Chu
1 MS 0825 9100 C. W. Peterson
1 MS 0826 9100 D. K. Gartling
1 MS 0825 9110 W. Hermina
1 MS 0834 9112 S. J. Beresh
1 MS 1310 9113 S. N. Kempka
1 MS 0834 9114 J. E. Johannes
1 MS 0834 9114 K. S. Chen
1 MS 0834 9114 R. R. Rao
1 MS 0834 9114 P. R. Schunk
1 MS 0825 9115 B. Hassan
1 MS 0825 9115 M. Barone
1 MS 0825 9115 F. G. Blottner
1 MS 0825 9115 D. W. Kuntz

1	MS 0825	9115	J. L. Payne
1	MS 0825	9115	D. L. Potter
1	MS 0825	9115	W. P. Wolfe
1	MS 0836	9116	E. S. Hertel
1	MS 0836	9116	D. Dobranich
1	MS 0836	9116	R. E. Hogan
1	MS 0836	9117	R. O. Griffith
1	MS 0836	9117	R. J. Buss
1	MS 0139	9120	P. J. Wilson
1	MS 0555	9122	M. S. Garrett
1	MS 0893	9123	J. Pott
1	MS 0847	9124	J. M. Redmond
1	MS 0557	9124	T. G. Carne
1	MS 0847	9124	R. V. Field
1	MS 0557	9124	T. Simmermacher
1	MS 0553	9124	D. O. Smallwood
1	MS 0847	9124	S. F. Wojtkiewicz
1	MS 0557	9125	T. J. Baca
1	MS 0557	9125	C. C. O'Gorman
1	MS 0372	9126	R. A. May
1	MS 0372	9126	T. D. Hinnerichs
1	MS 0372	9126	K. E. Metzinger
1	MS 0372	9127	J. Jung
1	MS 0824	9130	J. L. Moya
1	MS 0821	9132	L. A. Gritzo
1	MS 1135	9132	J. T. Nakos
1	MS 0836	9132	C. Romero
1	MS 1135	9132	S. R. Tieszen
3	MS 0828	9133	M. Pilch
1	MS 0828	9133	A. R. Black
1	MS 0828	9133	K. J. Dowding
1	MS 0828	9133	A. A. Giunta
1	MS 0779	9133	J. C. Helton
5	MS 0828	9133	W. L. Oberkampf
1	MS 0557	9133	T. L. Paez
1	MS 0828	9133	J. R. Red-Horse
1	MS 0828	9133	V. J. Romero
1	MS 0828	9133	M. P. Sherman
1	MS 0828	9133	A. Urbina
1	MS 0847	9133	W. R. Witkowski
1	MS 1135	9134	S. Heffelfinger
1	MS 0847	9134	S. W. Attaway
1	MS 0384	9140	H. S. Morgan
1	MS 0382	9141	E. A. Boucheron
1	MS 0380	9142	K. F. Alvin
1	MS 0380	9142	M. L. Blanford
1	MS 0380	9142	M. W. Heinstein
1	MS 0380	9142	S. W. Key
1	MS 0380	9142	G. M. Reese
1	MS 0382	9143	J. R. Stewart
1	MS 0382	9143	K. M. Aragon
1	MS 0382	9143	H. C. Edwards
1	MS 0382	9143	G. D. Sjaardema
1	MS 0321	9200	W. J. Camp
1	MS 0318	9200	G. S. Davidson
1	MS 1110	9210	D. E. Womble
1	MS 0370	9211	S. A. Mitchell
1	MS 0370	9211	R. A. Bartlett
1	MS 0370	9211	S. S. Collis
1	MS 0370	9211	M. S. Eldred
1	MS 0370	9211	D. M. Gay
1	MS 0370	9211	L. P. Swiler
5	MS 0370	9211	T. G. Trucano
1	MS 0370	9211	B. G. van Bloemen Waanders
1	MS 0310	9212	M. D. Rintoul
1	MS 1110	9212	S. J. Plimpton
1	MS 1110	9214	J. DeLaurentis
1	MS 1110	9214	R. B. Lehoucq
1	MS 1110	9215	S. K. Rountree
1	MS 1111	9215	B. A. Hendrickson
1	MS 1110	9215	R. Carr
1	MS 1110	9215	W. E. Hart
1	MS 1111	9215	P. Knupp
1	MS 1110	9215	V. J. Leung
1	MS 1110	9215	C. A. Phillips
1	MS 0318	9216	J. E. Nelson
1	MS 1109	9216	R. J. Pryor
1	MS 0321	9220	R. W. Leland
1	MS 0370	9220	J. A. Ang
1	MS 1110	9223	N. D. Pundit
1	MS 0817	9224	D. W. Doerfler
1	MS 0376	9226	T. D. Blacker
1	MS 0822	9227	D. R. White
1	MS 0822	9227	C. F. Diegert
1	MS 0316	9230	P. Yarrington
1	MS 0378	9231	R. M. Summers
1	MS 0378	9231	S. P. Burns
1	MS 0378	9231	M. A. Christon
1	MS 0378	9231	R. R. Drake
1	MS 0378	9231	A. C. Robinson
1	MS 0378	9231	T. Voth

1	MS 0378	9231	M. K. Wong
1	MS 0378	9232	P. F. Chavez
1	MS 0370	9232	M. E. Kipp
1	MS 0378	9232	S. A. Silling
1	MS 0378	9232	P. A. Taylor
1	MS 0316	9233	S. S. Dosanjh
1	MS 0316	9233	D. R. Gardner
1	MS 0316	9233	S. A. Hutchinson
1	MS 1111	9233	A. G. Salinger
1	MS 0316	9233	J. N. Shadid
1	MS 0310	9235	J. B. Aidun
1	MS 0310	9235	H. P. Hjalmarson
1	MS 0661	9514	M. A. Ellis
1	MS 0629	9519	D. S. Eaton
1	MS 0139	9900	M. O. Vahle
1	MS 0139	9904	R. K. Thomas
1	MS 0139	9905	S. E. Lott
1	MS 0428	12300	D. D. Carlson
1	MS 0428	12301	V. J. Johnson
1	MS 0638	12316	D. L. Knirk
1	MS 0638	12316	D. E. Peercy
1	MS 0829	12323	W. C. Moffatt
1	MS 0829	12323	J. M. Sjulin
1	MS 0829	12323	B. M. Rutherford
1	MS 0829	12323	F. W. Spencer
1	MS 0405	12333	T. R. Jones
1	MS 0405	12333	S. E. Camp
1	MS 0434	12334	R. J. Breeding
1	MS 0830	12335	K. V. Diegert
1	MS 1030	12870	J. G. Miller
1	MS 1221	15100	J. L. McDowell
1	MS 1002	15230	P. D. Heermann
1	MS 1170	15310	R. D. Skocypec
1	MS 1176	15312	D. J. Anderson
1	MS 1176	15312	J. E. Campbell
1	MS 1176	15313	R. M. Cranwell
1	MS 1153	15331	L. C. Sanchez
1	MS 1179	15340	J. R. Lee
1	MS 1179	15341	L. Lorence
1	MS 1162	15414	W. H. Rutledge
1	MS 9018	8945-1	Central Technical Files
2	MS 0899	9616	Technical Library